The Mass Transfer and Charge Transport Properties of Osmium bis(2,2'-bipyridyl)- containing 4-Vinylpyridine / Styrene Copolymers.

David Michael Kelly

A Thesis submitted for the Degree of

Doctor of Philosophy.

School of Chemical Sciences,

Dublin City University.

March 1996.

Declaration

I hereby declare that the contents of this thesis, except where otherwise stated, are based entirely on my own work, which was carried out in the School of Chemical Sciences, Dublin City University and in the School of Chemistry, University of Leicester.

David Kelly

David Michael Kelly

This thesis is dedicated to my parents.

Acknowledgements.

My sincerest thanks to Prof. Johannes G. Vos for his support, guidance and encouragement during the course of this work. My thanks also to Prof. A. Robert Hillman for providing me with the opportunity to work with the EQCM and for his endless help in the preparation of this thesis.

My thanks to Dr. R.J. Forster for his insights into the many facets of electron transfer theory.

My deepest and sincerest thanks to Eva for her love, support and friendship.

My thanks to Patxi, Niall, Dave and Mary for their encouragement and good company.

Thanks to the members of the Vos research group; Andy, Alan, Margaret, Frances, Karen, Miriam and Tia, and to the members of the Hillman research group; Dave, Lou, Sally and Helen for their extraordinary help during my time in Dublin and Leicester.

Thanks to the technical staff at D.C.U; Veronica, Maurice, Damien and Ann for their invaluable help.

Finally, my thanks to Joey and Des for their kindness and to my parents for their love and constant encouragement and for always being there.

Abstract.

The Mass Transfer and Charge Transport Properties of Osmium bis(2,2'-bipyridyl)-containing 4-Vinylpyridine / Styrene Copolymers.

In Chapter 1, some of the techniques used for the characterisation of the electrochemical properties of electrode modifying materials are introduced. A brief review of the mass transfer and charge transport studies of redox materials is presented.

In Chapter 2, the admittance characteristics of crystal coatings are studied. This analysis allows the rigidity and resident layer mass of the coatings to be probed as a function of the electrolyte type and concentration. In Chapter 3, the charge transport properties of $[Os(bipy)_2(PVP_x)_{10}Cl]^+$, where x signifies the percentage of poly 4-vinylpyridine in the poly 4-vinylpyridine/styrene copolymer backbone, are probed as a function of the electrolyte type and concentration. Activation parameters are evaluated to aid diagnosis of the rate determining steps.

The remainder of the thesis deals with the mass transfer properties of the highest and lowest styrene content metallopolymers. In Chapters 4 and 5, the redox-switching-induced mass changes of $[Os(bipy)_2(PVP_{33})_{10}Cl]^+$ coated crystals are investigated as a function of the $HClO_4$ and $LiClO_4$ concentration of the contacting electrolyte and the experimental timescale using the Electrochemical Quartz Crystal Microbalance (EQCM). Comparison with $[Os(bipy)_2(PVP_{100})_{10}Cl]^+$ is made and a relationship between the ease of solvent transfer and the rate of charge transport is suggested.

In Chapter 6, the effect of acetonitrile on the mass transfer and charge transport properties of $[Os(bipy)_2(PVP_{100})_{10}Cl]^+$ crystal coatings is investigated. The relationship between the degree of polymer swelling, the ease of mass transfer and the rate of charge transport is illustrated.

Contents

Chapter 2. The Effect of $HClO_4$ and $LiClO_4$ Concentrations On the Rigidity and Layer Mass of $[Os(bipy)_2(PVP_x)_{10}Cl]^+$ Copolymer Films.

Chapter 1.

Introduction, Theory and Review of Redox Polymer Modified Electrodes.

1.1. Introduction.

The electrode surface can be a powerful tool. By controlling the electrode potential, the electrode can be used as a variable free energy source or sink of electrons. In addition, electrons crossing the solution-electrolyte interface can be determined with great sensitivity by measuring current. As with most measurement tools, however, electrodes encounter specific phenomena that reduce their applicability to analytical and synthetic schemes. Chief among these are fouling of the electrode by unwanted precipitation or absorption processes and the slow electrochemical reaction rates of some species. These limitations have led to the development of modified electrodes, which may be designed to be either selective for a particular analyte or capable of mediating redox reactions that are slow or not possible at a bare unmodified electrode.

The range of modifying materials is vast, varying from metal deposits and metal oxide layers to the use of organic materials, enzymes and polymers. The availability of considerable numbers of different modifying materials means that the properties of traditional electrode materials can be altered to meet the requirements of a particular application. Multilayer coverages are often achieved by modification of the electrode with polymer layers [1-4]. Polymer materials offer synthetic flexibility and inherent stability as well as ease of application to electrode substances. Methods that achieve this include electrochemical polymerisation of the monomer and, most commonly, drop, dip or spin-coating of a solution of the polymer. For a more complete insight into the synthesis and preparation of electrode coatings the reader is referred to the excellent reviews in References 1-4.

Modification of electrode surfaces with thin polymer films carrying redox sites has become a major area of electrochemistry for more than a decade [1-11]. Such rapid growth of modified electrodes can be understood in view of their many potential applications which includes, for example, their use in electrocatalysis [12,13]. Electroactive polymers containing fixed redox sites may be classified as

redox polymers or ion exchange polymers. Redox polymers contain the electroactive centre as a part of the polymer chain backbone, or the electroactive centre may be covalently bound to a pre-formed functional polymer. In these systems the redox sites are immobile beyond a close vicinity of their attachment to the matrix. Ion exchange polymer films on electrodes, however, depend on drawing ionic redox substances from their solutions into the film as counterions [1,14-16]. This process has been termed "electrostatic binding" [1,14,16].

A large body of research on chemical modification of electrodes that has been generated over the years is concerned with the dynamics of charge transport in the electrode films (see references 1,11 and 16 for reviews). In virtually all applications, the functioning of these systems depends on the efficiency of charge transport across the electrode film. It is, therefore, not surprising that the understanding of charge transport and related processes has always been emphasised in this area of research. The work presented in this thesis deals with the charge transport and associated mass transfer properties of redox polymers based on osmium poly(pyridyl) complexes covalently attached to pre-formed poly(4-vinylpyridine)/ styrene copolymer backbones. In the course of this work, the influence of the polymer backbone on these transport processes is probed as a function of the bathing electrolyte type and concentration. The influence of organic solvent-induced swelling phenomena is also considered. These studies involve the evaluation of charge transport rates and activation parameters for electron transfer using electrochemical techniques; while the Electrochemical Quartz Crystal Microbalance (EQCM), is used to probe interfacial mass transfer processes.

In this chapter the techniques used in the charge and mass transport investigations undertaken in this work are introduced and reviewed. Particular emphasis is placed on previous studies of the redox polymers which are the subject of this thesis, however reference is also made to other electrode modifying materials.

1.2. Charge Transport Processes in Redox Polymers.

1.2.1. General Considerations.

For redox polymers in which electroactive sites are fixed, the electroactive sites that are remote from the electrode surface cannot be oxidised/ reduced unless successive electron transfer between electroactive sites occurs i.e. it is considered that charge transport through the film can only occur via an electron hopping process between the electroactive centres [16-18]. This propagation of electrons is generally accompanied by the movement of electroinactive counterions (to maintain electroneutrality), solvent and polymer chain segments [1,2,11]. Therefore, while electron hopping may be the mechanism for electron transport, the charge transport rate will be governed by either (i) the electron self-exchange reaction, (ii) charge-compensating counterion motion, which is necessarily coupled to electron transfer, or (iii) segmental motion of the polymer chains. The charge transport process is diffusive in nature, so the rate of electron transport can therefore be characterised by an observable parameter, the apparent diffusion coefficient, D_{CT} [19,20,11].

1.2.2. Estimation of Charge transport rates.

The two most commonly used techniques for the estimation of homogeneous charge transport rates in electroactive electrode modifying layers are cyclic voltammetry and potential step chronoamperometry.

1.2.2.1. Cyclic Voltammetry (CV).

Cyclic voltammetry has been used extensively to characterise the electroactivity of polymer modified electrodes and for the evaluation of charge transport rates. In this technique the potential sweep commences at a potential where no reaction occurs, proceeds to a potential where the species of interest is

electroactive and then to a final switching potential from where the scan direction is reversed.

Quantitative data regarding charge transport have been largely obtained from studies of the current response of the modifying layer at high voltammetric scan rates where solution (semi-infinite diffusion) conditions prevail [19,21-27]. For an electroactive layer undergoing a reversible electrode reaction, under a semi-infinite regime, the peak current is defined by the Randles-Sevcik equation [28]:

$$i_p = \frac{0.4463(nF)^{3/2} AD_{CT}^{1/2} C\nu^{1/2}}{(RT)^{1/2}} \qquad (1.2.1.)$$

where i_p is the peak current, n is the number of electrons transferred, F is the Faraday constant, A is the electrode area, D_{CT} is the apparent diffusion coefficient, C is the concentration of electroactive sites within the film, ν is the scan rate, R is the gas constant and T is the absolute temperature. In addition, the following conditions prevail:

$$E_p = E_{pa} - E_{pc} = \frac{0.0592}{n} \text{ V at } 25^0\text{C} \qquad (1.2.2.)$$

$$i_{pa} / i_{pc} = 1 \qquad (1.2.3.)$$

where E_{pa} and E_{pc} , i_{pa} and i_{pc} are the anodic and cathodic peak potentials and current respectively.

Equation 1.2.1 has been used in the evaluation of charge transport rates in osmium and ruthenium redox polymers [21-27,29], where typically semi-infinite diffusion conditions prevail at sweep rates in excess of 50 mVs^{-1}. The magnitude of the charge transport rates estimated by cyclic voltammetry are typically within the

range of 10^{-10} - 10^{-12} cm^2s^{-1} for these osmium and ruthenium based redox polymers.

At slow sweep rates, when the modifying layer is exhaustively oxidised/ reduced, surface or thin-layer behaviour is observed. Under these conditions the peak current varies linearly with scan rate and the following conditions prevail [28,30]:

$$i_p = \frac{n^2 F^2 A \Gamma_T \nu}{4RT} \qquad (1.2.4.)$$

$$E_{pa} = E_{pc} \qquad (1.2.5.)$$

$$FWHM = \frac{90.6}{n} \text{ mV at } 25^0\text{C} \qquad (1.2.6.)$$

where FWHM is the full peak width at half height. Γ_T is the total quantity of electroactive material on the electrode surface and may be evaluated, under thin-layer conditions, using the relationship:

$$\Gamma_T = Q / nFA \qquad (1.2.7.)$$

where Q is the total charge passed and may be determined by integrating the area under the anodic or cathodic branch of the cyclic voltammogram. Surface behaviour is typically observed for osmium and ruthenium redox polymers at scan rates of 1-5 mVs^{-1} [21-27].

1.2.2.2. Chronoamperometry (PS).

Charge transport rates are most frequently evaluated using potential step techniques. The timescale of the potential step is manipulated to ensure a semi-infinite diffusional response, where the current decay conforms to the Cottrell equation [28]:

$$i(t) = \frac{nFAD_{CT}^{1/2}C}{(\pi t)^{1/2}} \qquad (1.2.8.)$$

Charge transport rates estimated by potential step techniques are typically within the range of 10^{-8} - 10^{-10} for osmium and ruthenium redox polymers [21-27].

1.2.3. Evaluation of Activation Parameters.

For a more definitive evaluation of the processes involved in charge transport, activation parameters are frequently determined [19-27,29,31-33].

Activation parameters for homogeneous charge transport can be evaluated from the temperature dependence of D_{CT}, which typically exhibits an Arrhenius-type relationship [19]:

$$D_{CT} = D_{CT}^{0} \exp\left[-E_a / RT\right] \qquad (1.2.9.)$$

The entropy of activation may be estimated from the Eyring equation [19]:

$$D_{CT}^{0} = e\delta^2 \left(k_B T / h\right) \exp\left(\Delta S^{\neq} / R\right) \qquad (1.2.10.)$$

where e is the base of the natural log, δ is the intersite separation between redox sites, k_B is the Boltzmann constant and h is Planck's constant.

The absolute values of these entropy terms are acknowledged to be of limited accuracy since the intersite separation of the redox sites (δ in equation 1.2.10) is only approximated using a rigid rod model of the polymer structure [34]. However, even allowing for a large variation in polymer swelling, a significant departure from the assumed value of δ does not change the sign of the entropy terms calculated and the observed trends should remain valid [24]. Negative entropies are associated with either electron hopping or ion motion rate determining steps [19] whilst positive entropies can be assigned to disordering polymer chain motion [21,23].

1.2.4. Review of Charge Transport Processes in $[M(bipy)_2(Pol)_nCl]^+$ Redox Polymers.

The ultimate goal of polymer modified electrodes is in their practical applications. The redox polymers $[M(bipy)_2(Pol)_nCl]^+$ where M signifies osmium or ruthenium metal centres, bipy is 2,2'-bipyridyl; Pol is Poly 4-vinylpyridine (PVP), Poly N-vinylimidazole (PVI) or PVP: Styrene copolymer backbones; and n is the metal to polymer unit loading (typically $5 \leq n \leq 100$) have proven particularly useful as electrocatalysts. The mediated oxidation of Fe^{2+} by $[Ru(bipy)_2(PVP)_nCl]Cl$ [12,13,31,35-37], reduction of Fe^{3+} by $[Os(bipy)_2(PVP)_{10}Cl]Cl$ [36,38] and $[Os(bipy)_2(PS)_{7.5}(DMAP)_{2.5}Cl]Cl$ [39] where PS is polystyrene and DMAP is poly[4-(methyl-N-p-vinylbenzylamino) pyridine], and the detection of both nitrite [40] and ascorbic acid [41] with $[Os(bipy)_2(PVP)_{10}Cl]Cl$ have been successfully demonstrated. Furthermore, enzymatic sensors based on the redox polymer $[Os(bipy)_2(PVP)_nCl]Cl$ have been developed [42-44]. These studies are beyond the scope of this thesis and the reader is referred to References 12,13,31,35-44. The success of any attempt to exploit polymer modified electrodes for the electrocatalytic detection of substrates lies in a detailed understanding of the mechanisms and rates of charge transport. Consequently, the charge transport properties of these and similar redox materials have attracted considerable attention in the last decade. These investigations are the primary focus of this review.

In a series of comprehensive studies, the influence of electrolyte type and concentration, redox site loading, experimental timescale and temperature on the charge transport properties of $[Os(bipy)_2(PVP)_nCl]^+$ [21-24], $[Os(bipy)_2(PVI)_nCl]^+$ [26] and $[Os(bipy)_2(PVI)_n]^{2+}$ [25] electrode coatings were investigated. In these redox polymers, anion dependent changes in D_{CT} of up to 1-2 orders of magnitude were observed [21-25]. These variations in D_{CT} with electrolyte anion type are a consequence of the anion dependence of the polymer structure and are considered to reflect changes in the relative ease of ion motion [21,25] e.g. for

$[Os(bipy)_2(PVP)_nCl]^+$ in pTSA electrolytes, in which these layers are swollen [45-47], D_{CT} is of the order of 10^{-10} cm^2s^{-1}; whilst in perchlorate electrolytes, in which these layers are compact [47,48], D_{CT} is of the order of 10^{-11} cm^2s^{-1}. Similar anion dependent variations in D_{CT} have been reported for $[Ru(bipy)_2(QPVP)_nCl]^+$ where QPVP signifies quaternised PVP and $4 \leq n \leq 80$ [20]. For $[Os(bipy)_2(PVP)_nCl]^+$ polymers, D_{CT} typically increases with increasing electrolyte concentration and is considered to reflect reduced ion transport limitations [21-24].

The dependence of D_{CT} on the redox site concentration has also received considerable attention [20-26,31,49,50]. Whilst it is considered that the charge transport rate will increase with increasing metal loading, this behaviour is typically only observed over a limited range of metal loadings [20-26,31,50]. This behaviour is a consequence of the fact that D_{CT} is dependent not only on the rate of electron self-exchange but on the availability and mobility of ions and solvent. It has been illustrated that the conditions necessary for rapid electron transfer i.e. a high concentration of orientated sites and facile ion diffusion are mutually exclusive [23,24,51]. Consequently, whilst increasing the redox site loading favours rapid electron transport it also results in ion diffusion limitations. For $[Ru(bipy)_2(PVP)_nCl]^+$ polymers, where $4 \leq n \leq 80$, the activation energy for the charge transport process, E_a, was observed to increase with decreasing redox site loading and was attributed to the increased requirement for polymer chain motions to reduce the intersite separation [31].

The influence of the polymer backbone on the charge transport process has been probed. For $[Ru(bipy)_2(QPVP)_nCl]^+$ polymers, E_a increased with increased crosslinking of the polymer backbone using α,α'-dibromo-m-xylene crosslinker [20]. This increase in E_a was attributed to rate limiting polymer motion [20]. For $[Os(bipy)_2(QPVP)_6Cl]^+$ at pH 7.0, D_{CT} was observed to increase with increasing quaternisation of the polymer backbone [52]. At pH 2.0, where the polymer is protonated [45,48], D_{CT} was observed to decrease with increasing crosslinking of the

polymer [52]. These observations were discussed in terms of relative changes in the mobility of the polymer chains [52]. The effect of crosslinking of the polymer backbone on the rate of charge transport in $[Os(bipy)_2(PVP)_{10}Cl]Cl$ has been addressed [53]. Using 1,5-dibromopentane as a crosslinker, D_{CT} was enhanced by crosslinking of up to 20% of the pyridine units. However, further crosslinking of the polymer resulted in decreased charge transport rates [53]. These observations were considered to reflect a "trade-off" between reduced redox site separation (increased D_{CT}) and more hindered ion transport (decreased D_{CT}) with increased crosslinking of the polymer [53].

The relationship between the polymer properties and the rate and mechanism for charge transport has been clearly demonstrated for the redox polymer $[Ru(bipy)_2(PVP_x)_{10}Cl]^+$ where x signifies the percentage of PVP in a PVP: Styrene copolymer [27]. In a series of polymers of increasing styrene content, the rate of charge transport was found to increase in perchlorate electrolyte. Concurrently, the activation energy for the charge transport process, E_a, was found to decrease with increasing styrene content. It has been suggested that the perchlorate anion may crosslink these polymers through the pyridine moieties of the polymer backbone [54,55]. Consequently, the observed decrease in E_a was attributed to the more facile ion permeation within the less crosslinked polymer structure of higher styrene content [27].

1.3. The Electrochemical Quartz Crystal Microbalance.

1.3.1. Introduction.

The quartz crystal microbalance (QCM) is a piezoelectric device capable of extremely sensitive mass measurements [56-60]. It consists of a thin wafer of quartz sandwiched between two concentric electrodes which are bonded to the surface on opposite sides of the quartz disk. This arrangement is shown in Fig. 3.1. Application of an alternating electric field across a piezoelectric material induces a standing acoustic wave within the quartz with the node at the centre and antinodes at the two surfaces. This is the converse piezoelectric effect [56-58]. The quartz resonator can be made to oscillate by including the wafer in an appropriately designed oscillator circuit [56,57].

The superior mechanical and piezoelectric properties of alpha quartz make it ideal for this application. The mode of vibration depends on the crystallographic orientation of the quartz, the shape and configuration of the electrodes and the supporting structure. Unwanted modes of vibration can therefore be suppressed by careful design and control of the crystal cut and electrode arrangement. Crystals are precisely cut from a natural or synthetic single crystal of quartz at certain angles to the crystalline axes [56,57].

The thickness shear mode of vibration, in which motion of the crystal surface is parallel to the crystal face, is the most sensitive to the addition and removal of mass [57]. "AT" and "BT" crystal cuts, which oscillate in this mode, are most frequently used. Standard AT crystals, cut at an angle of 35° 15', are insensitive to temperature changes in the region around room temperature which makes them particularly useful [56].

A typical crystal design is highlighted in Fig. 3.1. The vibration of quartz is confined to the area between the two electrodes. This orientation allows the quartz

Fig. 1.1. Laboratory Quartz Crystal.

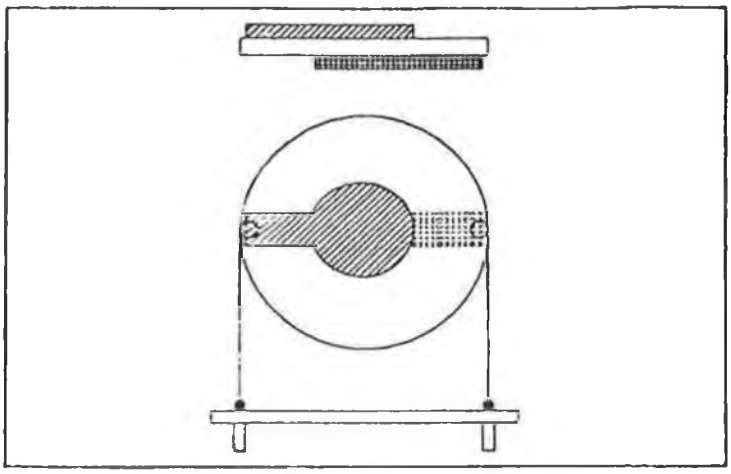

plate to be held by mechanical supports near its edge without adversely affecting the crystal resonance.

1.3.2. Mass-Frequency Relationship.

The resonant frequency of these oscillating devices is sensitive to the addition/ removal of mass. In 1959 Sauerbrey demonstrated that the shift in resonant frequency of an oscillating quartz crystal could be used to accurately determine the mass of rigidly attached material [61]. The mass-frequency relationship which he derived is given by:

$$\Delta f = -\left(\frac{2}{\rho v}\right)\Delta M f_o^2 \qquad (1.3.1.)$$

where f_o is the base frequency of the quartz crystal (10 MHz in our case), ΔM is the change in areal mass ($ngcm^{-2}$), ρ is the density of quartz (2.648 gcm^{-3}) and v is the wave velocity within it (3.34 x 10^5 cmHz). The negative sign signifies that an increase

in the mass of the quartz crystal results in an decrease in the resonant frequency.

Up until quite recently it was believed that the QCM would not function in a liquid medium as a result of excessive energy loss from viscosity effects of the contacting solution. However, in 1980 Konash and Bastiaans successfully demonstrated the application of the QCM to the determination of mass changes in a liquid environment [62]. In 1985 the Electrochemical Quartz Crystal Microbalance (EQCM) was developed in which one of the quartz electrodes served as the working electrode in a three-electrode electrochemical cell [63]. The development of this technique allowed for the simultaneous measurement of electrochemical parameters and the accompanying mass transfer associated with these electrochemical processes.

1.3.3. Immersion in Solution.

On immersion of one side of a resonator in liquid, a decrease in the resonant frequency is observed. This change in resonant frequency arises from coupling of the quartz shear oscillations with the liquid medium, which results in a damped propagation of the shear wave [63-65]. The associated boundary layer, which is dragged along the disk surface, behaves as a rigidly attached mass. The thickness of this liquid boundary layer, i.e. the degree of penetration of the shear wave, depends on the viscosity and density of the liquid and the degree of coupling between the two. The shift in resonant frequency on immersion is given by [64,65]:

$$\Delta f = -f_o^{3/2}\left(\frac{\eta_L \rho_L}{\pi \rho_q \mu_q}\right)^{1/2} \qquad (1.3.2.)$$

where η_L is the liquid viscosity, ρ_L is the liquid density and μ_q is the shear modulus of quartz. The decay length, which represents the effective thickness of the rigidly bound liquid deposit, is ca. 300 nm thick for a 10 MHz quartz crystal in an aqueous

medium [66].

The dependence of the oscillation frequency of the piezoelectric crystal on the physical parameters of the contacting liquid; viscosity, density, dielectric constant and specific conductivity; have been studied in detail [63-65,67-75]. Corrections for these phenomena may be achieved by separately measuring the shift in resonant frequency on immersion and by subsequent subtraction. Alternately a dual QCM may be used in which both the sensing and reference crystals are immersed. This approach provides a more accurate and facile means of compensating for these affects [76-78].

The Sauerbrey equation allows for the evaluation of the mass of a loaded crystal resonator based on the shift in resonant frequency. There are, however, a number of conditions under which deviations from a linear mass-frequency relationship may be observed. These are briefly outlined in the following section.

1.3.4. Non-ideal Behaviour.

The microscopic "roughness" of the quartz may effect the behaviour of the QCM in solution [79-81]. Solvent molecules trapped in surface cavities will increase the mass change observed and may be incorrectly assigned to some other process. This behaviour has been observed during the oxidation of gold, silver and copper layers [80,81]. Oxidation of these layers resulted in frequency changes that were substantially greater than anticipated for the formation of the oxide layers. Roughening of the surface, and the subsequent trapping of solvent molecules was identified [80,81].

The radial sensitivity function of crystals has been shown to exhibit a Gaussian distribution, which is greatest at the centre and decreases towards the edge of the electrodes [82-84]. This distribution reflects the Gaussian distribution of the shear amplitude within the quartz, which has been verified for uncoated crystals in air using a tungsten probe [85]. The integral or average sensitivity however remains constant for a given crystal over the quartz electrode area [83,84]. It is therefore

essential that homogenous mass changes are observed over the entire crystal area and that coated films are evenly distributed.

The effects of both film [83] and liquid [79] induced stresses on the behaviour of the QCM have been noted. It has been demonstrated that, for a heavily stressed film on one face of the crystal, the sensitivity of the centre of the crystal increases dramatically whilst the sensitivity at the electrode edges decreases to insignificance [83]. The integral sensitivity remains constant however, again emphasising the need for films of even thickness.

The primary underlying assumption of the Sauerbrey equation is that the foreign mass behaves as a rigid, perfectly elastic layer. Deviations from this "rigid layer approximation" may result in viscous damping of the acoustic shear wave within the polymer film and may thus compromise the mass-frequency relationship. The viscoelastic behaviour of each material must, therefore, be studied before accurate mass measurements can be made. One approach is to verify that changes in deposit thickness or surface coverage scale linearly with changes in the resonant frequency. This requires that some parameter, such as charge, be found which provides independent measure of thickness and coverage. In the absence of film viscosity contributions to the resonant frequency, a plot of mass against the charge passed should be linear [47,48,57,86]. Viscous films will exhibit concave curvature, indicating loss of sensitivity due to damping of the shear wave as it travels through the film [57,86].

An alternative approach is to study the crystal resonance i.e. the admittance (or conductance) response at a range of frequencies around the resonant frequency [45,47,48,60,86-90]. In this qualitative approach, the viscoelastic properties of the layer are characterised in terms of the shape of the admittance response. A significant contribution of the viscosity of the polymer layer to the resonant frequency, i.e. non rigid layer behaviour, is characterised by a decrease in the admittance maximum and broadening of the admittance response [45,47,48,60,86-90].

1.3.5. Review of Mass Transfer Properties of Electroactive Polymers.

Since its development, the EQCM has found considerable application in the electrogravimetric study of fundamental electrochemical processes (see References 57-60,79 and 91 for a review). The EQCM has proven particularly useful in the study of changes in the ion and solvent populations of thin electroactive polymer layers during electrochemical processes. Identification of the counterion component of the redox-switching-induced mass change may be achieved by systematic variation of the electrolyte cation or anion, whilst the use of deuterated solvents can provide a useful and unambiguous means of identifying the solvent component of the redox induced mass charge. The mass changes accompanying redox switching of electroactive polymer layers are the subject of the following review.

A number of conducting polymers have been investigated using the EQCM technique. Studies of the changes in layer mass during redox switching of polypyrrole have demonstrated that both counter-anions and cations are transferred in response to electroneutrality constraints. It was observed that, for pyrrole films grown with small anions (BF_4^- [92], ClO_4^- [92-94] and Cl^- [95]), counter-anion motion dominated the redox-switching-induced mass change, while, for films grown with large anions (poly(4-styrenesulphonate) [92,93,96,97], polyvinyl sulphonate [92] and dodecylbenzenesulfonate [98]) cation motion dominated. For films grown with dodecylbenzenesulfonate, the level of solvent transfer accompanying cation motion has been quantified as 6.0, 4.5, 4.0, and 1.7 molecules of water per Li^+, Na^+, K^+ and Cs^+ cation respectively [98].

For polyaniline in aqueous electrolytes, at pH > 2, counter-anion ingress and cation egress were identified as the ions responsible for the maintain of electroneutrality during the first [86,99,100] and second [86,99] polymer oxidations respectively. Anion insertion with very little solvent movement was observed during oxidation [86,100]. At more acidic pH, proton expulsion during oxidation was also in

evidence [86,100]. Redox switching of polybithiophene films was observed to result in counter-anion ingress/ egress [66,101-105]. This anion motion was accompanied by exactly balancing motion of solvent and salt in opposing directions. This behaviour has been termed "apparent permselectivity" [66,103].

Mass transfer accompanying redox switching of Prussian Blue [106,107] and its analogues [108,109] has been investigated. Dominant cation transfer during redox processes has been clearly illustrated by systematic variation of the molecular weight of the electrolyte cation [107-109]. The simultaneous motion of solvent, in the direction opposite to that of cation motion, has been verified by isotopic substitution of H_2O with D_2O [108].

Changes in the ion and solvent populations of polyvinylferrocene (PVF) [66,103,110,111-118] and $[Os(bipy)_2(PVP)_{10}Cl]^+$ [45-48,114,119] redox polymers, during redox processes, have been studied in some detail. In perchlorate electrolytes, PVF [111] and $[Os(bipy)_2(PVP)_{10}Cl]^+$ [46-48] layers are permselective. For PVF under these conditions, the changes in layer mass during redox processes, obtained at slow cyclic voltammetric scan rates, indicated that mass transfer was due to the interfacial movement of a single perchlorate counter-anion and 4-5 solvent molecules [111]. In an earlier investigation [113], considerably less solvent movement with the perchlorate anion was observed. Similarly, in perchloric acid, oxidation/ reduction of $[Os(bipy)_2(PVP)_{10}Cl]^+$ films was observed to be accompanied by the ingress/ egress of a single perchlorate counter-anion and 2-3 molecules of solvent [48]. In sodium perchlorate electrolytes however, anion transfer was apparently unaccompanied by solvent [46,47].

The influence of electrolyte concentration on the mass transfer processes within these and tetracyanoquinodimethane (TCNQ) [120-122] polymer layers has been probed. For PVF [111] and $[Os(bipy)_2(PVP)_{10}Cl]^+$ [48] crystal coatings, permselectivity apparently fails in electrolyte concentrations in excess of ca. 1.0M ClO_4^- and interfacial salt transfer occurs during redox switching. In TCNQ films,

cation motion maintains electroneutrality within the polymer during redox cycling and the mass changes observed were found to be dominated by the concomitant movement of water of hydration [120,121]. In high electrolyte concentrations the mass changes observed decreased. This behaviour was explained in terms of decreased solvent activity and compaction and restricted segmental polymer motion within the polymer layer [120,121].

The dependence of the mass transfer processes within these electroactive films on the degree of polymer swelling has been clearly demonstrated [45-48,120]. The importance of counter-anion type has been addressed. For PVF, an almost linear relationship between the observed mass change and anion molecular weight has been observed [111], with slight deviations attributed to variations in polymer structure affecting solvent movement. However, more pronounced changes in PVF morphology with changes in counter-anion type have been observed [113]. In PF_6^- electrolyte no solvent transfer was observed, however in Cl^- electrolyte, extensive delamination of the polymer from the electrode occurred during oxidation [113].

Similar counter-anion effects have been observed in $[Os(bipy)_2(PVP)_{10}Cl]^+$ [45-48,114]. In perchlorate electrolytes, only small quantities of solvent are transferred [45-48,114]. In para-toluene sulphonate, NO_3^-, SO_4^{2-}, and Cl^- electrolytes, significant solvent transfer was observed [45-47]. This was related to the increased solvent content of the polymer layers in the initial state when converted to these salt forms [46]. The considerable movement of solvent in pTS^- electrolytes was confirmed from isotopic substitution of H_2O with D_2O [45,47].

The kinetics of mobile species transfer has been addressed for many of the polymers discussed in this review. In PVF, under potential step conditions, counter-anion motion maintains electroneutrality at short timescales [103,115]. At low electrolyte concentrations, solvent movement was found to be slower than ion motion [103,115,116]. This delineation of solvent was termed "kinetic permselectivity", in

which the mass change observed was that of counter-anion only [101,116]. At high electrolyte concentrations salt transfer also occurs, but at a slightly faster rate than solvent movement [103,110,115,116,118]. Similarly, for polybithiophene [66,101], polythionine [66] and $[Os(bipy)_2(PVP)_{10}Cl]^+$ [123], net neutral species have been identified as the slowest species transferred during redox switching. For these systems, transient non-equilibrium states are used to maintain electroneutrality under more dynamic conditions, which may be achieved independently of the thermodynamic requirements of the charge transport process itself.

EQCM studies of the dynamics of mass transfer in $[Os(bipy)_2(PVP)_{10}Cl]^+$ have been considered. It has been illustrated that there is good correlation between the water content of the polymer and the apparent charge transport diffusion coefficient, D_{CT} [47,114,123] and that the presence of solvent facilitates redox switching. These observations are examined in the course of the work presented here.

1.4. Conclusions.

Through the unique properties of modified electrodes, many potential applications for these devices have been proposed. Of primary importance to the successful application of these materials is a knowledge and understanding of the charge transport mechanism within them. The techniques discussed in this review provide a means for examining not only the charge transport processes within electrode modifying materials but also the accompanying mass transfer processes. Only through detailed studies of the charge transport and mass transfer properties of these materials will these processes be understood.

1.5. References.

1. A.R. Hillman, Electrochemical Science and Technology of Polymers, R.G. Linford (Ed.), Elsevier, Amsterdam, (1987), Chs. 5 and 6.
2. R.W. Murray, Electroanalytical Chemistry, A.J. Bard (Ed.), Marcel Dekker, New York, 13 (1984) 191.
3. R.W. Murray, Molecular Design of Electrode Surfaces, R.W. Murray (Ed.), Wiley, New York, (1992) Ch. 1.
4. R.J. Forster and J.G. Vos, Comprehensive Analytical Chemistry, Vol. XXVII, M.R. Smyth and J.G. Vos (Ed.), Elsevier, Amsterdam, (1992), Ch. 7.
5. M.D. Imisides, G.G. Wallace and E.A. Wilke, Trends in Anal. Chem., 7 (1988) 143.
6. M.S. Wrighton, Science, 231 (1986) 32.
7. A.R. Guadalupe and H.D. Abruna, Anal. Chem., 57 (1985) 142.
8. R.W. Murray, A.G. Ewing and R.A. Durst, Anal. Chem., 59 (1987) 379A.
9. C.E.D. Chidsey and R.W. Murray, Science, 231 (1986) 25.
10. R.W. Murray, Acc. Chem. Res., 13 (1980) 135.
11. M. Majda, Molecular Design of Electrode Surfaces, R.W. Murray (Ed.), Wiley, New York, (1992) Ch. 4.
12. S. Geraty and J.G. Vos, J. Electroanal. Chem., 176 (1984) 389.
13. O.Haas, M. Kriens and J.G. Vos, J. Am. Chem. Soc., 103 (1981) 1318.
14. H.S. White, J. Leddy and A.J. Bard, J. Am. Chem. Soc., 104 (1982) 4811.
15. M. Shin, E-Y Kim, J. Kwak and I.C. Jeon, J. Electroanal. Chem., 394 (1995) 87.
16. N. Oyama and T. Ohsaka, Molecular Design of Electrode Surfaces, R.W. Murray (Ed.), Wiley, New York, (1992) Ch. 7.
17. F.B. Kaufman, A.H. Schroeder, E.M. Engler, S.R. Kramer and J.Q. Chambers, J. Am. Chem. Soc., 102 (1980) 483.

18. O. Hatazoki, T. Ohsaka and N. Oyama, J. Phys. Chem., 96 (1992) 10492.

19. P. Daum, J.R. Lenhard, D.R. Rolison and R.W. Murray, J. Am. Chem. Soc., 102 (1980) 4649.

20. S.M. Oh and L.R. Faulkner, J. Am. Chem. Soc., 111 (1989) 5613.

21. R.J. Forster, A.J. Kelly, J.G. Vos and M.E.G. Lyons, J. Electroanal. Chem., 270 (1989) 365.

22. R.J. Forster and J.G. Vos, J. Electroanal. Chem., 314 (1991) 135.

23. R.J. Forster, J.G. Vos and M.E.G. Lyons, J. Chem. Soc. Faraday Trans., 87 (1991) 3761.

24. R.J. Forster and J.G. Vos, Electrochim. Acta, 37 (1992) 159.

25. R.J. Forster and J.G. Vos, J. Inorganic and Organometallic Polymers, 1 (1991) 67.

26. R.J. Forster and J.G. Vos, Langmuir, 10 (1994) 4330.

27. D. Leech, R.J. Forster, M.R. Smyth and J.G. Vos, J. Mater. Chem., 1 (1991) 629.

28. A.J. Bard and L.R. Faulkner, Electrochemical Methods: Fundamentals and Applications, Wiley, New York, (1980).

29. M.E.G. Lyons, H.G. Fay, J.G. Vos and A.J. Kelly, J. Electroanal. Chem., 250 (1988) 207.

30. A.P. Brown and F.C. Anson, Anal. Chem., 49 (1977) 1589.

31. C.P. Andrieux, Electrochemistry, Sensors and Analysis, M.R. Smyth and J.G. Vos (Ed.), Analytical Symposia Series, 25 (1986) 235.

32. W.J. Albery, M.G. Boutelle. P.J. Colby and A.R. Hillman, J. Electroanal. Chem., 133 (1982) 135.

33. M. Sharp and H. Larsson, J. Electroanal. Chem., 386 (1995) 189.

34. D. Ghesquiere, B. Ban and C. Chachaty, Macromolecules, 10 (1977) 743.

35. C.P. Andrieux, O. Haas and J.M. Saveant, J. Am. Chem. Soc., 108 (1986) 8175.

36. A.P. Doherty, R.J. Forster, M.R. Smyth and J.G. Vos, Anal. Chem., 64 (1992) 572.

37. O.Haas and B. Sandmeier, J. Phys. Chem., 91 (1987) 5072.

38. R.J. Forster and J.G. Vos, J. Chem. Soc. Faraday Trans., 87 (1991) 1863.

39. A.P. Doherty, M.A. Stanley, G. Arana, C.E. Koning, R.H.G. Brinkhuis and J.G. Vos, Electroanalysis, 4 (1995) 333.

40. A.P. Doherty and J.G. Vos, J. Chem. Soc. Faraday Trans., 88 (1992) 2903.

41. A.P. Doherty, M.A. Stanley and J.G. Vos, Analyst, 120 (1995) 2371.

42. B.A. Gregg and A. Heller, J. Phys. Chem., 95 (1991) 5970.

43. B.A. Gregg and A. Heller, J. Phys. Chem., 95 (1991) 5976.

44. B.A. Gregg and A. Heller, Anal.Chem., 62 (1990) 258.

45. A.P. Clarke, J.G. Vos, A.R. Hillman and A. Glidle, J. Electroanal. Chem., 389 (1995) 129.

46. A.J. Kelly, T. Ohsaka, N. Oyama, R.J. Forster and J.G. Vos, J. Electroanal. Chem., 287 (1990) 185.

47. A.J. Kelly and N. Oyama, J. Phys. Chem., 95 (1991) 9579.

48. A.P. Clarke, J.G. Vos, A. Glidle and A.R. Hillman, J. Chem. Soc. Faraday Trans., 89 (1993) 1695.

49. H. Larsson and M. Sharp, J. Electroanal. Chem., 381 (1995) 133.

50. J.S. Facci, R.H. Schmehl and R.W. Murray, J. Am. Chem. Soc., 104 (1982) 4959.

51. G. Inzelt, Electrochim. Acta, 34 (1989) 83.

52. A. Aoki, R. Rajagopalan and A. Heller, J. Phys. Chem., 99 (1995) 5102.

53. A.P. Doherty, T. Buckley, D. Kelly and J.G. Vos, Electroanalysis, 6 (1994) 553.

54. E.F. Bowden, M.F. Dautartas and J.F. Evans, J. Electroanal. Chem., 219 (1987) 91.

55. S.M. Oh and L.R. Faulkner, J. Electroanal. Chem., 269 (1989) 77.

56. C. Lu and A.W. Czanderna (Eds.), Applications of Piezoelectric Crystal Microbalances, Vol. 7, Elsevier, New York, (1984).

57. D.A. Buttry, Applications of the Quartz Crystal Microbalance to Electrochemistry, in A.J. Bard (Ed.), Electroanalytical Chemistry, Marcel Dekker, New York, 17 (1991) 1.

58. M.R. Deakin and D.A. Buttry, Anal. Chem., 61 (1989) 1147A.

59. M.D. Ward and D.A. Buttry, Science, 249 (1990) 1000.

60. D.A. Buttry and M.D. Ward, Chem. Rev., 92 (1992) 1355.

61. G. Sauerbrey, Z. Phys. 155 (1959) 206.

62. P.L. Konash and G.J. Bastiaans, Anal. Chem., 52 (1980) 1929.

63. S. Bruckenstein and M. Shay, Electrochim. Acta., 30 (1985) 1295.

64. K.K. Kanazawa and J.G. Gordon, Anal. Chem., 57 (1985) 1770.

65. K.K. Kanazawa and J.G. Gordon, Anal. Chim. Acta., 175 (1985) 99.

66. A.R. Hillman, D.C. Loveday, M.J. Swann, S. Bruckenstein and C.P. Wilde, J. Chem. Soc. Faraday Trans., 87 (1991) 2047.

67. T. Nomura and T. Nagamune, Anal. Chim. Acta., 155 (1983) 231.

68. T. Nomura and M. Maruyama, Anal. Chim. Acta., 147 (1983) 365.

69. T. Nomura and M. Okuhara, Anal. Chim. Acta., 142 (1982) 281.

70. T. Nomura, N. Watanabe and T.S. West, Anal. Chim. Acta., 175 (1985) 107.

71. S.Z. Yao and T.A. Zhou, Anal. Chim Acta., 212 (1988) 61.

72. Z.A. Shana, H. Zong, F. Josse and D.C. Jeutter, J. Electroanal. Chem., 379 (1994) 21.

73. S. Kurosawa, H. Kitajima, Y. Ogawa, M. Muratsugu, E. Nemoto and N. Kamo, Anal. Chim. Acta., 274 (1993) 209.

74. S. Kurosawa, E. Tawara, N. Kamo and Y. Kobatake, Anal. Chim. Acta., 230 (1990) 41.

75. H. Ghourchian and N. Kamo, Analyst, 120 (1995) 2737.

76. O. Lau, B. Shao and W. Zhang, Anal. Chim. Acta., 312 (1995) 217.

77. S. Bruckenstein, M. Michalski, A. Fensore, Z. Li and A.R. Hillman, Anal. Chem., 66 (1994) 1847.

78. G.C. Dunham, N.H. Benson, D. Petelenz and J. Janata, Anal. Chem., 67 (1995) 267.

79. R. Schumacher, Angew. Chem. Int. Ed. Engl. 29 (1990) 329.

80. R. Schumacher, G. Borges and K.K. Kanazawa, Surface Science, 163 (1985) L621.

81. R. Schumacher, J.G. Gordon and O. Melroy, J. Electroanal. Chem., 216 (1987) 127.

82. M.D. Ward and E.J. Delawski, Anal. Chem., 63 (1991) 63.

83. D.M. Ullevig, J.F. Evans and M.G. Albrecht, Anal. Chem., 54 (1982) 2341.

84. C. Gabrielli, M. Keddam and R. Torresi, J. Electrochem. Soc., 138 (1991) 2657.

85. B.A. Martin and H.E. Hager, J. Appl. Phys., 65 (1989) 2630.

86. D.Orata and D.A. Buttry, J. Am. Chem. Soc., 109 (1987) 3574.

87. R. Borjas and D.A. Buttry, J. Electroanal. Chem., 280 (1990) 73.

88. A. Glidle, A.R. Hillman and S. Bruckenstein, J. Electroanal. Chem., 318 (1991) 411.

89. S. Yamaguchi, T. Shimomura, T. Tatsuma and H. Oyama, Anal. Chem., 65 (1993) 1925.

90. A.P. Clarke, J.G. Vos, H.L. Bandey and A.R. Hillman, J. Phys. Chem., 99 (1995) 15973.

91. M. Minunni, M. Mascini, G.G. Guilbault and B. Hock, Anal. Letters, 28 (1995) 749.

92. K. Naoi, M. Lien and W.H. Smyrl, J. Electrochem. Soc., 138 (1991) 440.

93. K. Naoi, M.M. Lien and W.H. Smyrl, J. Electroanal. Chem., 272 (1989) 273.

94. C.S.C. Bose, S. Basak and K. Rajeshwar, J. Phys. Chem., 96 (1992) 9899.

95. J.Y. Lim, W. Paik and I.H. Yeo, Synthetic Metals, 69 (1995) 451.

96. S.D. Champagne, J.R. Reynolds and M. Pomerantz, Chem. Mater., 7 (1995) 277.

97. M. Pyo and J.R. Reynolds, J. Phys. Chem., 99 (1995) 8249.

98. R.M. Torresi, S.I. Cordoba de Torresi, T. Matencio and M.-A. de Paoli, Synthetic Metals, 72 (1995) 283.

99. H. Daifuku, T. Kawagoe, N. Yamamoto, T. Ohsaka and N. Oyama, J. Electroanal. Chem., 274 (1989) 313.

100. M.C. Miras, C. Barbero, R. Kotz and O. Haas, J. Electroanal. Chem., 369 (1994) 193.

101. A.R. Hillman, M.J. Swann and S. Bruckenstein, J. Phys. Chem., 95 (1991) 3271.

102. A.R. Hillman, M.J. Swann and S. Bruckenstein, J. Electroanal. Chem., 291 (1990) 147.

103. A.R. Hillman, D.C. Loveday, M.J. Swann, S. Bruckenstein and C.P. Wilde, Analyst, 117 (1992) 1251.

104. A.R. Hillman and A. Glidle, J. Electroanal. Chem., 379 (1994) 365.

105. L. Torsi, P.G. Zambonin, A.R. Hillman and D.C. Loveday, J. Chem. Soc. Faraday Trans., 89 (1993) 3941.

106. A. Dostal, B. Meyer, F. Scholz, U. Schroder, A.M. Bond, F. Marken and S.J. Shaw, J. Phys. Chem., 99 (1995) 2096.

107. B.J. Feldman and O.R. Melroy, J. Electroanal. Chem., 234 (1987) 213.

108. S.J. Lasky and D.A. Buttry, J. Am. Chem. Soc., 110 (1988) 6258.

109. J. Bacskai, K. Martinusz, E. Crirok, G. Inzelt, P.J. Kulesza and M.A. Malik, J. Electroanal. Chem., 385 (1995) 241.

110. A.R. Hillman, D.C. Loveday, S. Bruckenstein and C.P. Wilde, J. Chem. Soc. Faraday Trans., 86 (1990) 437.

111. A.R. Hillman, D.C. Loveday and S. Bruckenstein, J. Electroanal. Chem., 274 (1989) 157.

112. A.R. Hillman, N.A. Hughes and S. Bruckenstein, J. Electrochem. Soc., 139 (1992) 74.

113. P.T. Varineau and D.A. Buttry, J. Phys. Chem., 91 (1987) 1292.

114. A.R. Hillman, D.C. Loveday, A. Glidle, J.G. Vos, A.P. Clarke, D. Kelly and S. Bruckenstein, Macromol. Symp., 80 (1994) 323.

115. A.R. Hillman, D.C. Loveday and S. Bruchenstein, J. Electroanal. Chem., 300 (1991) 67.

116. A.R. Hillman, N.A. Hughes and S. Bruckenstein, Analyst, 119 (1994) 167.

117. A.R. Hillman and S. Bruckenstein, J. Chem. Faraday Trans., 89 (1993) 339.

118. A.R. Hillman and S. Bruckenstein, J. Chem. Faraday Trans., 89 (1993) 3779.

119. A.P. Clarke, J.G. Vos and A.R. Hillman, J. Electroanal. Chem., 356 (1993) 287.

120. G. Inzelt, J. Electroanal. Chem., 287 (1990) 171.

121. G. Inzelt and J. Bacskai, J. Electroanal. Chem., 308 (1991) 255.

122. G. Inzelt, Electroanalysis, 7 (1995) 895.

123. A.P. Clarke, Ph.D. Thesis, Dublin City University, (1992).

Chapter 2.

The Effect of $HClO_4$ and $LiClO_4$ Concentrations On the Rigidity and Layer Mass of $[Os(bipy)_2(PVP_x)_{10}Cl]^+$ Copolymer Films.

2.1. Introduction.

The primary apprehension about the applicability of polymer modifying layers to electroanalysis concerns their stability on the electrode surface, particularly in flowing systems. A number of procedures have been reported for improving the long-term stability of polymer coatings. Overlaying of a $[Ru(bipy)_2(PVP)_5Cl]Cl$ polymer with conducting polymers resulted in improved life times of the redox polymer with the half life increasing from 8 to 48 hours [1]. However, it was noted that the presence of the overlayer reduced the sensitivity towards substrates [1]. An alternative approach is to reduce the solubility of the electroactive polymer in the contacting electrolyte by modifying the polymer backbone [2,3,4]. It has been illustrated that the stability of $[Os(bipy)_2(PVP)_{10}Cl]Cl$ electrode coatings may be greatly enhanced by chemical crosslinking of the polymer backbone with p-dibromobenzene, 1,5-dibrompentane and 1,10-dibromodecane [2]. For an uncrosslinked film the surface coverage in a thin-layer flow cell was reduced by 50% after 48 hours. However, for the corresponding crosslinked film, over 90% of the film was still intact after 72 hours under identical experimental conditions [2].

An alternative approach to the stabilisation of these polymer layers is the incorporation of hydrophobic moieties into the PVP backbone [3,4]. The resulting $[Ru(bipy)_2(PVP_x)_{10}Cl]Cl$ polymers, where x signifies the percentage of Poly 4-vinylpyridine (PVP) in a PVP: styrene copolymer, were stable for over 14 days in a flowing system, whilst the homopolymer was slowly stripped from the electrode surface [4].

Ideally, stabilisation should not hinder the mass and charge transport processes in the electroactive polymer. It is known that the requirements for stability of redox polymers are mutually opposed to the requirements for rapid mass and charge transport [5]. Good stability is achieved with unswollen compact polymer films, while charge transport is optimum in swollen films [5]. This is further complicated by the fact that the conditions for fast electron transport and rapid

counter ion motion can be mutually opposed, so the optimum degree of polymer swelling is a compromise between electron transport and counter ion motion [2,6,7]

For the $[Ru(bipy)_2(PVP_x)_{10}Cl]Cl$ polymers, improvements in layer stability upon incorporation of styrene into the polymer backbone were clearly illustrated [4]. However, the influence of the styrene moieties on the charge transport properties of these materials was only briefly addressed [3]. Consequently, the primary focus of the work presented in this thesis is the study of the influence of the styrene content of the polymer backbone on the mass transfer and charge transport processes in the corresponding osmium redox polymers, $[Os(bipy)_2(PVP_x)_{10}Cl]Cl$. The general structure of these metallopolymers is given in Fig. 2.1. These studies were undertaken in perchlorate electrolytes, $HClO_4$ and $LiClO_4$, because it was anticipated that the crosslinking properties of the perchlorate anion would result in extremely stable electrode coatings of these materials.

It has been demonstrated previously that the rate of charge transport through $[Os(bipy)_2(PVP)_{10}Cl]^+$ electrode coatings is strongly dependent on the electrolyte type and concentration [6-11]. Furthermore, EQCM studies have shown that the quantity of solvent transferred during redox switching of this polymer is influenced by the bathing electrolyte [12-15]. These effects have been attributed to changes in the morphology of the polymer. Consequently, before probing the mass transfer and charge transport properties of the $[Os(bipy)_2(PVP_x)_{10}Cl]^+$ polymers, the resident layer mass of these materials was examined as a function of the contacting perchlorate electrolyte concentration. These layer mass studies are the focus of the work presented in this chapter.

Accurate mass changes can only be determined from the Sauerbrey equation under rigid layer conditions. It is therefore necessary to probe for deleterious swelling of the modifying layers. Analysis of the admittance characteristics of a coated quartz crystal i.e. the admittance (or conductance) response at a range of frequencies around the crystal resonance, provides a means of studying both the rigidity and resident

Fig. 2.1. Chemical structure of $[Os(bipy)_2(PVP_x)_{10}Cl]^+$ metallopolymers. The sum of m and n in this structure is 9.

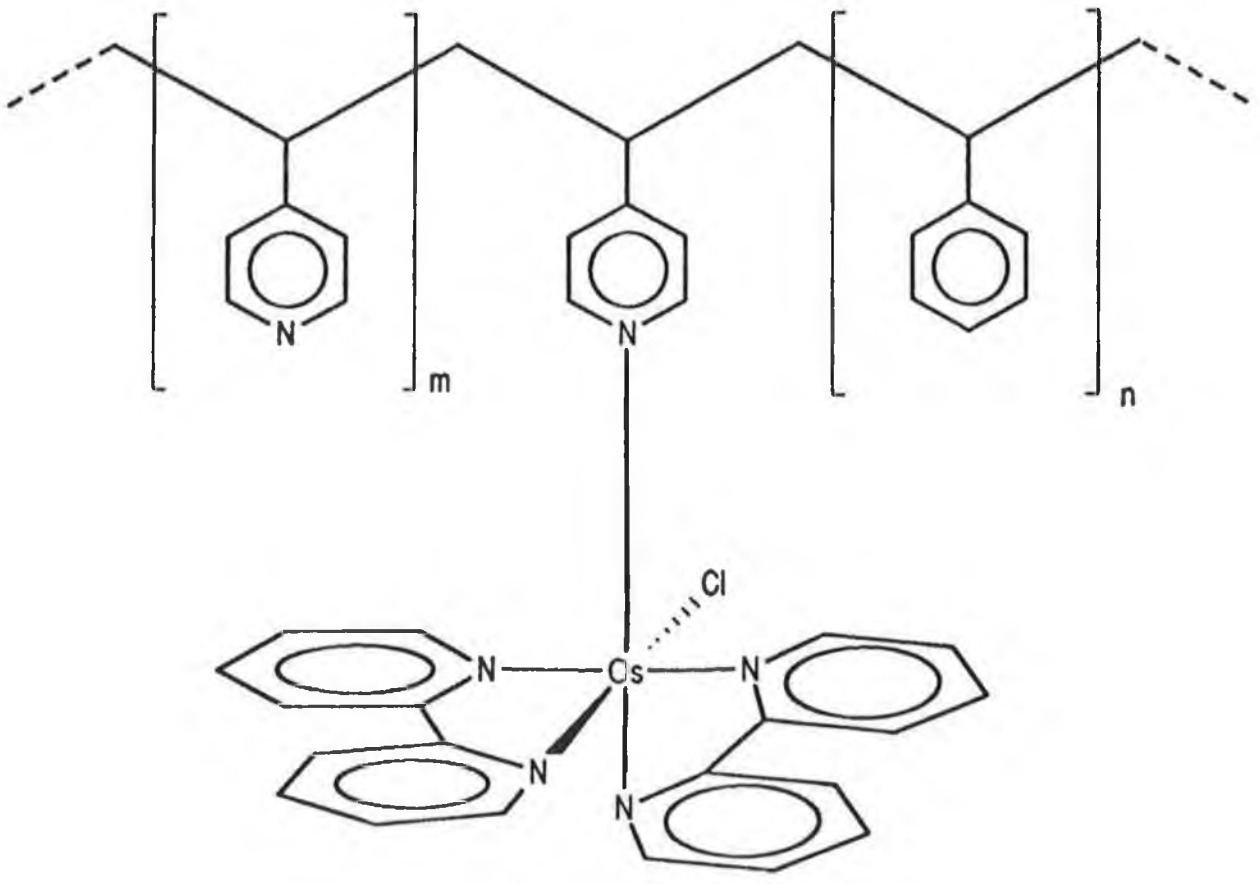

layer mass of the attached layer. Firstly, the shape of the crystal resonance may be used as a probe of layer rigidity [12,13,15-21]. A decrease in admittance and a broadening of the resonance (as characterised by the peak width at half height), is a qualitative reflection of a decrease in layer rigidity, which may be equated with morphology changes occurring within the polymer [12,13,15-21]. Secondly, the shift in resonant frequency, determined from the frequency of maximum admittance, when corrected for the viscous load of the contacting electrolyte, may be used to probe the layer mass. In this chapter the rigidity and resident layer mass of $[Os(bipy)_2(PVP_x)_{10}Cl]^+$ coated crystals are studied as a function of the styrene content of the polymer backbone and the $HClO_4$ electrolyte concentration. Characterisation of the layer mass of these coated polymers, as a function of the $HClO_4$ concentration, enables the pK_a^{app} of the PVP units to be measured [12]. These studies therefore provide a means of probing the changing chemical properties of these metallopolymers upon incorporation of styrene moieties into the polymer backbone. For comparison, similar studies are undertaken for the $OsPVP_{100}$ and $OsPVP_{33}$ polymers in $LiClO_4$ electrolytes.

2.2. Experimental.

2.2.1. Apparatus.

UV-visible spectra were recorded using a Hewlett-Packard 342A diode array spectrophotometer. Electrochemical measurements were performed using an EG and G PAR 363 potentiostat.

10 MHz AT-cut laboratory monitor crystals were used as supplied from International Crystal Manufacturing Company Inc., Oklahoma City, USA. The crystals had a 90 nm thick layer of gold sputter coated onto each side. The calibrated mass-sensitivity of the crystals was 0.232 $Hzcm^2ng^{-1}$ and the electrochemically active area was 0.23 cm^2.

Crystal admittance measurements were made using a Hewlett-Packard 8753A network analyser (used in the reflectance mode [19]). Scans were made over a 16 kHz bandwidth, with the computer software centred on the peak admittance maximum. The sweep time was 400 ms, with a sweep repetition rate of 2.9 s. Measurements were made at 801 points centred about the fundamental resonant frequency giving a frequency resolution of 20 Hz. Electrochemical experiments were carried out using an Oxford Electrodes potentiostat. A saturated potassium chloride calomel reference electrode (SCE) and a platinum mesh counter electrode were used.

2.2.2. Materials.

Polymers

4-vinylpyridine was distilled under vacuum at 45^{O} C. Poly 4-vinylpyridine (PVP) was prepared by bulk polymerisation of the freshly distilled 4-vinylpyridine under nitrogen atmosphere using 2,2'-azobisisobutyronitrile (500:1 w/w) as initiator, at 75^{0}C. The resulting polymer was purified by repeated precipitation in diethyl-ether from methanol and was dried at 60^{0}C in vacuo overnight. The molecular weight of the polymer, as determined by viscometry in absolute ethanol using the Mark-Houwink

equation, $[\eta] = 2.5 \times 10^{-4} M_v^{0.68}$, was found to be ca. 325,000 $gmol^{-1}$.

The poly 4-vinylpyridine: styrene copolymers, PVP_{75}, PVP_{67}, PVP_{50} and PVP_{33} were prepared and characterised by Dr. D. Leech [3,4]. These polymers are identified in terms of the percentage of poly 4-vinylpyridine in the copolymer backbone i.e. PVP_{33} signifies a copolymer of 33% 4-vinylpyridine and 67% styrene.

$[Os(bipy)_2(PVP_x)_{10}Cl]Cl$

The metallopolymers were prepared as described previously [22]. In a typical syntheses of $[Os(bipy)_2(PVP_{100})_{10}Cl]Cl$, 40 mg of $[Os(bipy)_2Cl_2]$ were dissolved in 30 cm^3 of ethanol and refluxed for 30 min. A total of 73 mg of PVP in 10 cm^3 of ethanol were then added and refluxing continued for ca. 72 h. The reaction was continually monitored using uv-visable spectrophotometry and cyclic voltammetry. The metallopolymer was isolated by precipitation into diethyl ether and purified by repeated precipitation (2x) in diethyl ether from ethanol. Cyclic voltammetry confirmed the presence of a single redox centre.

Metallopolymers of the copolymers were prepared in a similar manner. Reaction times typically increased with increasing styrene content and varied from 3-11 days. A constant 1 in 10 metal to polymer-unit loading was prepared in each case. These metallopolymers are identified as $OsPVP_{100}$, $OsPVP_{75}$, $OsPVP_{67}$, $OsPVP_{50}$ and $OsPVP_{33}$, in order of increasing styrene content of the polymer backbone. The general structure of these metallopolymers is illustrated in Fig. 2.1.

2.2.3. Procedures.

Polymer films were drop coated from 0.25% (w/v) ethanolic solutions of the polymer and were allowed to dry in air for 24 hours. Uneven films were discarded and the quartz crystals were soaked in methanol overnight to remove the dried polymer. Polymer coatings on crystals that have been cleaned in this manner, exhibited the same qualitative and quantitative trends as coatings on previously

unused crystals. Coated crystals were attached to the base of electrochemical cells using a non-corrosive rubber sealant (RTV1000 Dow Corning) and were allowed to cure for ca 8 hours. Care was taken to ensure that the polymer film was not exposed to this sealant. Gravimetric surface coverages (Γ_g) were estimated from the shift in resonant frequency of the quartz crystals upon deposition of the polymer layers.

The equilibrium solvent and ion populations within $OsPVP_{100}$, $OsPVP_{75}$, $OsPVP_{67}$ and $OsPVP_{33}$ crystal coatings were measured at open circuit (Os^{II} oxidation state) as a function of the electrolyte concentration. In a typical experiment, a polymer coated crystal was first exposed to H_2O and the level of solvent imbibition was determined from the shift in resonant frequency. The rigidity and layer mass of the crystal coating was then probed as a function of increasing $HClO_4$ electrolyte concentration. Equilibration times of up to 3 hours were required for a stable frequency reading to be obtained. This experiment was then repeated with decreasing $HClO_4$ electrolyte concentration. The layer was voltammetrically cycled for 3 hours at each electrolyte concentration, prior to the recording of the open circuit admittance spectrum (Os^{II} oxidation state).

The cell and crystal were washed with Milli-Q water between each $HClO_4$ electrolyte concentration. All experiments were carried out at 20 ($\pm$ 2)^{0}C. The duration of the experiments was such that temperature fluctuations were negligible. A constant volume of solution was used for all experiments so that the height of liquid above the crystal was kept approximately constant. All solutions were purged with argon to remove oxygen, while the Ar stream was directed over the solution during data acquisition to maintain quiescent solution conditions.

For comparison, the equilibrium solvent and ion populations within $OsPVP_{100}$ and $OsPVP_{33}$ crystal coatings were investigated as a function of the $LiClO_4$ concentration of the bathing electrolyte.

The conditions used in these experiments are discussed in greater detail in the following sections.

2.3. Results and Discussion.

2.3.1. Solvent Imbibition.

The driving force for solvent uptake is the tendency for the polymer segments and contacting solvent to inter-diffuse [23]. Furthermore, the tendency for the fixed and mobile ions to form solvation shells will lead to additional solvent uptake [23]. This tendency of the polar and ionic constituents of the matrix to surround themselves with solvent is accompanied by expansion of the elastic polymer matrix. Swelling equilibrium is attained when the swelling tension imposed on the polymer segments, by the overall structural framework, balances the driving forces for solvent uptake [23].

The uptake of solvent by the $OsPVP_{100}$ - $OsPVP_{33}$ series of metallopolymers was studied. On immersion of these polymer coated crystals in de-oxygenated Milli-Q water, the resonant frequency of the coated crystal decreased slowly with time, reflecting the slow imbibition of solvent. Frequency readings were taken when the resonant frequency varied by less than 0.5 Hz per minute. Beyond this equilibration point the resonant frequency varied very little with time. Equilibration times for solvent uptake increased with styrene content of the polymer backbone and typically varied from ca. 1 hour for the $OsPVP_{100}$ polymer to ca. 3 hours for the highest styrene content polymer ($OsPVP_{33}$). It is suggested that this slower uptake of solvent is a consequence of the greater difficulty in attaining equilibrium levels of solvent in the more hydrophobic styrene based copolymers. For each polymer studied, the shift in resonant frequency on immersion was corrected for the viscous load of the solvent by subtraction of the frequency shift observed on immersion of an uncoated crystal in this solvent. The level of solvent uptake is expressed in terms of the number of absorbed water molecules per $[Os(bipy)_2(PVP_x)_{10}Cl]Cl$ polymer unit. These results were determined for at least two different coatings for each polymer and are presented in Table 2.1.

Table 2.1. Solvent uptake by the $OsPVP_{100}$ - $OsPVP_{33}$ series of metallopolymers, on immersion in H_2O.

Polymer	Solvent content [a,b] (mol polymer equiv.$^{-1}$)
$OsPVP_{100}$	42 (5)
$OsPVP_{75}$	9 (1)
$OsPVP_{67}$	3 (1)
$OsPVP_{33}$	0.7 (0.1)

(a) Estimated from the shift in resonant frequency (corrected for solution viscosity).

(b) Errors quoted in brackets represent the variations between 2 different films.

A central assumption of these calculations is that the shift in resonant frequency, on immersion of an uncoated crystal in solvent, may be used to compensate for the corresponding shift in frequency of a coated crystal in the same solvent. The greater surface roughness of the polymer layer will likely result in greater trapping of solvent in pores at the polymer/ solvent interface compared with the uncoated crystal/ solution interface [24-26]. Compensation for the frequency shift due to the viscous load of the solvent using an uncoated crystal may therefore be incomplete. Consequently, the level of solvent uptake is possibly less than that quoted in Table 2.1. These values may therefore be viewed as the upper limit for solvent imbibition into these polymer layers.

Fig. 2.2 illustrates the admittance spectra obtained for each metallopolymer on immersion in water. The x-axis for these plots have been adjusted for presentation purposes and the apparent "shift" in resonant frequency is a result of this presentation. In Fig. 2.2, the shape of the crystal resonance, as characterised by the admittance maximum and the peak width at half maximum admittance, is sharper for the higher styrene content polymers. This behaviour signifies that, in water, the contributions of the viscoelastic properties of the polymers to the resonant frequency are less for the higher styrene content copolymers and that these polymers are more compact and rigid than the higher PVP content polymers. However, it is important to note that, despite the greater swelling of the $OsPVP_{100}$ polymer, this polymer is still rigid in H_2O [12].

The uptake of 44±5 molecules of water per $[Os(bipy)_2(PVP_{100})_{10}Cl]^+$ polymer unit on immersion in H_2O has been previously reported for the $OsPVP_{100}$ polymer [12]. A similar solvent level of 42±4 molecules of water per polymer unit was observed for this polymer during the experiments reported here.

From Table 2.1, it is apparent that the level of solvent imbibition is greatly reduced for the styrene copolymers and decreases quite dramatically with increasing styrene content. For the $OsPVP_{33}$ polymer, the uptake of 0.7±0.1 molecules of water per polymer unit is nearly 60 times less than that observed for the $OsPVP_{100}$ polymer [12]. This point is reflected in Fig. 2.2 which illustrates that the shape of the crystal resonance becomes broader and, therefore, the degree of swelling of the polymer layers increases, with increasing PVP content. For the $OsPVP_{33}$ polymer, it would appear that the lower level of solvent ingress, compared with the higher PVP content polymers, results in a comparatively more compact polymer structure.

For all polymers studied, the chloride salt form of the polymer was used. All other parameters such as metal loading, surface coverage etc. were similar in each case. It is, therefore, anticipated that the trends observed reflect the changing nature/ properties of the polymer backbone on incorporation of the styrene moieties. The

Fig. 2.2. Admittance spectra for the $OsPVP_{100}$ - $OsPVP_{33}$ series of metallopolymers, on immersion in H_2O. The frequency axis has been offset for presentation purposes (see text).

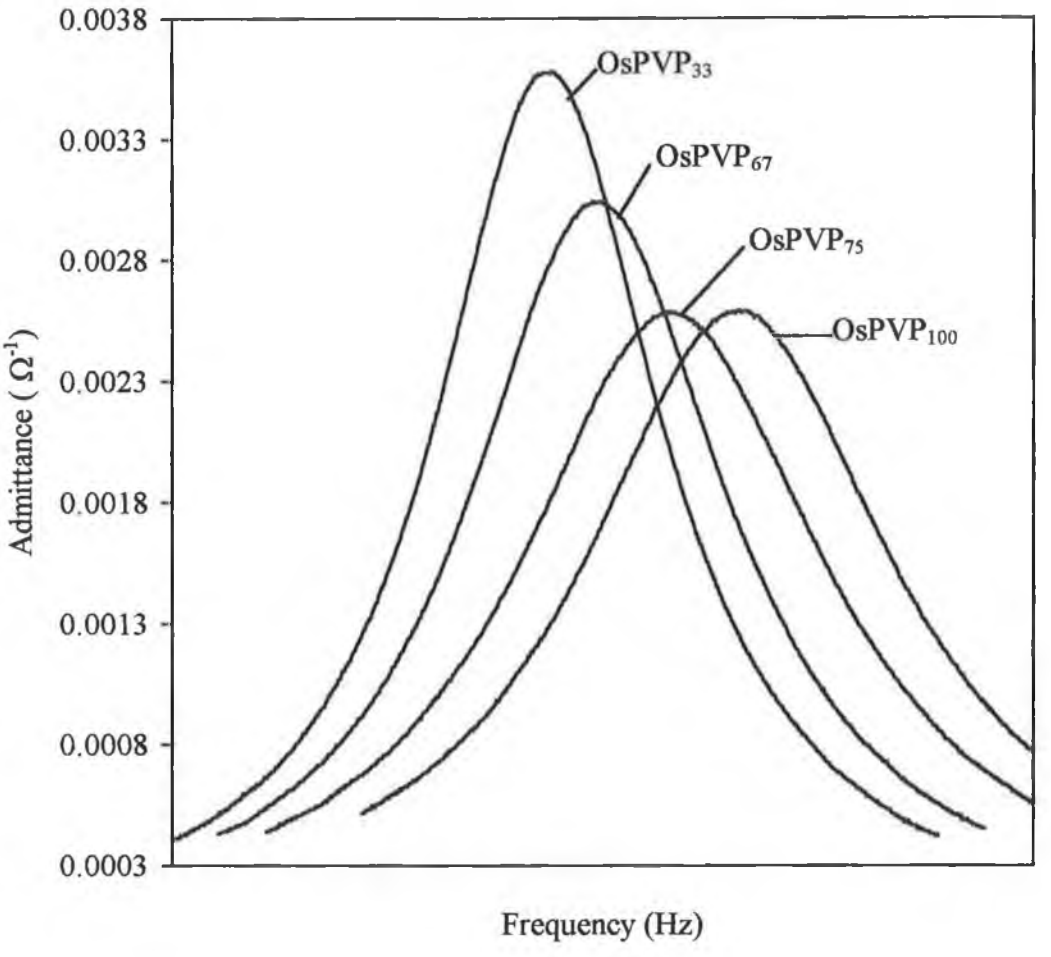

decrease in the level of polymer solvation and the greater layer rigidity of the polymer matrix with increasing styrene content likely reflects the more hydrophobic nature of the styrene moiety compared with the PVP moiety. This behaviour emphasises the importance of the physico-chemical properties of the polymer backbone on the overall layer properties of these metallopolymer compounds. This more compact and rigid nature of the styrene based copolymers will, as anticipated, result in greater adhesion of these layers to the underlying electrode.

2.3.2. Effect of $HClO_4$ Concentration on Layer Rigidity.

Admittance spectra were recorded for $OsPVP_{75}$, $OsPVP_{67}$ and $OsPVP_{33}$ crystal coatings in a series of $HClO_4$ electrolyte concentrations to investigate the $HClO_4$ concentration dependence of the rigidity and resident layer mass of these materials. Prior to these admittance studies, the polymer layers were voltammetrically cycled over the $Os^{II/III}$ redox couple in 0.1M $HClO_4$ to exchange the polymer counterions, yielding the complex $[Os(bipy)_2(PVP_x)_{10}Cl]ClO_4$. Upon immersion and voltammetric cycling in 0.1M $HClO_4$, from H_2O, a mass change of 71±6 g polymer equiv.$^{-1}$, corresponding to this exchange process, was noted in each case. This value was corrected for the mass influx associated with protonation of the layer at this electrolyte concentration (see below) and is in addition to the initially imbibed solvent.

The reported hydration numbers for chloride and perchlorate ions in aqueous solution are 3.9 and 2.6 respectively [12,27]. If it is assumed that solvated Cl^- and ClO_4^- ions are exchanged, then a mass change of 41 g pol equiv.$^{-1}$ is anticipated. However, if it is assumed that unsolvated ions are exchanged, then a mass change of 64 g pol equiv.$^{-1}$ is anticipated. The observed mass change therefore suggests that all the polymer counterions are exchanged and that this exchange process occurs between unhydrated counterions. However, the lack of detailed information regarding the hydration of ionic species in polymer networks precludes a more detailed discussion of these points.

The polymers films were subsequently stored in Milli-Q water prior to use. For the admittance studies, the admittance spectra of the modified crystals were recorded in a series of $HClO_4$ electrolyte concentrations, as the concentration was increased from water to 1.0M $HClO_4$. The cell was cleaned with Milli-Q water between each electrolyte concentration. No voltammetry was performed at this stage of the experiment and equilibration times varied from 2 to 3 hours, depending on the particular polymer under investigation. The higher content styrene copolymers i.e.

$OsPVP_{67}$ and $OsPVP_{33}$ typically required longer periods of equilibration. Similar behaviour was observed during the solvent imbibition experiments (see Section 2.3.1) and highlights the difficulty in attaining equilibrium solvent and ion populations within these hydrophobic polymers. Admittance spectra were also recorded as a function of decreasing electrolyte concentration. In these experiments the polymer layers were voltammetrically scanned at each concentration for two hours; intermittently changing from 1 to 50 mVs^{-1} scan rates, prior to the recording of the open circuit admittance spectra. All spectra were recorded for the polymers in the Os^{II} oxidation state.

As mass changes occurring within these polymers can only be quantitatively evaluated when layer rigidity has been established, the change in polymer morphology with changing electrolyte concentration is considered first. This is followed by a more quantitative interpretation of the mass changes which occur within the polymer layers.

2.3.2.1. $OsPVP_{75}$.

Fig. 2.3 illustrates the change in the admittance response (crystal resonance) of an $OsPVP_{75}$ coated crystal, as the electrolyte concentration is increased from pure solvent to 1.0M $HClO_4$. The gravimetric surface coverage was 1.09×10^{-8} $molcm^{-2}$. No voltammetry was performed at this stage of the experiment and all spectra were recorded at open circuit (Os^{II} oxidation state). Column A of Table 2.2 summarises the characteristic features of the admittance spectra i.e. admittance maximum, peak width at half maximum admittance and the shift in resonant frequency. The shift in resonant frequency has been corrected for the viscous load of the bathing electrolyte. Fig. 2.4 illustrates the corresponding set of admittance spectra obtained with the same layer, as the electrolyte concentration was decreased. The layer was voltammetrically cycled at each concentration prior to the recording of the open circuit crystal resonance. Column B of Table 2.2 summarises the characteristic features of these

Figs. 2.3. and 2.4. Admittance spectra for an $OsPVP_{75}$ coated crystal in $HClO_4$. Gravimetric surface coverage is 1.09×10^{-8} molcm^{-2}.

Fig. 2.3. Increasing electrolyte concentration, no voltammetry.

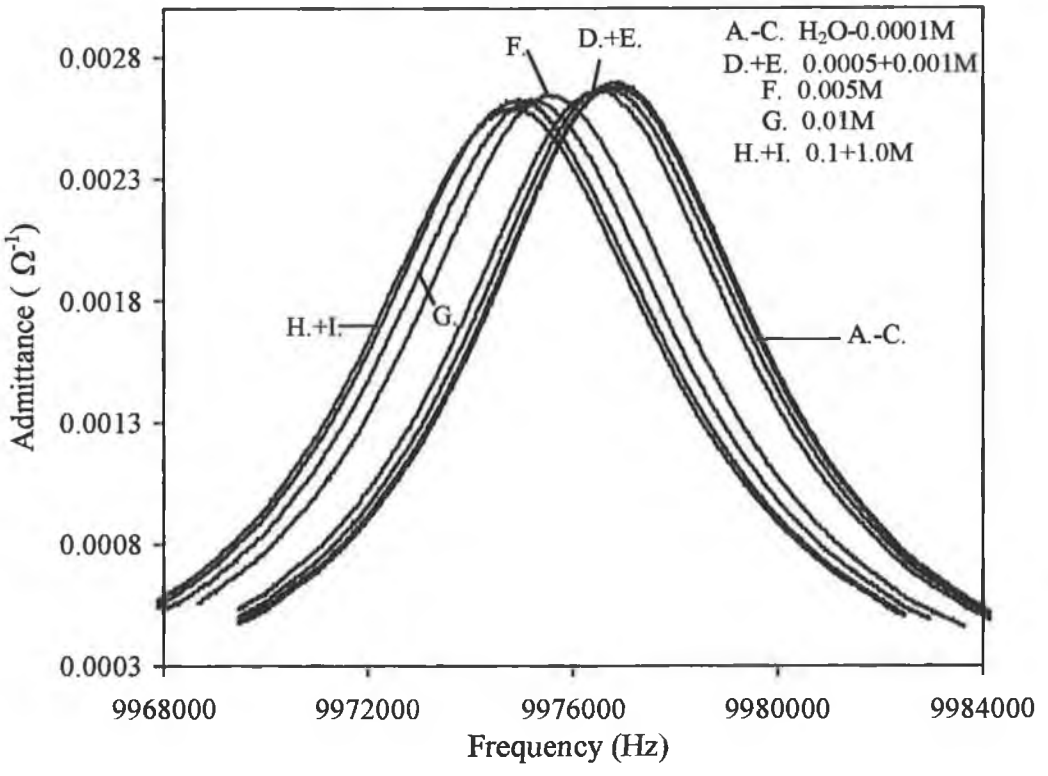

Fig. 2.4. Decreasing electrolyte concentration, with voltammetry.

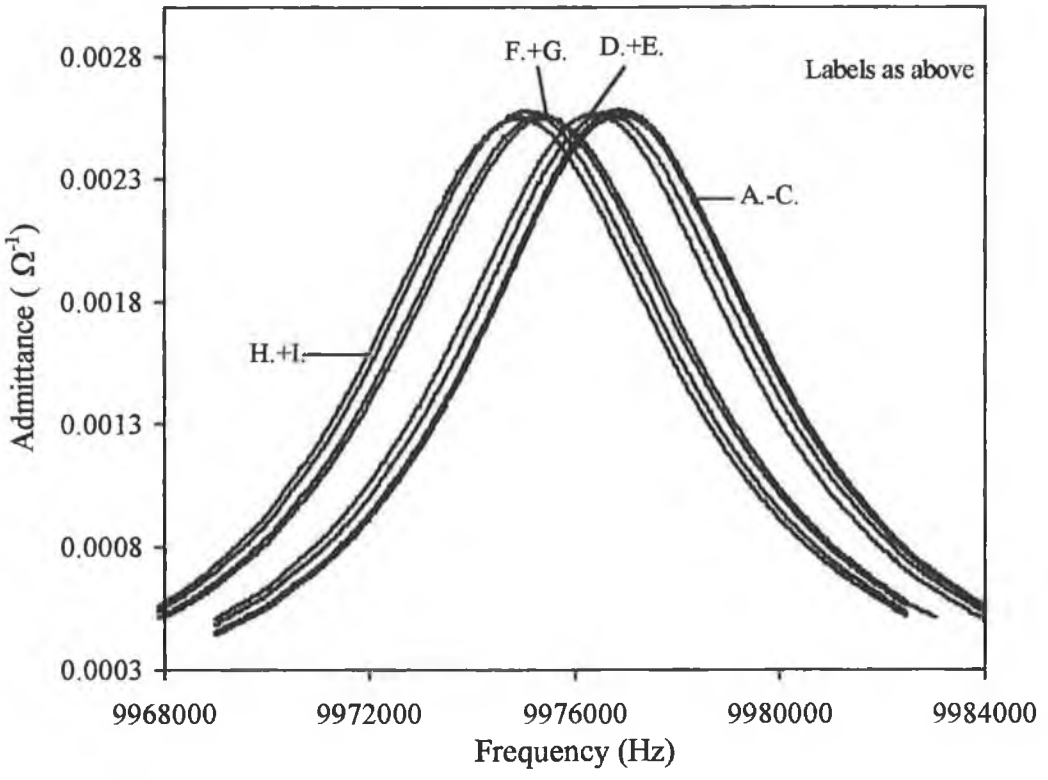

Table 2.2. Admittance data obtained at open circuit for an $OsPVP_{75}$ coated crystal in $HClO_4$. Gravimetric surface coverage is 1.09×10^{-8} molcm^{-2}.

$HClO_4$ Conc. (M)	Admittance[a] ($\Omega^{-1} \times 10^{-2}$)		PWHM[a] (Hz)		Δf[a,b] (Hz)	
	A.	B.	A.	B.	A.	B.
H_2O	0.271	0.259	6947	7303	0	-49
1×10^{-5}	0.270	0.256	6975	7396	-38	-38
1×10^{-4}	0.268	0.258	7050	7312	-94	-86
5×10^{-4}	0.267	0.258	7069	7398	-225	-292
1×10^{-3}	0.267	0.257	7097	7398	-338	-537
5×10^{-3}	0.264	0.256	7238	7500	-1219	-1358
0.01	0.262	0.256	7312	7500	-1560	-1419
0.1	0.263	0.258	7294	7444	-1692	-1617
1.0	0.259	0.256	7350	7529	-1702	-1721

(a) Data resolution is 20Hz.

(b) Estimated from the shift in resonant frequency and corrected for the viscous load of electrolyte.

Column A is data obtained with increasing concentration, no voltammetry.

Column B is data obtained with decreasing concentration, following electrochemical cycling at each concentration.

spectra.

In Fig. 2.3, there is a decrease in the frequency of maximum admittance, corresponding to a decrease in the resonant frequency of the coated crystal with increasing electrolyte concentration. This shift in resonant frequency is indicative of an increase in the layer mass of the polymer, which is in addition to the initial imbibed solvent and is considered to be associated with the protonation of the PVP units of the polymer backbone and the subsequent influx of perchlorate counter-anions to maintain electroneutrality.

As the concentration of the bathing solution is increased, the shape of crystal resonance remains essentially constant up to, and including, 0.001M $HClO_4$. This behaviour suggests that the rigidity of this layer is unchanged within this concentration range. The increase in layer mass at these concentrations is, therefore, not accompanied by swelling of the polymer matrix. This behaviour is likely a consequence of the crosslinking properties of the perchlorate anion [28-30]. Within the concentration range of 0.005M to 0.1M $HClO_4$, slight broadening of the crystal resonance is observed, which is not associated with the viscous load of the bathing electrolyte and therefore indicates swelling of the polymer matrix. Similar behaviour has been previously observed for the $OsPVP_{100}$ polymer in 0.01M $HClO_4$ and suggests that the substantial mass influx observed in these $HClO_4$ concentrations is not accompanied by extensive crosslinking of the polymer layer.

Broadening of the crystal resonance in 1.0M $HClO_4$ is associated with the viscous properties of this electrolyte and does not indicate swelling of the polymer layer. Therefore, as the concentration of the bathing electrolyte is increased above 0.1M $HClO_4$, a return to rigid layer behaviour is observed. This behaviour is likely a result of the extensive crosslinking of the polymer backbone which occurs as the degree of polymer protonation increases.

Fig. 2.4 illustrates the change in crystal resonance with decreasing electrolyte concentration, following electrochemical cycling at each concentration. The

admittance spectra do not retrace those obtained with increasing electrolyte concentration. At all concentrations, the crystal resonance shape broadens slightly following electrochemical cycling of the layer, which suggests that there is a slight loss in rigidity of the attached layer. However, excluding 0.001M and 0.005M $HClO_4$ concentrations, this polymer expansion is not accompanied by an increase in layer mass, as one might anticipate. In fact, the mass changes observed are almost identical to those observed with increasing electrolyte concentration. It is therefore apparent that equilibrium solvent and ion populations are achieved in this polymer in the absence of voltammetric experiments. This behaviour is clearly highlighted in Fig. 2.5, which illustrates the shift in resonant frequency of this coated crystal as a function of the bathing $HClO_4$ electrolyte concentration.

Overall, there are changes in the morphology of this metallopolymer with changes in the $HClO_4$ concentration. However, these changes are extremely small and correspond to less than a 4% change in the PWHM of the admittance spectra over the complete $HClO_4$ concentration range.

2.3.2.2. $OsPVP_{67}$.

Fig. 2.6 illustrates the change in crystal resonance of an $OsPVP_{67}$ coated crystal as the electrolyte concentration is increased from pure solvent to 1.0M $HClO_4$. No voltammetry was performed at this stage of the experiment and all spectra were recorded at open circuit (Os^{II} oxidation state). The gravimetric surface coverage was 1.07×10^{-8} $molcm^{-2}$. The characteristic features of these spectra are summarised in Column A of Table 2.3. Fig. 2.7 illustrates the corresponding admittance spectra obtained as a function of decreasing $HClO_4$ electrolyte concentration, following voltammetry at each concentration. The characteristic features of these spectra are summarised in Column B of Table 2.3.

The behaviour of this polymer, under these experimental conditions, is similar to that observed for the $OsPVP_{75}$ polymer. In Fig. 2.6, there is a decrease in

Fig. 2.5. Solvent corrected shift in the resonant frequency of coated crystals as a function of A) decreasing electrolyte pH and B) increasing electrolyte pH.

1.09×10^{-8} molcm^{-2} $OsPVP_{75}$

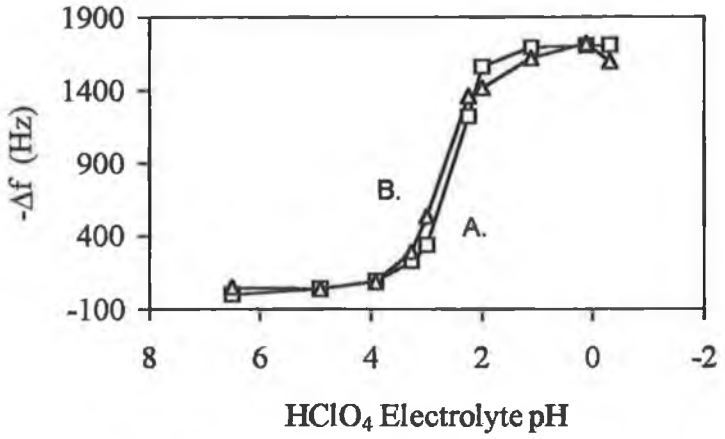

1.07×10^{-8} molcm^{-2} $OsPVP_{67}$

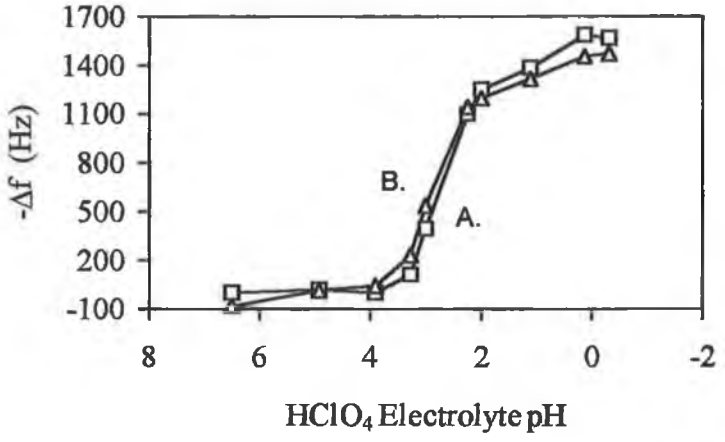

1.34×10^{-8} molcm^{-2} $OsPVP_{33}$

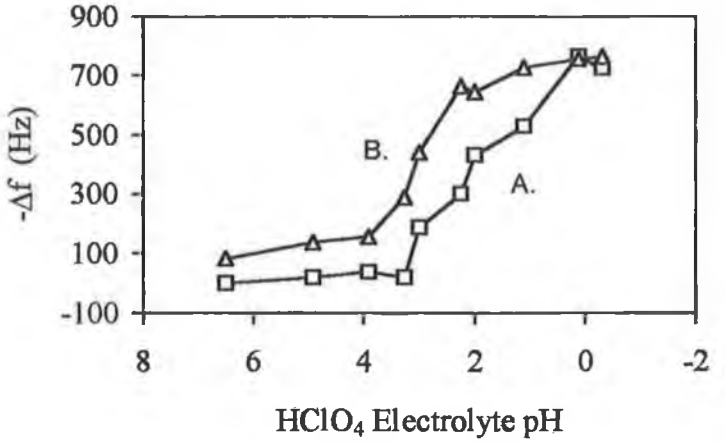

Figs. 2.6. and 2.7. Admittance spectra for an $OsPVP_{67}$ coated crystal in $HClO_4$. Gravimetric surface coverage is 1.07×10^{-8} molcm^{-2}.

Fig. 2.6. Increasing electrolyte concentration, no voltammetry.

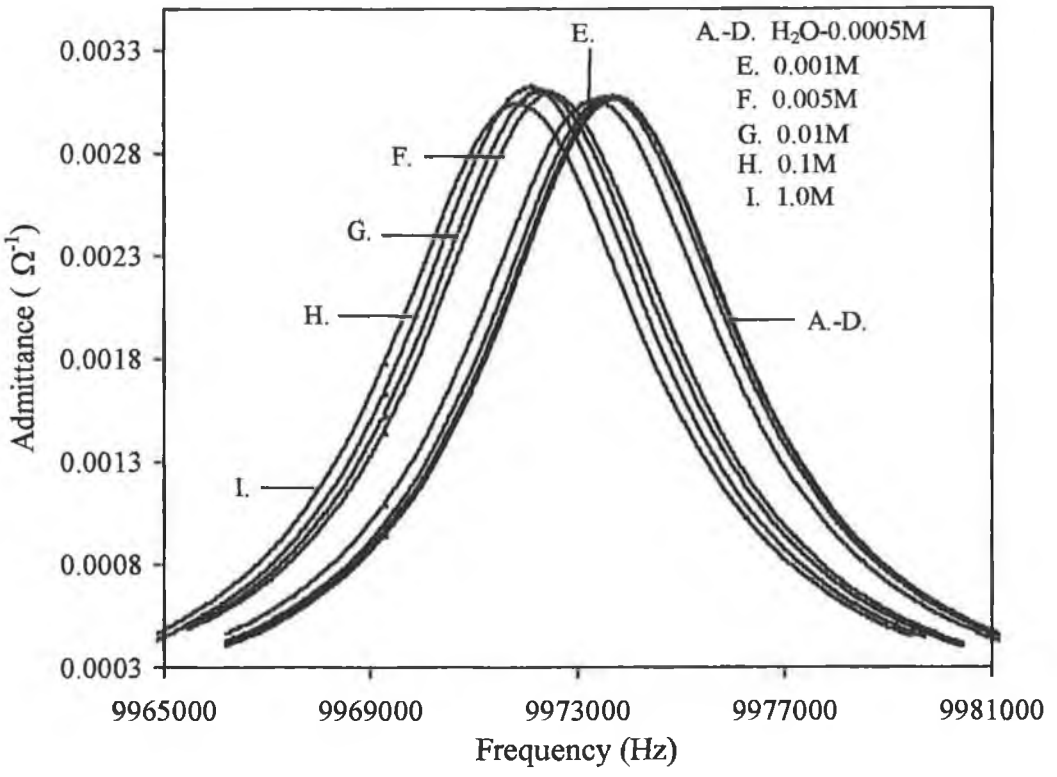

Fig. 2.7. Decreasing electrolyte concentration, with voltammetry.

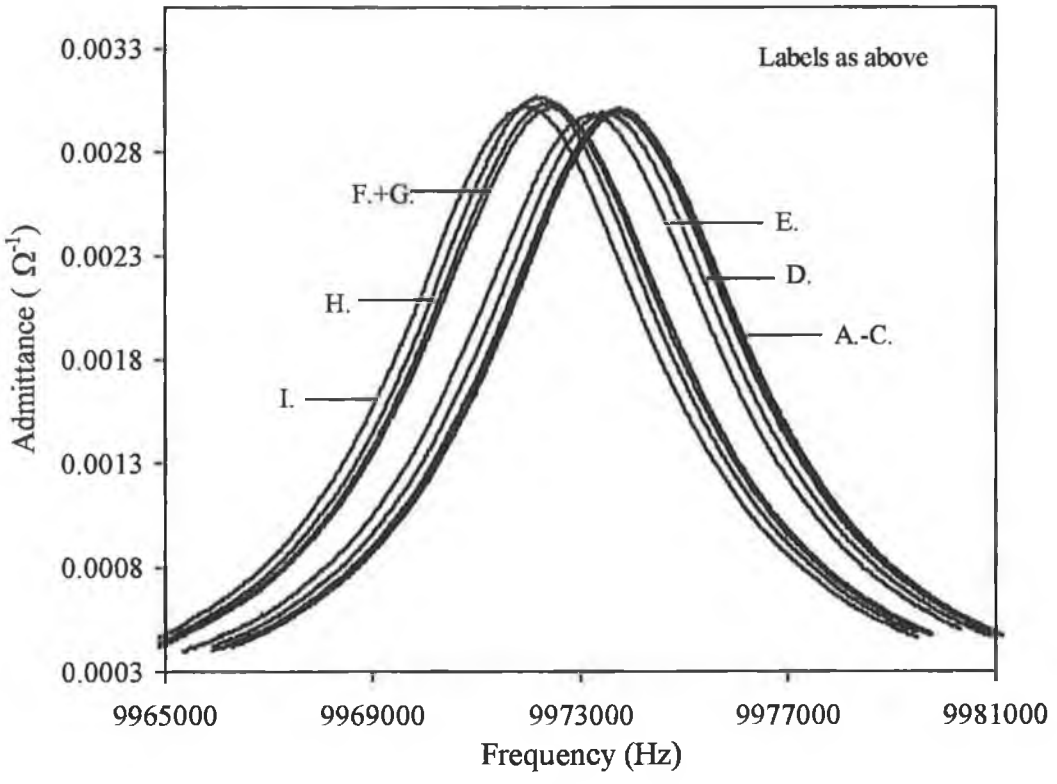

Table 2.3. Admittance data obtained at open circuit for an $OsPVP_{67}$ coated crystal in $HClO_4$. Gravimetric surface coverage is 1.07×10^{-8} molcm^{-2}.

$HClO_4$ Conc. (M)	Admittance[(a)] ($\Omega^{-1} \times 10^{-2}$)		PWHM[(a)] (Hz)		Δf[(a,b)] (Hz)	
	A.	B.	A.	B.	A.	B.
H_2O	0.307	0.300	6056	6215	0	+83
1×10^{-5}	0.307	0.301	6084	6187	-19	-11
1×10^{-4}	0.308	0.299	6046	6233	0	-41
5×10^{-4}	0.308	0.299	6102	6234	-112	-228
1×10^{-3}	0.306	0.298	6169	6253	-394	-536
5×10^{-3}	0.310	0.302	6093	6243	-1099	-1140
0.01	0.311	0.304	6093	6188	-1248	-1196
0.1	0.312	0.307	6019	6131	-1384	-1316
1.0	0.304	0.302	6196	6206	-1586	-1452

(a) Data resolution is 20 Hz.

(b) Estimated from the shift in resonant frequency and corrected for the viscous load of electrolyte.

Column A is data obtained with increasing concentration, no voltammetry.

Column B is data obtained with decreasing concentration, following electrochemical cycling at each concentration.

the resonant frequency of this $OsPVP_{67}$ coated crystal corresponding to an increase in the resident layer mass. Furthermore, in Fig. 2.6, with the possible exception of 0.001M $HClO_4$, the crystal resonance shape becomes slightly sharper as the bathing solution concentration is increased. This behaviour clearly illustrates that, as the layer mass increases, layer rigidity is maintained at each electrolyte concentration. This increase in layer mass, accompanied by a constant resonance shape, is likely a consequence of the crosslinking properties of the perchlorate anion [28-30]. In 1.0M $HClO_4$, the apparent broadening of the crystal resonance shape reflects the highly viscous nature of this electrolyte and therefore does not indicate swelling of the polymer layer.

Comparison with the corresponding data obtained for the $OsPVP_{75}$ coated crystal (see Section 2.3.2.1) illustrates that the crystal resonance shape of the $OsPVP_{67}$ coated crystal is sharper in all electrolyte concentrations. It is anticipated that the $OsPVP_{75}$ polymer is crosslinked to a greater extent than the $OsPVP_{67}$ polymer, as the number of protonated pyridine units in the backbone is greater. However, despite this expectation of a lower degree of crosslinking, the higher styrene content $OsPVP_{67}$ polymer exhibits greater layer rigidity over the complete $HClO_4$ concentration range. This behaviour is likely a consequence of the reduced requirement for anion influx within this lower PVP content polymer and may also reflect the more hydrophobic nature of this higher styrene content polymer.

Fig. 2.7 illustrates the change in crystal resonance of the same $OsPVP_{67}$ layer as the electrolyte concentration is decreased. The layer was voltammetrically cycled at each electrolyte concentration prior to the recording of the open circuit admittance response. As was observed for the $OsPVP_{75}$ polymer, these admittance spectra do not retrace those obtained with increasing electrolyte concentration. There is slight broadening of the crystal resonance in all $HClO_4$ concentrations, which is more apparent in lower $HClO_4$ concentrations, and may indicate slight expansion of the polymer matrix. However, excluding 0.005M and 0.001M $HClO_4$, this expansion of

the polymer is not accompanied by an increase in layer mass. Consequently, as was observed for the $OsPVP_{75}$ polymer, equilibrium solvent and ion populations are achieved in the $OsPVP_{67}$ polymer in the absence of voltammetric experiments. This behaviour is clearly highlighted in Fig. 2.5. Overall, the changes in layer morphology that occur as a function of the bathing $HClO_4$ electrolyte concentration are extremely small and constitute less than 4% change in the PWHM.

2.3.2.3. $OsPVP_{33}$.

Fig. 2.8 illustrates the change in crystal resonance of an $OsPVP_{33}$ coated crystal, obtained at open circuit (Os^{II} oxidation state), as the electrolyte concentration is increased from pure solvent to 1.0M $HClO_4$. The gravimetric surface coverage was 1.34×10^{-8} molcm^{-2}. No voltammetry was performed at this stage of the experiment. Column A of Table 2.4 summarises the characteristic features of these admittance spectra. Fig. 2.9 illustrates the corresponding set of admittance spectra, obtained with the same layer, as the electrolyte concentration was decreased. The layer was voltammetrically scanned at each concentration prior to the recording of the open circuit crystal resonance.

The shift in resonant frequency, on increasing the $HClO_4$ electrolyte concentration, is summarised in Column A of Table 2.4. The data have again been corrected for the solution viscous load and reflect the increase in layer mass associated with the protonation process. The relative shifts in resonant frequency are smaller than those observed for the $OsPVP_{75}$ and $OsPVP_{67}$ polymers. This reflects the lower number of protonable pyridine units and the lower requirement for compensating counterions. This point is discussed in greater detail in Section 2.3.3. In Fig. 2.8, with increasing concentration, the crystal resonance behaviour for this polymer is quite similar to that observed for the $OsPVP_{67}$ polymer. At all concentrations, with the possible exception of 0.0005M and 0.001M $HClO_4$, the crystal resonance shape becomes slightly sharper. Therefore, the increase in layer

Figs. 2.8. and 2.9. Admittance spectra for an $OsPVP_{33}$ coated crystal in $HClO_4$. Gravimetric surface coverage is 1.34×10^{-8} molcm^{-2}.

Fig. 2.8. Increasing electrolyte concentration, no voltammetry.

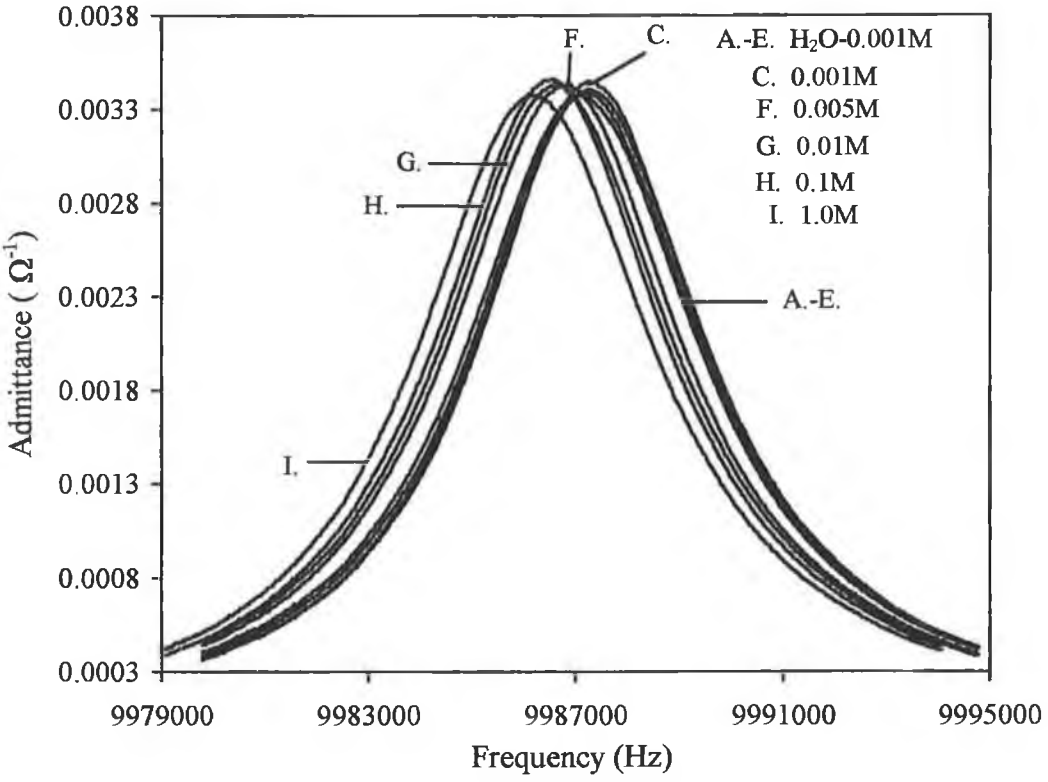

Fig. 2.9. Decreasing electrolyte concentration, with voltammetry.

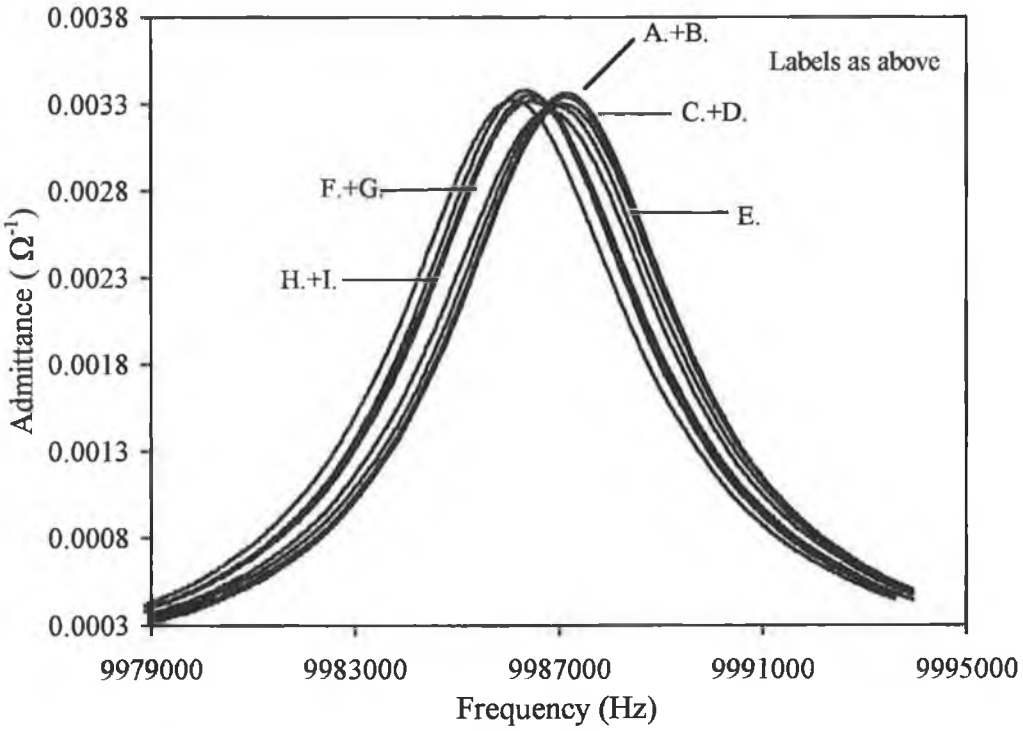

Table 2.4. Admittance data obtained at open circuit for an $OsPVP_{33}$ coated crystal in $HClO_4$. Gravimetric surface coverage is 1.34×10^{-8} molcm^{-2}.

$HClO_4$ Conc. (M)	Admittance[(a)] ($\Omega^{-1} \times 10^{-2}$)		PWHM[(a)] (Hz)		Δf[(a,b)] (Hz)	
	A.	B.	A.	B.	A.	B.
H_2O	0.342	0.337	5391	5504	0	-82
1×10^{-5}	0.341	0.335	5446	5541	-19	-138
1×10^{-4}	0.345	0.330	5372	5606	-38	-157
5×10^{-4}	0.339	0.330	5456	5578	-19	-288
1×10^{-3}	0.338	0.326	5542	5681	-187	-439
5×10^{-3}	0.343	0.333	5512	5652	-300	-664
0.01	0.343	0.335	5502	5365	-431	-644
0.1	0.346	0.338	5457	5587	-529	-727
1.0	0.338	0.333	5606	5700	-764	-756

(a) Data resolution is 20 Hz.

(b) Estimated from the shift in resonant frequency and corrected for the viscous load of electrolyte.

Column A is data obtained with increasing concentration, no voltammetry.

Column B is data obtained with decreasing concentration, following electrochemical cycling at each concentration.

mass associated with the protonation process does not result in a loss in layer rigidity.

The "apparent" broadening of the crystal resonance in 1.0M $HClO_4$ again reflects the viscous load of the electrolyte and does not indicate swelling of the polymer layer. The slight broadening of the resonance in 0.0005M and 0.001M $HClO_4$ concentrations is not related to the viscous load of the solution and may therefore indicate partial swelling of the polymer layer.

Comparison with the corresponding data obtained for the $OsPVP_{75}$ and $OsPVP_{67}$ coated crystals illustrates that the crystal resonance shape of the $OsPVP_{33}$ coated crystal is sharper in all electrolyte concentrations. Consequently, as anticipated, this $OsPVP_{33}$ is more compact than the other polymers. This behaviour is likely a consequence of the reduced requirement for anion influx into this lower PVP content polymer and the more hydrophobic nature of this higher styrene content polymer.

Fig. 2.9 illustrates the change in crystal resonance for this $OsPVP_{33}$ layer as the electrolyte concentration is decreased. The layer was voltammetrically cycled at each concentration. Excluding 0.01M $HClO_4$, there is a slight broadening of the resonance at all concentrations which suggests that there is slight swelling of the layer following electrochemical cycling. This behaviour is accompanied by a decrease in the resonant frequency and, by implication, an increase in resident layer mass. This behaviour is summarised in Table 2.4 and illustrated in Fig. 2.5. The increase in layer mass upon voltammetric cycling reflects the difficulty in attaining equilibrium levels of solvent and ions within this compact layer, which is only facilitated by the extensive counterion and solvent transfer that occurs during electrochemical cycling. This behaviour is referred to as a "break-in" effect and has been observed many times previously [31-34]. It is analogous to the variation between the first and subsequent electrochemical responses which is frequently observed for electroactive polymers [31-34]. This "break-in" effect was not observed for the $OsPVP_{75}$ and $OsPVP_{67}$ polymers and thus illustrates the greater difficulty in attaining equilibrium solvent

levels within the more compact and hydrophobic $OsPVP_{33}$ polymer. This point is further supported by the fact that equilibration times, on initial exposure to these electrolyte concentrations, were greater for the higher styrene content polymers.

Overall, as was observed for the $OsPVP_{75}$ and $OsPVP_{67}$ polymer coatings, there are changes in the morphology of $OsPVP_{33}$ crystal coatings in $HClO_4$ electrolytes. However, these swelling phenomena are extremely small and constitute only a 4% change in the PWHM. Whilst the absolute change in PWHM that a polymer must undergo before the rigid layer approximation is compromised, is unknown, these changes are insignificant in comparison with the swelling of polymer layers in contact with organic solvents (see Chapter 6).

In summary, $OsPVP_{75}$, $OsPVP_{67}$ and $OsPVP_{33}$ electrode coatings are rigid in all $HClO_4$ electrolyte concentrations under investigation. This rigidity is a consequence of both the crosslinking properties of the perchlorate anion and the hydrophobic nature of the styrene moiety of the copolymer backbone. On increasing the styrene content of the polymer backbone, the rigidity of the layer increases as a consequence of the reduced requirement for anion ingress and the enhanced hydrophobicity of the polymer backbone.

For all polymers, an increase in layer mass is observed with increasing $HClO_4$ electrolyte concentration. This mass influx is associated with the influx of counter-anions to maintain electroneutrality within the protonated polymer matrix. Having demonstrated that these polymers are rigid at all $HClO_4$ electrolyte concentrations it is now possible to give a quantitative assessment of the mass changes within the layer using the Sauerbrey equation.

2.3.3. Change in resident layer mass with increasing $HClO_4$ Concentration.

Fig. 2.10 illustrates the change in layer mass, with increasing electrolyte pH, for $OsPVP_{75}$, $OsPVP_{67}$ and $OsPVP_{33}$ polymer layers. At each concentration, the shift in resonant frequency resulting from the change in viscous load was corrected for, by subtracting the frequency shift observed for an uncoated crystal. Tables 2.5 - 2.7 give the corresponding sets of data. All mass changes were calculated using a mass sensitivity of 0.232 $Hzcm^2ng^{-1}$ [35]. It is anticipated that these mass changes result from the influx of perchlorate anions, in response to the electroneutrality constraints imposed by the protonated polymer backbone.

Columns A and B of each table are estimates of the number of perchlorates required for electroneutrality, assuming the influx of A) unhydrated perchlorate ($H^+ClO_4^-$) and B) hydrated perchlorate ($H^+ClO_4^- 2.6H_2O$). Assuming the influx of hydrated perchlorate anions, the level of anion influx is less than that anticipated for protonation of the backbone. This suggests incomplete protonation of the backbone, which is considered unlikely at concentrations so far to the acid side of the pK_a of the pyridine units (pK_a = 3.3 [36]). However, there would appear to be excellent agreement between the unhydrated data and the electroneutrality requirement, assuming complete protonation of the polymer layers at pH 0. Taking the $OsPVP_{33}$ polymer as an example, the $OsPVP_{33}$ polymer unit $[Os(bipy)_2(PVP_{33})_{10}Cl]^+$ comprises 3.3 pyridine units, one of which is bound to the osmium redox centre. There are, therefore, 2.3 pyridine units available for protonation. The influx of 2.4 perchlorate anions (see Table 2.7) is close to the anticipated influx of 2.3 perchlorates, on complete protonation of the polymer. Similarly, for the $OsPVP_{75}$ and $OsPVP_{67}$ polymers, the data illustrate the influx of 6.6. and 5.8 perchlorate anions respectively, which is close to the anticipated influx of 6.5 and 5.7 perchlorates. Furthermore, the influx of 9 perchlorate anions was reported for the $OsPVP_{100}$ polymer under similar experimental conditions [12]. This behaviour suggests that

Fig. 2.10. Change in layer mass as a function of $HClO_4$ electrolyte pH.

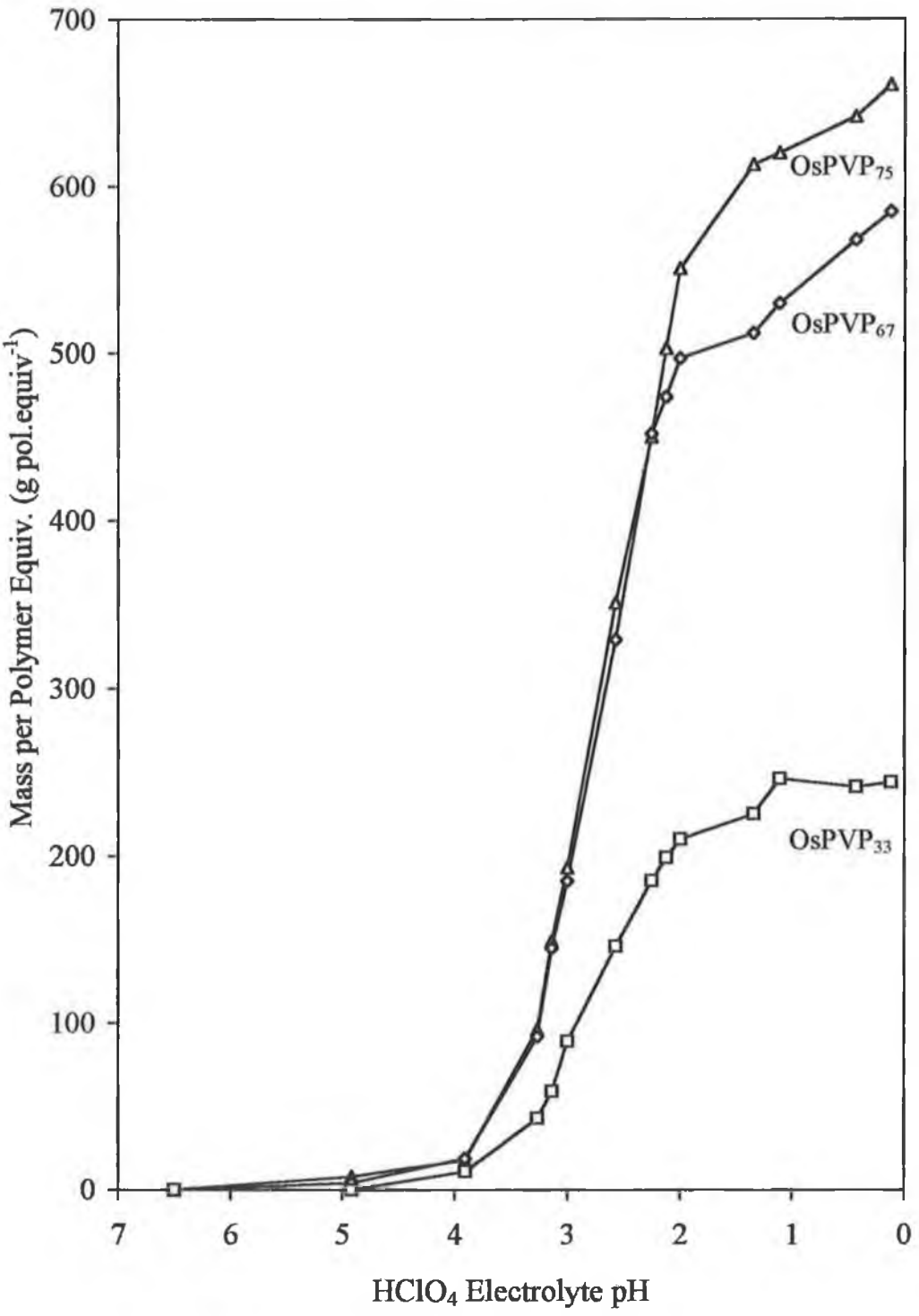

Table 2.5. Changes in layer mass as a function of $HClO_4$ electrolyte pH for an $OsPVP_{75}$ coated crystal. Gravimetric surface coverage is 1.09×10^{-8} $molcm^{-2}$.

$HClO_4$ pH	Δf (Hz)	$\Delta M^{(a)}$ ($ngcm^{-2}$)	Mass per polmer unit[(b)] (g pol equiv.$^{-1}$)	ClO_4^- content[(c)] (mol pol equiv.$^{-1}$)	
				A.	B.
6.50	0	0	0	0	0
4.92	+19	81	8	0.1	0.1
3.91	-45	196	18	0.2	0.1
3.27	-243	1047	96	1.0	0.7
3.14	-377	1624	149	1.5	1.0
3.00	-488	2103	193	1.9	1.3
2.57	-888	3827	351	3.5	2.4
2.25	-1138	4905	450	4.5	3.1
2.12	-1274	5478	503	5.0	3.4
2.00	-1393	6006	551	5.5	3.7
1.34	-1549	6676	613	6.1	4.2
1.11	-1568	6758	620	6.2	4.2
0.43	-1624	7000	642	6.4	4.4
0.12	-1672	7207	661	6.6	4.5

(a) Calculated using mass sensitivity of 0.232 $Hzcm^2ng^{-1}$.

(b) Calculated from the gravimetric surface coverage.

(c) Column A : Calculated assuming the insertion of unhydrated ClO_4^- and H^+.

Column B : Calculated assuming the insertion of hydrated ClO_4^- (hydration number 2.6) and H^+.

Table 2.6. Changes in layer mass as a function of $HClO_4$ electrolyte pH for an $OsPVP_{67}$ coated crystal. Gravimetric surface coverage is 1.07×10^{-8} $molcm^{-2}$.

$HClO_4$ pH	Δf (Hz)	$\Delta M^{(a)}$ ($ngcm^{-2}$)	Mass per polmer unit[(b)] (g pol equiv.$^{-1}$)	ClO_4^- content[(c)] (mol pol equiv.$^{-1}$)	
				A.	B.
6.50	0	0	0	0	0
4.92	-11	47	4	0	0
3.91	-47	203	19	0.2	0.1
3.27	-228	982	92	1.0	0.6
3.14	-360	1551	145	1.4	1.0
3.00	-460	1982	185	1.8	1.3
2.57	-817	3521	329	3.3	2.2
2.25	-1121	4831	452	4.5	3.1
2.12	-1177	5073	474	4.7	3.2
2.00	-1234	5318	497	4.9	3.4
1.34	-1271	5478	512	5.1	3.5
1.11	-1316	5672	530	5.3	3.6
0.43	-1410	6077	568	5.7	3.9
0.12	-1452	6258	585	5.8	4.0

(a) Calculated using mass sensitivity of 0.232 $Hzcm^2ng^{-1}$.

(b) Calculated from the gravimetric surface coverage.

(c) Column A : Calculated assuming the insertion of unhydrated ClO_4^- and H^+.

Column B : Calculated assuming the insertion of hydrated ClO_4^- (hydration number 2.6) and H^+.

Table 2.7. Changes in layer mass as a function of $HClO_4$ electrolyte pH for an $OsPVP_{33}$ coated crystal. Gravimetric surface coverage is 1.51×10^{-8} $molcm^{-2}$.

$HClO_4$ pH	Δf (Hz)	$\Delta M^{(a)}$ ($ngcm^{-2}$)	Mass per polmer unit[(b)] (g pol equiv.$^{-1}$)	ClO_4^- content[(c)] (mol pol equiv.$^{-1}$)	
				A.	B.
6.50	0	0	0	0	0
4.92	-0	0	0	0	0
3.91	-37	159	11	0.1	0.1
3.27	-150	646	43	0.4	0.3
3.14	-207	892	59	0.6	0.4
3.00	-312	1344	89	0.9	0.6
2.57	-510	2198	146	1.5	1.0
2.25	-648	2794	185	1.8	1.3
2.12	-697	3004	199	2.0	1.4
2.00	-735	3168	210	2.1	1.4
1.34	-788	3396	225	2.2	1.5
1.11	-863	3719	246	2.4	1.7
0.43	-844	3637	241	2.4	1.6
0.12	-855	3685	244	2.4	1.7

(a) Calculated using mass sensitivity of 0.232 $Hzcm^2ng^{-1}$.

(b) Calculated from the gravimetric surface coverage.

(c) Column A : Calculated assuming the insertion of unhydrated ClO_4^- and H^+.

Column B : Calculated assuming the insertion of hydrated ClO_4^- (hydration number 2.6) and H^+.

these polymers are completely protonated in 0.5M $HClO_4$ and that the observed mass changes are associated solely with the protonation process. Furthermore, it suggests that the styrene moieties act merely as diluents and do not inhibit protonation of the neighbouring pyridine units. The data in Column A of Tables 2.5 - 2.7 suggest that, for each individual metallopolymer, all the pyridine units of the polymer backbone are protonated.

An important consideration that has, as yet, not been addressed is the nature of the frequency response. The observed shifts in resonant frequency represent the net change in layer mass and, therefore, will not highlight counterbalancing ion motion (i.e. simultaneous motion in opposing directions). It seems unlikely that the initially imbibed solvent will remain constant, as the solvent activity of the bathing solution is decreased. It is anticipated, therefore, that water egress will occur, in response to activity constraints, as the bathing electrolyte concentration is increased. If solvent egress does occur then the number of perchlorate ions that enter the layer is greater than that quoted in Tables 2.5 - 2.7. However, for the $OsPVP_{33}$ polymer at least, this should not result in a serious discrepancy as the initial solvent level in this polymer is only 0.7 ± 0.1 molecules of water per polymer unit. Assuming complete egress of this solvent at higher electrolyte concentrations accounts for an additional influx of only 0.14 molecules of perchlorate per polymer unit i.e. the influx of 2.54 perchlorate anions as opposed to 2.4 anions (see Table 2.7). The fact remains, that there is a relationship between the mass influx and the electroneutrality requirement and that the presence of styrene moieties in the polymer backbone does not appear to adversely affect the protonation process.

For the $OsPVP_{100}$ polymer, the mass of the layer continues to increase with increasing $HClO_4$ concentration in excess of 0.5M $HClO_4$ and is, therefore, in excess of that anticipated for the protonation process [12]. This behaviour reflects the breakdown in permselectivity of this layer [12]. This behaviour is also observed for the $OsPVP_{75}$ and $OsPVP_{67}$ polymers reported here. However, for the $OsPVP_{33}$

polymer, there is little variation in the resident layer mass at concentrations in excess of 0.5M $HClO_4$, suggesting that this polymer layer behaves permselectively, even at these high electrolyte concentrations. This also suggests that the mass influx is associated solely with the protonation process and that this process is complete in 0.5M $HClO_4$. The concentration of fixed charge sites within this polymer, estimated from floatation experiments in non swelling solvents, is 0.75M. Protonation of the PVP units of the backbone and compaction of the layer by crosslinking will increase this concentration further. Consequently, for the $OsPVP_{33}$ polymer, the fixed site concentration will be greater than the $HClO_4$ concentration of the bathing solution at all concentrations and Donnan exclusion will prevail. As a result, this layer is apparently permselective in all $HClO_4$ concentrations examined. The primary effect of this behaviour is the absence of free electrolyte in this polymer network in all $HClO_4$ concentrations. In comparison, the failure of permselectivity in the $OsPVP_{75}$ and $OsPVP_{67}$ polymers in higher electrolyte concentrations likely reflects the less compact nature of these polymers.

To test the reproducibility of these results, the change in layer mass on immersion of three different $OsPVP_{75}$ - $OsPVP_{33}$ polymer layers in 1.0 M $HClO_4$ (from H_2O) was examined. The data obtained from these experiments is summarised in Table 2.8. Clearly, there is excellent agreement between the data in Table 2.8 and the corresponding data quoted in Tables 2.5 - 2.7, for the original polymer layers in this electrolyte concentration.

Table 2.8. Change in layer mass on immersion of the $OsPVP_{75}$ - $OsPVP_{33}$ series of metallopolymers in 1.0M $HClO_4$ (from H_2O).

Polymer	Γ_G[(a)] ($molcm^{-2}$)	Δf[(b)] (Hz)	ΔM per pol equiv. (g pol equiv.$^{-1}$)	ClO_4- content[(c)] (mol pol equiv.$^{-1}$)	
				A.	B.
$OsPVP_{75}$	1.52×10^{-8}	-2253	639	6.4	4.3
$OsPVP_{67}$	9.98×10^{-9}	-1321	576	5.7	3.9
$OsPVP_{33}$	1.11×10^{-8}	-647	251	2.5	1.7

(a) Gravimetric surface coverage.

(b) Corrected for solution viscosity.

(c) Column A : Calculated assuming the insertion of unhydrated ClO_4^- and H^+.

Column B : Calculated assuming the insertion of hydrated ClO_4^- (hydration number 2.6) and H^+.

2.3.4. Estimation of the pK_a^{app} of the Pyridine Units.

The change in layer mass with increasing electrolyte pH may be viewed as a titration of the unbound pyridine units of the polymer backbone and may therefore be used to estimate the apparent pK_a of the protonated pyridine units, pK_a^{app}. The relationship between the solution pH and the pK_a^{app} is given by [12]:

$$pH = pK_a^{app} + \log \{ \left(\frac{\Delta M_{Total}}{\Delta M} \right) - 1 \} \qquad (2.3.1.)$$

ΔM_{Total} is the total mass change observed on increasing the pH from 5.0 to ca. pH 0.0. ΔM is the individual mass change observed at each intermediate pH.

Fig. 2.11 illustrates plots of $\log \{ \left(\frac{\Delta M_{Total}}{\Delta M} \right) - 1 \}$ vs pH for the three polymers under investigation. Equation 2.3.1 predicts a linear plot of slope 1 with an intercept with the x-axis (i.e. the pH at which this term goes to zero) corresponding to the pK_a^{app} of the pyridine units of the polymer backbone. The relevant data from these plots are given in the Table 2.9.

Linear plots with slopes approaching unity were obtained in all cases. The near unity slopes for each plot suggests that protonation proceeds as dictated by the pH of the bathing solution. The pK_a^{app} values, evaluated for each polymer, are almost identical in each case, which suggests that the presence of the styrene moieties in the polymer backbone does not adversely affect the protonation of the pyridine units and re-iterates what was stated in Section 2.3.3. The pK_a of the PVP backbone of these metallopolymers is clearly more acidic than the pK_a of the PVP homopolymer in solution i.e. 2.66 ±0.06 compared with 3.30 [36]. This likely reflects the compact and dehydrated nature of these copolymers and the resulting difficulty in protonation of the PVP units due to the electroneutrality requirement for anion-insertion. This observation is supported by the protonation behaviour of the $OsPVP_{100}$ polymer in

Fig. 2.11. Plots of log [($\Delta M_{total}/\Delta M$)-1] vs electrolyte pH for the series of polymers under investigation.

1.09 x 10^{-8} molcm^{-2} $OsPVP_{75}$

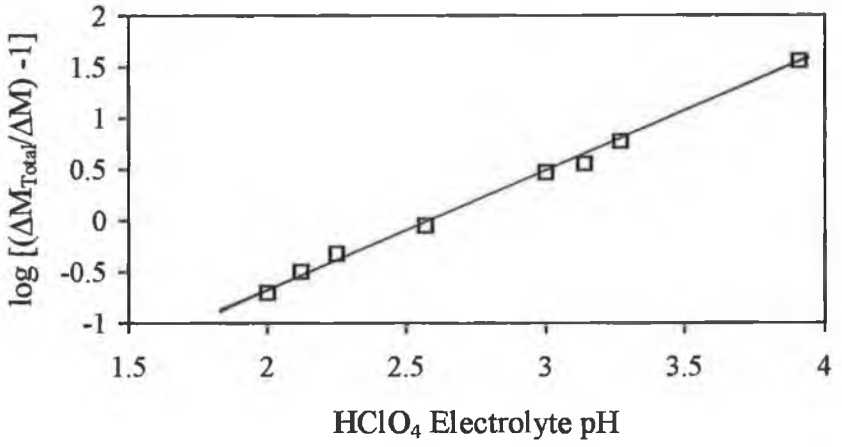

1.07 x 10^{-8} molcm^{-2} $OsPVP_{67}$

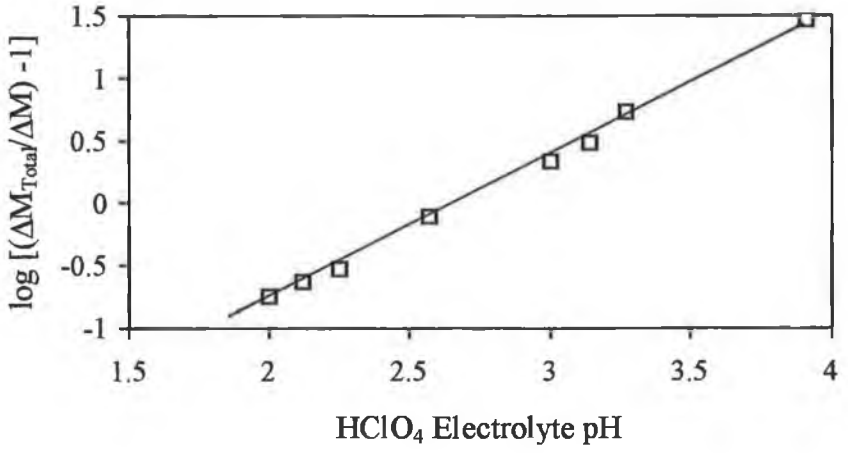

1.51 x 10^{-8} molcm^{-2} $OsPVP_{33}$

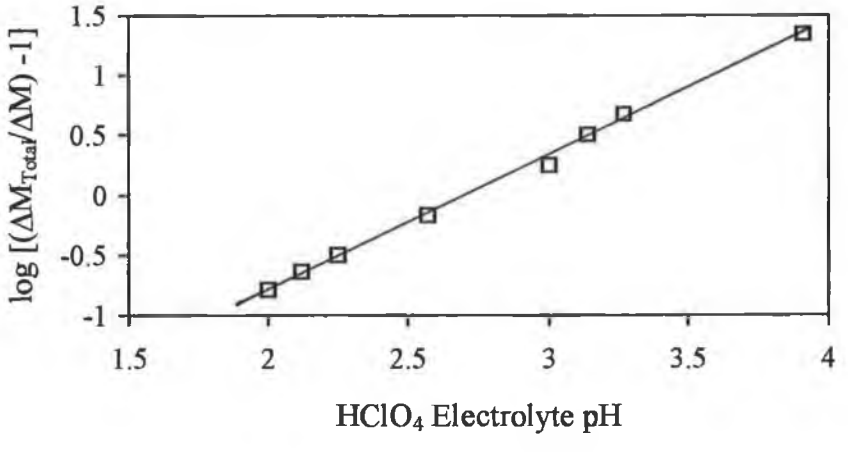

Table 2.9. Change in pK_a^{app} of PVP with increasing styrene content of the copolymer backbone.

Polymer	Slope	Intercept: pK_a^{app}
$OsPVP_{75}$	1.14 (0.03)	2.59 (0.05)
$OsPVP_{67}$	1.16 (0.02)	2.68 (0.04)
$OsPVP_{33}$	1.11 (0.02)	2.71 (0.04)

para-toluene sulphonic acid [13]. In this electrolyte, the polymer is extensively swollen as a result of the large volume of the bulky anion [13]. The ingress of this species is anticipated to occur more easily into the swollen polymer network that exists in this electrolyte. This point is indicated by the observed pK_a^{app} of 3.0, which is closer to the reported pK_a of the homopolymer.

The general behaviour of the $OsPVP_{100}$ polymer is decidedly different from that reported here for the copolymer systems. In both $HClO_4$ and pTSA electrolytes, dual sloped pK_a^{app} plots were observed, with two distinct regions of differing behaviour [12,13]. In $HClO_4$, this transition occurred at pH 2.5 and is related to the observed change in polymer morphology at 0.01M $HClO_4$. At pH above 2.50 a slope of 0.60 was observed, whilst at pH more acidic than this, a slope of 1.20 was noted [12]. A pK_a of 2.54 for the protonated pyridine units was reported [12]. The slope of less than unity was discussed in terms of Donnan exclusion at low $HClO_4$ concentrations and suggests that protonation of the pyridine units is hindered and does not proceed as dictated by the pH of the external solution [12].

This dual sloped behaviour was not observed for the copolymers reported

here. It is clear from the data that Donnan exclusion exists for these polymers in all $HClO_4$ concentrations. Furthermore, the rigidity studies reveal that these polymers are more compact than the higher PVP content polymers. The styrene polymers under these conditions behave more "ideally" than the less compact $OsPVP_{100}$ polymer and would appear to provide a less hindered path for anion influx. This behaviour is quite surprising and one might tentatively suggest that it may reflect the reduced requirement for compensating counterions within these lower PVP content polymers. At pH greater than 2.5, the behaviour of the $OsPVP_{100}$ polymer is comparable with that observed for the copolymers [12].

In summary, in $HClO_4$ electrolyte concentrations up to and including 1.0M $HClO_4$, layer rigidity is maintained. With increasing electrolyte concentration, there is an increase in layer mass associated with the influx of charge compensating counterions. With decreasing PVP content of the polymers, the level of anion influx is reduced proportionally. For each polymer, the perchlorate level is related to the requirements of electroneutrality. The ingress of this species is not apparently accompanied by the ingress of solvent, assuming of course that mass transfer occurs in one direction only. Protonation of the pyridine moieties of the copolymer backbone is more acidic than that observed for the homopolymer and likely reflects the compact nature of these structures.

2.3.5. Effect of $LiClO_4$ Concentration on Layer Rigidity.

For comparison, the influence of $LiClO_4$ electrolyte concentration on the resident layer mass of $OsPVP_{33}$ and $OsPVP_{100}$ modifying layers was studied. As mass changes occurring within these polymers can only be quantitatively evaluated when layer rigidity has been established, the change in polymer morphology with changing electrolyte concentration is considered first. Admittance spectra were recorded for $OsPVP_{100}$ and $OsPVP_{33}$ crystal coatings in a series of $LiClO_4$ electrolyte concentrations. Admittance spectra were recorded as a function of increasing electrolyte concentration, with no voltammetry, and decreasing concentration following voltammetric cycling of the layers. All spectra were recorded at open circuit (Os^{II} oxidation state).

Prior to these admittance studies, the coated crystals were cycled in 0.1M $LiClO_4$, following immersion in Milli-Q water, to exchange the polymer counterion. The mass change accompanying this process was similar to that observed for the $HClO_4$ experiments i.e. 62±10 g pol equiv^{-1}. No correction was made for other mass changes as there is no apparent electrolyte uptake in this $LiClO_4$ concentration due to Donnan exclusion (see below). The coatings were then stored in water prior to use.

2.3.5.1. $OsPVP_{100}$.

Fig. 2.12 illustrates the change in crystal resonance of an $OsPVP_{100}$ coated crystal, as the electrolyte concentration is increased from pure solvent to 4.0M $LiClO_4$. The gravimetric surface coverage was 2.16×10^{-8} molcm^{-2}. The characteristic features of these spectra are summarised in Column A of Table 2.10. Fig. 2.13 illustrates the change in crystal resonance for the same coating as a function of decreasing $LiClO_4$ concentration. The layer was voltammetrically cycled at each concentration, prior to the recording of the open circuit spectra. The characteristic features of these spectra are summarised in Column B of Table 2.10.

In Fig. 2.12, with the exception of 4.0 M $LiClO_4$, there is no variation in the

shape of the crystal resonance of this coated crystal compared with that observed for an uncoated crystal i.e. at each concentration the change in the shape of the crystal resonance is related to the viscous load of the solution and is not associated with changes in the viscoelastic properties of the polymer coating. Therefore, the morphology of this layer is not affected by the concentration of the bathing solution within the concentration range of 0.01M to 2.0M $LiClO_4$. Broadening of the crystal resonance in 4.0M $LiClO_4$ is only partially related to the viscous load of the electrolyte and therefore illustrates a slight expansion of the polymer network.

The shift in resonant frequency observed at each concentration is summarised in Column A of Table 2.10. The data have been corrected for the viscous load of the contacting electrolyte. With increasing electrolyte concentration, from 0.01M to 0.1M $LiClO_4$, the observed shift in resonant frequency is associated solely with the viscosity of the bathing solution, which suggests that the layer mass does not change. As was discussed in Section 2.3.3, the concentration of fixed sites within these polymer layers is ca. 0.7M. If the electrolyte concentration is more dilute, then a concentration difference will exist between the polymer phase and the contacting electrolyte which will result in the establishment of a membrane potential difference across the polymer/ solution interface. This Donnan potential will serve to exclude electrolyte from the polymer pore liquid. The existence of this exclusion barrier is suggested by the absence of changes in the layer mass in these electrolyte concentrations. Under these conditions the polymer layer is permselective.

On immersion of this $OsPVP_{100}$ coated crystal in 0.01M $LiClO_4$, from pure solvent, the crystal's resonant frequency increases. This increase is not related to the viscosity of this solution and thus represents a decrease in the layer mass. Fig. 2.12 illustrates that there is slight sharpening of the crystal resonance shape in this electrolyte concentration, which reflects compaction of the polymer layer. The decrease in layer mass and associated compaction of the layer may be a consequence of either the partial delamination of the polymer layer from the electrode or the egress

Figs. 2.12. and 2.13. Admittance spectra for an $OsPVP_{100}$ coated crystal in $LiClO_4$. Gravimetric surface coverage is 2.16×10^{-8} molcm^{-2}.

Fig. 2.12. Increasing electrolyte concentration, no voltammetry.

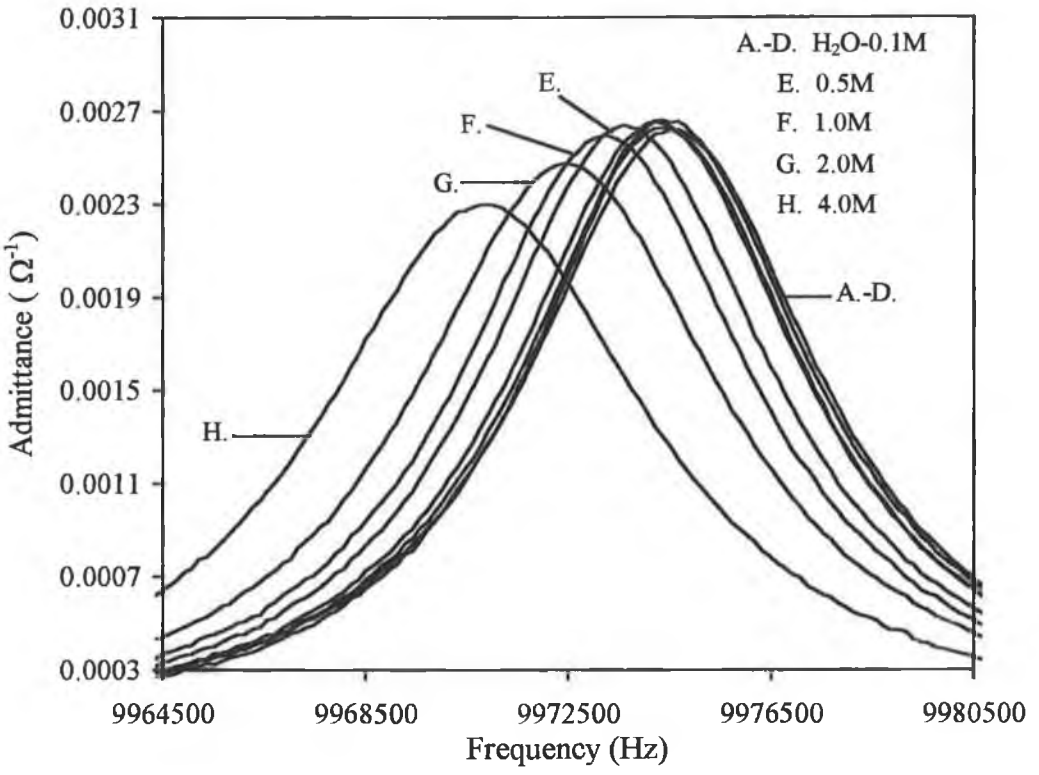

Fig. 2.13. Decreasing electrolyte concentration, with voltammetry.

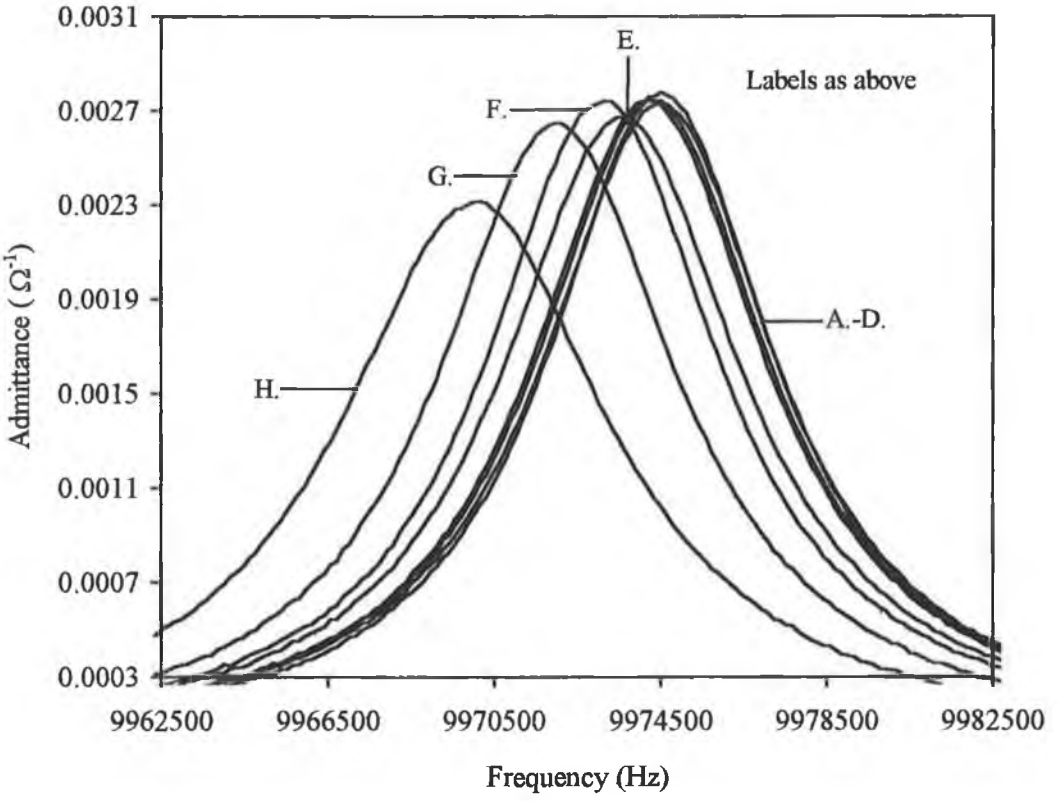

Table 2.10. Admittance data obtained at open circuit for an $OsPVP_{100}$ coated crystal in $LiClO_4$. Gravimetric surface coverage is 2.16×10^{-8} molcm^{-2}.

$LiClO_4$ Conc. (M)	Admittance[a] ($\Omega^{-1} \times 10^{-2}$)		PWHM[a] (Hz)		Δf[a,b] (Hz)	
	A.	B.	A.	B.	A.	B.
H_2O	0.263	0.278	6825	6675	0	+168
0.01	0.262	0.275	6825	6750	+153	+131
0.05	0.266	0.275	6975	6825	0	0
0.10	0.265	0.275	7050	6875	0	-19
0.50	0.264	0.267	7125	7125	-274	-282
1.00	0.259	0.274	7125	6900	-548	-550
2.00	0.247	0.265	7500	7125	-1270	-1706
4.00	0.230	0.232	8175	7950	-2264	-3019

(a) Data resolution is 20 Hz.

(b) Estimated from the shift in resonant frequency and corrected for the viscous load of electrolyte.

Column A is the data obtained with increasing concentration, no voltammetry.

Column B is the data obtained with decreasing concentration, following electrochemical cycling at each concentration.

of species from within the layer. Within the concentration range of 0.05 to 0.1 M $LiClO_4$, Donnan exclusion prevents the influx of bathing electrolyte into the layer. Therefore, at concentrations lower than 0.05M $LiClO_4$, where Donnan exclusion will be more prevalent, it is considered unlikely that sufficient electrolyte will enter the film to swell and cause delamination. The frequency increase observed in this electrolyte concentration is more likely related to a decrease in layer mass associated with the loss of initially imbibed solvent. This mass loss may result from the decrease in solution activity of the bathing electrolyte compared with pure solvent and corresponds to 30 g pol equiv^{-1}, which is associated with the loss of ca. 2 of the 42 initially imbibed water molecules.

With increasing bathing electrolyte concentration, from 0.5M to 4.0M $LiClO_4$, the resonant frequency of this coated crystal decreases, reflecting an increase in the layer mass. As the concentration of the external solution approaches the concentration of fixed polymer sites, the failure of Donnan exclusion and the subsequent influx of electrolyte is anticipated. This behaviour is identified by the increase in layer mass observed in 0.5M $LiClO_4$, which is associated with the influx of electrolyte ($Li^+ClO_4^-$) and associated solvent. The polymer layer is no longer permselective at these higher electrolyte concentrations.

Fig. 2.13 illustrates the change in crystal resonance for the same $OsPVP_{100}$ coating, with decreasing electrolyte concentration. These spectra do not retrace those obtained with increasing electrolyte concentration (see Table 2.10). At all concentrations, with the exception of 0.5M $LiClO_4$, the shape of the crystal resonance becomes slightly sharper following voltammetric cycling, which suggests that the layer compacts. The shift in resonant frequency with decreasing $LiClO_4$ concentration is summarised in Column B of Table 2.10. Within the concentration range of 0.01M to 1.0M $LiClO_4$, the shift in resonant frequency observed at each concentration is similar to that observed with increasing electrolyte concentration. Permselective layer behaviour is once more observed within the concentration range

of 0.01M to 0.1M $LiClO_4$. This behaviour is highlighted in Fig. 2.14, which illustrates the shift in resonant frequency of this coated crystal with increasing and decreasing $LiClO_4$ concentration. In 2.0M and 4.0M $LiClO_4$, there is a increase in layer mass following voltammetry. In these electrolyte concentrations the layer behaves non-permselectively and this behaviour reflects the further influx of electrolyte. This suggests that, in these electrolyte concentrations, equilibrium solvent and ion populations are achieved only following voltammetric cycling of the layer.

Overall, there are changes in the morphology of this metallopolymer with changes in the $LiClO_4$ concentration. However, these changes are extremely small and the rigid layer approximation is valid.

2.3.5.2. $OsPVP_{33}$.

The rigidity and resident layer mass of $OsPVP_{33}$ crystal coatings were studied as a function of the $LiClO_4$ bathing electrolyte concentration. In the course of these experiments, surface coverage dependent behaviour was observed. Only two $OsPVP_{33}$ polymer layers were studied over the complete $LiClO_4$ concentration range. However, the observed behaviour has been reproduced on at least one other film. The results obtained for these coatings are discussed individually.

7×10^{-9} molcm^{-2} $OsPVP_{33}$.

Fig. 2.15 illustrates the change in crystal resonance for an $OsPVP_{33}$ coated crystal, as the electrolyte concentration is increased from pure solvent to 4.0M $LiClO_4$. The characteristic features of these spectra are summarised in Column A of Table 2.11. Fig. 2.16 illustrates the change in crystal resonance for the same coating, as a function of decreasing $LiClO_4$ concentration, following voltammetry at each concentration. The characteristic features of these spectra are summarised in Column B of Table 2.11.

The behaviour of this $OsPVP_{33}$ coating is similar to that observed for the

Fig. 2.14. Shift in resonant frequency of an $OsPVP_{100}$ coated crystal as a function of A) increasing $LiClO_4$ concentration and B) decreasing $LiClO_4$ concentration. Gravimetric surface coverage is 2.16×10^{-8} molcm^{-2}.

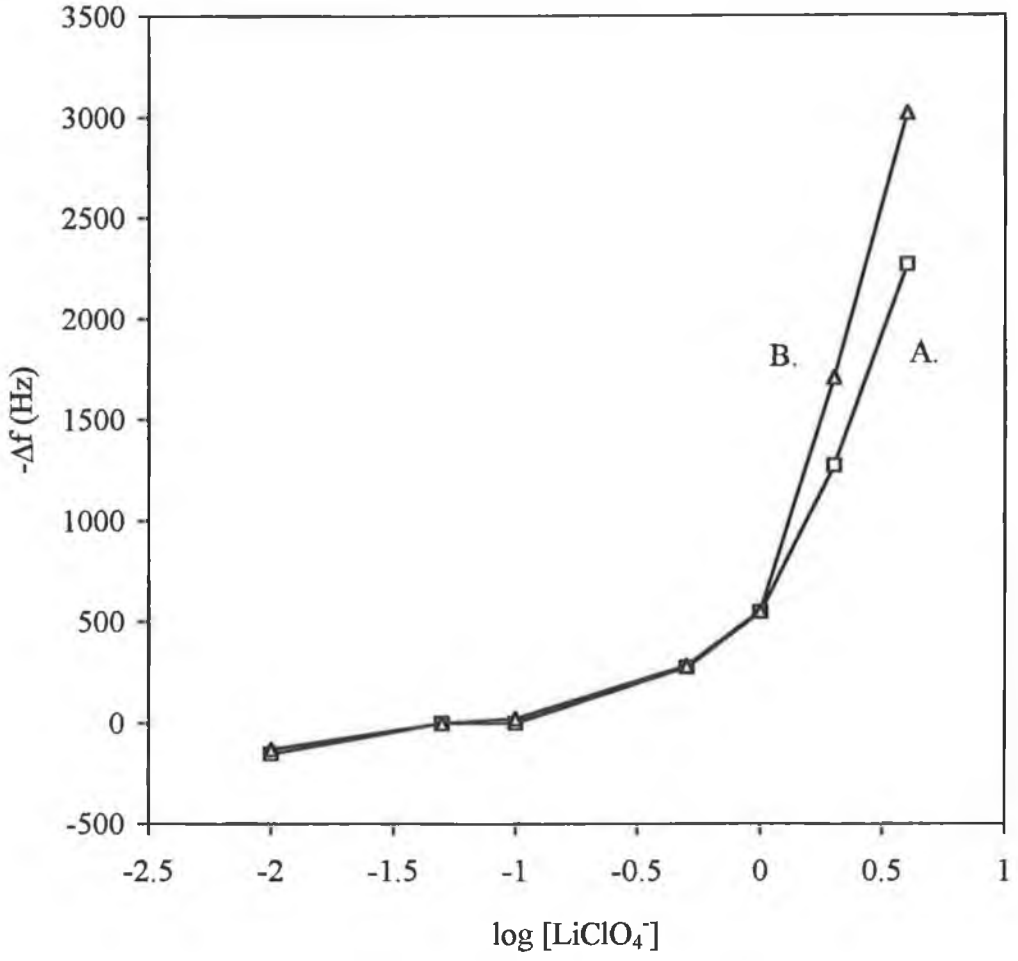

$OsPVP_{100}$ polymer (see Section 2.3.5.1). In Fig. 2.15, the shape of the crystal resonance exhibits the same characteristic features as the $OsPVP_{100}$ polymer. At all concentrations, with the exception of 4.0M $LiClO_4$, the shape of the crystal resonance remains essentially constant. In 4.0M $LiClO_4$, broadening of the crystal resonance signifies an expansion of the polymer matrix. The shift in resonant frequency accompanying the increase in electrolyte concentration is summarised in

Figs. 2.15. and 2.16. Admittance spectra for an $OsPVP_{33}$ coated crystal in $LiClO_4$. Gravimetric surface coverage is 7.0×10^{-9} molcm^{-2}.

Fig. 2.15. Increasing electrolyte concentration, no voltammetry.

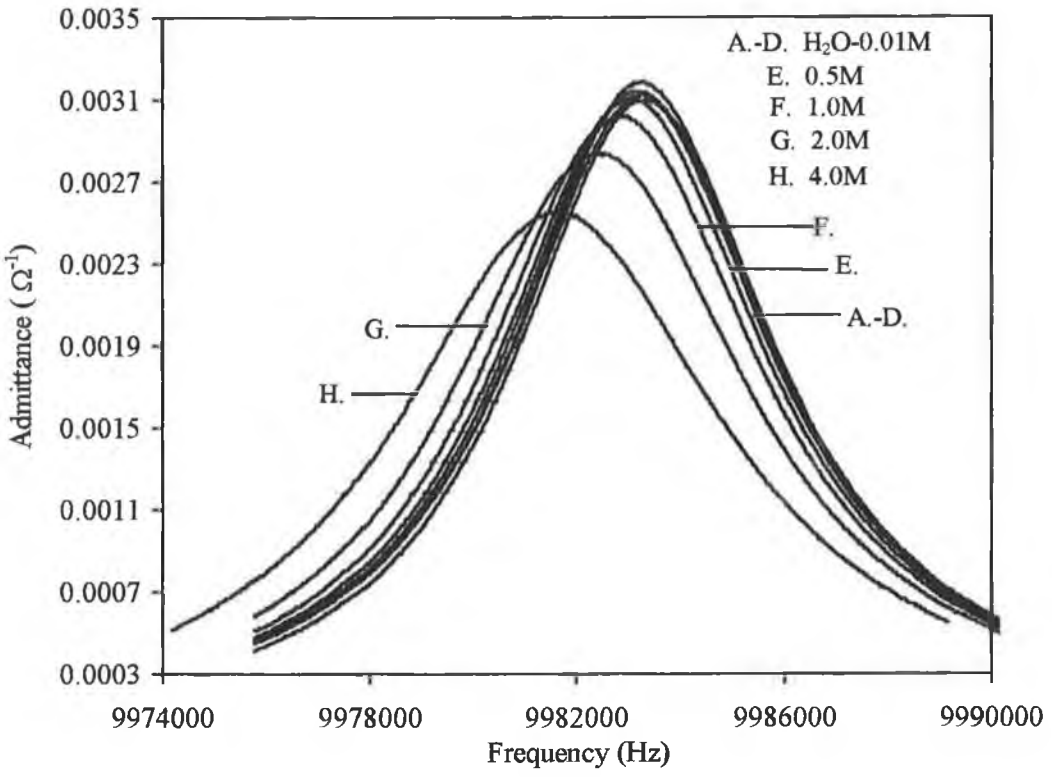

Fig. 2.16. Decreasing electrolyte concentration, with voltammetry.

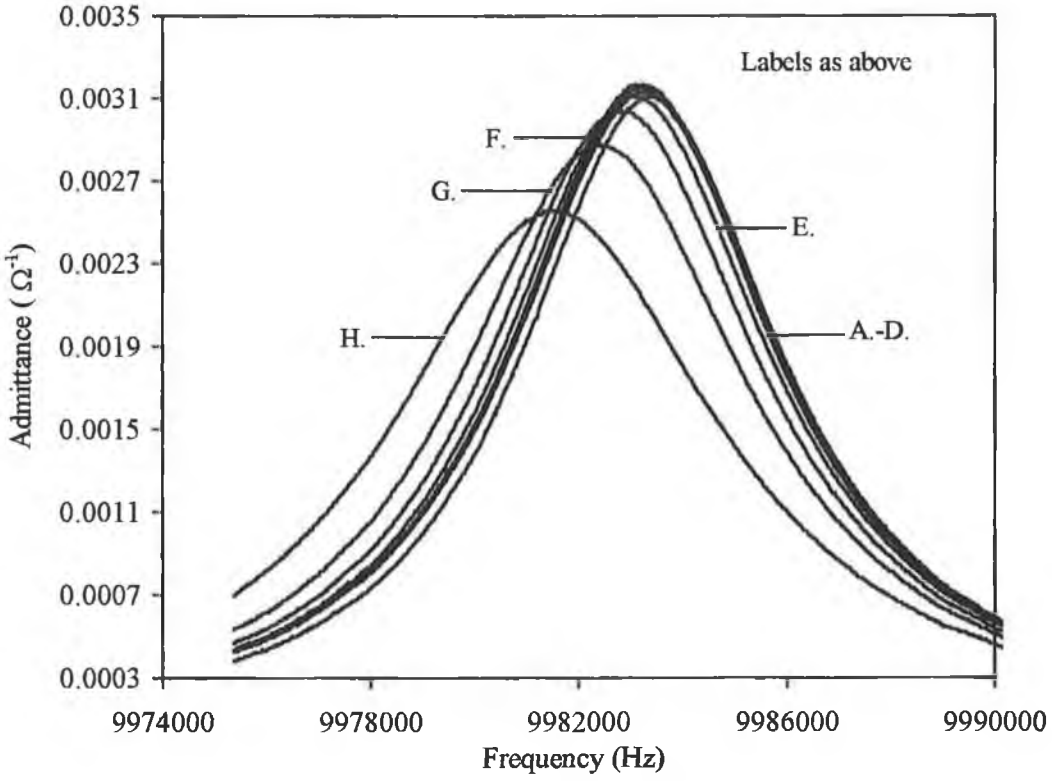

Table 2.11. Admittance data obtained at open circuit for an $OsPVP_{33}$ coated crystal in $LiClO_4$. Gravimetric surface coverage is 7×10^{-9} molcm^{-2}.

$LiClO_4$ Conc. (M)	Admittance[a] ($\Omega^{-1} \times 10^{-2}$)		PWHM[a] (Hz)		Δf[a,b] (Hz)	
	A.	B.	A.	B.	A.	B.
H_2O	0.310	0.311	6132	6160	0	+20
0.01	0.313	0.313	6254	6281	+19	+19
0.05	0.318	0.316	6169	6253	0	+27
0.10	0.314	0.317	6244	6225	0	-9
0.50	0.311	0.311	6300	6308	-20	-29
1.00	0.302	0.304	6515	6440	-56	-86
2.00	0.284	0.287	6891	6835	-187	-255
4.00	0.256	0.256	7687	7669	-540	-573

(a) Data resolution is 20 Hz.

(b) Estimated from the shift in resonant frequency and corrected for the viscous load of electrolyte.

Column A is the data obtained with increasing concentration, no voltammetry.

Column B is the data obtained with decreasing concentration, following electrochemical cycling at each concentration.

Column A of Table 2.11. This $OsPVP_{33}$ layer behaves permselectively in electrolyte concentrations up to 0.1M $LiClO_4$. In electrolyte concentrations in excess of 0.1M $LiClO_4$, the breakdown in layer permselectivity and the subsequent influx of electrolyte is illustrated by the observed increase in layer mass. This behaviour contrasts with that observed in $HClO_4$ (see Fig. 2.10). In $HClO_4$, Donnan exclusion exists in all concentrations, however, protonation of the backbone provides sufficient driving force for the influx of ions across this membrane potential.

In 0.01M $LiClO_4$, there is an increase in the resonant frequency of this coated crystal. However, this frequency shift is only 19 Hz, which is also the point to point resolution of these admittance spectra and is therefore of limited accuracy.

In Fig. 2.16, the change in crystal resonance shape with decreasing electrolyte concentration, retraces the corresponding set of spectra obtained with increasing concentration. This behaviour suggests that the layer morphology is not affected by voltammetric cycling at each $LiClO_4$ concentration. The shift in resonant frequency, with decreasing electrolyte concentration, is summarised in Column B of Table 2.11. This data suggests that, with the exception of 2.0M $LiClO_4$, there is little variation in the layer mass before and after voltammetry and that equilibrium solvent and solute levels are achieved in the absence of electrochemical cycling. This behaviour is illustrated in Fig. 2.17. Overall, as was observed for the $OsPVP_{100}$ polymer, the changes in the morphology of this $OsPVP_{33}$ polymer layer as a function of the contacting $LiClO_4$ concentration are extremely small.

3.27×10^{-8} molcm^{-2} $OsPVP_{33}$.

Fig. 2.18 illustrates the change in crystal resonance for an $OsPVP_{33}$ coated crystal, as the electrolyte concentration is increased from pure solvent to 4.0M $LiClO_4$. The characteristic features of these spectra are summarised in Column A of Table 2.12. Fig. 2.19 illustrates the change in crystal resonance, for the same coating, as a function of decreasing $LiClO_4$ concentration, following voltammetry at each

Fig. 2.17. Shift in resonant frequency of an $OsPVP_{33}$ coated crystal as a function of A) increasing $LiClO_4$ concentration and B) decreasing $LiClO_4$ concentration. Gravimetric surface coverage is 7.0×10^{-9} molcm^{-2}.

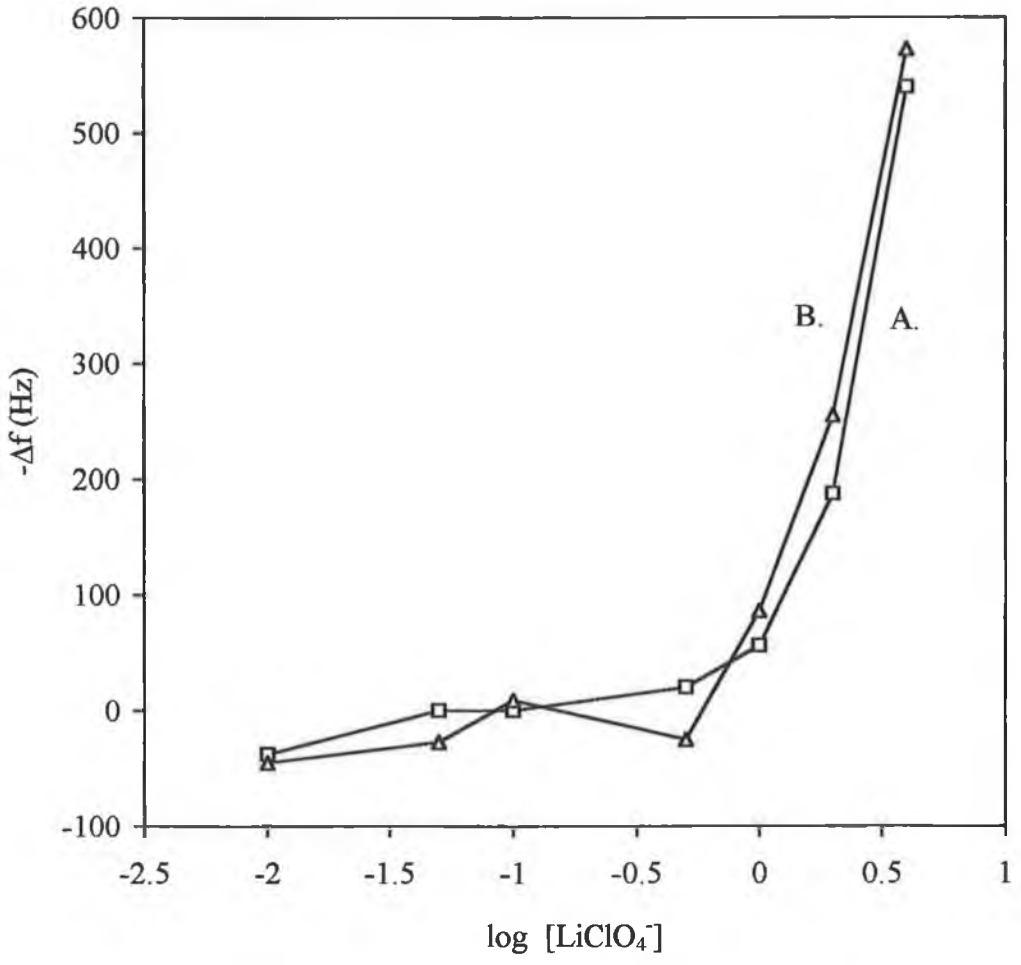

concentration. The characteristic features of these spectra are summarised in Column B of Table 2.12.

In Fig. 2.18, with the exception of 4.0M $LiClO_4$, layer rigidity is maintained in each electrolyte concentration. In 4.0M $LiClO_4$ the polymer matrix expands. The shift in resonant frequency, summarised in Column A of Table 2.12, suggests that this layer is permselective for electrolyte concentrations up to 0.1M $HClO_4$ and is non-

Figs. 2.18. and 2.19. Admittance spectra for an $OsPVP_{33}$ coated crystal in $LiClO_4$. Gravimetric surface coverage is 3.27×10^{-8} molcm^{-2}.

Fig. 2.18. Increasing electrolyte concentration, no voltammetry.

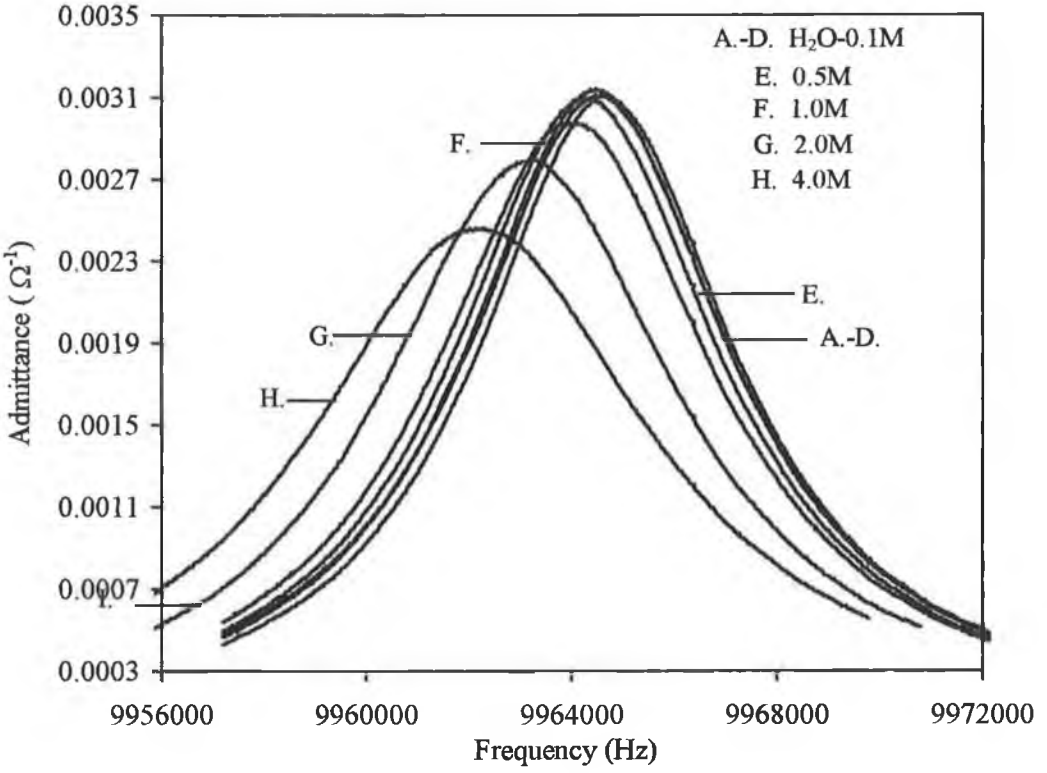

Fig. 2.19. Decreasing electrolyte concentration, with voltammetry.

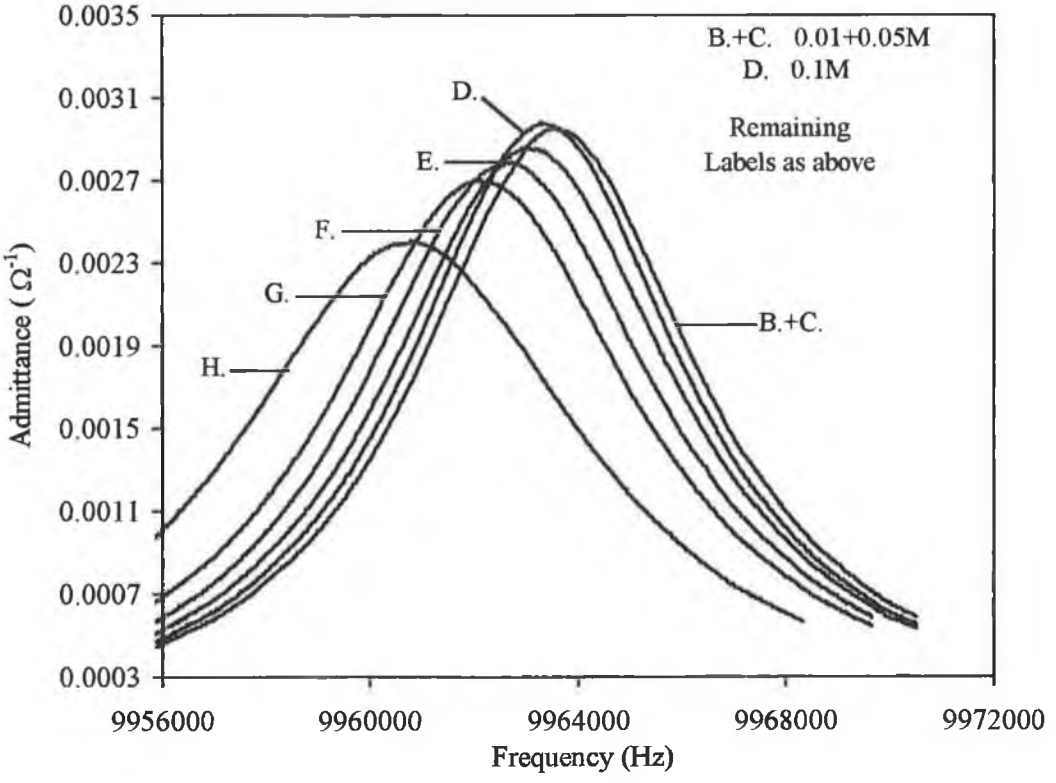

Table 2.12. Admittance data obtained at open circuit for an $OsPVP_{33}$ coated crystal in $LiClO_4$. Gravimetric surface coverage is 3.27×10^{-8} molcm^{-2}.

$LiClO_4$ Conc. (M)	Admittance ($\Omega^{-1} \times 10^{-2}$)		PWHM (Hz)		Δf (Hz)	
	A.	B.	A.	B.	A.	B.
H_2O	0.311	0.298	6160	6404	0	-949
0.01	0.311	0.296	6309	6638	-19	-949
0.05	0.313	0.296	6290	6647	-20	-1043
0.10	0.314	0.298	6262	6591	-20	-1174
0.50	0.310	0.286	6328	6881	-169	-1437
1.00	0.298	0.279	6610	7012	-300	-1609
2.00	0.280	0.270	7013	7275	-739	-1909
4.00	0.246	0.241	8025	8268	-1298	-2614

a) Estimated from the shift in resonant frequency and corrected for the viscous load of electrolyte.

Column A is the data obtained with increasing concentration, no voltammetry.

Column B is the data obtained with decreasing concentration, following electrochemical cycling at each concentration.

permselective in electrolyte concentrations in excess of 0.1M $LiClO_4$. Similar behaviour was observed for the thinner $OsPVP_{33}$ coating. The admittance characteristics of this layer, with decreasing electrolyte concentration, are decidedly different from those observed for the $OsPVP_{100}$ polymer and for the thinner $OsPVP_{33}$ polymer layer. In Fig. 2.19, broadening of the crystal resonance shape occurs at all concentrations and is associated with a substantial decrease in the resonant frequency of this coated crystal. This decrease in resonant frequency is highlighted in Fig. 2.20.

This behaviour reflects the expansion of the polymer matrix and suggests that some morphology change has occurred. Within the concentration range of 0.01M to 4.0M $LiClO_4$, this expansion corresponds to a 4-8% change in the PWHM after cycling, which suggests that the Sauerbrey equation may be invalid. However, the total mass change per polymer equivalent, observed on increasing the electrolyte concentration from water to 4.0M $LiClO_4$, is similar for both $OsPVP_{33}$ coatings. This observation suggests that the rigid layer approximation is still valid for the thicker $OsPVP_{33}$ layer. This behaviour is discussed in greater detail in Section 2.3.6. The shift in resonant frequency, following cycling in 4.0M $LiClO_4$, represents an approximate doubling of the layer mass. This is associated with the difficulty in attaining equilibrium levels of solute in this thicker polymer layer, which is only achieved by electrochemical cycling. With decreasing electrolyte concentration, this solute remains trapped within the layer and this behaviour is reflected by the difference in the resonant frequencies of the crystal in Milli-Q water before and after this analysis.

Fig. 2.20. Shift in resonant frequency of an $OsPVP_{33}$ coated crystal as a function of A) increasing $LiClO_4$ concentration and B) decreasing $LiClO_4$ concentration. Gravimetric surface coverage is 3.27×10^{-8} molcm^{-2}.

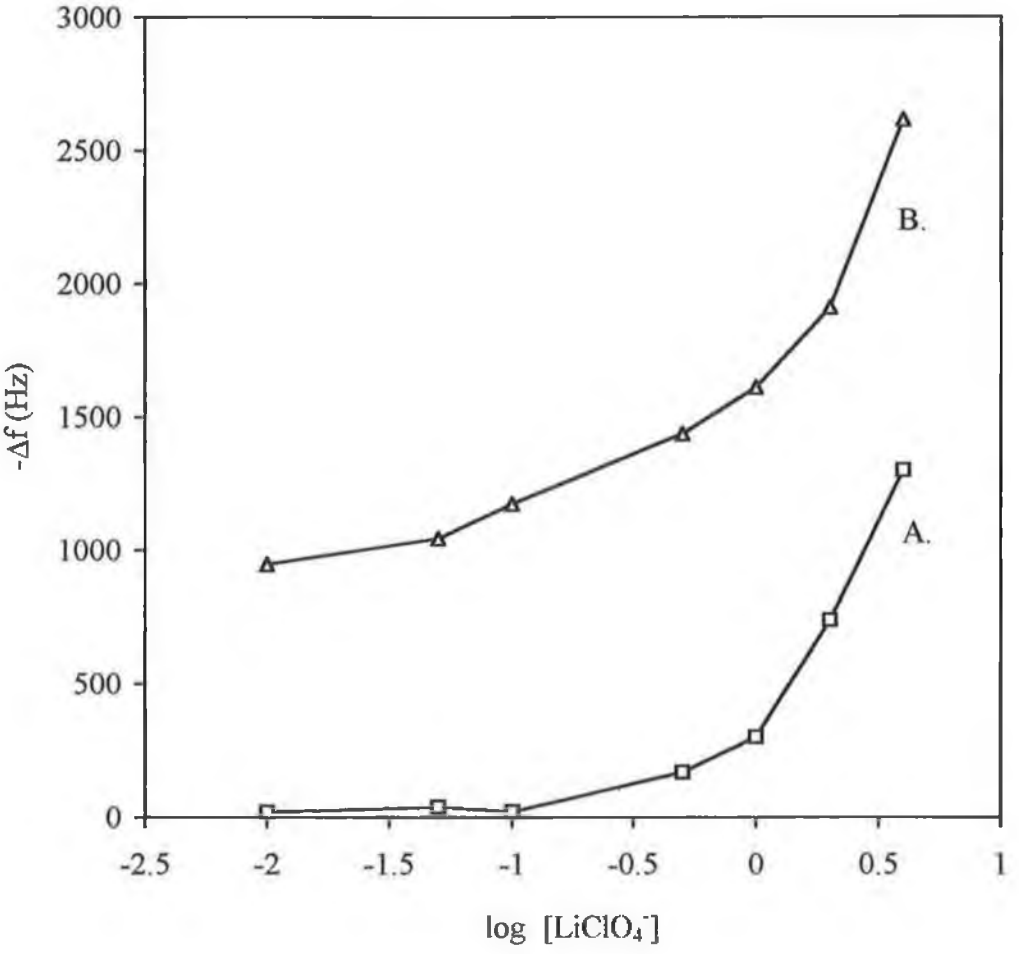

2.3.6. Changes in resident layer mass with increasing $LiClO_4$ Concentration.

In Section 2.3.5, the influence of $LiClO_4$ electrolyte concentration on the rigidity of $OsPVP_{100}$ and $OsPVP_{33}$ layers was discussed. The rigidity of $OsPVP_{100}$ and thin $OsPVP_{33}$ layers is essentially independent of the electrolyte concentration up to 2.0M $LiClO_4$. In 4.0M $LiClO_4$ these layers swell slightly. It is considered, however, that this expansion process is insufficient to prevent the use of the Sauerbrey equation. The accurate evaluation of changes in the layer mass is therefore anticipated. The level of polymer expansion is considerably greater for thicker $OsPVP_{33}$ coatings in this electrolyte and reflects the greater influx of mobile species to establish equilibrium solvent and ions levels within this thicker layer. This behaviour is particularly prevalent in 4.0M $LiClO_4$.

The total change in layer mass on increasing the electrolyte concentration from Milli-Q water to 4.0M $LiClO_4$, is quoted in Table 2.13. These data are taken from Tables 2.10 - 2.12 and are calculated from the observed shift in resonant frequency at these electrolyte concentrations. Columns A and B of Table 2.13 illustrate the ClO_4^- content of these layers, assuming the influx of unhydrated $LiClO_4$ and hydrated $LiClO_4$ respectively. The hydration numbers used in this calculation were $Li^+ = 7.4$ and $ClO_4^- = 2.6$ [27]. A total mass change of 602 g pol equiv^{-1} is observed for the $OsPVP_{100}$ layer. This corresponds to the influx of 5.7 molecules of unhydrated $LiClO_4$ or 2.1 molecules of hydrated $LiClO_4$ per polymer equivalent. If it is assumed that egress of initially imbibed solvent occurs at high $LiClO_4$ concentrations (see Section 2.3.3), then these values may be viewed as the lower limit for electrolyte influx. The influx of electrolyte is in response to activity constraints and represents a breakdown in the permselectivity of the layer.

The level of electrolyte/ salt ingress into the thin $OsPVP_{33}$ polymer coating is 3.3 (unhydrated $LiClO_4$) or 1.2 (hydrated $LiClO_4$) molecules per polymer equivalent. These values reflect the lower limit of salt influx for this polymer and are

Table 2.13. Change in layer mass of $OsPVP_{100}$ and $OsPVP_{33}$ polymers on immersion in 4.0M $LiClO_4$ (following voltammetric cycling of the layer).

Polymer	Γ_g[(a)] ($\times 10^{-8}$ molcm^{-2})	Mass per polymer unit[(b)] (g pol equiv.$^{-1}$)	ClO_4^- content[(c)] (mol pol equiv.$^{-1}$)	
			A.	B.
$OsPVP_{100}$	2.16	602	5.7	2.1
$OsPVP_{33}$	0.70	353	3.3	1.2
$OsPVP_{33}$	3.27	345	3.2	1.2

(a) Gravimetric surface coverage.

(b) Estimated from the total shift in resonant frequency, following voltammetry, on increasing the electrolyte concentration from Milli-Q H_2O to 4.0M $LiClO_4$.

(c) Column A : Calculated assuming the insertion of unhydrated Li^+ and ClO_4^-.

Column B : Calculated assuming the insertion of hydrated Li^+ (7.4 H_2O) and ClO_4^- (2.6 H_2O).

approximately a factor of 1.7 smaller than the corresponding values for the $OsPVP_{100}$ polymer. This lower level of salt influx for the $OsPVP_{33}$ polymer is likely a consequence of the more hydrophobic and compact nature of this copolymer. The level of electrolyte influx for the thicker $OsPVP_{33}$ polymer coating is almost identical to that observed for the thinner coating. This observation suggests that, although substantial broadening of the resonance was observed, the layer is sufficiently rigid to allow for accurate mass measurements. For the thicker $OsPVP_{33}$ layer, half the

observed mass change occurs following voltammetry, whilst for the thinner $OsPVP_{33}$ coating, most of the electrolyte influx occurs before voltammetry. This behaviour illustrates the greater difficulty in obtaining equilibrium solute levels in thicker polymer films. The movement of ions and solvent, that accompanies voltammetry, greatly assists the equilibration process.

The polymer layer morphology of $OsPVP_{100}$ and $OsPVP_{33}$ polymer coatings is dependant on the concentration of $LiClO_4$. However, for $OsPVP_{100}$ and thin $OsPVP_{33}$ coatings, these morphology changes are small and the Sauerbrey equation is valid. For thick $OsPVP_{33}$ layers, although the degree of polymer swelling is greater in high $LiClO_4$ electrolyte concentrations, it appears that the Sauerbrey equation is still valid. Permselective layer behaviour is observed for all layers within the concentration range of 0.01M to 0.1M $LiClO_4$. Breakdown in layer permselectivity and the accompanying ingress of electrolyte occurs in 0.5M $LiClO_4$. The amount of salt uptake by the $OsPVP_{100}$ polymer is nearly twice that observed for the $OsPVP_{33}$ polymer. It is considered that this behaviour reflects the more compact and hydrophobic nature of the styrene based $OsPVP_{33}$ polymer. This behaviour highlights the different polymer properties of these polymers.

2.4. Conclusions.

In $HClO_4$ and $LiClO_4$ electrolytes, $[Os(bipy)_2(PVP_x)_{10}Cl]^+$ layers are compact and rigid. This behaviour is a consequence of the crosslinking and dehydrating properties of the perchlorate anion. Furthermore, as anticipated, there is an increase in polymer rigidity with increasing styrene content of the polymer backbone. This reflects the reduced ion and solvent content of the higher styrene content polymers, which is a consequence of the more hydrophobic nature of the styrene moieties. This behaviour highlights the different chemical properties of these polymers. The contacting electrolyte type has a profound influence on the resident layer mass of these metallopolymers. In perchloric acid electrolytes, protonation of the pyridine units of the polymer backbone provides the driving force for anion ingress. For the $OsPVP_{75}$ - $OsPVP_{33}$ polymers investigated here, there is a good correlation between the number of free protonable pyridine units and the quantity of anion ingress, assuming the uptake of a single unhydrated anion per protonated site.

In lithium perchlorate electrolytes, for the $OsPVP_{100}$ and $OsPVP_{33}$ polymers, there is no apparent change in the resident layer mass within the concentration range of 0.01M to 0.1M $LiClO_4$. On increasing the electrolyte concentration above 0.1M $LiClO_4$, these layers are no longer permselective and electrolyte ingress is in evidence. The level of electrolyte ingress is dependent on the styrene content of the polymer backbone, with the $OsPVP_{33}$ polymer exhibiting a reduced layer content compared with the $OsPVP_{100}$ polymer. This behaviour is again likely a consequence of the more compact nature of the lower PVP content polymer.

2.5. References.

1. G.G. Wallace, M. Meaney, M.R. Smyth and J.G. Vos, Electroanalysis, 1 (1989) 357.
2. A.P. Doherty, T. Buckley, D. Kelly and J.G. Vos, Electroanalysis, 6 (1994) 553.
3. D. Leech, R.J. Forster, M.R. Smyth and J.G. Vos, J. Mater. Chem., 1 (1991) 629.
4. D. Leech, Ph.D Thesis, Dublin City University, (1992).
5. R.J. Forster and J.G. Vos, Comprehensive Analytical Chemistry, Vol. XXVII, M.R. Smyth and J.G. Vos (Ed.), Elsevier, Amsterdam, (1992) Ch. 7.
6. R.J. Forster and J.G. Vos, Electrochim. Acta, 37 (1992) 159.
7. R.J. Forster and J.G. Vos, J. Inorganic and Organometallic Polymers, 1 (1991) 67.
8. R.J. Forster, A.J. Kelly, J.G. Vos and M.E.G. Lyons, J. Electroanal. Chem., 270 (1989) 365.
9. R.J. Forster and J.G. Vos, J. Electroanal. Chem., 314 (1991) 135.
10. R.J. Forster, J.G. Vos and M.E.G. Lyons, J. Chem. Soc. Faraday Trans., 87 (1991) 3761.
11. R.J. Forster and J.G. Vos, Langmuir, 10 (1994) 4330.
12. A.P. Clarke, J.G. Vos, A. Glidle and A.R. Hillman, J. Chem. Soc. Faraday Trans., 89 (1993) 1695.
13. A.P. Clarke, J.G. Vos, A.R. Hillman and A. Glidle, J. Electroanal. Chem., 389 (1995) 129.
14. A.J. Kelly, T. Ohsaka, N. Oyama, R.J. Forster and J.G. Vos, J. Electroanal. Chem., 287 (1990) 185.
15. A.J. Kelly and N. Oyama, J. Phys. Chem., 95 (1991) 9579.
16. D.A. Buttry and M.D. Ward, Chem. Rev., 92 (1992) 1355.

17. R. Borjas and D.A. Buttry, J. Electroanal. Chem., 280 (1990) 73.

18. D.Orata and D.A. Buttry, J. Am. Chem. Soc., 109 (1987) 3574.

19. A. Glidle, A.R. Hillman and S. Bruckenstein, J. Electroanal., 318 (1991) 411.

20. S. Yamaguchi, T. Shimomura, T. Tatsuma and H. Oyama, Anal. Chem., 65 (1993) 1925.

21. A.R. Hillman, D.C. Loveday, A. Glidle, J.G. Vos, A.P. Clarke, D. Kelly and S. Bruckenstein, Macromol. Symp., 80 (1994) 323.

22. R.J. Forster and J.G. Vos, Macromolecules, 23 (1990) 4372.

23. F. Hellfrich, Ion-Exchange, McGraw-Hill, New York, (1962).

24. R. Schumacher, Angew. Chem. Int. Ed. Engl. 29 (1990) 329.

25. R. Schumacher, G. Borges and K.K. Kanazawa, Surface Science, 163 (1985) L621.

26. R. Schumacher, J.G. Gordon and O. Melroy, J. Electroanal. Chem., 216 (1987) 127.

27. Y. Marcus, Ion Solvation, Wiley-Interscience, New York, (1985).

28. S.M. Oh and L.R. Faulkner, J. Electroanal. Chem., 269 (1989) 77.

29. S.M. Oh and L.R. Faulkner, J. Am. Chem. Chem. Soc., 111 (1989) 5613.

30. E.F. Bowden, M.F. Dautartas and J.F. Evans, J. Electroanal. Chem., 219 (1987) 91.

31. A.R. Hillman, N.A. Hughes and S. Bruckenstein, J. Electrochem. Soc., 139 (1992) 74.

32. A.R. Hillman and S. Bruckenstein, J. Chem. Faraday Trans., 89 (1993) 339.

33. G. Inzelt, J. Electroanal. Chem., 287 (1990) 171.

34. G. Inzelt and J. Bacskai, J. Electroanal. Chem., 308 (1991) 255.

35. S. Bruckenstein and M. Shay, Electrochim. Acta, 30 (1985) 1295.

36. P. Ferruti and R. Barbucci, Adv. Polym. Sci., 58 (1984) 55.

Chapter 3.

The Charge Transport Properties of $[Os(bipy)_2(PVP_x)_{10}Cl]^+$ Metallopolymer Films in Perchlorate Electrolytes.

3.1. Introduction.

Extensive studies into the charge transport properties of electrodes modified with $[M(bipy)_2(Pol)_nCl]^+$ [1-12] and $[M(bipy)_2(Pol)_n]^{2+}$ [13] have been undertaken, where M signifies osmium [1-8,13] or ruthenium [9-12] metal centres and Pol signifies Poly 4-vinylpyridine (PVP) [1-10], poly N-vinylimidazole (PVI) [13], or PVP: Styrene [11] and PVP: poly (methylmethacrylate) [12] copolymer backbones. The influence of experimental variables such as the metal loading, electrolyte type and concentration and the temperature on the charge transport properties of these materials have been probed [1-13]. A comprehensive review of these investigations was presented in Chapter 1. What has clearly emerged from these studies is that the rate of the charge transport through these materials depends greatly on the physico-chemical properties of the polymer backbone [3,4,10-13]. This relationship between polymer structure and charge transport rates is most clearly illustrated by the anion dependence of the charge transport properties of these redox polymers [1,3,4,13].

To-date, however, relatively little attention has been paid to the effects of systematic structural variations in the polymer backbone on the rate of charge transport rate through these coatings [8,10,11]. The relationship between the physico-chemical characteristics of the polymer phase and the rate and mechanism for charge transport has been clearly demonstrated for the redox polymer $[Ru(bipy)_2(PVP_x)_{10}Cl]^+$, where x signifies the percentage of PVP in a PVP: styrene copolymer [11]. In a series of polymers of increasing styrene content, $RuPVP_{100}$ - $RuPVP_{33}$, the rate of charge transport was found to increase in perchlorate electrolyte. Concurrently, the activation energy for the charge transport process, E_a, was found to decrease with increasing styrene content. It has been suggested that the perchlorate anion may crosslink these polymers through the pyridine moieties of the polymer backbone [14,15]. Consequently, the observed decrease in E_a was attributed to the more facile ion permeation within the less crosslinked polymer structure of the higher styrene content polymers [11].

In this chapter the charge transport properties of electrode coatings of the $OsPVP_{100}$ - $OsPVP_{33}$ metallopolymers are investigated as a function of the perchlorate electrolyte type and concentration. In Chapter 2, the influence of the $HClO_4$ and $LiClO_4$ contacting electrolyte concentration on the rigidity and layer mass of these metallopolymers was reported. The charge transport studies presented in this chapter, combined with the structural information obtained from Chapter 2, provide the means for investigating the influence of polymer structural changes on the charge transport properties of these materials. The results are discussed in terms of the styrene content of the polymer backbone.

The electrochemical techniques used for the evaluation of the apparent charge transport diffusion coefficient, D_{CT}, are as outlined in Section 1.2.2. Activation parameters, evaluated from the temperature dependence of D_{CT}, are also determined to aid in the diagnosis of the rate determining step in the charge transport process. Comparison with the previous study of the ruthenium analogues is made [11].

3.2. Experimental.

3.2.1. Apparatus.

Electrochemical measurements were performed using an EG and G PAR 363 potentiostat, with a Philips 3311 digital storage oscilloscope interfaced to a BBC microcomputer for data capture and interrogation for the potential step experiments. Coulometric measurements were made using an EG and G PAR 379 digital coulometer.

3.2.2. Materials.

The synthesis of the $[Os(bipy)_2(PVP_x)_{10}Cl]Cl$ metallopolymers was described in Chapter 2. Perchloric acid and lithium perchlorate electrolytes were prepared with Milli-Q H_2O.

3.2.3. Procedures.

Glassy carbon electrodes of 3 or 7mm diameter, mounted in Teflon shrouds, were polished to a mirror finish using a 0.5 μm alumina slurry on a felt bed, followed by thorough washing with methanol and Milli-Q water. Electrode coatings were prepared by droplet evaporation of 0.25% w/v ethanolic solutions of the metallopolymers onto the electrode surface. Coatings were allowed to dry in a solvent saturated chamber for 24 hours prior to use. A saturated potassium chloride calomel reference electrode (SCE) and a platinum mesh counter electrode were used as reference and counter electrodes, respectively. The electrochemical cell was thermostated to $\pm 1\ ^0C$.

In the absence of thin layer voltammetric behaviour at slow scan rates (see Section 3.3.1), surface coverages were estimated by coulometry. In this approach, the potential of the working electrode was stepped to 1.0 V (approximately 600 mV

past the formal potential of the $Os^{II/III}$ couple) and the charge passed during the exhaustive oxidation of the modifying layer was monitored. Surface coverages for the five metallopolymers were typically in the range of 3.0 to 6.0 x 10^{-8} molcm^{-2}.

Charge transport rates were estimated by cyclic voltammetry, under semi-infinite diffusion conditions (50-500 mVs^{-1}), using the Randles-Sevcik equation. Chronoamperometry was used to determine charge transport rates by stepping from -0.3V to 1.0V over the time range of 0 to 20ms. Potential steps for background correction were made between -0.3V and 0.0V, where no redox reaction occurred. For both the redox active potential step and for background correction, 5 current decays were averaged. Where necessary, IR compensation was achieved via positive feedback circuitry.

The experimentally determined variable for these charge transport studies is $D_{CT}^{1/2}C$, where D_{CT} is the apparent rate of charge transport and C is the concentration of electroactive sites in the polymer. C was estimated from the individual densities of the dry metallopolymers which were measured by floatation in non-swelling solvents, hexane and carbon tetrachloride [11]. The concentrations determined for the individual polymers under investigation were : $OsPVP_{100}$ 0.70M, $OsPVP_{75}$ 0.71M, $OsPVP_{67}$ 0.72M, $OsPVP_{50}$ 0.74M and $OsPVP_{33}$ 0.75M. These concentrations were used to estimate D_{CT} from $D_{CT}^{1/2}C$.

Diffusion coefficients and activation parameters were estimated on fresh coatings in order to minimise memory effects [16]. Diffusion coefficients were typically reproducible to within 10% for determinations on different coatings and 4% for repeated determinations on single coatings. Activation parameters were reproducible to within 15% for determinations on different coatings and 7% for repeated determinations on single coatings.

3.3. Results and Discussion.

3.3.1. General Electrochemical Characteristics.

The cyclic voltammetric characteristics of the $OsPVP_{100}$ - $OsPVP_{33}$ series of metallopolymers were probed as a function of the voltammetric scan rate (1 to 500 mVs^{-1}) in $HClO_4$ and $LiClO_4$ electrolytes. In these electrolytes, ideal surface or thin layer behaviour was not observed for any of the metallopolymers, even at scan rates as low as 1 mVs^{-1}. This behaviour is likely a result of the slow transport of charge through these metallopolymers, reflecting their compact and dehydrated nature in perchlorate electrolytes (see Chapter 2). Similar observations have been previously reported for the $OsPVP_{100}$ polymer in $HClO_4$ electrolyte [17]. The voltammetric characteristics of these metallopolymers, over the complete range of scan rates, are characteristic of a diffusion controlled voltammetric response.

The formal potential of the $Os^{II/III}$ couple in these polymers was taken as the average of the anodic and cathodic peak potentials. These formal potentials were shifted positively in all electrolytes upon incorporation of styrene into the polymer backbone. This positive shift indicates that it becomes more difficult to oxidise the Os^{II} sites on incorporation of styrene into the polymer backbone. Whilst the exact origins of this effect are unknown, it is likely a consequence of the hydrophobic nature of the styrene moieties. Similar behaviour was observed for the ruthenium analogues of these polymers [11].

3.3.2. Investigation of Charge Transport Processes.

For the cyclic voltammetric experiments, linear peak-current versus square root of scan rate plots were observed for scan rates of 1 to 500 mVs^{-1}, suggesting semi-infinite diffusion conditions prevail and permitting the evaluation of the charge transport rate as the apparent diffusion coefficient, $D_{CT}(CV)$, using the Randles-

Sevcik equation. Fig. 3.1 illustrates the dependence of the anodic peak current on the square root of scan rate for the $OsPVP_{100}$ and $OsPVP_{33}$ polymers at scan rates of 50 to 500 mVs^{-1} in 0.1M $LiClO_4$. The characteristics of these plots are representative of the general behaviour of the five metallopolymers in $LiClO_4$ and $HClO_4$ electrolytes.

Potential step chronoamperometry was employed in conjunction with the Cottrell equation to estimate charge transport rates as the apparent diffusion coefficient, $D_{CT}(PS)$. Fig. 3.2 illustrates Cottrell plots for the $OsPVP_{100}$ and $OsPVP_{33}$ polymers in 0.1M $LiClO_4$. In general, plots of i(t) vs $t^{-1/2}$ were linear over the timescale 0 to 20ms and exhibited zero current intercepts for all polymer/ electrolyte combinations. The accurate evaluation of charge transport rates using the models employed in this study requires that the response be diffusional in character and that migrational effects be absent. Perturbation of the diffusional current by other components is indicated by a non zero intercept on the current axis of the Cottrell plot [18] or by a peak in the $it^{1/2}$ vs $t^{1/2}$ plot [19]. Neither of these conditions are observed for the metallopolymers under investigation, suggesting that migrational effects are absent.

Activation parameters have been used previously to aid in the diagnosis of the rate determining step of the charge transport process [1-5,9-13]. Activation energies for the charge transport process were estimated from the temperature dependence of the charge transport diffusion coefficient, as estimated by cyclic voltammetry and chronoamperometry, over the temperature range of 278 to 308 K. Linear Arrhenius plots of ln D_{CT} vs T^{-1} were observed for all polymer/ electrolyte combinations over this temperature range. Fig. 3.3 illustrates the temperature dependence of $D_{CT}(CV)$ for the $OsPVP_{33}$ polymer in 0.1M $HClO_4$. Activation entropies were estimated from the Eyring equation. The absolute values of these entropy terms are acknowledged to be of limited accuracy since the intersite separation of the redox sites is only approximated using a rigid rod model of the polymer structure [20]. However, even allowing for a large variation in polymer swelling, a significant departure from the

Fig. 3.1. Plots of anodic peak current vs the square root of scan rate (50 to 500 mVs^{-1}) for the $OsPVP_{33}$ and $OsPVP_{100}$ metallopolymers in 0.1M $LiClO_4$.

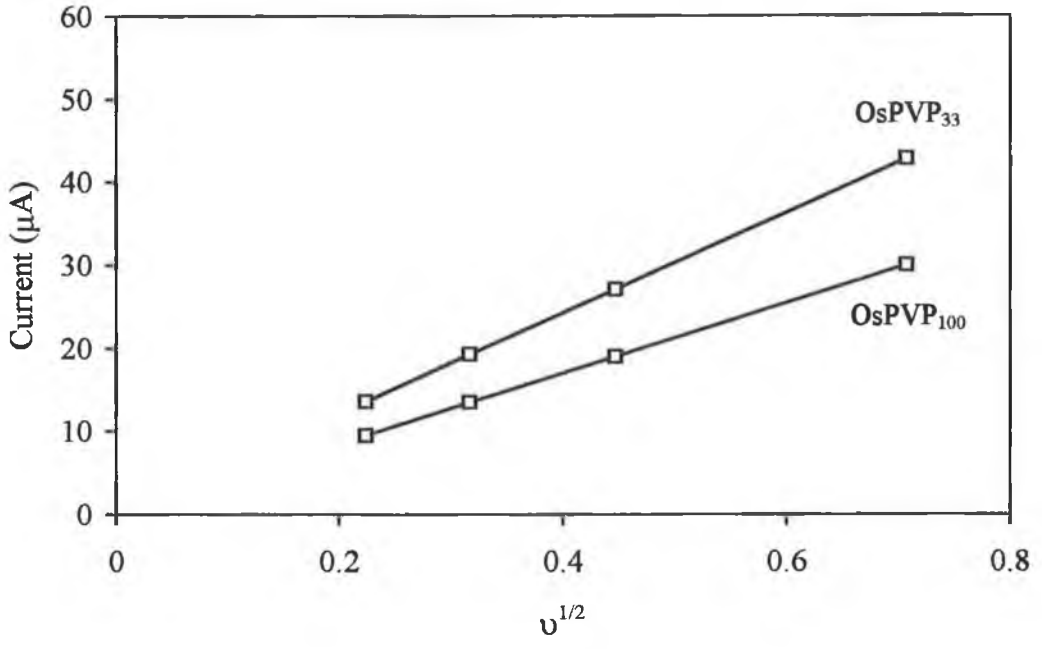

Fig. 3.2. Cottrell response of $OsPVP_{33}$ and $OsPVP_{100}$ polymers in 0.1M $LiClO_4$.

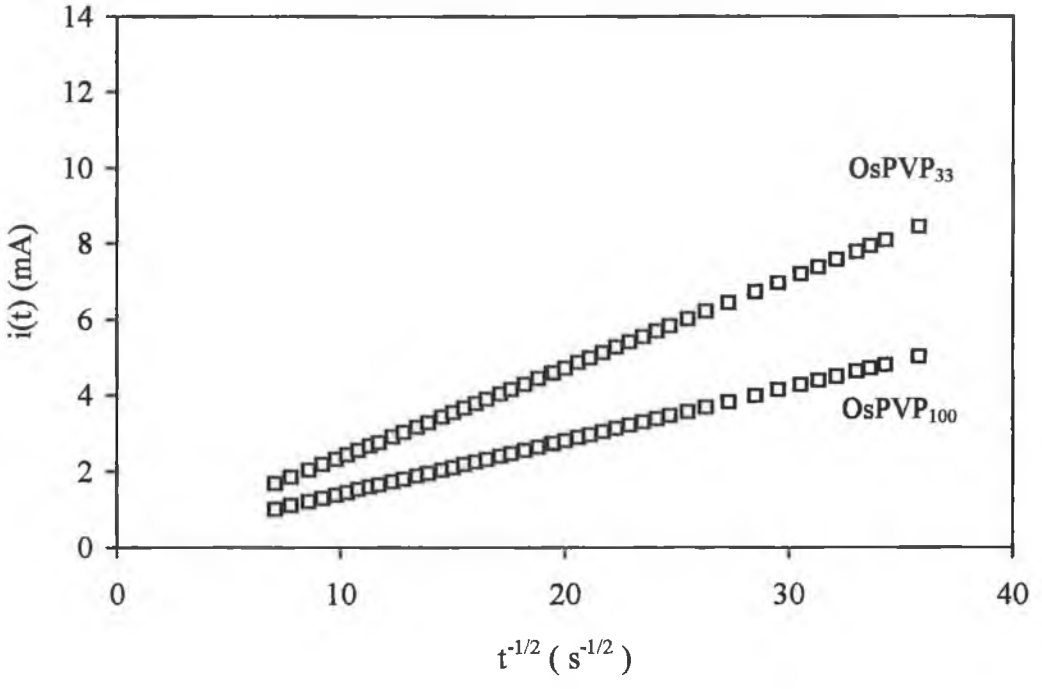

Fig. 3.3. The temperature dependence of $D_{CT}(CV)$ for the $OsPVP_{33}$ polymer in 0.1M $HClO_4$.

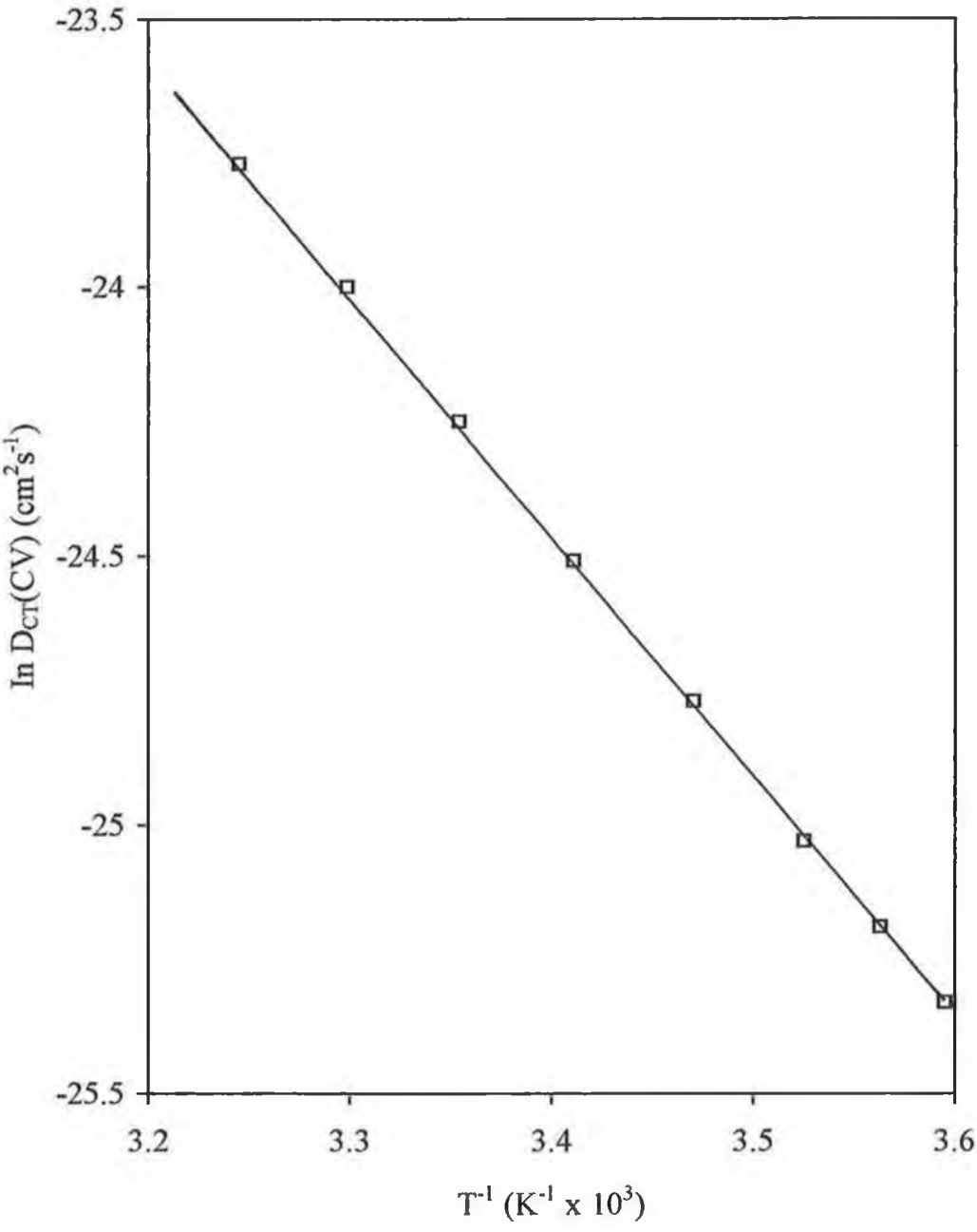

assumed value of δ does not change the sign of the entropy terms calculated and the observed trends should remain valid [4]. It has been suggested previously that negative entropies are associated with either electron hopping or ion motion rate determining steps [21] whilst positive entropy can be assigned to disordering polymer chain motion [1-4]. In the analysis presented here, this interpretation is followed.

3.3.2.1. Perchloric Acid.

In Chapter 2, the influence of $HClO_4$ electrolyte concentration on the resident layer mass and rigidity of the $OsPVP_{75}$ - $OsPVP_{33}$ metallopolymers was probed. In this electrolyte, the strong interaction between the perchlorate anion and the PVP units of the polymer backbone [14,15] results in crosslinked, dehydrated layers (see Chapter 2). Furthermore, in Chapter 2, it was found that the rigidity of these metallopolymers increases with increasing styrene content of the copolymer backbone as a result of the reduced solvent and ion content. This behaviour is a consequence of the increased hydrophobic nature of these polymers with increasing styrene content of the polymer backbone and the reduced requirement for anion influx to maintain electroneutrality within the protonated polymer.

Table 3.1 summarises the apparent charge transport diffusion coefficients for the $Os^{II/III}$ oxidation, estimated for the $OsPVP_{100}$ - $OsPVP_{33}$ metallopolymers in 0.1M and 1.0M $HClO_4$ electrolytes. Fig. 3.4 illustrates the dependence of $D_{CT}(CV)$ on the styrene content of the metallopolymer backbone in 0.1M and 1.0M $HClO_4$ (data taken from Table 3.1).

0.1M $HClO_4$

In 0.1M $HClO_4$, addition of styrene to the polymer backbone causes $D_{CT}(CV)$ to initially decrease and then increase for the higher styrene content polymers. In the estimation of these charge transport rates the experimentally determined variable is $D_{CT}^{1/2}C$. Therefore, comparative differences in $D_{CT}^{1/2}C$ may result from either

Table 3.1. The effect of $HClO_4$ electrolyte concentration on the rate of charge transport through $OsPVP_{100}$ - $OsPVP_{33}$ electrode coatings, as determined by cyclic voltammetry (CV) and potential step (PS) techniques.

Polymer	$HClO_4$ Conc. (M)	$E_{1/2}$[(a)] (V)	$D_{CT}(CV)$[(b)] $x10^{-11}$ cm^2s^{-1}	$D_{CT}(PS)$[(b)] $x10^{-10}$ cm^2s^{-1}
$OsPVP_{100}$	0.1M	0.249	5.42	1.64
	1.0M	0.197	0.12	2.83
$OsPVP_{75}$	0.1M	0.264	2.09	1.45
	1.0M	0.222	2.21	2.44
$OsPVP_{67}$	0.1M	0.264	2.54	1.52
	1.0M	0.217	2.79	2.54
$OsPVP_{50}$	0.1M	0.262	2.85	1.27
	1.0M	0.204	3.11	2.58
$OsPVP_{33}$	0.1M	0.262	2.95	1.76
	1.0M	0.201	3.30	2.77

(a) Estimated from the 1 mVs^{-1} cyclic voltammogram.

(b) The variations between individual coatings are ±10%.

Fig. 3.4. The dependence of $D_{CT}(CV)$ on the styrene content of $OsPVP_{100}$ - $OsPVP_{33}$ electrode coatings in 0.1M (□) and 1.0M (◊) $HClO_4$.

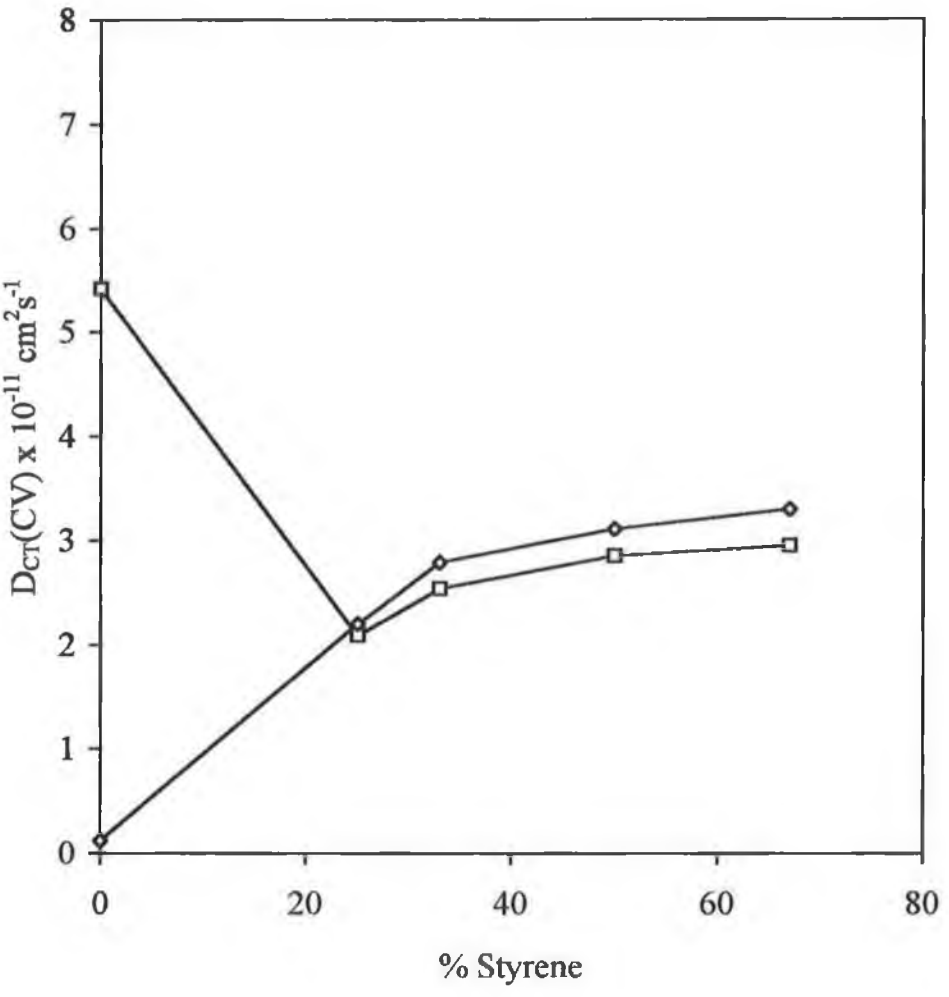

variations in the actual diffusion coefficient or variations in the individual redox site concentrations of these polymers. For the $OsPVP_{75}$ - $OsPVP_{33}$ polymers, the observed increase in $D_{CT}(CV)$ with increasing styrene content is quite small and may reflect the greater concentration of fixed sites within the more compact, higher styrene content polymers (see Chapter 2). For the $OsPVP_{100}$ polymer, the observed increase in $D_{CT}(CV)$ is considered to be real as the fixed site concentration will likely decrease with increasing PVP content of the polymer backbone (see Chapter 2). This increase in $D_{CT}(CV)$ may result from the more favourable interfacial mass transfer processes associated with this comparatively more swollen polymer.

Table 3.2 summarises the activation parameters for the charge transport process in 0.1M and 1.0M $HClO_4$, as determined by cyclic voltammetry. For the $OsPVP_{75}$ - $OsPVP_{33}$ series of polymers, the activation energies are essentially constant ($E_a = 36 \pm 6$ kJmol^{-1}) and independent of the styrene content of the polymer backbone. This observation suggests that the same process limits the rate of charge transport through these $OsPVP_{75}$ -$OsPVP_{33}$ polymers and is consistent with the observation of only small changes in the charge transport rate for these materials, as a function of the styrene content of the polymer backbone. These activation energies are all coupled with large negative entropy terms which may reflect either electron hopping or ion motion limitations [21]. However, it is considered that ion motion rather than electron hopping represents the rate determining step of charge transport in these polymers as charge transport rates for electron hopping are typically two orders of magnitude higher than those quoted here [5]. This ion diffusion limitation is likely a consequence of the compact and dehydrated nature of these materials in perchloric acid electrolytes.

In 0.1M $HClO_4$, Arrhenius plots for the $OsPVP_{100}$ polymer exhibit two distinct linear regions. This behaviour has been observed previously for this particular polymer [1,3] and for a ruthenium copolymer [12] in perchlorate electrolytes. At temperatures less than 288K, $E_a(CV)$ is 35 kJmol^{-1} and is of a similar magnitude to

Table 3.2. Activation parameters for charge transport through $OsPVP_{100}$ - $OsPVP_{33}$ electrode coatings in $HClO_4$ electrolytes, as determined by cyclic voltammetry (CV).

	0.1M $HClO_4$			1.0M $HClO_4$		
Polymer	$E_a(CV)$ ($kJmol^{-1}$)	$\Delta S(CV)^{\neq}$ ($Jmol^{-1}K^{-1}$)	$\Delta G(CV)^{\neq}$ ($kJmol^{-1}$)	$E_a(CV)$ ($kJmol^{-1}$)	$\Delta S(CV)^{\neq}$ ($Jmol^{-1}K^{-1}$)	$\Delta G(CV)^{\neq}$ ($kJmol^{-1}$)
$OsPVP_{100}$				92	105	58
T<288 K	35	-104	63			
T>288 K	159	290	70			
$OsPVP_{75}$	40	-83	62	47	-59	62
$OsPVP_{67}$	41	-76	61	42	-71	61
$OsPVP_{50}$	35	-97	61	39	-89	63
$OsPVP_{33}$	29	-115	61	35	-93	60

The variations between individual coatings are ±15%.

the activation energies observed for the other polymers. This small activation energy and coupled negative entropy term again suggest that ion motion is limiting [21]. At temperatures in excess of 288K, E_a(CV) increases to 159 $kJmol^{-1}$ and the entropy term becomes positive. This large activation energy and coupled positive entropy term may indicate that polymer chain motions are limiting [1-4]. It has been suggested previously that the $OsPVP_{100}$ polymer may swell at temperatures in excess of 288K and that the large positive entropy may reflect the requirement for polymer chains motions to reduce the intersite separation to allow for electron transfer to occur [3]. This behaviour is consistent with the observations made in Chapter 2 that, in this electrolyte, the $OsPVP_{100}$ polymer is comparatively more swollen than the styrene based copolymers. This behaviour is not observed for the styrene based copolymers which illustrates that their inherent polymer properties are different

1.0M $HClO_4$

On increasing the electrolyte concentration to 1.0M $HClO_4$, the rate of charge transport through the $OsPVP_{100}$ polymer decreases. The rigidity, and therefore the fixed site concentration, of the $OsPVP_{100}$ [17] and $OsPVP_{75}$ - $OsPVP_{33}$ polymers (see Chapter 2) is maintained on increasing the electrolyte concentration from 0.1M to 1.0M $HClO_4$. The observed decrease in D_{CT}(CV) for the $OsPVP_{100}$ is therefore real and is not a consequence of a decrease in the fixed site concentration. For the $OsPVP_{75}$ - $OsPVP_{33}$ polymers, D_{CT}(CV) remains largely unchanged with increasing perchloric acid concentration. Table 3.2 summarises the activation parameters for these polymers in 1.0M $HClO_4$. For the $OsPVP_{75}$ - $OsPVP_{33}$ polymers, E_a(CV) is clearly independent of the styrene content of the polymer backbone and exhibits little variation between 0.1M and 1.0M $HClO_4$ electrolyte concentrations. This concentration independence of the activation data for $OsPVP_{75}$ - $OsPVP_{33}$ reflects the concentration independence of D_{CT}(CV) and illustrates that the rate limiting process (ion motion) is unaffected by increasing the electrolyte concentration. This behaviour

again reflects the compact nature of these polymers in these $HClO_4$ electrolytes.

For $OsPVP_{100}$, $D_{CT}(CV)$ decreases by a factor of approximately 50 on increasing the electrolyte concentration to 1.0M $HClO_4$. $E_a(CV)$ is 92 $kJmol^{-1}$ for this polymer in this electrolyte. This large activation energy coupled with the positive entropy term suggests that polymer motions are rate limiting [1-4]. It has been suggested previously that the observed decrease in $D_{CT}(CV)$ for this polymer is a consequence of further compaction of the layer with increasing $HClO_4$ electrolyte concentration and that the large positive entropy term in 1.0M $HClO_4$ reflects the requirement for polymer chain motions to allow for anion and solvent ingress [1]. More recently, however, it has been demonstrated that the rigidity of $OsPVP_{100}$ coatings do not in fact change on increasing the electrolyte concentration from 0.1M to 1.0M $HClO_4$ [17]. However, it is likely that the degree of crosslinking by the perchlorate anion will increase with increasing $HClO_4$ electrolyte concentration. Therefore, the observed decrease in $D_{CT}(CV)$ in 1.0M $HClO_4$ may actually reflect the greater difficulty in anion ingress as a consequence of this enhanced crosslinking effect. This suggestion is consistent with EQCM studies of the $OsPVP_{100}$ polymer in these electrolytes which clearly illustrate that, on increasing the $HClO_4$ electrolyte concentration, interfacial mass transfer becomes more impeded [22]. This behaviour is not observed for the $OsPVP_{75}$ - $OsPVP_{33}$ polymers which may reflect the smaller PVP content of these polymers and,thus, a reduction in this crosslinking effect. The influence of interfacial mass transfer limitations on the charge transport process is examined in Chapter 4 and Chapter 5.

Table 3.1 and Fig. 3.5 illustrate the dependence of $D_{CT}(PS)$ on the styrene content of the metallopolymer backbone in 0.1M and 1.0M $HClO_4$. In these experiments, $D_{CT}(PS)$ is an order of magnitude greater than $D_{CT}(CV)$. Similar observations have been reported previously for the $OsPVP_{100}$ polymer in perchlorate electrolytes and are discussed below [1,3,4]. Table 3.3 summarises the associated

Fig. 3.5. The dependence of $D_{CT}(PS)$ on the styrene content of $OsPVP_{100}$ - $OsPVP_{33}$ electrode coatings in 0.1M (□) and 1.0M (◊) $HClO_4$.

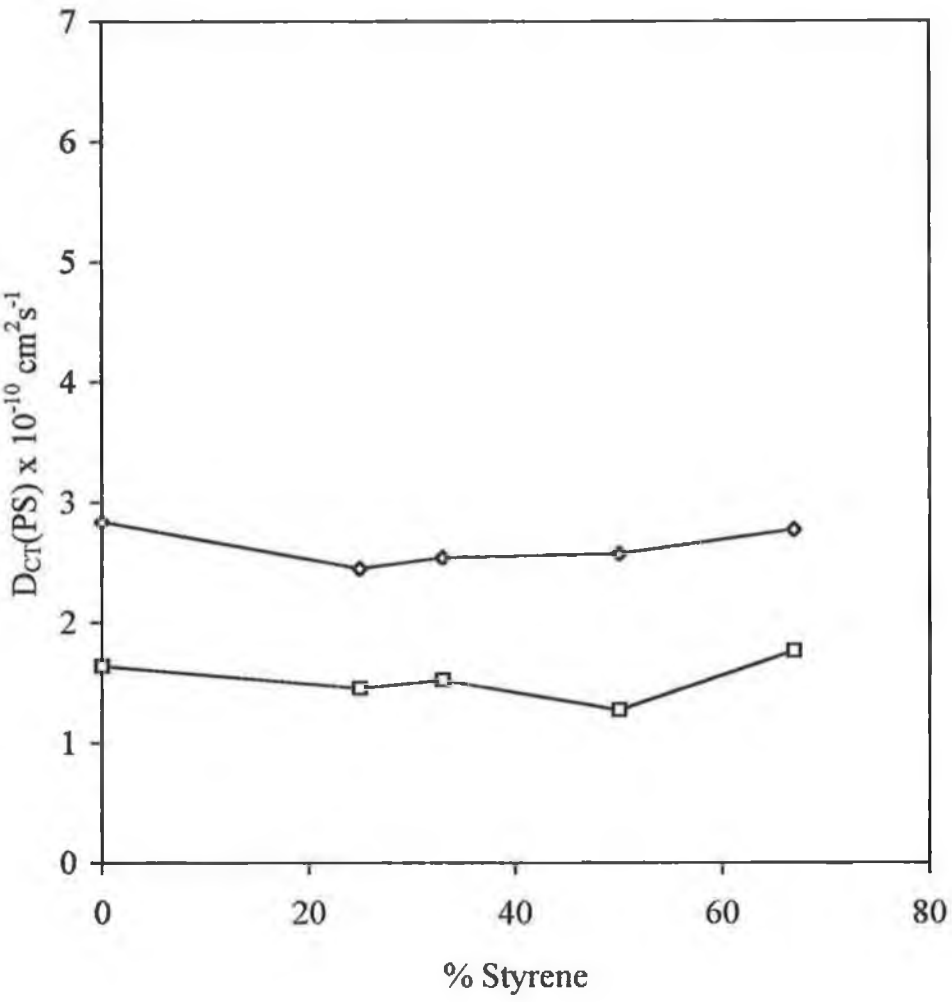

activation parameters, estimated from the temperature dependence of D_{CT}(PS). In 0.1M $HClO_4$, D_{CT}(PS) is largely independent of the styrene content of the polymer backbone, which suggests that a common process limits the rate of charge transport in these polymers. This observation is supported by the activation data. For these polymers, E_a(PS) is essentially independent of the styrene content of the polymer backbone. The small activation energies observed, coupled with the negative entropy terms, suggest, as was observed for the cyclic voltammetric experiments, that ion motion is rate limiting [21].

On increasing the electrolyte concentration to 1.0M $HClO_4$, D_{CT}(PS) increases slightly for these polymers and, as was observed in 0.1M $HClO_4$, is essentially independent of the styrene content of the polymer backbone (see Fig. 3.5). The activation parameters summarised in Table 3.3 illustrate that for $OsPVP_{75}$ - $OsPVP_{33}$ polymers, the activation parameters are almost identical to those observed in 0.1M $HClO_4$ and are independent of the styrene content of the polymer backbone. Consequently, as was observed for the cyclic voltammetric experiments, ion motion is possibly the rate determining step of charge transport in the $OsPVP_{75}$ - $OsPVP_{33}$ polymers in 0.1M and 1.0M $HClO_4$ electrolyte concentrations.

For the $OsPVP_{100}$ polymer in 1.0M $HClO_4$, the Arrhenius plot, as determined from D_{CT}(PS), exhibits two distinct linear regions. At temperatures less than 288K, E_a(CV) is 53 $kJmol^{-1}$ and is coupled with a small negative entropy which again suggests that ion motion is limiting [21]. At temperatures in excess of 288K, E_a(CV) increases to 134 $kJmol^{-1}$ and the entropy term becomes positive. This large activation energy and coupled positive entropy term suggest that polymer chain motions are limiting [1-4]. This behaviour contrasts with that observed for the copolymers and is surprising considering the independence of D_{CT}(PS) to the styrene content of the polymer backbone.

Table 3.3. Activation parameters for charge transport through $OsPVP_{100}$ - $OsPVP_{33}$ electrode coatings in $HClO_4$ electrolytes, as determined by chronoamperometry (PS).

	0.1M $HClO_4$			1.0M $HClO_4$		
Polymer	E_a(PS) ($kJmol^{-1}$)	$\Delta S(PS)^{\neq}$ ($Jmol^{-1}K^{-1}$)	$\Delta G(PS)^{\neq}$ ($kJmol^{-1}$)	E_a(PS) ($kJmol^{-1}$)	$\Delta S(PS)^{\neq}$ ($Jmol^{-1}K^{-1}$)	$\Delta G(PS)^{\neq}$ ($kJmol^{-1}$)
$OsPVP_{100}$	25	-108	55			
T<288 K				53	-25	58
T>288 K				134	251	57
$OsPVP_{75}$	17	-135	55	15	-153	58
$OsPVP_{67}$	12	-156	56	19	-140	58
$OsPVP_{50}$	12	-157	56	21	-126	56
$OsPVP_{33}$	21	-127	56	19	-131	56

The variations between individual coatings are ±15%.

In these studies, D_{CT}(PS) differs from D_{CT}(CV) by an order of magnitude. The dependence of the rate of charge transport on the experimental technique used in its measurement is commonly observed for osmium and ruthenium metallopolymers [1-4,11,13]. It has been proposed that these differences in D_{CT} may represent either a dependence on the experimental time scale or the region of the film in which it is evaluated [2-4,11]. For the $OsPVP_{75}$ - $OsPVP_{33}$ polymers, the activation parameters suggest that ion motion limitations control both D_{CT}(CV) and D_{CT}(PS). Furthermore, E_a(CV) is consistently larger than E_a(PS), which may reflect the existence of greater ion motion limitations. This is not surprising considering the nature of ion motion is decidedly different for the two techniques [3,4]. In CV, the more extensive oxidation of the layers requires counterion diffusion to occur over larger regions of the layer than in short timescale PS experiments. Furthermore, the quantity of diffusing counterions is considerably larger in cyclic voltammetry experiments. Alternatively, it is also possible that the larger D_{CT}(PS) may reflect a greater concentration of redox centres in the relatively more compact base layer. However, the difference between D_{CT}(CV) and D_{CT}(PS) would require differential swelling of over 300% [2-4,11].

For the $OsPVP_{100}$ polymer in 0.1M $HClO_4$, the activation parameters suggest that different equilibria are established during the cyclic voltammetry and potential step experiments. $\Delta S(CV)^{\neq}$ is positive which suggests that polymer chain motion represents the rate determining step of charge transport, whilst $\Delta S(PS)^{\neq}$ is negative which suggests that ion motion is rate limiting. These observations are likely a consequence of the fact that on longer timescales all mobile species, ions, electrons, polymer chains and solvent, can attain equilibrium positions. However, for potential step methods it is possible that only redox equilibrium can be established for counterions and electrons.

In summary, the data in Table 3.1 illustrate that in perchloric acid electrolytes the charge transport rates for the $OsPVP_{75}$ - $OsPVP_{33}$ polymers, as estimated by both

cyclic voltammetry and chronoamperometry, are essentially independent of the styrene content of the polymer backbone. This behaviour is reflected in the activation parameters (see Table 3.2 and Table 3.3) which illustrate that a common rate determining step, namely ion motion, exists for these metallopolymers under these conditions. Furthermore, increasing the electrolyte concentration from 0.1M to 1.0M $HClO_4$ appears to have little influence on the observed charge transport rates, with D_{CT}(CV) essentially independent of the electrolyte concentration and D_{CT}(PS) increasing by only ca. 2x on increasing the electrolyte concentration. This behaviour is again reflected by the activation parameters which are independent of the $HClO_4$ electrolyte concentration. These observations are likely a consequence of the compact nature of these metallopolymers in $HClO_4$ electrolytes.

For the $OsPVP_{100}$ polymer, the charge transport rates estimated by cyclic voltammetry are different from those observed for the copolymers. This suggests that the presence of styrene in the polymer backbone influences the charge transport properties of these materials. Furthermore, for the $OsPVP_{100}$ polymer, only the activation parameters obtained in the potential step experiments in 0.1M $HClO_4$ are comparable with the corresponding data obtained for the styrene based copolymers. The remaining activation data suggest that polymer chain motions are limiting in $OsPVP_{100}$. Therefore, while polymer chain motion limits the rate of charge transport in $OsPVP_{100}$, ion motion limits the rate of charge transport in the $OsPVP_{75}$ - $OsPVP_{33}$ polymers.

It is suggested that in 0.1M $HClO_4$ the polymer chain motion limitations of the $OsPVP_{100}$ polymer, at temperatures in excess of 288K, may represent the requirement for juxtaposition of the redox sites to allow for electron transfer to occur [3]. This suggestion is consistent with the observed decrease in layer rigidity with increasing PVP content of the polymer backbone (see Chapter 2). Under these conditions one might anticipate a transition in the rate determining step from ion motion control for the more compact styrene based copolymers to polymer motion

control for the relatively more swollen $OsPVP_{100}$ polymer. For the $OsPVP_{100}$ polymer in 1.0M $HClO_4$, it is suggested that the increased crosslinking of the layer in this $HClO_4$ concentration results in polymer chain motion limitations to allow for the influx of solvent and charge compensating counterions. As a consequence of this limitation, the charge transport rate for $OsPVP_{100}$ ($D_{CT}(CV)$) decreases dramatically in 1.0M $HClO_4$. This behaviour is not observed for any of the copolymers, which reflects their reduced PVP content and, by implication, a reduction in the crosslinking effect. These charge transport studies therefore highlight the different structural properties of these polymers.

3.3.2.2. Lithium Perchlorate.

Table 3.4 and Fig. 3.6 illustrate the dependence of $D_{CT}(CV)$ on the styrene content of the polymer backbone in 0.1M and 1.0M $LiClO_4$. The charge transport rates observed for the $OsPVP_{75}$ - $OsPVP_{33}$ polymers are of a similar magnitude to those observed in $HClO_4$, which suggests that the electrolyte cation plays only a minor role in the charge transport process. In 0.1M $LiClO_4$, $D_{CT}(CV)$ is independent on the styrene content of the polymer backbone. In 1.0M $LiClO_4$, there is a slight increase in $D_{CT}(CV)$ with increasing styrene content of the polymer backbone. In this electrolyte, the rigidity of $OsPVP_{33}$ and $OsPVP_{100}$ coatings are similar (see Chapter 2). This slight increase in $D_{CT}(CV)$ is therefore considered to be real.

Table 3.5 summarises the activation parameters associated with the change transport process, as determined by cyclic voltammetry. In 0.1M and 1.0M $LiClO_4$, $E_a(CV)$ varies only slightly as a function of the styrene content of the polymer backbone and the $LiClO_4$ concentration of the bathing electrolyte, for all five metallopolymers. These activation energies are coupled with negative entropies which suggest that ion motion is rate limiting in these polymers. For the $OsPVP_{75}$ - $OsPVP_{33}$ polymer, $E_a(CV)$ is of a similar magnitude to the corresponding data

Table 3.4. The effect of $LiClO_4$ electrolyte concentration on the rate of charge transport through $OsPVP_{100}$ - $OsPVP_{33}$ electrode coatings as determined by cyclic voltammetry (CV) and potential step (PS) techniques.

Polymer	$LiClO_4$ Conc. (M)	$E_{1/2}$[(a)] (V)	$D_{CT}(CV)$[(b)] $x10^{-11}$ cm^2s^{-1}	$D_{CT}(PS)$[(b)] $x10^{-10}$ cm^2s^{-1}
$OsPVP_{100}$	0.1M	0.241	1.48	1.11
	1.0M	0.208	0.65	2.57
$OsPVP_{75}$	0.1M	0.251	1.55	1.05
	1.0M	0.217	1.64	2.65
$OsPVP_{67}$	0.1M	0.269	1.71	1.06
	1.0M	0.217	1.83	2.73
$OsPVP_{50}$	0.1M	0.277	1.85	1.27
	1.0M	0.238	2.15	3.12
$OsPVP_{33}$	0.1M	0.284	1.70	1.57
	1.0M	0.230	2.76	3.19

(a) Estimated from the 1 mVs^{-1} cyclic voltammogram.

(b) The variations between individual coatings are ±10%.

Fig. 3.6. The dependence of $D_{CT}(CV)$ on the styrene content of $OsPVP_{100}$ - $OsPVP_{33}$ electrode coatings in 0.1M (□) and 1.0M (◊) $LiClO_4$.

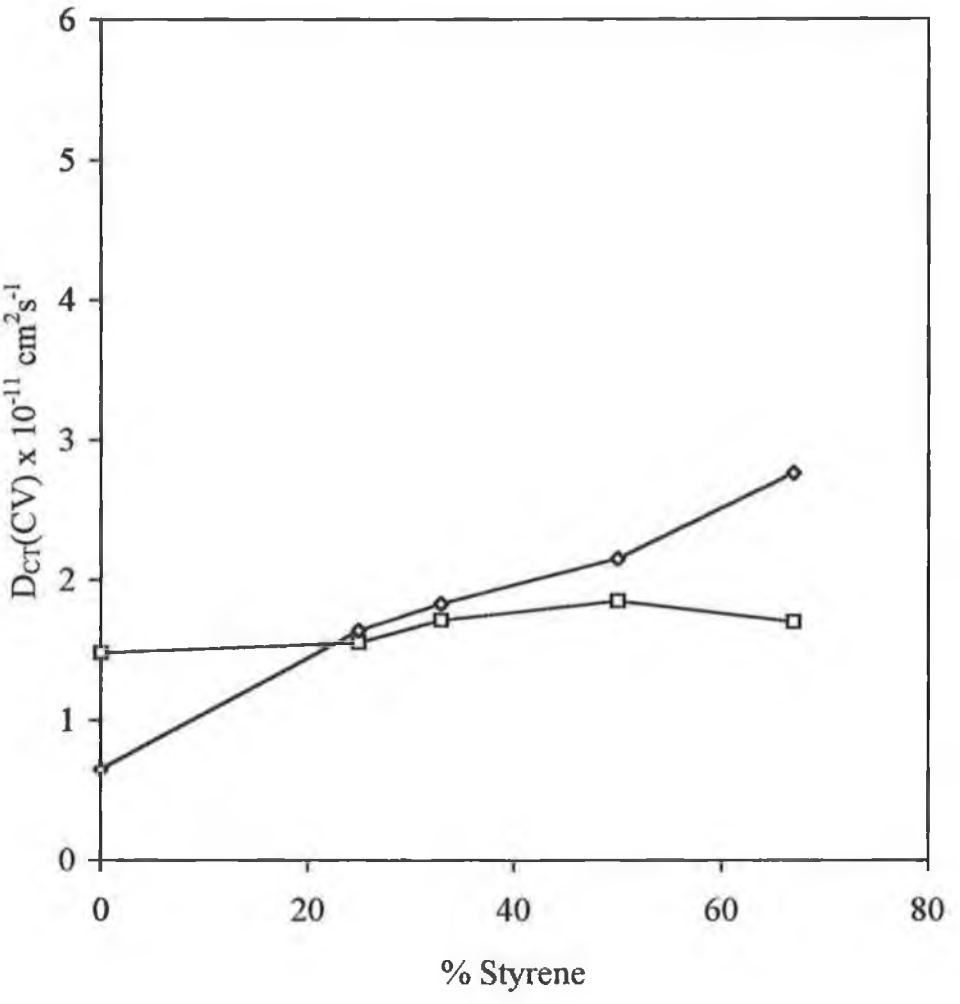

Table 3.5. Activation parameters for charge transport through $OsPVP_{100}$ - $OsPVP_{33}$ electrode coatings in $LiClO_4$ electrolytes, as determined by cyclic voltammetry (CV).

	0.1M $LiClO_4$			1.0M $LiClO_4$		
Polymer	$E_a(CV)$ ($kJmol^{-1}$)	$\Delta S(CV)^{\neq}$ ($Jmol^{-1}K^{-1}$)	$\Delta G(CV)^{\neq}$ ($kJmol^{-1}$)	$E_a(CV)$ ($kJmol^{-1}$)	$\Delta S(CV)^{\neq}$ ($Jmol^{-1}K^{-1}$)	$\Delta G(CV)^{\neq}$ ($kJmol^{-1}$)
$OsPVP_{100}$	44	-72	63	52	-42	62
$OsPVP_{75}$	27	-116	59	33	-107	62
$OsPVP_{67}$	35	-89	59	29	-114	61
$OsPVP_{50}$	42	-78	63	35	-94	61
$OsPVP_{33}$	42	-70	60	32	-103	60

The variations between individual coatings are ±15%.

obtained in $HClO_4$ (see Table 3.2). Consequently, the charge transport properties of these polymers are controlled by the same process in $LiClO_4$ and $HClO_4$ electrolytes.

On increasing the electrolyte concentration to 1.0M $LiClO_4$, $D_{CT}(CV)$ decreases slightly for $OsPVP_{100}$, remains constant for $OsPVP_{75}$ - $OsPVP_{50}$ and increases slightly for $OsPVP_{33}$. It is considered that these variations in $D_{CT}(CV)$ are real and do not reflect variations in the redox site concentration (see Chapter 2). The increase in $D_{CT}(CV)$ for the $OsPVP_{33}$ polymer may reflect the slightly less compact nature of this polymer in 1.0M $LiClO_4$ (see Chapter 2) and its more favourable mass transfer properties (see Chapter 5). For the $OsPVP_{100}$ polymer in $HClO_4$ electrolytes, $D_{CT}(CV)$ decreased on increasing the electrolyte concentration from 0.1M to 1.0M $HClO_4$ (see Section 3.3.2.1). This behaviour is again observed for this polymer in $LiClO_4$ electrolytes, however the effect is greatly reduced i.e. $D_{CT}(CV)$ decreases by only 2x in $LiClO_4$ compared with 50x in $HClO_4$. Furthermore, in $LiClO_4$ electrolytes the activation parameters are independent of the $LiClO_4$ electrolyte concentration and suggest that ion motion is rate limiting. However, in 1.0M $HClO_4$ the activation parameters suggest that polymer chain motions are limiting. In $HClO_4$, it was suggested that the decrease may reflect the increased crosslinking of the polymer in the higher electrolyte concentration (see Section 3.3.2.1). It is anticipated that this crosslinking effect will be greatly reduced in $LiClO_4$ electrolytes, as the PVP units of the polymer backbone are unprotonated. This suggestion is consistent with the observed smaller decrease in $D_{CT}(CV)$ in $LiClO_4$ electrolytes.

Table 3.4 and Fig. 3.7 illustrate the dependence of $D_{CT}(PS)$ on the styrene content of the polymer backbone in 0.1M and 1.0M $LiClO_4$. The charge transport rates observed in these electrolytes are almost identical to the corresponding data obtained in $HClO_4$ electrolytes (see Section 3.3.2.1). In 0.1M and 1.0M $LiClO_4$, $D_{CT}(PS)$ is largely independent of the styrene content of the polymer backbone. Table 3.6 summarises the activation parameters associated with these charge transport processes. $E_a(PS)$ is independent of the styrene content of the polymer backbone and

Fig. 3.7. The dependence of $D_{CT}(PS)$ on the styrene content of $OsPVP_{100}$ - $OsPVP_{33}$ electrode coatings in 0.1M (□) and 1.0M (◊) $LiClO_4$.

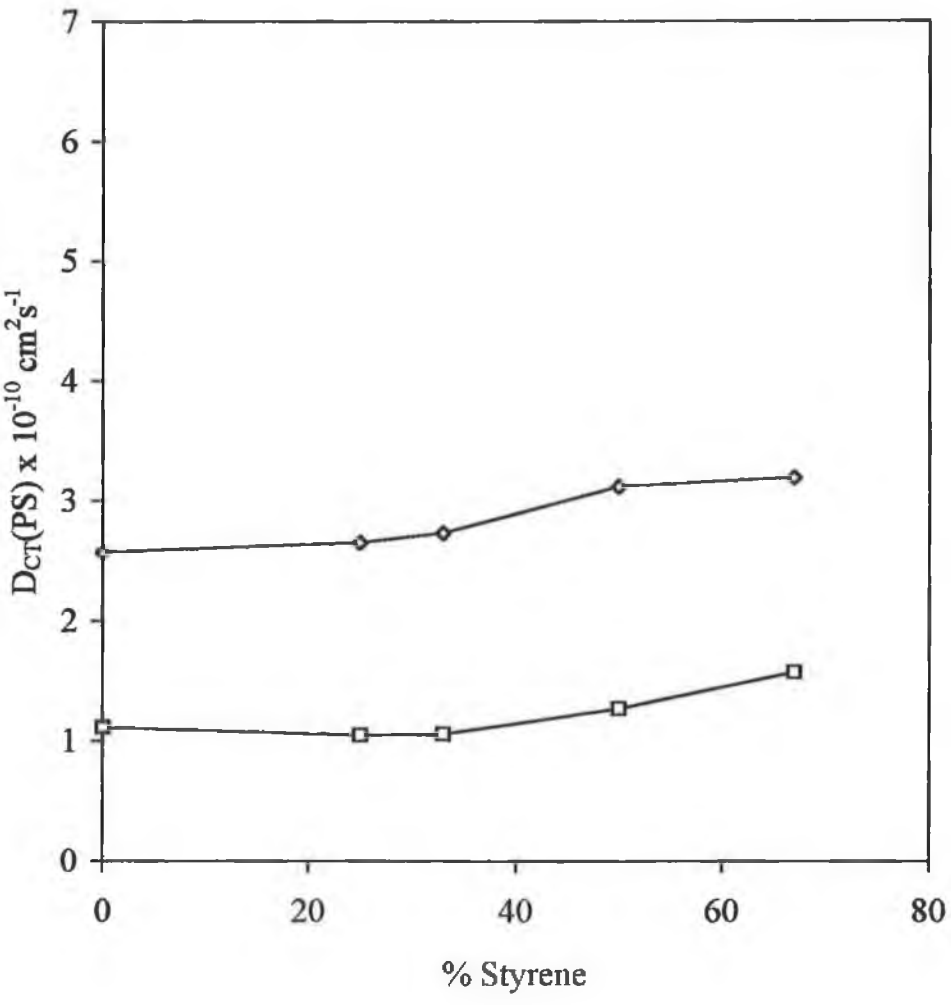

Table 3.6. Activation parameters for charge transport through $OsPVP_{100}$ - $OsPVP_{33}$ electrode coatings in $LiClO_4$ electrolytes, as determined by chronoamperometry (PS).

	0.1M $LiClO_4$			1.0M $LiClO_4$		
Polymer	$E_a(PS)$ ($kJmol^{-1}$)	$\Delta S(PS)^{\neq}$ ($Jmol^{-1}K^{-1}$)	$\Delta G(PS)^{\neq}$ ($kJmol^{-1}$)	$E_a(PS)$ ($kJmol^{-1}$)	$\Delta S(PS)^{\neq}$ ($Jmol^{-1}K^{-1}$)	$\Delta G(PS)^{\neq}$ ($kJmol^{-1}$)
$OsPVP_{100}$	20	-135	58	12	-161	58
$OsPVP_{75}$	11	-168	59	17	-142	57
$OsPVP_{67}$	13	-153	56	17	-138	56
$OsPVP_{50}$	9	-171	57	14	-150	56
$OsPVP_{33}$	7	-174	56	12	-156	56

The variations between individual coatings are ±15%.

the $LiClO_4$ electrolyte concentration. As was observed in $HClO_4$, the entropy terms are all negative, which again suggests that ion motion limitations exist in these polymers.

In summary, in $LiClO_4$ and $HClO_4$ electrolytes, the charge transport properties of the $OsPVP_{75}$ - $OsPVP_{33}$ polymers vary only slightly as a function of both the perchlorate electrolyte type and concentration and the styrene content of the polymer backbone. In these electrolytes, the activation parameters suggest that ion diffusion represents the rate determining step of charge transport in these redox copolymers. This observation is considered to reflect the compact and dehydrated nature of these coatings in these electrolytes (see Chapter 2). For the $OsPVP_{100}$ polymer in these electrolytes, the charge transport rates estimated by chronoamperometry are almost identical to those observed for the copolymers. Similarly, the activation data evaluated from the temperature dependence of $D_{CT}(PS)$ illustrate that, excluding the data obtained at temperatures in excess of 288K in 1.0M $HClO_4$, ion motion likely limits the charge transport processes in the $OsPVP_{100}$ polymer. However, for the $OsPVP_{100}$ polymer, the charge transport rates estimated by cyclic voltammetry are, with the exception of $D_{CT}(CV)$ in 0.1M $LiClO_4$, different from the charge transport rates obtained for the $OsPVP_{75}$ - $OsPVP_{33}$ polymers. The activation data evaluated from the temperature dependence of $D_{CT}(CV)$ illustrate that, excluding the data in $LiClO_4$, polymer chain motions may limit charge transport in the $OsPVP_{100}$ polymer. It is suggested that these polymer chain motion limitations may reflect the more swollen (0.1M $HClO_4$) and crosslinked (1.0M $HClO_4$) structure of the $OsPVP_{100}$ polymer in these electrolytes.

3.3.2.3. Comparison with $[Ru(bipy)_2(PVP_x)_{10}Cl]^+$ Films.

The charge transport properties of the ruthenium analogues of these metallopolymers, $RuPVP_{100}$ - $RuPVP_{33}$, have been probed as a function of the styrene content of the polymer backbone [11]. In 0.1M and 1.0M $HClO_4$, $D_{CT}(CV)$ increases with increasing styrene content. Activation entropies for the $RuPVP_{75}$ - $RuPVP_{33}$ polymers in these electrolytes are all negative and independent of the $HClO_4$ electrolyte concentration and the styrene content of the polymer backbone. Similar behaviour is reported here for the osmium analogues. It has been suggested that the increase in $D_{CT}(CV)$ with increasing styrene content of the backbone is a consequence of more facile ion transport within the less compact higher styrene content polymers [11]. However, the admittance data in Chapter 2 clearly illustrate that the rigidity of the osmium polymers increases with increasing styrene content.

In Section 3.3.2.1, reference was made to the findings of an EQCM study of the mass transfer properties of the $OsPVP_{100}$ polymer [22] in which good correlation was observed between the rate of charge transport and the ease of solvent transfer through this particular polymer. In Chapter 4 and Chapter 5, the mass transfer properties of the $OsPVP_{100}$ and $OsPVP_{33}$ polymers are studied as a function of the $LiClO_4$ and $HClO_4$ ($OsPVP_{33}$ only) electrolyte concentration to probe for a similar correlation in these polymers.

3.4. Conclusions.

The charge transport properties of the $OsPVP_{100}$ - $OsPVP_{33}$ polymers were probed as a function of the $HClO_4$ and $LiClO_4$ electrolyte concentration. With the exception of $D_{CT}(CV)$ in $HClO_4$, there appears to be only small variations in the rate of charge transport through these materials with increasing styrene content of the polymer backbone. This observation has important implications for the future application of these materials, as it illustrates that the rigidity and therefore the stability of these electrode modifying materials may be improved without adversely affecting their charge transport properties. The activation parameters suggest, however, that depending on the experimental timescale and the perchlorate electrolyte type, the rate determining step of charge transport is altered upon incorporation of styrene moieties into the polymer backbone. The potential step activation data suggest that, in general, ion motion is the rate determining step of charge transport in these redox polymers. Similar observations were made from the cyclic voltammetric activation parameters in $LiClO_4$. However, in $HClO_4$, the cyclic voltammetric activation data suggest that the rate limiting step is changed from ion motion for the $OsPVP_{75}$ - $OsPVP_{33}$ to polymer motion for the $OsPVP_{100}$ polymer. It is considered that this transition in the rate determining step may reflect the more swollen structure of the higher PVP content polymer.

3.5. References.

1. R.J. Forster, A.J. Kelly, J.G. Vos and M.E.G. Lyons, J. Electroanal. Chem., 270 (1989) 365.
2. R.J. Forster and J.G. Vos, J. Electroanal. Chem., 314 (1991) 135.
3. R.J. Forster, J.G. Vos and M.E.G. Lyons, J. Chem. Soc. Faraday Trans., 87 (1991) 3761.
4. R.J. Forster and J.G. Vos, Electrochim. Acta, 37 (1992) 159.
5. R.J. Forster and J.G. Vos, Langmuir, 10 (1994) 4330.
6. H. Larsson and M. Sharp, J. Electroanal. Chem., 381 (1995) 133.
7. M. Sharp and H. Larsson, J. Electroanal. Chem., 386 (1995) 189.
8. M.F. Mathias and O. Haas, J. Phys. Chem., 97 (1993) 9217.
9. C.P. Andrieux in, Electrochemistry, Sensors and Analysis, Analytical Symposia Series, Elsevier, Amsterdam, Vol. 25 (1986) 235.
10. S.M. Oh and L.R. Faulkner, J. Am. Chem. Soc., 111 (1989) 5813.
11. D. Leech, R.J. Forster, M.R. Smyth and J.G. Vos, J. Mater. Chem., 1 (1991) 629.
12. M.E.G. Lyons, H.G. Fay, J.G. Vos and A.J. Kelly, J. Electroanal. Chem., 250 (1988) 207.
13. R.J. Forster and J.G. Vos, J. Inorganic and Organometallic Polymers, 1 (1991) 67.
14. E.F. Bowden, M.F. Dautartas and J.F. Evans, J. Electroanal. Chem., 219 (1987) 91.
15. S.M. Oh and L.R. Faulkner, J. Electroanal. Chem., 269 (1989) 77.
16. A.P. Clarke, J.G. Vos and A.R. Hillman, J. Electroanal. Chem., 356 (1993) 287.
17. A.P. Clarke, J.G. Vos, A. Glidle and A.R. Hillman, J. Chem. Soc. Faraday Trans., 89 (1993) 1695.

18. W.T. Yap, R.A. Durst, E.A. Blubaugh and D.D. Blubaugh, J. Electroanal. Chem., 144 (1983) 69.

19. W.T. Yap and R.A. Durst, J. Electroanal. Chem., 216 (1987) 11.

20. D. Ghesquiere, B. Ban and C. Chachaty, Macromolecules, 10 (1977) 743.

21. P. Daum, J.R. Lenhard, D.R. Rolison and R.W. Murray, J. Am. Chem. Soc., 102 (1980) 4649.

22. A.P. Clarke, Ph.D. Thesis, Dublin City University, (1992).

Chapter 4.

The Mass and Charge Transport Properties of $[Os(bipy)_2(PVP_{33})_{10}Cl]^{+}$ Metallopolymer Films in $HClO_4$ Electrolytes.

4.1. Introduction.

The combination of the QCM with traditional electrochemical techniques (the EQCM) has proven particularly useful for the study of redox-switching-induced mass changes within surface-immobilised electroactive polymer films (see Chapter 1 for review). The sensitivity of the EQCM makes it ideal for these investigations. However, the generality of detection of this technique necessarily requires that the sometimes complex changes in layer mass must be analysed with care. The EQCM frequency data contain information about the interfacial transfer of all mobile species (charged and net neutrals). The electrochemical data however pertain only to the transfer of charged species [1]. Separation of the individual contributions of these mobile species to the overall redox-switching-induced mass change requires that the mass and charge relationship be defined. The approach used in this work is that proposed by Hillman et al. [1-7] and is outlined in brief in the following section.

4.2. Mass Changes Accompanying Redox Switching.

Redox switching of electroactive polymer films is accompanied by the motion of charged species, net neutrals (solvent and salt) and polymer chain segments. Ionic species are transferred in response to electroneutrality constraints imposed by the changing oxidation state of the redox sites. During oxidative processes, electroneutrality may be maintained by either the ingress of solution species i.e. anion influx, or the egress of mobile polymer species i.e. co-ion egress. The change in ionic concentration of the internal polymer pore liquid during redox processes is likely to result in a change in activity of the interstitial solvent [8]. Changes in the polymer solvent populations are therefore anticipated. The transfer of other net neutrals, such as "salt" (ion pairs and undissociated molecules), is a consequence of the breakdown in the permselectivity of the layer [9,10] and is frequently observed in electrolyte concentrations in excess of 1.0M [11,12].

These mass transfer processes are driven by their associated electrochemical potentials. For charged species the electrochemical potential contains both an activity gradient and a potential gradient term. Solvent molecules and net neutrals are transferred in response to activity gradients [4,5,13].

During redox switching, the total net change in layer mass per unit area (ΔM_{TOT}) is the sum of the contributions associated with ionic and neutral species transfer:

$$\Delta M_{TOT} = \Delta M_{ION} + \Delta M_{SOLVENT} + \Delta M_{SALT} \qquad (4.2.1.)$$

Or

$$\Delta M_{TOT} = \Sigma m_i \Delta\Gamma_i + \Sigma m_{so} \Delta\Gamma_{so} + \Sigma m_{sa} \Delta\Gamma_{sa} \qquad (4.2.2.)$$

where m is the molar mass and $\Delta\Gamma$ is the change in film population ($molcm^{-2}$) of the designated species. The subscripts i, so and sa signify ionic, solvent and salt species respectively.

The EQCM cannot differentiate between the interfacial transfer of charged and neutral species. However, the change in ionic species populations is associated with the charge change during the redox reaction and may be estimated from the electrochemical data using Faraday's law:

$$\Delta\Gamma_i = -\frac{Q}{z_i F} \qquad (4.2.3.)$$

where z_iF is the charge carried per mole of the ionic species i. In this analysis the charge is defined as positive for film oxidation.

Combining equation 4.2.2 and equation. 4.2.3 yields

$$\frac{\Delta M_{TOT} F}{Q} = \frac{\left(\Sigma m_i \Delta\Gamma_i + \Sigma m_{so} \Delta\Gamma_{so} + \Sigma m_{sa} \Delta\Gamma_{sa}\right)}{\Sigma z_i \Delta\Gamma_i} \qquad (4.2.4.)$$

which represents the net change in layer mass per mole of redox sites converted ($gmol^{-1}$) and is referred to as the normalised mass change.

Neutral species transfer contributes to the mass but not the charge. To eliminate the counterion contribution of the observed mass change, the Φ_j function is introduced. Substituting equation 4.2.3 into equation. 4.2.2 and re-arranging yields

$$\Phi_j = \Delta M_{TOT} + \frac{m_i Q}{z_i F} = m_{so} \Delta\Gamma_{so} + m_{sa} \Delta\Gamma_{sa} \qquad (4.2.5.)$$

The Φ_j function is a linear combination of the mass change observed and the mass change associated with the movement of the chosen ion (j) if it alone maintains electroneutrality. It represents the additional mass transfer of all mobile species to that anticipated for the motion of the chosen ion and therefore, provides a direct dynamic monitor of neutral species transfer during redox switching. The identity of the neutral species component of ΔM_{TOT} depends on the permselectivity of the layer. Equation 4.2.6 and equation. 4.2.7 represent the general equations for permselective and non-permselective cases respectively:

$$\Phi^{Perm} = \Delta M_{TOT}^{Perm} + \frac{m_i Q}{z_i F} = m_{so} \Delta\Gamma_{so} \qquad (4.2.6.)$$

$$\Phi^{Non-Perm} = \Delta M_{TOT}^{non-Perm} + \frac{m_i Q}{z_i F} = m_{so}\Delta\Gamma_{so} + m_{sa}\Delta\Gamma_{sa} \qquad (4.2.7.)$$

Separation of the individual components of the total mass change may be achieved kinetically [1-5,13-18]. These components; ions, solvent and salt, likely transfer at different rates [2,6,7] and, as a consequence, different species dominate the mass response at different experimental timescales. The existence of kinetic barriers to mass transfer have been illustrated for PVF [2-5,13,14], polythionine [4,13-16], polybithiophene [1,4], nitrated polystyrene [17] and $OsPVP_{100}$ [18] polymer systems under dynamic experimental conditions. For PVF, it has been suggested that the relative rates of species transfer increase in the order of [2,5]:

polymer reconfiguration < solvent transfer < salt transfer < ion transfer.

That salt and solvent motion is typically slower than ion motion is considered to reflect their differing driving forces [6]. An interesting consequence of this approach is the observation of "kinetic permselectivity" for short timescale experimental conditions [3,19].

In Chapter 2, the influence of the polymer backbone on the rigidity and resident layer mass of $[Os(bipy)_2(PVP_x)_{10}Cl]^+$ coated crystals was investigated in $HClO_4$ and $LiClO_4$ electrolytes. As anticipated, the rigidity of these coatings increases with increasing styrene content of the metallopolymer backbone. This behaviour reflects the reduced layer mass of the higher styrene content copolymers and is a consequence of the hydrophobic nature of the styrene moiety and the reduced requirement for anion influx during protonation of the pyridine units (in $HClO_4$).

The charge transport properties of $OsPVP_{33}$ electrode coatings were

investigated in Chapter 3. Within the electrolyte concentration range of 0.1 to 1.0M $HClO_4$, the rate of charge transport through $OsPVP_{33}$ coatings, as determined by cyclic voltammetry, is constant i.e. 3.13 ($\pm$ 0.2) x 10^{-11} cm^2s^{-1}. Activation parameters, estimated from the temperature dependence of the charge transport process, suggest that ion motion is limiting.

It is the purpose of this chapter to study the redox-switching-induced mass changes of $OsPVP_{33}$ layers as a function of the $HClO_4$ electrolyte concentration and the experimental timescale. The dynamic mass transfer experiments reported in this chapter provide additional insight into the processes limiting charge transfer within these metallopolymers. Comparison is made with the data reported for the $OsPVP_{100}$ polymer under similar experimental conditions [11,20-23]. The influence of the polymer backbone and the polymer ion content on the redox-switching-induced mass changes of these metallopolymers is probed.

4.3. Experimental.

4.3.1. Apparatus.

The electrochemical cell, oscillator circuit and its power supply were described by Bruckenstein and Shay [24]. All frequency measurements were made with respect to a reference crystal. Changes in the resonant frequency were monitored using a Hewlett Packard 5334B frequency counter, which was accurate to ±0.1 Hz in 10 Mhz. All data; frequency changes, potential, charge and current were recorded via a Keithley Data Acquisition System 570 interfaced to an IBM ATX computer. Electrochemical data were recorded on Bryans 60 000 series xy-recorders. All interfacing and computer programmes were written by M.J. Swann and D.C. Loveday of Leicester University.

4.3.2. Materials.

The synthesis of $[Os(bipy)_2(PVP_{33})_{10}Cl]Cl$ was described in Chapter 2. $HClO_4$ electrolytes were prepared with Milli-Q H_2O.

4.3.3. Procedures.

$OsPVP_{33}$ coated crystals were prepared as described in Chapter 2. The modifying layers were equilibrated in each $HClO_4$ electrolyte concentration by voltammetrically scanning over the $Os^{II/III}$ couple for a minimum of 3 hours. Scan rates of 1 mVs^{-1} and 50 mVs^{-1} were alternately used. The change in layer mass accompanying redox switching of these $OsPVP_{33}$ layers was studied as a function of the $HClO_4$ concentration of the contacting electrolyte (0.01M to 4.0M $HClO_4$) and the experimental timescale (1 to 500 mVs^{-1}). The profound influence of memory effects on the mass transfer properties of $OsPVP_{100}$ coated crystals has been previously demonstrated [25]. For the work reported here, the observed mass

changes were independent of the electrolyte concentration to which the layer had been previously exposed. Re-immersion in any $HClO_4$ concentration following exposure to higher or lower electrolyte concentrations did not affect the mass changes occurring during redox processes. All determinations were carried out on at least two different polymer layers in each $HClO_4$ concentration.

Polymer surface coverages, as determined by gravimetry, were in the range of 0.5 to 3.0 x 10^{-8} molcm^{-2}. The coulometric surface coverage, estimated from the area under the anodic peak of 1 mVs^{-1} cyclic voltammograms was typically 25-35% smaller than the gravimetric surface coverage. This suggests that only 65-75% of the Os^{II} sites are electroactive on the timescale of these voltammetric. These observations were verified with exhaustive coulometric experiments on coated 3 mm glassy carbon electrodes.

4.4. Results and Discussion.

4.4.1. Layer Mass Changes during Redox Switching of $OsPVP_{33}$ Films.

In Chapter 2, the change in layer mass of $OsPVP_{33}$ coatings was studied as a function of the $HClO_4$ bathing electrolyte concentration for the Os^{II} polymer oxidation state. Within the concentration range of 0.01M to 4.0M $HClO_4$, the change in resident layer mass is apparently associated solely with the influx of counter-anions for the maintenance of electroneutrality within the protonated layer. The crystal resonance shape of $OsPVP_{33}$ coated crystals remains constant in all $HClO_4$ concentrations examined and illustrates that these layers are rigid under these conditions [11,17,19,22,23,26].

For the work reported here, the crystal resonance shape of $OsPVP_{33}$ coated crystals was studied as a function of the $Os^{II/III}$ oxidation states, to probe for possible deleterious swelling variations during redox switching. Fig. 4.1 and Fig. 4.2 illustrate the change in crystal resonance of an $OsPVP_{33}$ coated crystal during oxidative 5 mVs^{-1} cyclic voltammetric scans in 0.1M and 1.0M $HClO_4$ respectively. The gravimetric surface coverage was 2.87×10^{-8} $molcm^{-2}$. Only the initial (ca. -100 mV) and final spectra (ca. +600 mV) are illustrated. These figures are representative of the general behaviour of this $OsPVP_{33}$ coating in all $HClO_4$ concentrations studied.

In Fig. 4.1 and Fig. 4.2, the resonant frequency decreases during polymer oxidation. This behaviour represents an increase in layer mass and suggests that anion influx is responsible for the maintenance of electroneutrality. The shape of the crystal resonance, as characterised by the admittance maximum and peak width at half maximum admittance, is similar in both Os^{II} and Os^{III} redox states and indicates that the rigidity of the coating is not compromised during redox switching [11,17,19,22,23,26]. It is therefore anticipated that the change in layer mass

Fig. 4.1. Admittance spectra for an $OsPVP_{33}$ coated crystal during redox switching in 0.1M $HClO_4$ at 5 mVs^{-1}. Gravimetric surface coverage is 2.87 x 10^{-8} $molcm^{-2}$.

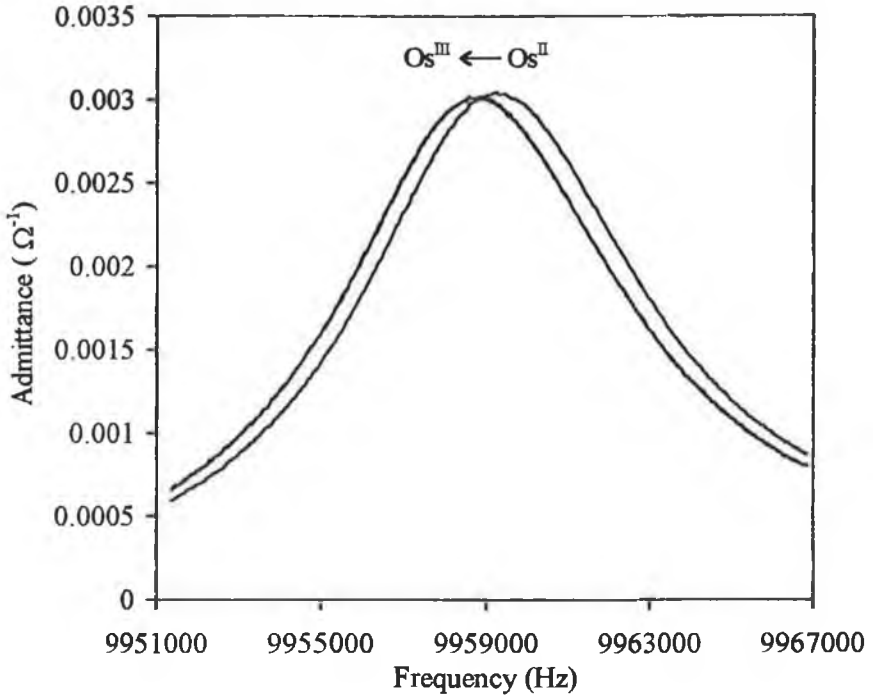

Fig. 4.2. Admittance spectra for an $OsPVP_{33}$ coated crystal during redox switching in 1.0M $HClO_4$ at 5 mVs^{-1}. Gravimetric surface coverage is 2.87 x 10^{-8} $molcm^{-2}$.

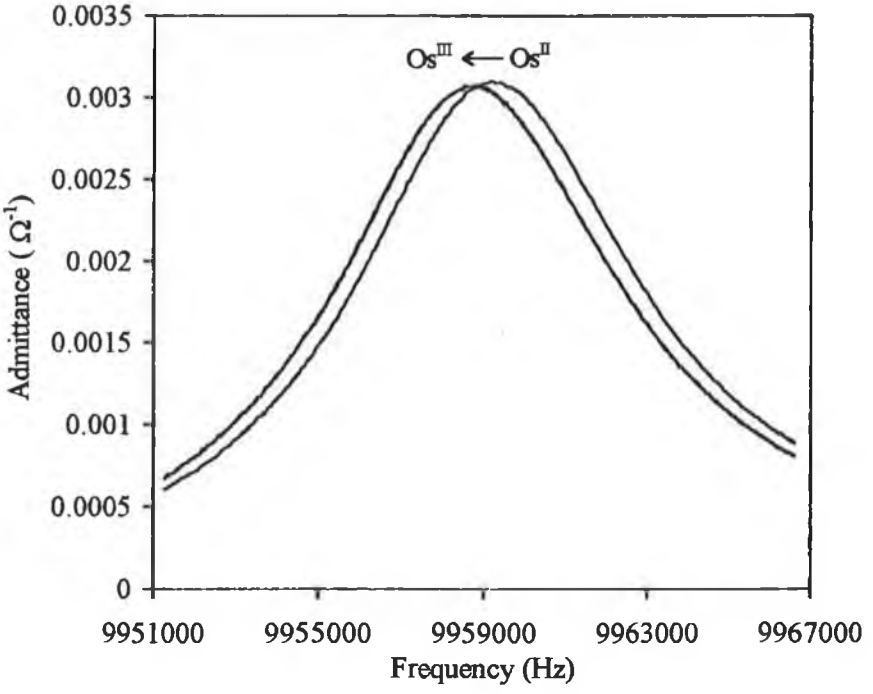

accompanying redox switching may be accurately evaluated from the shift in the resonant frequency using the Sauerbrey equation. This increase in layer mass accompanied by a constant resonance shape may reflect the crosslinking properties of the perchlorate anion [27-29].

Fig. 4.3 illustrates the change in layer mass of an $OsPVP_{33}$ coated crystal in 1.0M and 4.0M $HClO_4$. The scan rate was 5 mVs^{-1} and the gravimetric surface coverage was 8.07 x 10^{-9} $molcm^{-2}$. This behaviour is representative of the general mass transfer behaviour of all $OsPVP_{33}$ coatings examined under these experimental conditions, within the complete $HClO_4$ concentration range under investigation. Typically three successive voltammetric scans were obtained. However, the mass-potential plots for each scan are identical and only the first voltammetric scan is illustrated.

Table 4.1 summarises the overall change in layer mass of $OsPVP_{33}$ coated crystals during redox switching in $HClO_4$ electrolytes. The voltammetric scan rates were 1 and 5 mVs^{-1}. These mass changes are associated with the maintenance of electroneutrality within these $OsPVP_{33}$ coatings during the $Os^{II/III}$ oxidation process. The change in layer mass has been normalised with respect to the coulometric surface coverage and therefore reflects the mass influx per mole of osmium sites converted. This approach allows for the comparison of mass changes observed for different polymer surface coverages [10]. The normalised mass changes are reproducible to within 5% for determinations on different films and 3% for repeated determinations on a single film.

The overall normalised change in layer mass is independent of the $HClO_4$ concentration of the contacting electrolyte. Within experimental error, an average normalised mass change of 104 ($\pm$4) $gmol^{-1}$ is observed over the complete $HClO_4$ concentration range. This value is close to the molecular weight of the perchlorate anion and suggests that, during redox switching, electroneutrality is maintained by anion ingress/ egress.

Fig. 4.3. Mass-potential plots for an $OsPVP_{33}$ coated crystal in $HClO_4$ electrolytes. Scan rate is 5 mVs^{-1}. Gravimetric surface coverage is 8.07×10^{-9} $molcm^{-2}$.

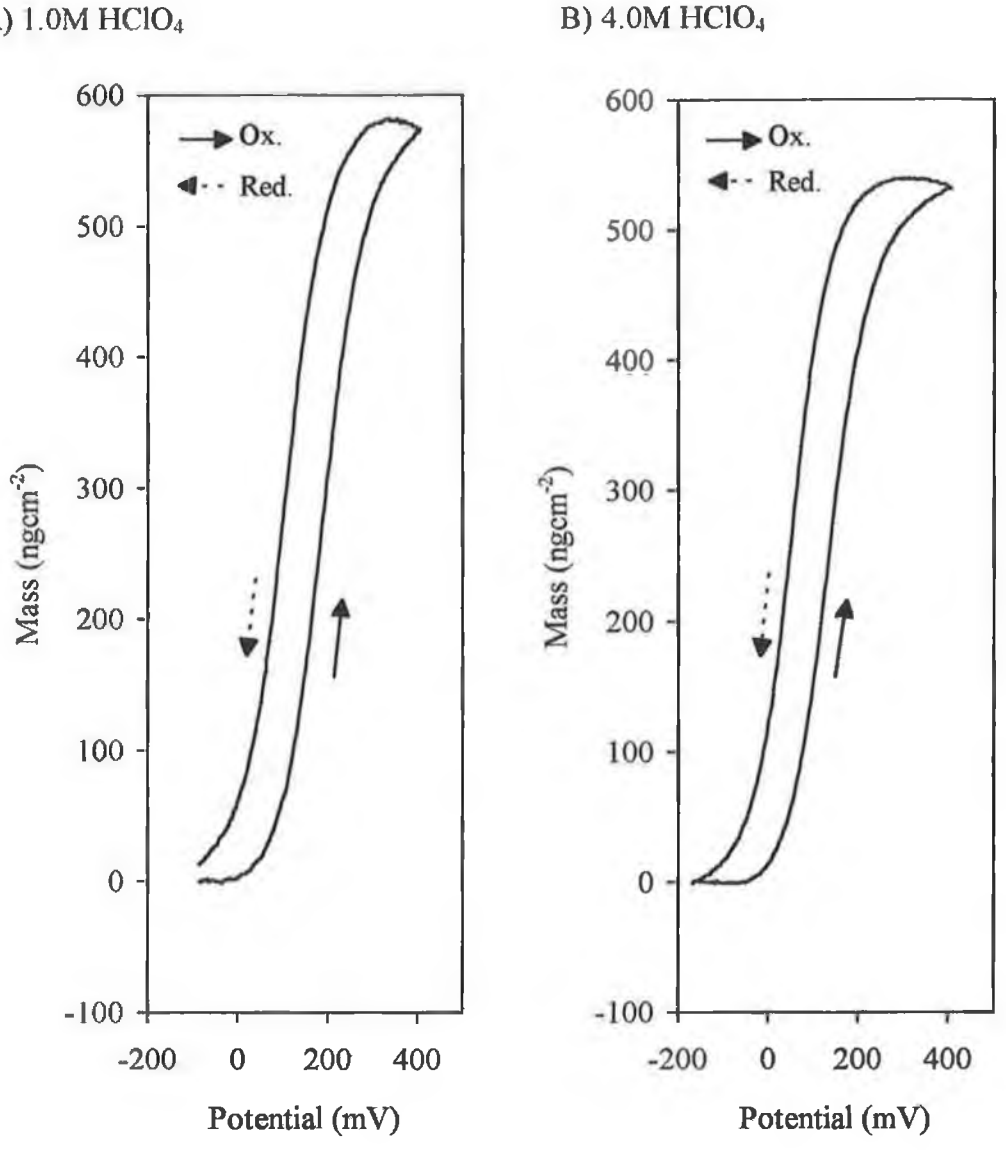

Table 4.1. The effect of $HClO_4$ electrolyte concentration on the normalised mass change accompanying redox switching of $OsPVP_{33}$ coated crystals.

$HClO_4$ Conc. (M)	Normalised Mass Change ($gmol^{-1}$)	
	A. 1 mVs^{-1} [a]	B. 5 mVs^{-1} [a]
0.01	104 (1)	104 (3)
0.10	100 (1)	101 (5)
0.50	104 (2)	108 (2)
1.00	100 (4)	104 (1)
2.00	103 (3)	101 (2)
4.00	101 (1)	102 (2)

(a) errors quoted in brackets represent the variations between 2 different films.

The mass changes observed for at least half the films studied are greater than 100 $gmol^{-1}$ and suggest that small quantities of neutral species are also transferred during redox processes. This solvent component of the redox-switching-induced mass change is illustrated under more dynamic experimental conditions in Section 4.4.2.

Table 4.2 summarises the potentials of half-total-charge change, $E_{1/2}(q)$, and half-total-mass change, $E_{1/2}(m)$, for both oxidative and reductive processes, obtained during 5 mVs^{-1} cyclic voltammetric experiments. Also included are the corresponding anodic and cathodic peak potentials. It is clear from the anodic and cathodic potentials that these layers do not exhibit true surface behaviour under these conditions. This behaviour is likely a result of slow charge transport through this polymer, reflecting its compact and dehydrated nature in this electrolyte (see Chapter 2). Within experimental error (±5 mV), the potentials of half-total-mass change and half-total-charge change coincide for all $HClO_4$ concentrations, reflecting concomitant mass and charge transfer [11,14,18,].

Fig. 4.4 illustrates the mass- and Φ_{ClO4^-} -charge plots for the 1.0M $HClO_4$ data in Fig. 4.3. The absence of hysteresis in the mass-charge plot, coupled with the scan rate independence of the normalised mass change (see Table 4.1), illustrates that these time scales are sufficiently long for all mobile species to attain at least pseudo-equilibrium, as dictated by the extent of oxidation of the polymer layer. The increase/ decrease in layer mass during oxidation/ reduction illustrates that electroneutrality is maintained by anion motion. The mechanism of co-ion expulsion can be neglected for two reasons; 1) in Chapter 2, it was noted that in all $HClO_4$ concentrations, the resident layer mass of $OsPVP_{33}$ coatings is associated solely with the protonated backbone and that no free electrolyte resides within these layers and 2) in Chapter 5, it is demonstrated that changing the electrolyte cation has no influence on the observed normalised mass changes of these layers.

Fig. 4.4 also illustrates the Φ_{ClO4^-} -charge plot for this data. The Φ_{ClO4^-} function represents the movement of all species other than the chosen ion, in this case

Table 4.2. The oxidation/ reduction potentials of the $Os^{II/III}$ couple and their associated half-mass and half-charge potentials for $OsPVP_{33}$ coated crystals in $HClO_4$ solutions.

$HClO_4$ Conc.(M)	Oxidation[a]			Reduction[a]		
	$E_{1/2}$ (Ox.)	$E_{1/2}$ (q)	$E_{1/2}$ (m)	$E_{1/2}$ (Red.)	$E_{1/2}$ (q)	$E_{1/2}$ (m)
0.01	355	355	370	245	254	248
0.10	285	285	289	190	190	190
0.50	242	244	249	147	148	155
1.00	224	224	231	130	129	122
2.00	193	191	194	109	103	107
4.00	151	150	150	80	80	82

(a) All potentials (mV vs SCE) measured at 1 mVs^{-1} at ambient temperatures (20 ± 2^{o} C).

Fig. 4.4. Mass- and Φ_{ClO4}^- -charge plots for data in Fig. 4.3.A.

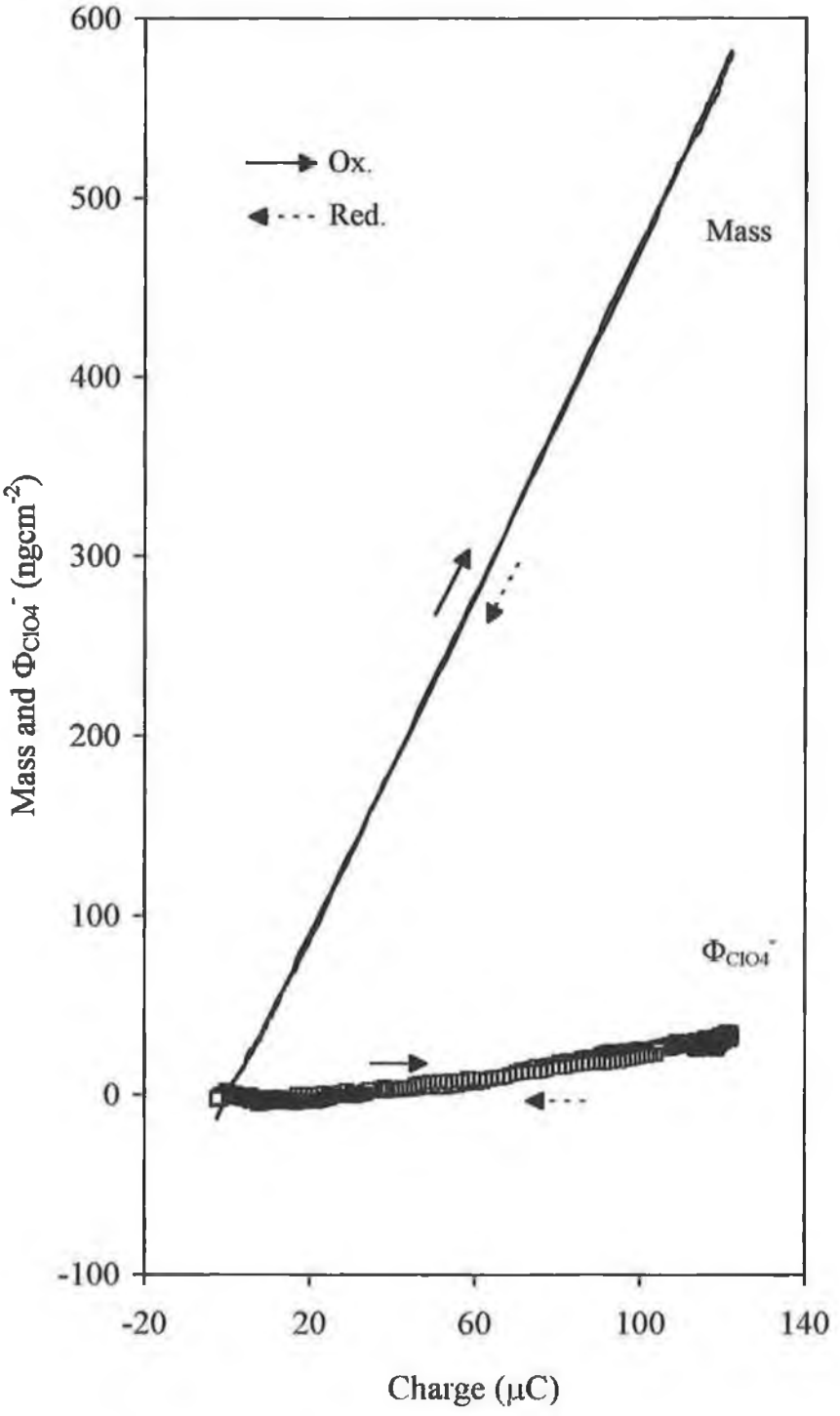

the perchlorate anion, assuming that this anion is solely responsible for the maintenance of electroneutrality (see Section 4.2). The absence of free residual electrolyte within $OsPVP_{33}$ polymer coatings (see Chapter 2) and the insensitivity of the redox-switching-induced mass changes of these coatings to the contacting $HClO_4$ electrolyte concentration (see Table 4.1) indicates that these layers are permselective under these experimental conditions. The Φ_{ClO4^-} data therefore represent the change in layer mass associated with the transfer of solvent molecules. In Fig. 4.4, the Φ_{ClO4^-} function is essentially zero for the first 25 μC of osmium oxidation. This corresponds to ca. 25% of the total charge passed during the oxidation process. The mass changes accompanying the initial oxidation of these layers are therefore associated solely with the influx of the perchlorate anion. Further oxidation of the layer (above 25 μC) is accompanied by solvent influx. This behaviour is independent of the polymer surface coverage, with solvent ingress typically occurring after ca. 25% of the total anodic charge is passed. The normalised mass changes, calculated from the individual slopes of the mass-charge plot in Fig. 4.4, are 100 $gmol^{-1}$ ($Q_{OX} < 25$ μC) and 108 $gmol^{-1}$ ($Q_{OX} > 25$ μC). These solvent transfer processes are reversed during the reductive scan. The existence of this dual-sloped mass-charge behaviour highlights the importance of considering not only the overall normalised mass changes, but the mass-charge relationship.

As a consequence of the permselectivity of these layers, the individual normalised mass changes of 100 $gmol^{-1}$ and 108 $gmol^{-1}$ (see above) can be equated with the initial sole influx of a single perchlorate anion and the subsequent influx of a single perchlorate anion and ca. 0.5 molecules of water per oxidised osmium site i.e. 1 water molecule per 2 osmium sites. Clearly, only small quantities of solvent are transferred during redox switching of $OsPVP_{33}$ coatings in these $HClO_4$ electrolytes. In Section 4.4.2, it is demonstrated that the anion and solvent transfer processes are delineated. It is therefore suggested that the solvent incorporated during redox switching is not part of the hydration sheet of the anion and that the incorporated

anions are unhydrated. The absence of anion hydration may be a consequence of steric considerations or may simply reflect the hydrophobic nature of the polymer backbone.

In Chapter 2, a solvent imbibition level of 0.7 ± 0.1 molecules of H_2O per $[Os(bipy)_2(PVP_{33})_{10}Cl]Cl$ polymer unit was reported for $OsPVP_{33}$ coatings in pure H_2O. The additional influx of 0.2 molecules of H_2O per osmium site, during redox switching (taken as the average solvent influx during polymer oxidation), represents an approximate 30% increase in the polymer solvent content. These solvent changes are extremely small and clearly reflect the hydrophobic nature of the styrene moieties.

Fig. 4.5 and Fig. 4.6 illustrate the mass- and Φ_{ClO4^-} -charge plots for an $OsPVP_{33}$ polymer coating in 0.01M and 4.0M $HClO_4$ respectively. The gravimetric surface coverage was 2.35×10^{-8} molcm^{-2}. The scan rate was 5 mVs^{-1}. These plots exhibit the same qualitative and quantitative trends as those observed in 1.0M $HClO_4$ (see Fig. 4.4). The absence of hysteresis in both mass-charge plots again reflects the establishment of pseudo-equilibrium mass changes on these experimental timescales. Neither plot exhibits any evidence for the existence of co-ion expulsion. The Φ_{ClO4^-} -charge plots illustrate that solvent transfer is again observed after 20 to 30% of the total anodic charge is passed. The normalised mass changes, calculated from the individual slopes of the mass-charge plots, are again 100 gmol^{-1} and 108 gmol^{-1}. This similarity in the mass transfer properties of $OsPVP_{33}$ coatings, in all $HClO_4$ concentrations studied, illustrates that, even in 4.0M $HClO_4$, these layers behave permselectively. This behaviour is surprising and is most likely a consequence of the compact and hydrophobic nature of these coatings. These layer characteristics differ from those reported for the $[Os(bipy)_2(PVP_{100})_{10}Cl]Cl$ polymer under similar experimental conditions [11].

Fig. 4.5. Mass- and Φ_{ClO4}^- -charge plots for an $OsPVP_{33}$ coated crystal in 0.01M $HClO_4$. Scan rate is 5 mVs^{-1}. Gravimetric surface coverage is 2.35 x 10^{-8} $molcm^{-2}$.

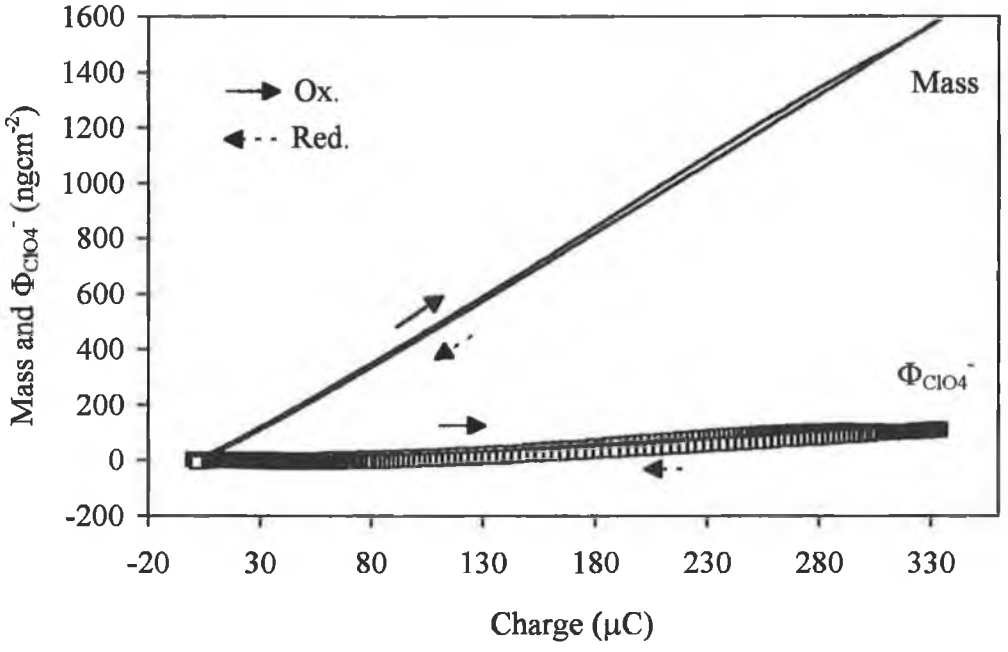

Fig. 4.6. Mass- and Φ_{ClO4}^- -charge plots for an $OsPVP_{33}$ coated crystal in 4.0M $HClO_4$. Scan rate is 5 mVs^{-1}. Gravimetric surface coverage is 2.35 x 10^{-8} $molcm^{-2}$.

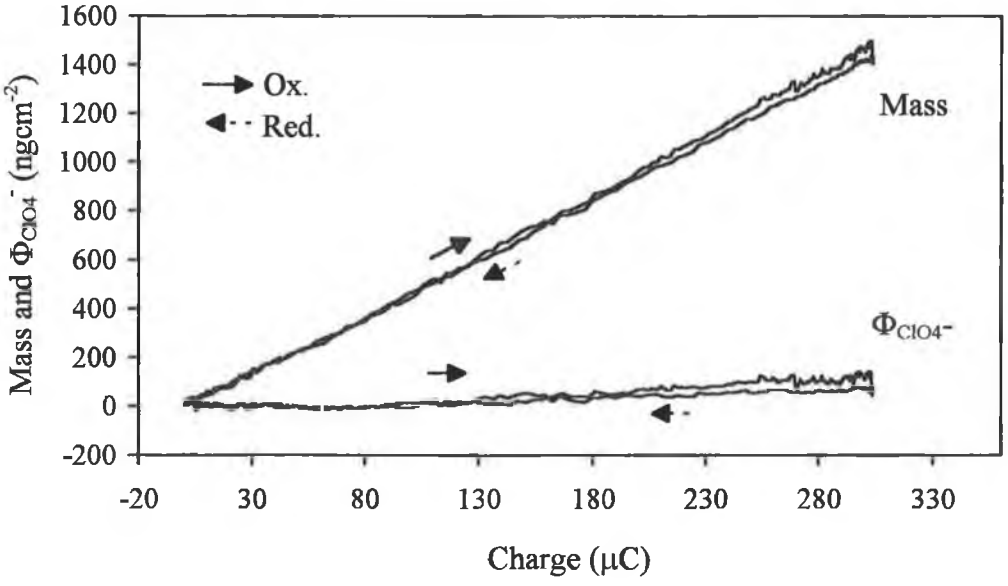

4.4.1.1. Comparison with $[Os(bipy)_2(PVP_{100})_{10}Cl]^+$ Films.

The normalised mass changes accompanying redox switching of $OsPVP_{100}$ layers, within the concentration range of 0.1M to 1.0M $HClO_4$, are associated with the ingress/ egress of a single perchlorate anion and ca. 2-3 water molecules [11]. This solvation level is close to the reported hydration number of the anion (2.6 [30]). However, experiments carried out under semi-infinite diffusion conditions illustrate that the anion and solvent transfer processes are delineated [18]. Similar qualitative behaviour is reported here for the $OsPVP_{33}$ copolymer. However, the level of solvent ingress during redox switching of $OsPVP_{33}$ is significantly smaller. Similarly, in Chapter 2 it was noted that, upon immersion of both polymers in pure H_2O, the level of solvent imbibition by the $OsPVP_{33}$ polymer is considerably less than that observed for the $OsPVP_{100}$ polymer [11]. This behaviour is a consequence of the relatively more hydrophobic and compact copolymer backbone of the $OsPVP_{33}$ polymer. Therefore, changing the nature of the backbone alters both the resident layer mass of the polymer coating and the magnitude of the mass response during redox switching.

In electrolyte concentrations in excess of 1.0M $HClO_4$, the normalised mass change accompanying redox switching of $OsPVP_{100}$ crystal coatings are substantially greater than those observed in lower $HClO_4$ concentrations [11]. These larger mass changes are considered to reflect the breakdown in layer permselectivity and the subsequent influx of $H_3O^+ClO_4^-$. However, for the $OsPVP_{33}$ polymer, the normalised mass changes are independent of the $HClO_4$ electrolyte concentration. Clearly, the relatively more compact and hydrophobic $OsPVP_{33}$ polymer prevents the ingress of $H_3O^+ClO_4^-$ and the layer remains permselective despite the high perchloric acid concentration of the bathing solution. The permselective nature of $OsPVP_{33}$ coatings in high perchloric acid concentrations was also noted in Chapter 2.

4.4.2. Effect of Experimental Timescale on Mass Transfer Through $OsPVP_{33}$ Films.

In Chapter 3, the influence of the styrene content of the polymer backbone on the rate of charge transport through $[Os(bipy)_2(PVP_x)_{10}Cl]^+$ metallopolymer coatings was investigated. In 0.1M and 1.0M $HClO_4$ electrolytes, the rate of charge transport, as determined by cyclic voltammetry, $D_{CT}(CV)$, was found to be independent of the $HClO_4$ concentration. Activation parameters, estimated for the change transport process, suggest that ion motion is rate limiting. In this section, the interfacial mass transfer processes are studied, using cyclic voltammetry, under semi-infinite diffusion conditions (scan rates of 50-500 mVs^{-1}) to probe for mass transfer limitations.

In Section 4.4.1, an investigation of the changes in the $OsPVP_{33}$ polymer populations during redox switching at slow voltammetric scan rates revealed that, under the permselective conditions exhibited by these $OsPVP_{33}$ layers, electroneutrality is maintained by the influx of a single perchlorate anion. Approximately 0.2 molecules of solvent per Os^{III} site are transferred during redox switching (averaged over the complete oxidation). This solvent component of the normalised mass transfer is delineated from the initial anion flux and is observed only after 20% to 30% of the total anodic charge is passed.

Table 4.3 summarises the overall normalised mass changes associated with the redox switching of $OsPVP_{33}$ coatings at scan rates of 50-500 mVs^{-1}, as a function of the $HClO_4$ electrolyte concentration. These values are reproducible to within 10% for determinations on different films and 7% for repeated determinations on a single film. Charge transport rates, $D_{CT}(CV)$, were estimated, as outlined in Chapter 3, from the anodic peak current using the Randles-Sevcik equation and are included in Table 4.3. These values are reproducible to within 10% for determinations on different layers and 5% for repeated determinations on a single film. The gravimetric surface coverages were of the order of 1.0 to 3.0 x 10^{-8} $molcm^{-2}$. All mass and charge transport data are independent of the polymer surface coverage within this range.

Table 4.3. The effect of $HClO_4$ electrolyte concentration on the normalised mass change accompanying redox switching of $OsPVP_{33}$ coated crystals at fast cyclic voltammetric scan rates.

$HClO_4$ Conc. (M)	D_{CT} (CV) x 10^{-11} cm^2s^{-1}	Scan Rate (mVs^{-1})	Normalised Mass Change ($gmol^{-1}$)
0.01	2.62	50	104 (2)
		100	106 (4)
		200	99*
		500	110*
0.10	2.75	50	104 (5)
		100	102 (4)
		200	106*
		500	108 (5)
0.50	2.68	50	107 (5)
		100	102 (4)
		200	107 (8)
		500	110 (5)
1.0	2.90	50	105 (1)
		100	104 (3)
		200	108 (7)
		500	107 (9)
2.0	2.71	50	106*
		100	103 (3)
		200	107 (5)
		500	101 (7)
4.0	2.24	50	106 (5)
		100	104 (2)
		200	103*
		500	109*

( ) errors quoted in brackets represent the variations between 2 different films.

* signifies measurements made on one film only.

It is apparent from Table 4.3 that the normalised mass changes are independent of both the experimental timescale and the $HClO_4$ electrolyte concentration. The average normalised mass change is 105 (±5) $gmol^{-1}$ and is of a similar magnitude to the slow scan mass changes discussed in Section 4.4.1. Fig. 4.7 and Fig. 4.8 illustrate the mass- and charge-potential plots for a 2.35 x 10^{-8} $molcm^{-2}$ $OsPVP_{33}$ crystal coating during a 100 mVs^{-1} cyclic voltammetric experiment in 1.0M $HClO_4$. For both the mass and charge data, 3-5 voltammetric scans are required before reproducible, steady-state changes are observed. Failure of both sets of data to return to their original baselines following each scan reflects the trapping of both charge and mass on the timescale of this experiment [6]. The original mass and charge baselines are renewed upon holding the polymer in the Os^{II} state for 10-15 minutes. The trapped charge is a result of the kinetic isolation of redox species on this experimental timescale [6]. The trapped mass is associated with these isolated redox sites and represents the trapping of a single perchlorate and ca. 0.2 molecules of water per trapped Os^{III} site.

Fig. 4.9 illustrates the mass- and Φ_{ClO4^-} -charge plots for the data in Fig. 4.7 and Fig. 4.8. The linearity of the mass-charge plot suggests that no reservoir of cations/ anions exists within the polymer layer. Oxidation therefore requires an external source of charge-compensating ions. Compared with the data in Fig. 4.4, for a 5 mVs^{-1} voltammetric experiment, this plot exhibits hysteresis which, using Hillman's diagnostic scheme [1,3-5], is considered to reflect hindered neutral species motion. Under the permselective layer conditions reported here, this hysteresis must reflect the slow influx of solvent. Therefore interfacial mass transfer is impeded, with solvent motion lagging anion ingress/ egress.

Table 4.3 summarises the charge transport properties of $OsPVP_{33}$ coatings as a function of the $HClO_4$ electrolyte concentration. The change in $D_{CT}(CV)$ with increasing $HClO_4$ electrolyte concentration is illustrated in Fig. 4.10. The $HClO_4$ concentration is illustrated in log format for presentation purposes. Fig. 4.10 also

Fig. 4.7. Mass-potential plots for an $OsPVP_{33}$ coated crystal in 1.0M $HClO_4$. Scan rate is 100 mVs^{-1}. Gravimetric surface coverage is 2.35 x 10^{-8} $molcm^{-2}$.

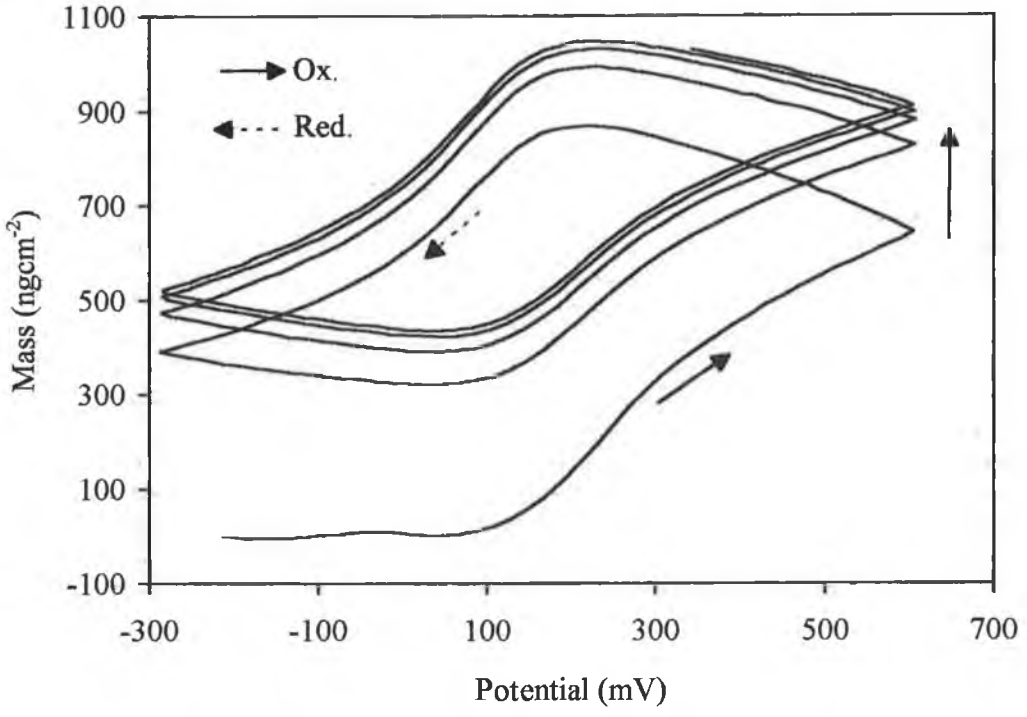

Fig. 4.8. Charge-potential plots for data in Fig. 4.7.

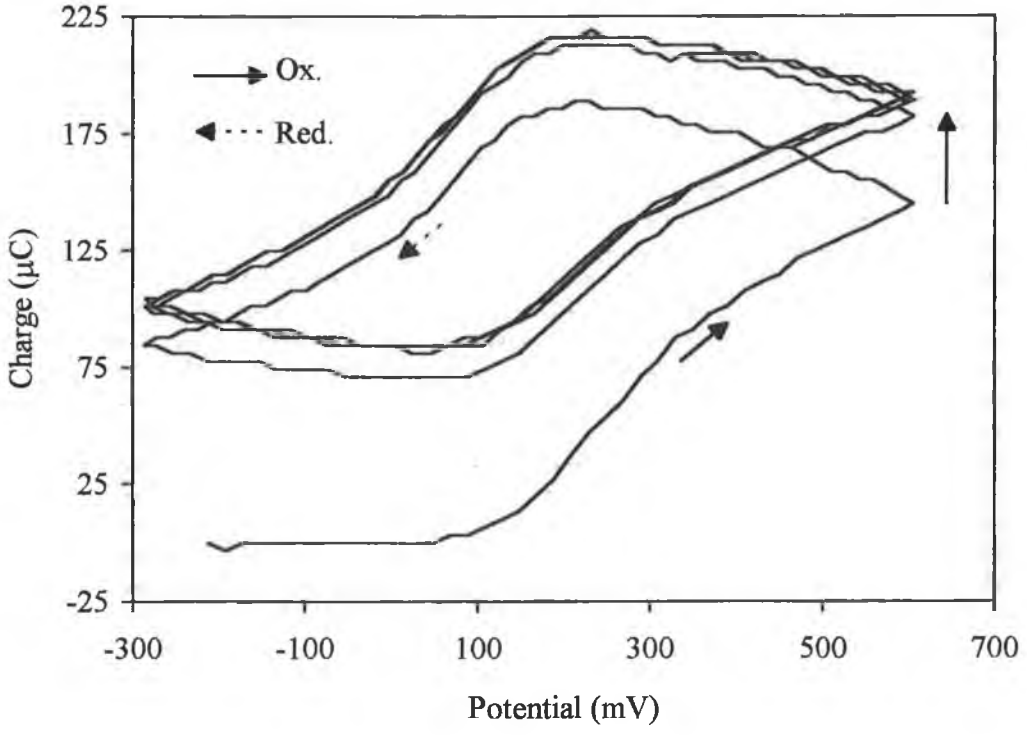

Fig. 4.9. Mass- and Φ_{ClO4}^- -charge plots for data in Fig. 4.7 and Fig. 4.8.

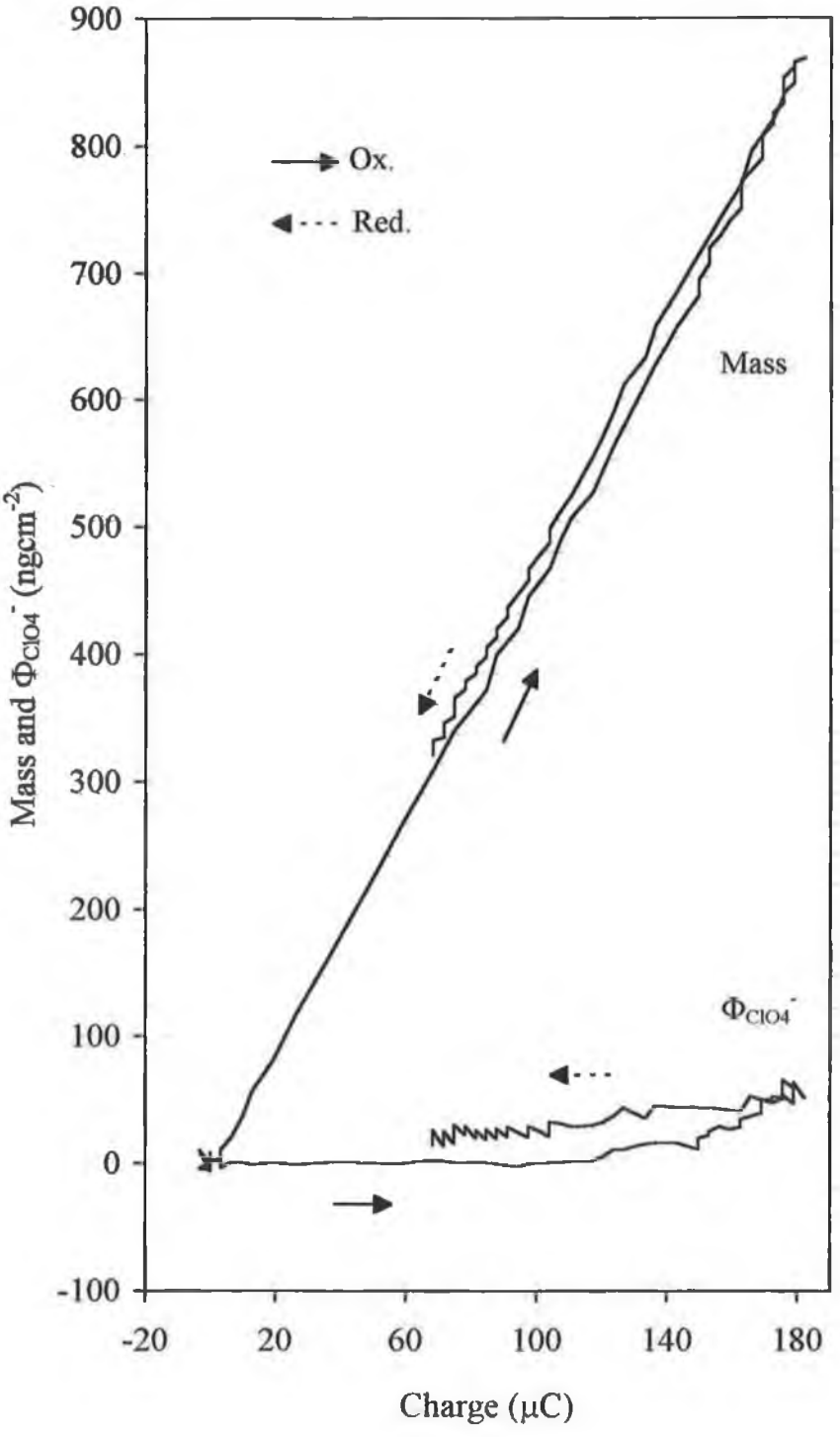

Fig. 4.10. The effect of $HClO_4$ electrolyte concentration on the rate of charge transport, $D_{CT}(CV)$, through $OsPVP_{33}$ (Δ) and $OsPVP_{100}$ (□) coated crystals. ($OsPVP_{100}$ data is taken from Ref. 18).

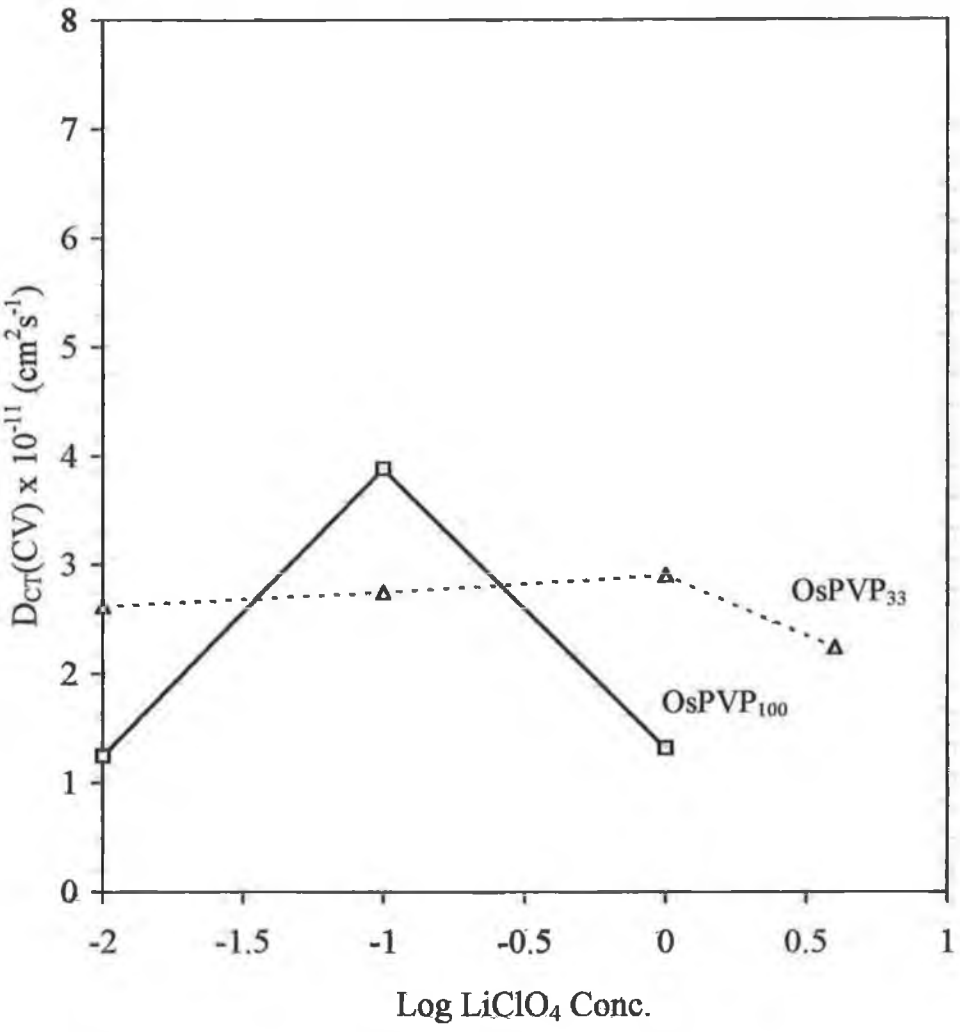

includes the corresponding charge transport rates for the $OsPVP_{100}$ polymer (from reference 18). The data in Table 4.3 and Fig. 4.10 illustrate that, with the possible exception of 4.0M $HClO_4$, the rate of charge transport within $OsPVP_{33}$ coatings is essentially independent of the $HClO_4$ electrolyte concentration over the complete range of concentrations studied. Similar behaviour was reported in Chapter 3, for $OsPVP_{33}$ coatings in 0.1M and 1.0M $HClO_4$. In Chapter 2, it was demonstrated that the rigidity of $OsPVP_{33}$ coatings changes very little over the complete $HClO_4$ concentration range studied. It is therefore considered unlikely that the concentration of electroactive sites will vary substantially within this $HClO_4$ concentration range and, therefore, this concentration independence of $D_{CT}(CV)$ is real.

In 4.0M $HClO_4$, the charge transport rates are slightly smaller than those observed in more dilute $HClO_4$ electrolytes. Fig. 4.11 and Fig. 4.12 illustrate the change in layer mass of a 2.35×10^{-8} $OsPVP_{33}$ coated crystal (same layer as in Fig. 4.7) during 100 mVs^{-1} voltammetric experiments in 0.01M and 4.0M $HClO_4$. The corresponding mass- and Φ_{ClO4^-} -charge plots are illustrated in Fig. 4.13 and Fig. 4.14 respectively. The mass- and Φ_{ClO4^-} -charge plots are essentially identical to those observed in 1.0M $HClO_4$ (see Fig. 4.9). As was noted above, the hysteresis in these plots indicates that interfacial solvent transfer is impeded [1,3-5]. The mass-potential plots in 0.01M $HClO_4$ (Fig. 4.11) are similar to those observed in 1.0M $HClO_4$ (see Fig. 4.7). In these $HClO_4$ electrolyte concentrations, typically 4-5 successive voltammetric scans are necessary before reproducible, steady-state mass changes are observed. However, in 4.0M $HClO_4$ (Fig. 4.12), the change in layer mass has not reached its steady-state following 6 successive scans. This behaviour illustrates that interfacial mass transfer is comparatively more hindered in 4.0M $HClO_4$ and, whilst the origins of this change in the facility for mass transfer remain unclear, it is suggested that they may be responsible for the slight decrease in $D_{CT}(CV)$ in this electrolyte concentration (see Fig. 4.10).

Fig. 4.11. Mass-potential plots for an $OsPVP_{33}$ coated crystal in 0.01M $HClO_4$. Scan rate is 100 mVs^{-1}. Gravimetric surface coverage is 2.35 x 10^{-8} $molcm^{-2}$.

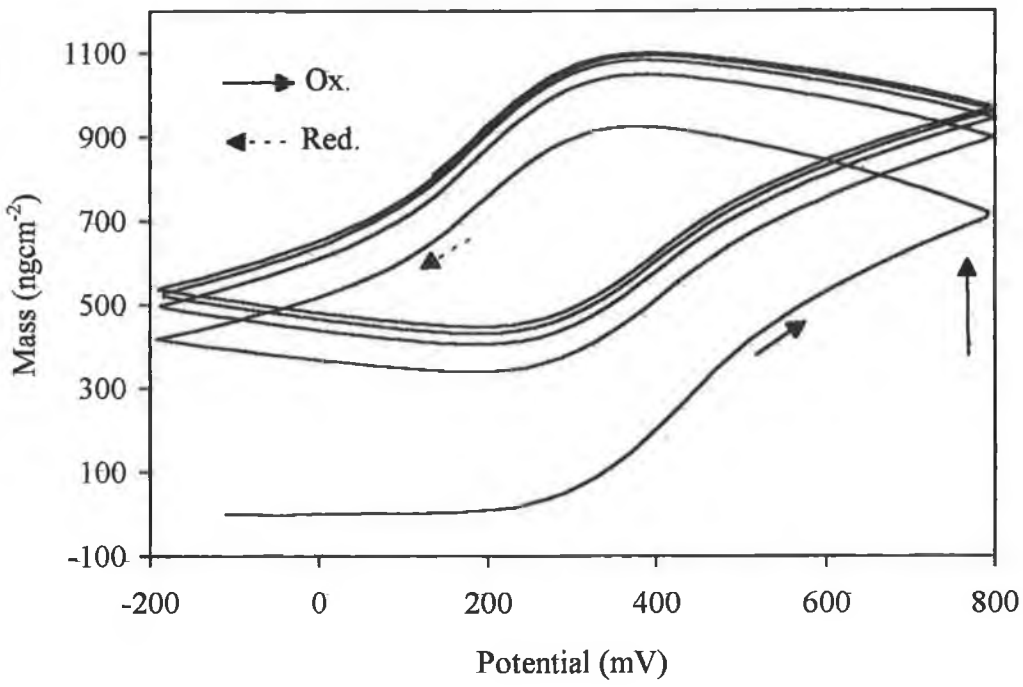

Fig. 4.12. Mass-potential plots for an $OsPVP_{33}$ coated crystal in 4.0M $HClO_4$. Scan rate is 100 mVs^{-1}. Gravimetric surface coverage is 2.35 x 10^{-8} $molcm^{-2}$.

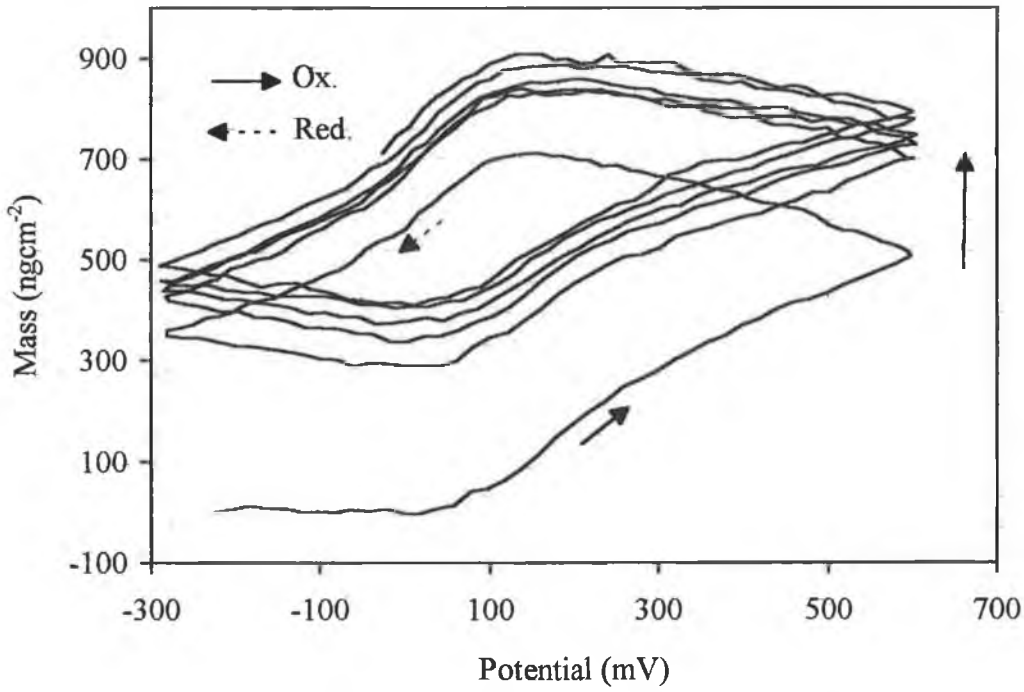

Fig. 4.13. Mass- and Φ_{ClO4}^- -charge plots for data in Fig. 4.11.

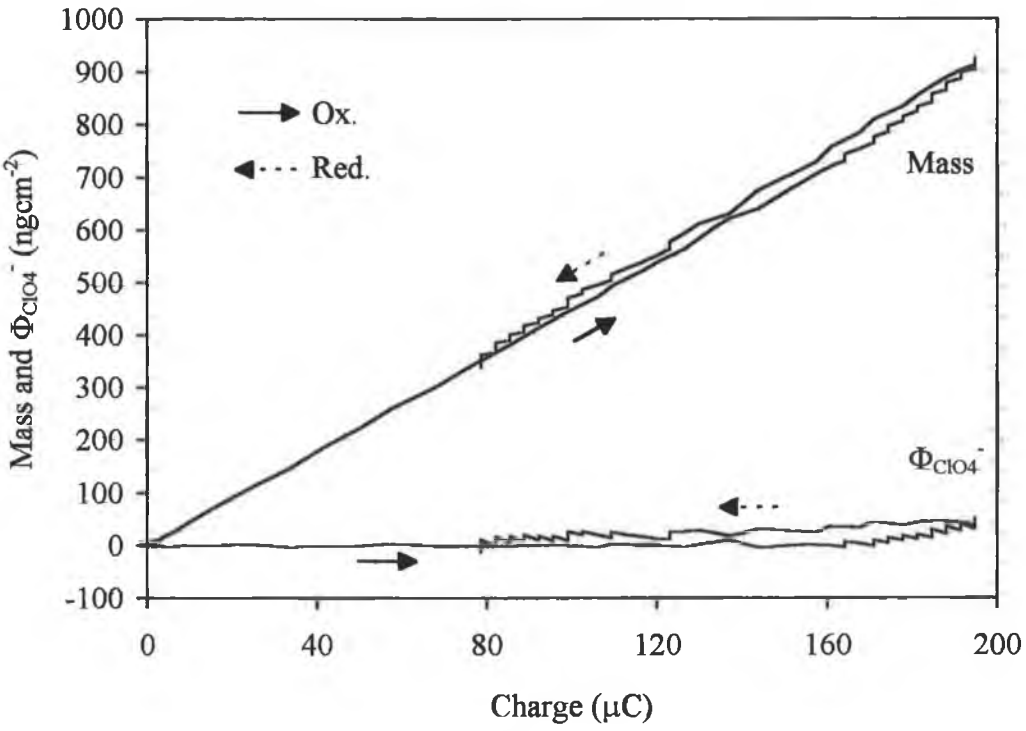

Fig. 4.14. Mass- and Φ_{ClO4}^- -charge plots for data in Fig. 4.12.

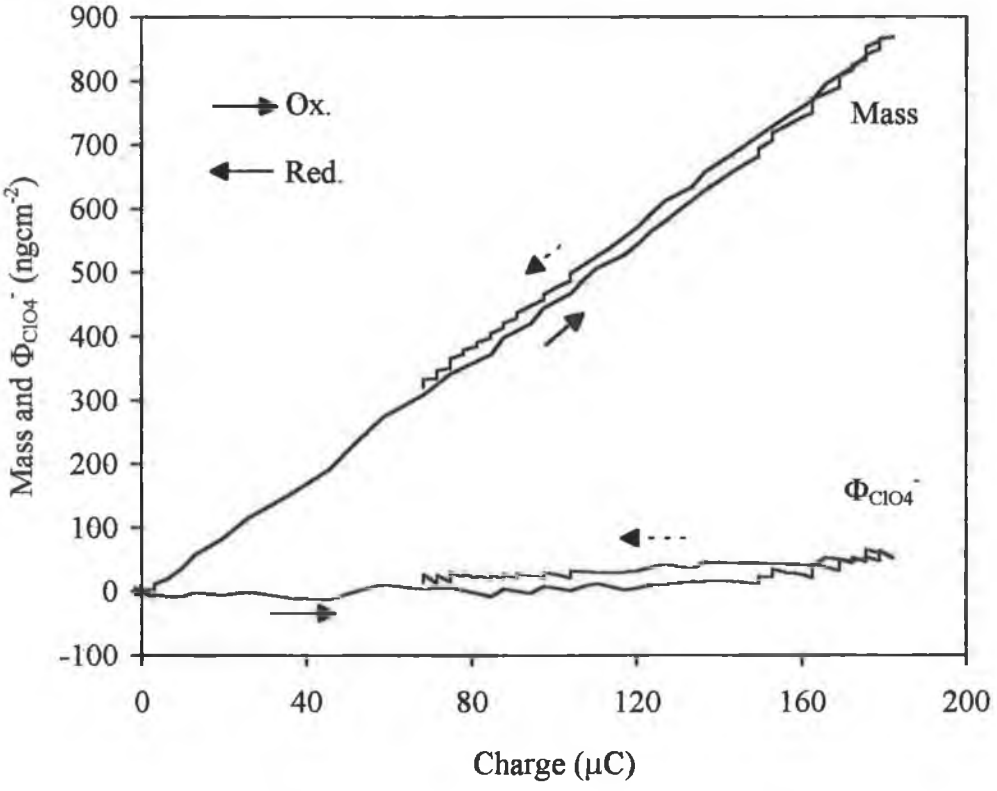

The mass transfer properties of $OsPVP_{100}$ coatings were reported under similar experimental conditions [18]. During polymer oxidation, under semi-infinite diffusion conditions, the mass of the $OsPVP_{100}$ coatings continues to increase following cessation of the anodic charge and is considered to reflect hindered solvent motion [18]. Fig. 4.10 illustrates the $HClO_4$ concentration dependence of $D_{CT}(CV)$ for $OsPVP_{100}$ coatings. $D_{CT}(CV)$ increases on increasing the $HClO_4$ concentration from 0.01M to 0.1M $HClO_4$. Within the concentration range of 0.1M to 1.0M $HClO_4$, $D_{CT}(CV)$ decreases. For the $OsPVP_{100}$ polymer, it has been suggested that, within the concentration range of 0.01M to 1.0M $HClO_4$, the changes in $D_{CT}(CV)$ reflect changes in the relative ease of solvent motion [18]. In 0.1M $HClO_4$, where solvent motion is most facile, the charge transport rate is faster than in all other $HClO_4$ concentrations. In 1.0M and 0.01M $HClO_4$, where solvent transfer is relatively more hindered, the observed charge transport rates are considerably reduced [18].

Similarly, for the $OsPVP_{33}$ polymer, interfacial solvent transfer is the slowest of the redox-switching-induced mass transfer processes. However, compared with the $OsPVP_{100}$ polymer, the rate of charge transport through the $OsPVP_{33}$ polymer is insensitive to the $HClO_4$ electrolyte concentration. This behaviour is a consequence of the fact that, with the possible exception of the 4.0M $HClO_4$ data, the facility for solvent transfer through the $OsPVP_{33}$ polymer does not vary with $HClO_4$ electrolyte concentration. Therefore, whilst the origins of the changes in the facility for solvent transfer in $OsPVP_{100}$ are unknown [18], it is suggested that they are responsible for the different change transport rates observed in the $OsPVP_{100}$ and $OsPVP_{33}$ polymers.

4.5. Conclusions.

The redox-switching-induced mass transfer properties of $OsPVP_{33}$ layers are insensitive to the $HClO_4$ concentration of the contacting electrolyte under both equilibrium and dynamic conditions. This behaviour reflects the permselective nature of these coatings and is likely a consequence of the hydrophobic and compact nature of these layers. Under slow scan conditions, scan rate 5 mVs^{-1}, electroneutrality is maintained by the ingress/ egress of the electrolyte anion. The normalised mass changes illustrate that anion ingress is accompanied by approximately 0.2 molecules of solvent per redox site converted. This solvent component of the normalised mass change is delineated from the anion under dynamic experimental conditions. With the exception of 4.0M $HClO_4$, the rate of charge transport through $OsPVP_{33}$ coatings is independent of the $HClO_4$ electrolyte concentration and reflects the concentration independence of the mass transfer processes in these layers. The overall mass transfer properties of this polymer are qualitatively similar to those observed in $OsPVP_{100}$. However, the level of solvent ingress is less for the $OsPVP_{33}$ polymer which is likely a consequence of the hydrophobic nature of the styrene moieties in this copolymer backbone.

4.6. References.

1. A.R. Hillman, M.J. Swann and S. Bruckenstein, J. Phys. Chem., 95 (1991) 3271.
2. A.R. Hillman, N.A. Hughes and S. Bruckenstein, Analyst, 119 (1994) 167.
3. A.R. Hillman, D.C. Loveday, M.J. Swann, S. Bruckenstein and C.P. Wilde, Analyst, 117 (1992) 1251.
4. A.R. Hillman, D.C. Loveday, M.J. Swann, B. Bruckenstein and C.P. Wilde, J. Chem. Soc. Faraday Trans., 87 (1991) 2047.
5. A.R. Hillman, D.C. Loveday and S. Bruckenstein, J. Electroanal. Chem., 300 (1991) 67.
6. A.R. Hillman and S. Bruckenstein, J. Chem. Soc. Faraday Trans., 89 (1993) 339.
7. A.R. Hillman and S. Bruckenstein, J. Chem. Soc. Faraday Trans., 89 (1993) 3779.
8. S. Bruckenstein and A.R. Hillman, J. Phys. Chem., 92 (1988) 4837.
9. S. Bruckenstein and A.R. Hillman, J. Phys. Chem., 95 (1991) 10748.
10. A.R. Hillman, M.J. Swann and S. Bruckenstein, J. Electroanal. Chem., 291 (1990) 147.
11. A.P. Clarke, J.G. Vos, A. Glidle and A.R. Hillman, J. Chem. Soc. Faraday Trans., 89 (1993) 1695.
12. A.R. Hillman, D.C. Loveday and S. Bruckenstein, J. Electroanal. Chem., 274 (1989) 157.
13. A.R. Hillman, D.C. Loveday, S. Bruckenstein and C.P. Wilde, J. Chem. Soc. Faraday Trans., 86 (1990) 437.
14. S. Bruckenstein, C.P. Wilde, M. Shay, A.R. Hillman and D.C. Loveday, J. Electroanal. Chem., 258 (1989) 457.

15. S. Bruckenstein, A.R. Hillman and M.J. Swann, J. Electrochem. Soc., 137 (1990) 1323.

16. S. Bruckenstein, C.P. Wilde and A.R. Hillman, J. Phys. Chem., 97 (1993) 6853.

17. R. Borjas and D.A. Buttry, J. Electroanal. Chem., 280 (1990) 73.

18. A.P. Clarke, Ph.D. Thesis, Dublin City University, (1992).

19. A.R. Hillman, D.C. Loveday, M.J. Swann, S. Bruckenstein and C.P. Wilde, in P.G. Edelman and J.G. Wang (Ed.) ACS Symposium Series, Ch. 12, 487.

20. A.J. Kelly and N. Oyama, J. Phys. Chem., 95 (1991) 9579.

21. A.R. Hillman, D.C. Loveday, A. Glidle, J.G. Vos, A.P. Clarke, D. Kelly and S. Bruckenstein, Macromol. Symp., 80 (1994) 323.

22. A.J. Kelly, T. Ohsaka, N. Oyama, R.J. Forster and J.G. Vos, J. Electroanal. Chem., 287 (1990) 185.

23. A.P. Clarke, J.G. Vos, A.R. Hillman and A. Glidle, J. Electroanal. Chem., 389 (1995) 129.

24. S. Bruckenstein and M. Shay, Electrochim. Acta, 30 (1985) 1295.

25. A.P. Clarke, J.G. Vos and A.R. Hillman, J. Electroanal. Chem., 356 (1993) 287.

26. A. Glidle, A.R. Hillman and S. Bruckenstein, J. Electroanal. Chem., 318 (1991) 411.

27. S.M. Oh and L.R. Faulkner, J. Electroanal. Chem., 269 (1989) 77.

28. S.M. Oh and L.R. Faulkner, J. Am. Chem. Chem. Soc., 111 (1989) 5613.

29. E.F. Bowden, M.F. Dautartas and J.F. Evans, J. Electroanal. Chem., 219 (1987) 91.

30. Y. Marcus, Ion Solvation, Wiley-Interscience, New York, (1985).

Chapter 5.

The Mass and Charge Transport Properties of $[Os(bipy)_2(PVP_{33})_{10}Cl]^+$ and $[Os(bipy)_2(PVP_{100})_{10}Cl]^+$ Metallopolymer Films in $LiClO_4$ Electrolytes.

5.1. Introduction.

In Chapter 2, the influence of the $LiClO_4$ bathing electrolyte concentration on the rigidity and resident layer mass of $OsPVP_{33}$ and $OsPVP_{100}$ crystal coatings was investigated. In these electrolytes, these metallopolymer layers are sufficiently rigid to allow for the application of the Sauerbrey equation. Under these conditions, $OsPVP_{33}$ (surface coverage 0.7×10^{-8} molcm^{-2}) and $OsPVP_{100}$ (surface coverage (2.16×10^{-8} molcm^{-2}) layers are permselective within the electrolyte concentration range of 0.01M to 0.1M $LiClO_4$. Consequently, the resident layer mass in these polymers consists of initially imbibed solvent molecules only. Within the electrolyte concentration range of 0.5M to 4.0M $LiClO_4$, breakdown in layer permselectivity is accompanied by the ingress of salt molecules. The layer mass characteristics of these polymers are therefore different in $HClO_4$ and $LiClO_4$ electrolytes (see Chapter 2).

Systematic variation of the bathing electrolyte anion/ cation can aid in the identification of the predominant ion responsible for the maintenance of electroneutrality within electroactive films [1-12]. In this chapter, the influence of $LiClO_4$ electrolyte concentration on the change in layer mass during redox switching of $OsPVP_{33}$ and $OsPVP_{100}$ crystal coatings is investigated. The contribution of the electrolyte co-ion to the redox-switching-induced mass change can be ascertained by comparison with the corresponding results obtained in $HClO_4$ electrolytes.

For the $OsPVP_{100}$ polymer, redox-switching-induced steady-state mass changes have been previously reported in $NaClO_4$ electrolytes [4,13]. It has been illustrated that, although the perchlorate anion is predominantly responsible for the maintenance on electroneutrality during redox switching in these electrolytes, there is evidence for counterbalancing mass transfer processes i.e. bi-directional mass transfer [4]. Consequently, the observed mass changes are less than those predicated based on the weight of the perchlorate anion. In this chapter, similar behaviour is reported for this polymer in $LiClO_4$ electrolytes.

5.2. Experimental.

5.2.1. Apparatus.

The EQCM was described in Chapter 4.

5.2.2. Materials.

The synthesis of $[Os(bipy)_2(PVP_{100})_{10}Cl]Cl$ and $[Os(bipy)_2(PVP_{33})_{10}Cl]Cl$ were described in Chapter 2. $LiClO_4$ electrolytes were prepared with Milli-Q H_2O.

5.2.3. Procedures.

Crystal coatings were prepared as described in Chapter 2. The modifying layers were equilibrated in each $LiClO_4$ concentration by voltammetrically scanning over the $Os^{II/III}$ couple for a minimum of 3 hours. Scan rates of 1 mVs^{-1} and 50 mVs^{-1} were alternately used. The change in layer mass accompanying redox switching of $OsPVP_{33}$ and $OsPVP_{100}$ polymer coatings was studied as a function of the $LiClO_4$ electrolyte concentration (0.01M to 4.0M $LiClO_4$) and the experimental timescale (1 to 500 mVs^{-1}). The change in layer mass was found to be independent of the electrolyte concentration to which the layer had been previously exposed. All determinations were carried out on at least 2 different polymer layers in each $LiClO_4$ concentration. The gravimetric surface coverages of these polymers were in the range of 5.0×10^{-9} to 5.8×10^{-8} $molcm^{-2}$. For both polymers, the coulometric surface coverages, estimated from the area under the anodic peak of 1 mVs^{-1} cyclic voltammograms, were typically 25-35% smaller than the gravimetric surface coverages. This suggests that only 65-75% of the Os^{II} sites are electroactive on the timescale of these voltammetric experiments.

5.3. Results and Discussion.

5.3.1. Layer Mass Changes during Redox Switching of $OsPVP_{33}$ Films.

The mass transfer properties of $OsPVP_{33}$ polymer coatings in $LiClO_4$ electrolytes are dependent on the gravimetric surface coverage. From the $OsPVP_{33}$ crystal coatings studied, two surface coverage ranges of different mass transfer behaviour were identified a) 0.5 to 0.99 x 10^{-8} molcm^{-2} and b) 1.1 to 5.8 x 10^{-8} molcm^{-2}.

5.3.1.1. Gravimetric surface coverages of 0.5 to 0.99 x 10^{-8} molcm^{-2}.

In Chapter 2, the admittance characteristics of a 0.7 x 10^{-8} molcm^{-2} $OsPVP_{33}$ coated crystal were examined as a function of the $LiClO_4$ bathing electrolyte concentration for the Os^{II} oxidation state. Within the concentration range of 0.01M to 0.1M $LiClO_4$, this layer exhibits permselective behaviour with no apparent change in the resident layer mass. Within the concentration range of 0.5M to 4.0M $LiClO_4$, breakdown in layer permselectivity is accompanied by the ingress of $Li^+ClO_4^-$. The shape of the crystal resonance remains essentially constant in all $LiClO_4$ concentrations, illustrating that these layers are rigid under these conditions [4,13-17].

For the work reported here, the crystal resonance shape of $OsPVP_{33}$ coated crystals was studied as a function of the $Os^{II/III}$ oxidation states, to probe for possible deleterious swelling variations during redox switching. Fig. 5.1 illustrates the change in crystal resonance of an $OsPVP_{33}$ coated crystal during an oxidative 5 mVs^{-1} cyclic voltammogram in 0.01 M $LiClO_4$. The gravimetric surface coverage was 9.1 x 10^{-9} molcm^{-2}. Only the initial (ca. -100 mV) and final (ca. +600 mV) spectra are illustrated. This figure is representative of the general behaviour of this $OsPVP_{33}$

Fig. 5.1. Admittance spectra for an $OsPVP_{33}$ coated crystal during redox switching in 0.01M $LiClO_4$ at 5 mVs^{-1}. Gravimetric surface coverage is 9.1 x 10^{-9} $molcm^{-2}$.

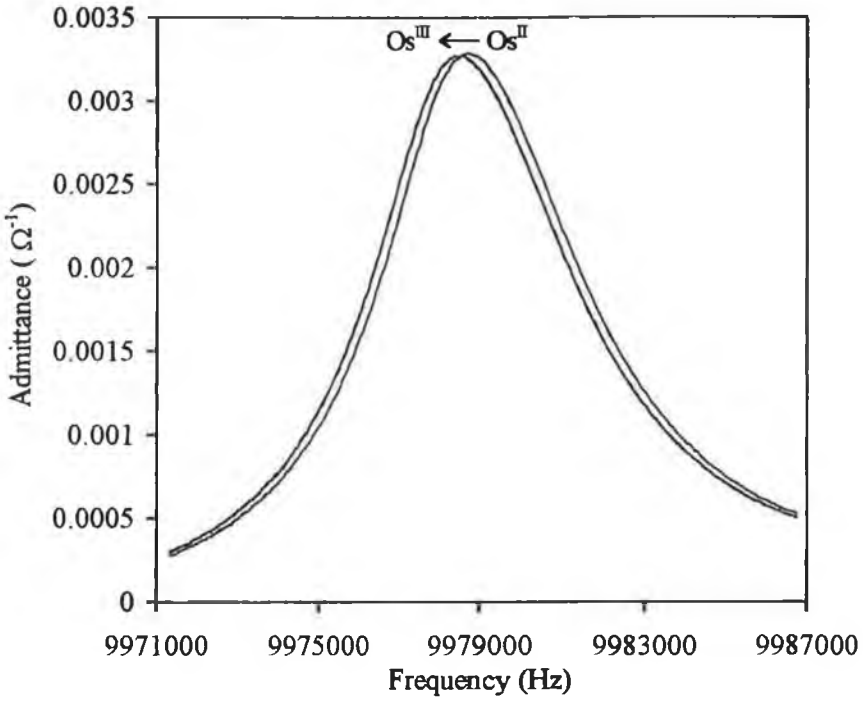

coating in all $LiClO_4$ concentrations studied.

The characteristics of Fig. 5.1 are similar to those observed for $OsPVP_{33}$ coatings in $HClO_4$ electrolytes (see Chapter 4). The resonant frequency decreases during polymer oxidation, which suggests that anion ingress is responsible for the maintenance of electroneutrality. The crystal resonance shape is essentially constant in both redox states, indicating that the layer remains compact during redox switching [4,13-17]. Therefore, the change in layer mass accompanying redox switching may be accurately evaluated from the shift in resonant frequency using the Sauerbrey equation.

Fig. 5.2 illustrates the change in layer mass during a 5 mVs^{-1} voltammetric

scan of an $OsPVP_{33}$ coated crystal in 0.01M $LiClO_4$. The gravimetric surface coverage was 5.0×10^{-9} molcm^{-2}. Fig. 5.2 is representative of the general mass transfer characteristics of this layer in all $LiClO_4$ electrolyte concentrations studied, for this experimental timescale. Table 5.1. summarises the overall change in layer mass of $OsPVP_{33}$ coated crystals (gravimetric surface coverage 0.5 to 0.99×10^{-8} molcm^{-2}) accompanying redox switching in $LiClO_4$ electrolytes. These normalised mass changes are associated with the maintenance of electroneutrality within these layers during the $Os^{II/III}$ oxidation process. The voltammetric scan rates were 1 and 5 mVs^{-1}. The normalised mass changes are reproducible to within 5% for determinations on different films and 3% for repeated determinations on a single film. Typically 3 successive voltammetric scans were obtained in each coating/ electrolyte concentration combination. The mass changes for the first and successive scans are identical and only those obtained for the first voltammetric scan are illustrated. The normalised mass change associated with the oxidation/ reduction of these layers is clearly independent of the $LiClO_4$ concentration of the contacting electrolyte and suggests that these layers are permselective in all $LiClO_4$ electrolyte concentrations under investigation.

Table 5.2. summarises the potentials of half-total-charge change, $E_{1/2}(q)$, and half-total-mass change, $E_{1/2}(m)$, for both oxidative and reductive processes, obtained during 5 mVs^{-1} cyclic voltammetric experiments. Also included are the corresponding anodic and cathodic peak potentials. As was observed in $HClO_4$ electrolytes (see Chapter 4), these layers do not exhibit true surface behaviour in $LiClO_4$ electrolytes. Within experimental error ($\pm$ 5 mV), the potentials of half-total-mass change and half-total-charge change coincide in all $LiClO_4$ concentrations above 0.01M $LiClO_4$, reflecting concomitant mass and charge transport [4,18,19].

Fig. 5.2. Mass-potential plot for an $OsPVP_{33}$ coated crystal in 0.01M $LiClO_4$. Scan rate is 5 mVs^{-1}. Gravimetric surface coverage is 5.0×10^{-9} $molcm^{-2}$.

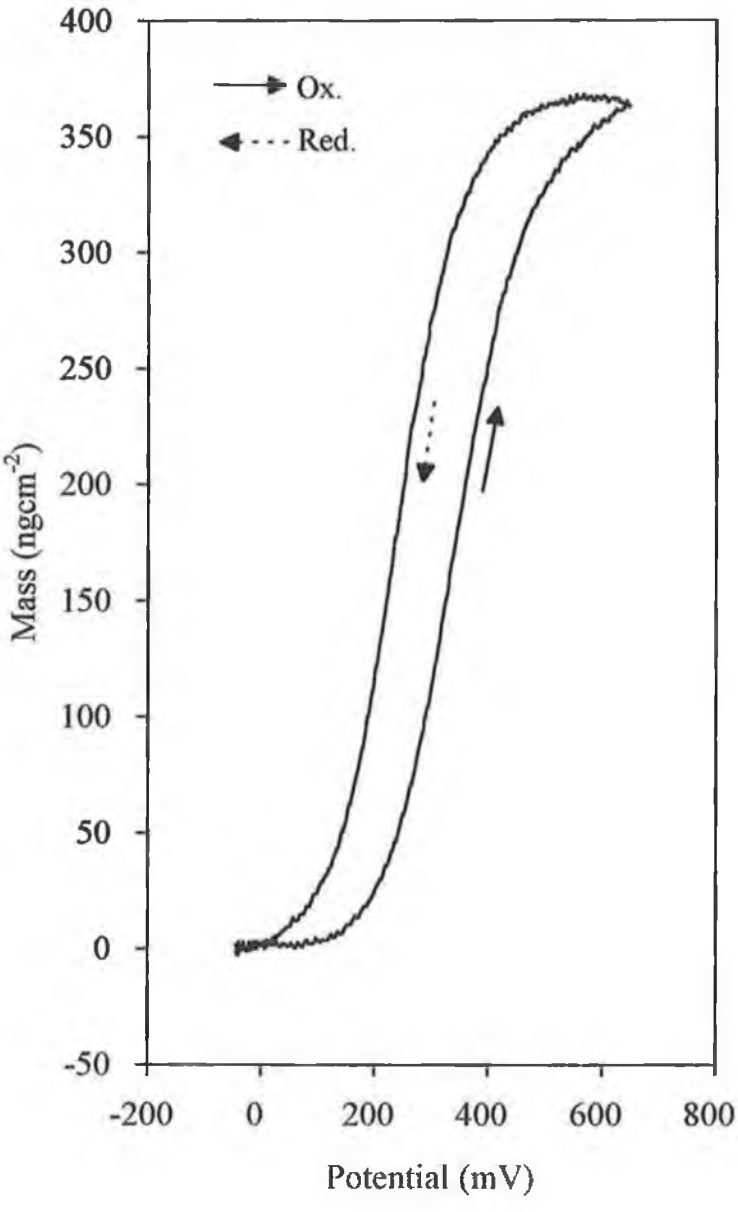

Table 5.1. The effect of $LiClO_4$ electrolyte concentration on the normalised mass change accompanying redox switching of $OsPVP_{33}$ coated crystals. Gravimetric surface coverages are 0.5 to 0.99 $x10^{-8}$ $molcm^{-2}$.

$LiClO_4$ Conc. (M)	Normalised Mass Change ($gmol^{-1}$)	
	A. 1 mVs^{-1} [a]	B. 5 mVs^{-1} [a]
0.01	103 (2)	105*
0.05	107 (1)	101 (5)
0.10	104 (1)	103 (1)
0.50	102 (1)	102 (1)
1.00	105 (2)	105 (3)
2.00	103 (2)	105 (1)
4.00	103 (1)	102 (2)

(a) errors quoted in brackets represent the variations between 2 different films.

* signifies measurements made on one film only.

Table 5.2. The oxidation/ reduction potentials of the $Os^{II/III}$ couple and their associated half-mass and half-charge potentials for $OsPVP_{33}$ coated crystals in $LiClO_4$.

$LiClO_4$ Conc.(M)	Oxidation[a]			Reduction[a]		
	$E_{1/2}$ (Ox.)	$E_{1/2}$ (q)	$E_{1/2}$ (m)	$E_{1/2}$ (Red.)	$E_{1/2}$ (q)	$E_{1/2}$ (m)
0.01	367	364	393	265	261	261
0.05	342	339	344	233	237	236
0.10	306	309	309	215	214	214
0.50	276	276	281	190	187	187
1.00	247	249	254	169	166	169
2.00	216	215	217	151	149	146
4.00	182	186	186	124	128	128

(a) All potentials (mV vs SCE) measured at 1 mVs^{-1} at ambient temperatures (20 ± 2^{o} C).

Fig. 5.3 illustrates the mass- and Φ_{ClO4^-} -charge plots for the data in Fig. 5.2. The minimal hysteresis, coupled with the scan rate independence of the normalised mass change (see Table 5.1.), reflects the attainment of at least pseudo-equilibrium on this experimental timescale. The minimal hysteresis in these plots suggests that mass transfer and charge transport occur concomitantly and corroborates the data in Table 5.2. This, coupled with the increase/ decrease in layer mass during oxidation/ reduction and the similarity in the behaviour in $LiClO_4$ and $HClO_4$ electrolytes, illustrates that electroneutrality is maintained by anion motion.

Under these conditions, the Φ_{ClO4^-} -charge plot represents the motion of solvent molecules in response to activity constraints imposed by the changing oxidation state of the polymer layer [20]. For the initial 35 μC of osmium oxidation, the Φ_{ClO4^-} data is zero, which suggests that anion influx occurs in the absence of solvent transfer. On further oxidation of the layer (above 30 μC), the Φ_{ClO4^-} data is greater than zero and indicates that solvent motion accompanies anion ingress. The normalised mass changes associated with these processes are 99 $gmol^{-1}$ and 110 $gmol^{-1}$ respectively. These mass changes are almost identical to those observed in $HClO_4$ solutions and can be equated with the initial sole influx of the anion and the subsequent influx of the anion with ca. 0.5 molecules of solvent per redox site converted. This level of solvent transfer is small and is delineated from the anion (see Section 5.3.3.1). Therefore, as was observed in $HClO_4$ solutions, the charge-compensating anion apparently enters the layer in the unhydrated form.

The mass transfer properties of $OsPVP_{33}$ coatings (gravimetric surface coverage 0.5 to 0.99 x 10^{-8} $molcm^{-2}$) are therefore clearly identical in $HClO_4$ and $LiClO_4$ electrolytes. Consequently, the electrolyte cation plays no apparent part in the maintenance of electroneutrality during redox switching of these materials. This behaviour is consistent with the observation that the electrolyte anion is solely responsible for the maintenance of electroneutrality within these layers during redox processes.

Fig. 5.3. Mass- and Φ_{ClO4^-} -charge plots for data in Fig. 5.2.

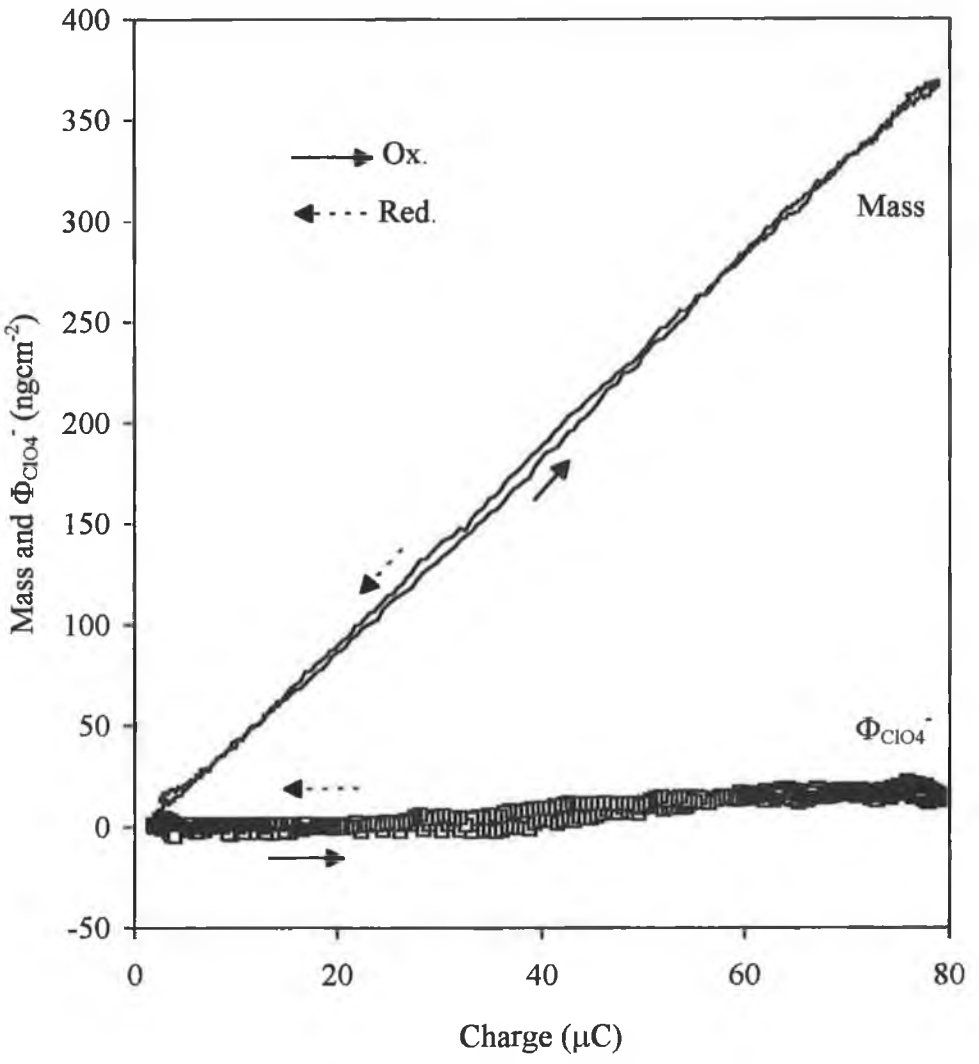

As was stated above, the data in Fig. 5.2 and Fig. 5.3 are representative of the redox-switching-induced mass transfer properties of these $OsPVP_{33}$ coating in all $LiClO_4$ concentrations under investigations. Table 5.1. illustrates that the overall mass changes accompanying redox switching are independent of the $LiClO_4$ electrolyte concentration. Therefore, even in concentrations in excess of 1.0M $LiClO_4$, these $OsPVP_{33}$ coatings behave permselectively during redox switching. This behaviour is surprising and likely reflects the compact nature of this polymer.

5.3.1.2. Gravimetric surface coverages of 1.1 to 5.8 x 10^{-8} molcm^{-2}.

In Chapter 2, the change in resident layer mass of a 3.27 x 10^{-8} molcm^{-2} $OsPVP_{33}$ coating was examined as function of the bathing $LiClO_4$ concentration. For this polymer, equilibrium ion and solvent levels are only achieved following voltammetric cycling of the layer. This behaviour is considered to reflect the difficulty in establishing equilibrium mobile species levels within this thick coating.

Fig. 5.4 and Fig. 5.5 illustrate the change in crystal resonance of a 2.87 x 10^{-8} molcm^{-2} $OsPVP_{33}$ coated crystal during an oxidative 5 mVs^{-1} scan in 0.01M and 1.0M $LiClO_4$ respectively. These spectra are representative of the general behaviour of this $OsPVP_{33}$ coating thickness in all $LiClO_4$ concentrations under investigation. In Fig. 5.4 and Fig. 5.5, the decrease in resonant frequency during polymer oxidation represents an increase in the layer mass and is associated with the influx of charge compensating counterions. The shape of the crystal resonance broadens during redox switching and suggests that the layer swells. This behaviour contrasts with the rigid layer behaviour of thinner $OsPVP_{33}$ layers in these $LiClO_4$ solutions (see Fig. 5.1) and may reflect the greater mass influx associated with the greater number of osmium sites within the thicker film. However, this broadening corresponds to only an approximate 3% change in the crystal resonance shape, which is unlikely to invalidate the Sauerbrey equation. It is therefore anticipated that the change in layer mass during redox switching may be accurately evaluated from the shift in resonant frequency using the Sauerbrey equation.

Fig. 5.4. Admittance spectra for an $OsPVP_{33}$ coated crystal during redox switching in 0.01M $LiClO_4$ at 5 mVs^{-1}. Gravimetric surface coverage is 2.87 x 10^{-8} $molcm^{-2}$.

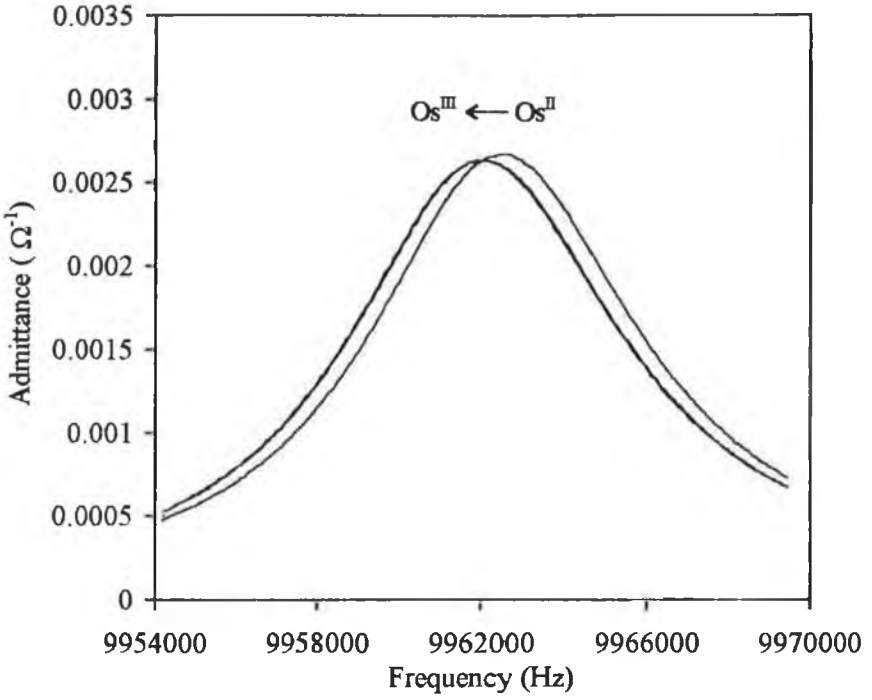

Fig. 5.5. Admittance spectra for an $OsPVP_{33}$ coated crystal during redox switching in 1.0M $LiClO_4$ at 5 mVs^{-1}. Gravimetric surface coverage is 2.87 x 10^{-8} $molcm^{-2}$.

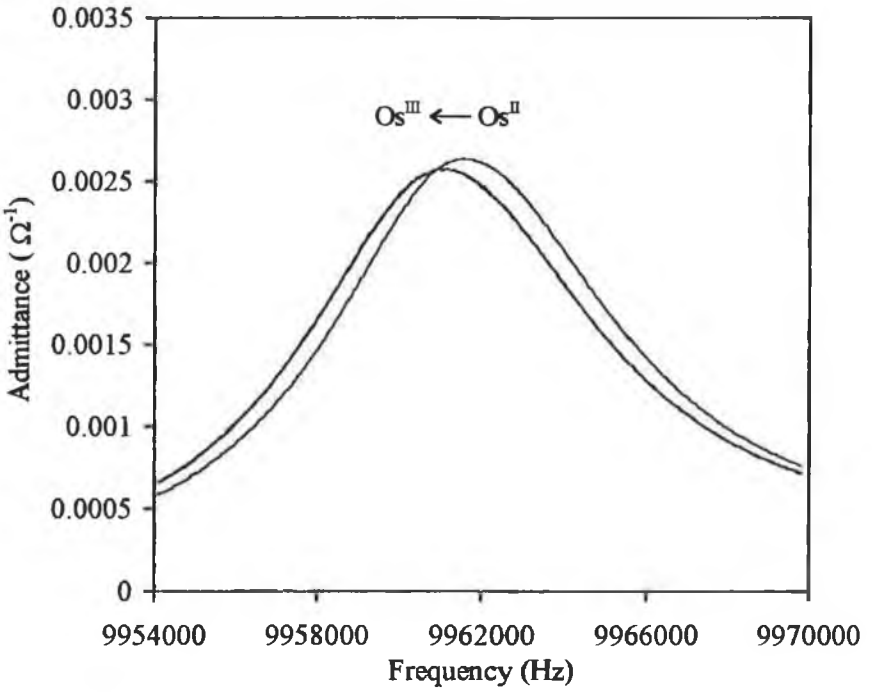

Fig. 5.6 illustrates the cyclic voltammogram and change in layer mass during a 5 mVs^{-1} voltammetric scan of an $OsPVP_{33}$ coated crystal in 1.0M $LiClO_4$. The gravimetric surface coverage was 1.75 x 10^{-8} $molcm^{-2}$. The cyclic voltammogram for the first and second voltammetric scans are essentially identical. However, the associated mass-potential plots for the first and second scans are different. This behaviour was not observed for thinner $OsPVP_{33}$ coatings under these conditions (see Fig. 5.2). The first mass-potential plot does not return to its original baseline mass following the completion of the first voltammetric scan. Therefore, some component of the mass transferred during the anodic scan remains trapped within the layer following the cathodic scan. For all voltammetric scans, the charge change during oxidation/ reduction is constant. Therefore, the mass trapped in the initial voltammogram is not associated with trapped ions and thus reflects the trapping of net neutral species. The original baseline mass is regenerated upon holding the layer in the Os^{II} oxidation state (i.e. -100 mV) for a minimum of 30 minutes. The second and subsequent mass potential-plots are identical and represent the establishment of steady-state mass changes. This behaviour, which has been observed previously for other polymer systems [13,15,21-25], is frequently referred to as a "break-in" effect.

Table 5.3. summarises the overall change in layer mass of $OsPVP_{33}$ coated crystals (gravimetric surface coverage 1.1 to 5.8 x 10^{-8} $molcm^{-2}$) accompanying redox switching in $LiClO_4$ electrolytes. The data were obtained at 1 and 5 mVs^{-1}. These normalised mass changes are reproducible to within 7% for determinations on different films and 3% for repeated determinations on a single film. Only the normalised mass changes associated with the first and second voltammetric scans are illustrated. In all $LiClO_4$ electrolyte concentrations under investigation, steady-state mass changes are achieved following the first voltammetric scan.

Within the concentration range of 0.05M to 4.0M $LiClO_4$, the overall normalised mass changes are independent of the $LiClO_4$ concentration of the contacting electrolyte (see Table 5.3.). The average normalised mass changes

Fig. 5.6. Cyclic voltammogram and mass-potential plot for an $OsPVP_{33}$ coated crystal in 1.0M $LiClO_4$. Scan rate is 5 mVs^{-1}. Gravimetric surface coverage is 1.75 x 10^{-8} $molcm^{-2}$.

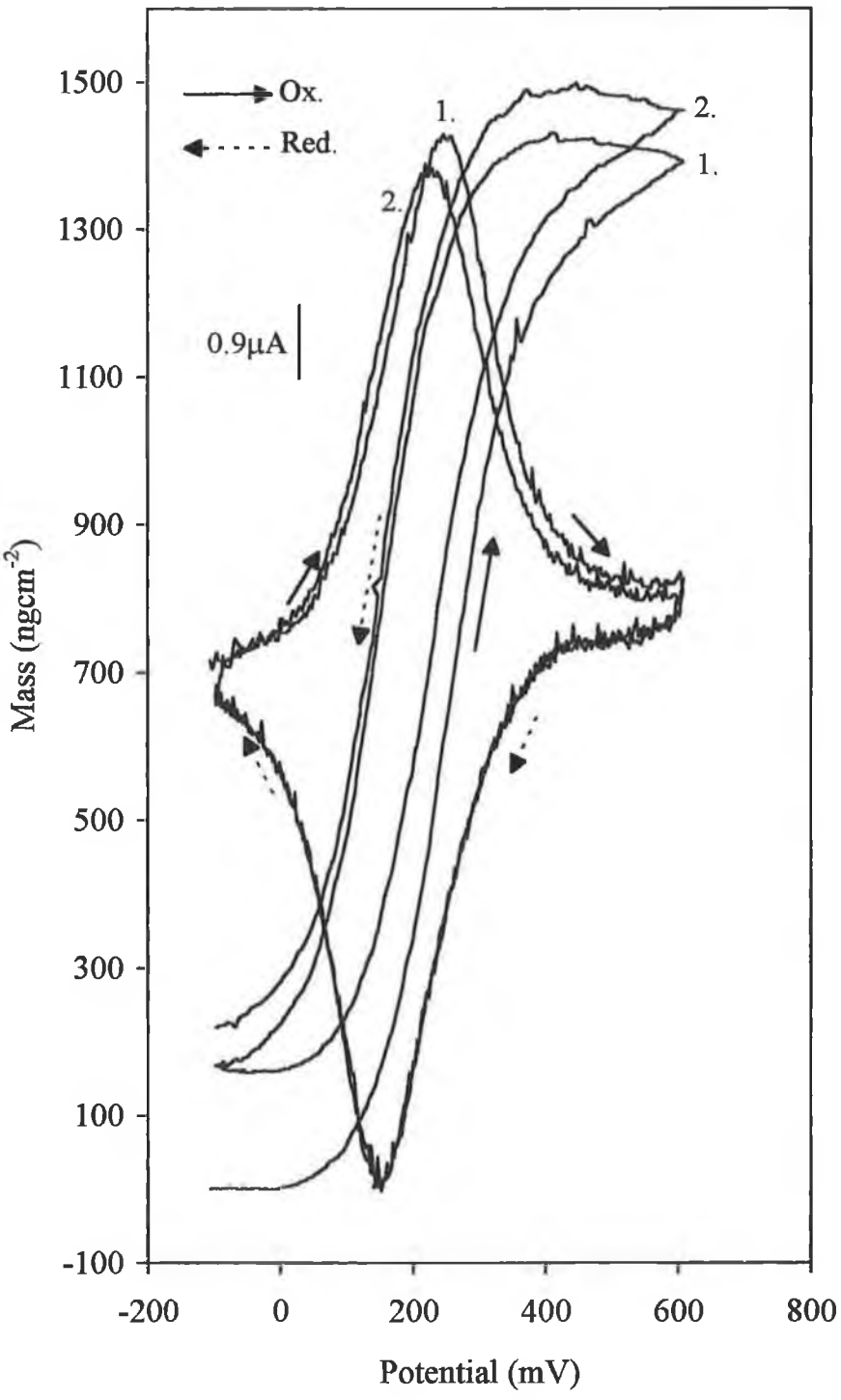

Table 5.3. The effect of $LiClO_4$ electrolyte concentration on the normalised mass change accompanying redox switching of $OsPVP_{33}$ coated crystals. Gravimetric surface coverages are 1.1 to 5.8 $x10^{-8}$ $molcm^{-2}$.

$LiClO_4$ Conc. (M)	Normalised Mass Change ($gmol^{-1}$)			
	1 mVs^{-1} [a]		5 mVs^{-1} [a]	
	Scan 1	Scan 2	Scan 1	Scan 2
0.01	145 (7)	134 (7)	146 (10)	135 (9)
0.05	119 (4)	102 (2)	115 (4)	103 (1)
0.10	115*	104*	112 (5)	102 (2)
0.50	115 (6)	101 (4)	111 (4)	99 (1)
1.00	114*	100 (1)	115 (2)	102 (4)
2.00			109 (3)	103 (2)
4.00	112*	100*	110 (2)	101 (1)

(a) Errors quoted in brackets represent the variations between 2 different films.

* signifies measurements made on one film only.

associated with the first and second voltammetric scans in these electrolyte concentrations are 113 (±3) $gmol^{-1}$ and 102 (±2) $gmol^{-1}$ respectively. The normalised mass changes associated with the second voltammetric scan are essentially identical to those observed for thinner $OsPVP_{33}$ coatings (see Section 5.3.1.1) and again reflect the predominant influx of the perchlorate anion. The insensitivity of the normalised mass change, for the first voltammetric scan, to the $LiClO_4$ electrolyte concentration, within the concentration range of 0.05M to 4.0M $LiClO_4$, suggests that these thicker layers behave permselectively during redox switching. The larger mass change observed during the first scan is therefore associated with the additional influx of solvent. This behaviour was not observed for thinner $OsPVP_{33}$ coatings (see Table 5.1.) and is considered to reflect the more swollen structure of these thicker coatings (see Fig. 5.4 and Fig. 5.5).

Fig. 5.7 illustrates the mass- and Φ_{ClO4^-} -charge plots for the data in Fig. 5.6. The mass charge plot for the first scan exhibits considerable hysteresis. In terms of Hillman's diagnostic scheme, it is considered that this hysteresis is indicative of hindered solvent motion [26-29]. Therefore, the system is under activity control rather than electroneutrality control. For the first voltammetric scan there is no apparent solvent motion for the first 85 μC of osmium oxidation (ca. 30% of total oxidation). Therefore, the mass changes observed are associated solely with anion motion. Further oxidation of the layer is accompanied by a sharp increase in Φ_{ClO4^-}, indicating solvent ingress. The normalised mass changes associated with these processes are 100 $gmol^{-1}$ and 120 $gmol^{-1}$ respectively (calculated from the individual slopes of the mass-charge plot). These mass changes may be equated with the initial ($Q_{OX} < 85$ μC) sole ingress of the perchlorate anion and the subsequent ($Q_{OX} > 85$ μC) ingress of one perchlorate anion and ca. 1 H_2O molecule per Os^{III} site. For the second scan data, the mass- and Φ_{ClO4^-} -charge plots are identical to those observed for thinner $OsPVP_{33}$ coatings in these electrolytes and for all $OsPVP_{33}$ coatings in $HClO_4$ electrolytes.

Fig. 5.7. Mass- and Φ_{ClO4}^- -charge plots for data in Fig. 5.6.

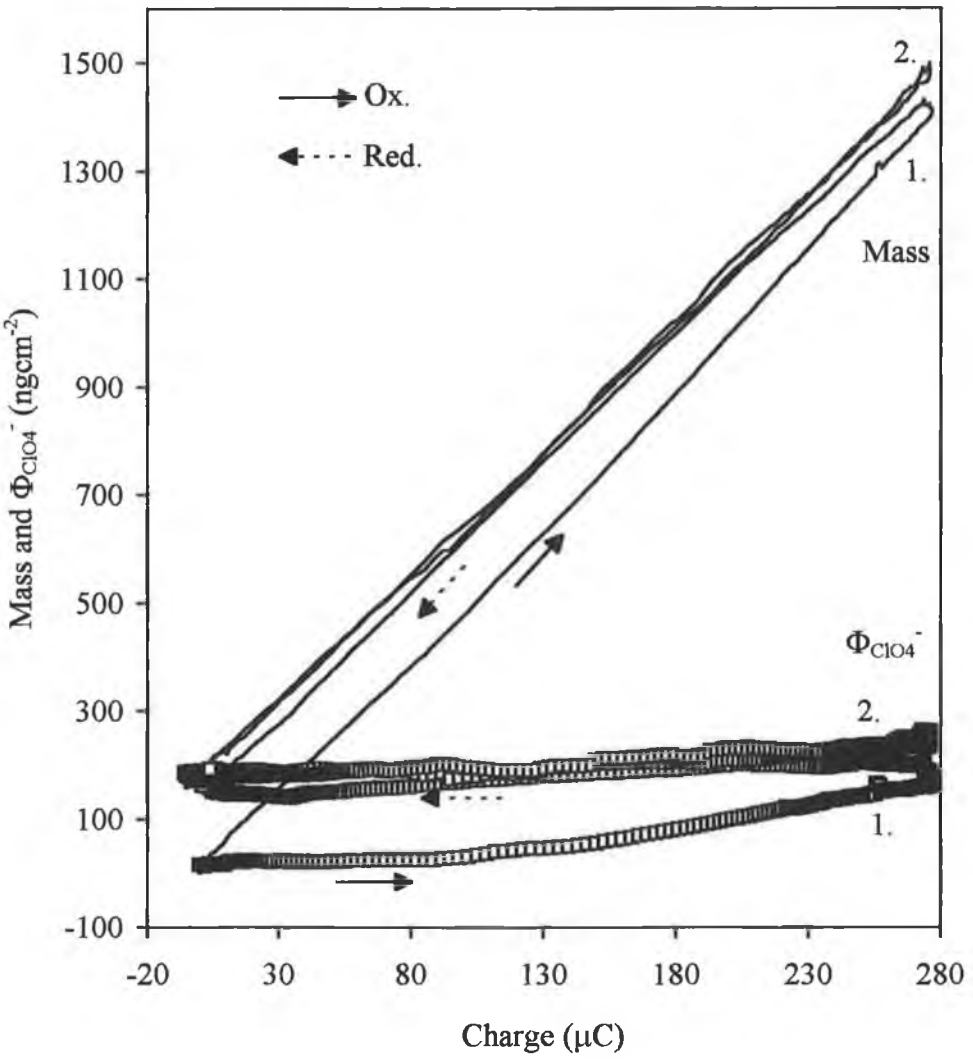

The normalised mass changes associated with the second scan are 101 gmol^{-1} (Q_{OX} < 85 μC) and 107 gmol^{-1} (Q_{OX} > 85 μC) and reflect the initial sole influx of the anion and the subsequent influx of the anion and ca. 0.5 molecules of solvent per Os^{III} site. The larger mass change observed for the first voltammetric scan, therefore represents an approximate two-fold increase in the level of solvent ingress during redox switching, This additional solvent component of the redox-switching-induced mass change is trapped during the first scan, as illustrated by the failure of the mass-

charge plot to close (see Fig. 5.7). We can therefore distinguish between different neutral components of the changing layer mass i.e. between solvent that is irreversibly transferred during the initial scan and solvent that is transferred reversibly during each scan.

In 0.01M $LiClO_4$, the overall normalised mass changes are 146 (±10) $gmol^{-1}$ and 135 (±9) $gmol^{-1}$ for the first and second voltammetric scans respectively (see Table 5.3.). Fig. 5.8 illustrates the mass- and Φ_{ClO4^-} -charge plots for an $OsPVP_{33}$ coated crystal in 0.01 M $LiClO_4$. The gravimetric surface coverage was 1.26 x 10^{-8} $molcm^{-2}$ and the scan rate was 5 mVs^{-1}. Compared with the data in Fig. 5.7, the mass-charge plots for both the first and second voltammetric scans exhibit hysteresis. Therefore, under these conditions, the system is under activity control during both voltammetric scans [26-29]. The larger normalised mass changes observed in 0.01M $LiClO_4$ may reflect additional solvent motion. The source of this additional solvent component is unknown. Assuming that anion motion is still responsible for the maintenance of electroneutrality, then, during redox switching, 2.5 (first scan) and 1.8 (second scan) molecules of solvent are transferred per redox site converted.

In summary, for $OsPVP_{33}$ coatings in $LiClO_4$ (and $HClO_4$) electrolytes, anion influx is responsible for the maintenance of electroneutrality during redox switching. For thin $OsPVP_{33}$ coatings, only small quantities of solvent are transferred during redox switching. Similar behaviour is observed for thicker layers once steady-state mass changes are obtained following the first voltammetric scan. These thicker layers are less compact during polymer oxidation and, as a result, the mass changes accompanying the first voltammetric scan are greater. These larger mass changes are considered to reflect the additional transfer of solvent. During the first voltammetric scan, this additional solvent component becomes trapped within the layer and all subsequent scans exhibit characteristics similar to those of thinner $OsPVP_{33}$ coatings.

Fig. 5.8. Mass- and Φ_{ClO4}^- -charge plots for an $OsPVP_{33}$ coated crystal in 0.01M $LiClO_4$. Scan rate is 5 mVs^{-1}. Gravimetric surface coverage is 1.26 x 10^{-8} $molcm^{-2}$.

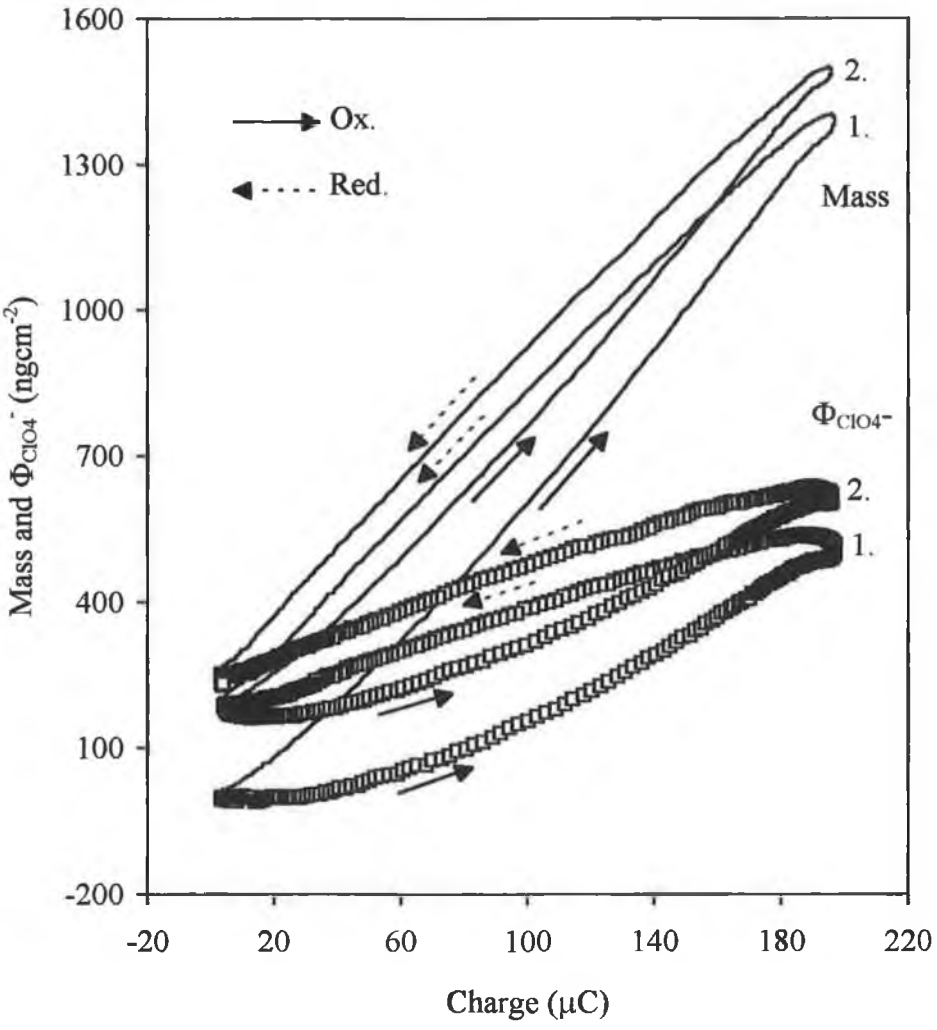

In $LiClO_4$ concentrations in excess of 0.5M $LiClO_4$, all $OsPVP_{33}$ layers appear to be permselective during redox switching, despite the apparent non-permselective nature of these coatings at open circuit in high $LiClO_4$ concentrations (see Chapter 2).

5.3.2. Layer Mass Changes during Redox Switching of $OsPVP_{100}$ Films.

In Chapter 2, the admittance characteristics of a 2.16 x 10^{-8} molcm^{-2} $OsPVP_{100}$ coated crystal were examined as a function of the $LiClO_4$ bathing electrolyte concentration, for the Os^{II} polymer oxidation state. Within the electrolyte concentration range of 0.01M to 0.1M $LiClO_4$, this layer exhibits permselective behaviour with no apparent change in the resident layer mass. Within the concentration range of 0.5M to 4.0M $LiClO_4$, this layer is no longer permselective and the resident layer mass increases. In all $LiClO_4$ concentrations, the shape of the crystal resonance is constant, which illustrates that layer rigidity is not compromised [4,13-17].

The crystal resonance shape of $OsPVP_{100}$ coated crystal were studied as a function of the $Os^{II/III}$ oxidation states. Fig. 5.9 illustrates the change in crystal resonance of a 2.16 x 10^{-8} molcm^{-2} $OsPVP_{100}$ coated crystal during an oxidative 5 mVs^{-1} scan in 0.01M $LiClO_4$. Only the initial (ca. -100 mV) and final spectra (ca. 600 mV) are illustrated. Fig. 5.9 is representative of the general behaviour of this $OsPVP_{100}$ coating in all $LiClO_4$ concentrations under investigation. As was observed for the $OsPVP_{33}$ polymer (see Fig. 5.4), the resonant frequency decreases during polymer oxidation and suggests that the influx of charge compensating counterions is responsible for the maintenance of electroneutrality. However, compared with the $OsPVP_{33}$ polymer (see Fig. 5.4), this increase in layer mass is accompanied by a sharpening of the crystal resonance shape. Therefore, despite the increase in layer mass, this layer apparently compacts during redox switching. This behaviour may be a consequence of either the crosslinking of the polymer layer by the perchlorate anion [30] or the egress of polymer species during polymer oxidation.

Fig. 5.9. Admittance spectra for an $OsPVP_{100}$ coated crystal during redox switching in 0.01M $LiClO_4$ at 5 mVs^{-1}. Gravimetric surface coverage is 2.16 x 10^{-8} $molcm^{-2}$.

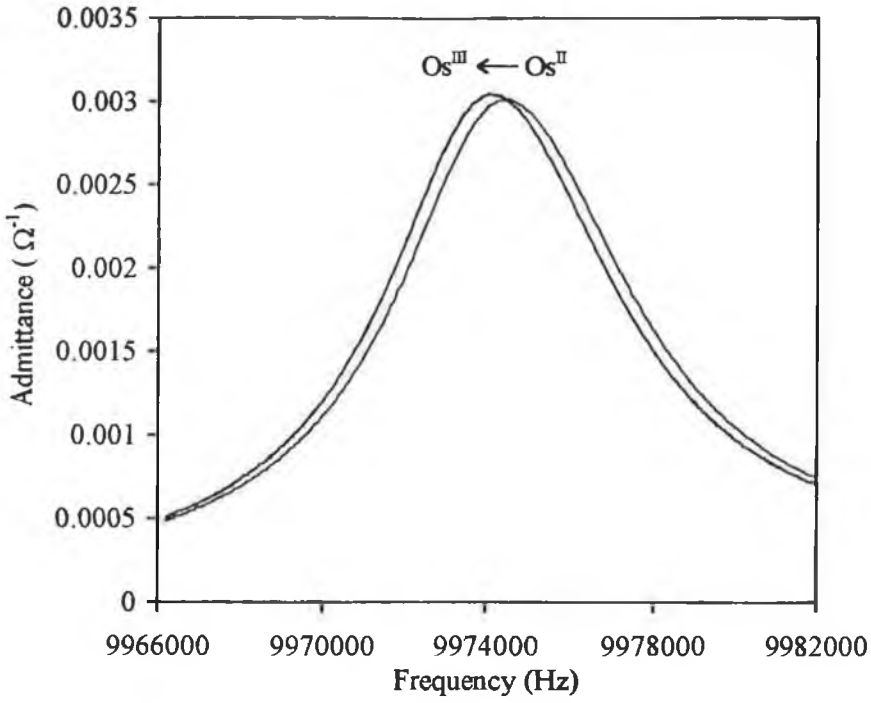

As was observed for $OsPVP_{33}$ coatings, the mass transfer properties of $OsPVP_{100}$ coated crystals are dependent on the polymer surface coverage.

5.3.2.1. Gravimetric surface coverages of 0.52 to 1.57 x 10^{-8} $molcm^{-2}$.

Fig. 5.10 illustrates the cyclic voltammogram and change in layer mass during a 5 mVs^{-1} voltammetric scan of an $OsPVP_{100}$ coated crystal in 0.1M $LiClO_4$. The gravimetric surface coverage was 1.03 x 10^{-8} $molcm^{-2}$. This behaviour is representative of the general mass and current characteristics of this layer in all $LiClO_4$ concentrations studied.

Fig. 5.10. Cyclic voltammogram and mass-potential plot for an $OsPVP_{100}$ coated crystal in 0.1M $LiClO_4$. Scan rate is 5 mVs^{-1}. Gravimetric surface coverage is 1.03×10^{-8} $molcm^{-2}$.

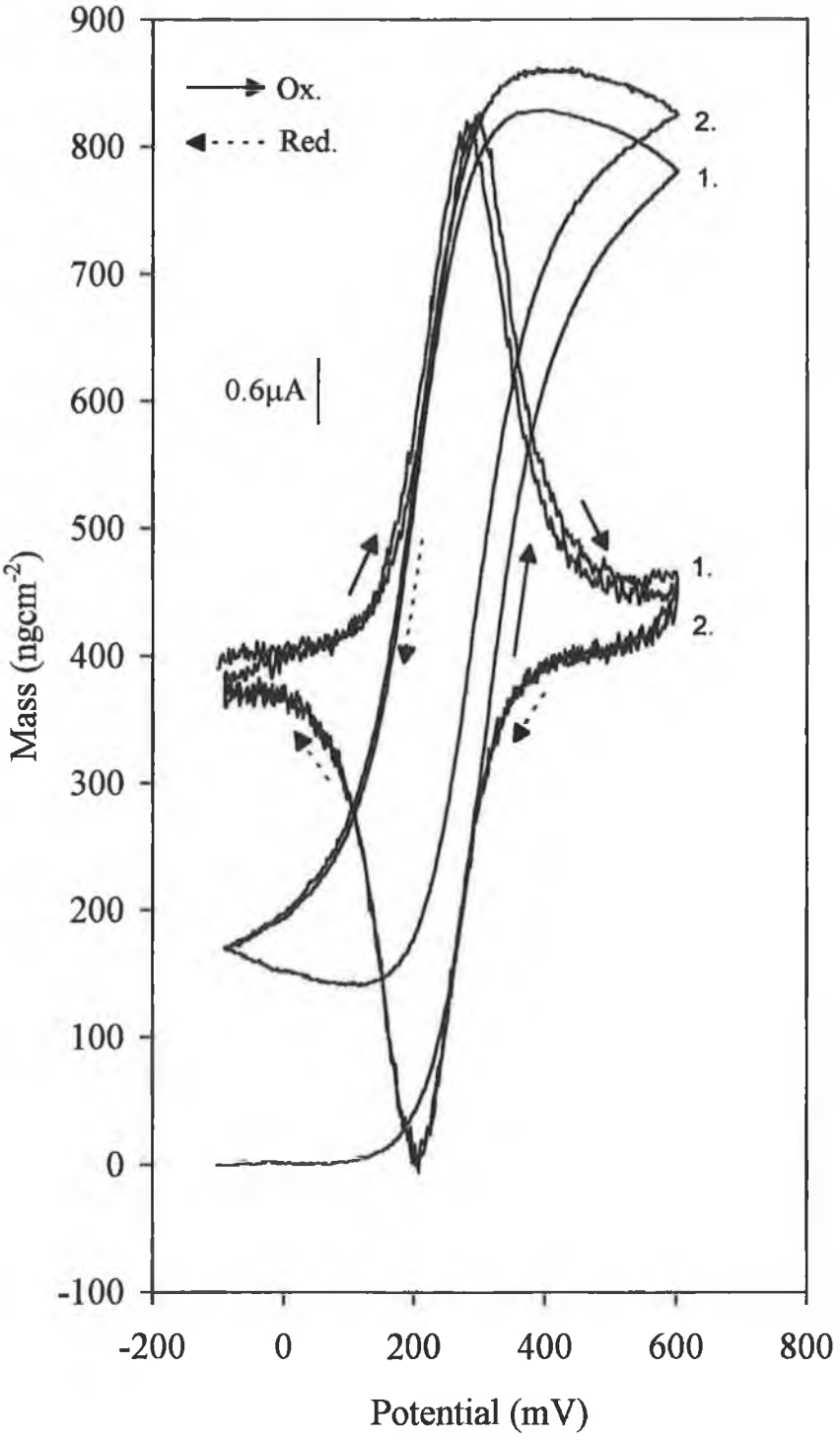

In Fig. 5.10, as was observed for all $OsPVP_{33}$ coatings, the cyclic voltammogram does not exhibit true surface behaviour. The characteristics of the mass-potential plots are similar to those observed for thicker $OsPVP_{33}$ coatings in these electrolytes (see Fig. 5.6). Failure of the mass-potential plot to close at the end of the first voltammetric scan reflects the trapping of mobile species within the layer during these redox processes. Steady-state mass changes are observed for the second and subsequent scans only.

Table 5.4. summarises the overall change in layer mass for $OsPVP_{100}$ coated crystals (gravimetric surface coverage of 0.52 to 1.57 x 10^{-8} molcm^{-2}) during redox switching in $LiClO_4$ electrolytes. The voltammetric scan rates were 1 and 5 mVs^{-1}. These normalised mass changes are reproducible to within 7% for determinations on different films and 4% for repeated determinations on a single film. Typically three successive voltammetric scans were obtained in each electrolyte concentration. A constant steady-state mass change is achieved following the first voltammetric scan. The normalised mass changes are qualitatively similar to those observed for $OsPVP_{33}$ coatings and suggest that the mass transfer processes are similar in both redox polymers.

The overall normalised mass changes for the first voltammetric cycle are independent of the bathing $LiClO_4$ concentration and are of a similar magnitude to the normalised mass changes observed for the first voltammetric scan of the thicker $OsPVP_{33}$ coatings in these electrolytes. An average normalised mass change of 114 ($\pm$4) gmol^{-1} is observed. The normalised mass changes associated with the second voltammetric scan are; less than those observed for the first scan, dependent on the electrolyte concentration and, more importantly, in electrolyte concentrations less than 0.5M $LiClO_4$, are less than those predicted for the influx of the perchlorate anion. It is therefore apparent that for the $OsPVP_{100}$ polymer, mass transfer occurs simultaneously in both directions i.e. anion ingress during polymer oxidation is accompanied by the egress of polymer phase species.

Table 5.4. The effect of $LiClO_4$ electrolyte concentration on the normalised mass change accompanying redox switching of $OsPVP_{100}$ coated crystals. Gravimetric surface coverages are 0.52 to 1.57 $x10^{-8}$ $molcm^{-2}$.

$LiClO_4$ Conc. (M)	Normalised Mass Change ($gmol^{-1}$)			
	1 mVs^{-1} (a)		5 mVs^{-1} (a)	
	Scan 1	Scan 2	Scan 1	Scan 2
0.01	111 (5)	90 (3)	115 (6)	93 (4)
0.05	112 (6)	92 (5)	114 (7)	94 (1)
0.10	115 (4)	91 (4)	112 (5)	92 (3)
0.50	113 (5)	99 (4)	113 (1)	101 (3)
1.00	118 (1)	101 (2)	115 (4)	102 (4)
2.00	112 (7)	107*	109 (6)	100 (2)
4.00	120 (5)	102 (5)	118 (3)	106*

(a) Errors quoted in brackets represent the variations between 2 different films.

* signifies measurements made on one film only.

Table 5.5. summarises the potentials of half-total-charge change and half-total-mass change for both oxidative and reductive processes, obtained during 5 mVs^{-1} cyclic voltammetric experiments. Also included are the corresponding anodic and cathodic peak potentials. In all $LiClO_4$ electrolyte concentrations, the potentials of half-total-mass change and half-total-charge change are delineated and thus illustrate that mass transfer is comparatively more hindered that charge transfer. This behaviour is discussed in the following sections.

Fig. 5.11 illustrates the mass- and Φ_{ClO4^-} -charge plots for the data in Fig. 5.10. During the first voltammetric scan, the Φ_{ClO4^-} -charge plot decreases for the first 35 μC of osmium oxidation. Therefore, the mass change observed is less than that anticipated for the influx of the charge compensating counterion, assuming that anion motion is responsible for the maintenance of electroneutrality. This behaviour may reflect either the simultaneous egress of net neutral species accompanying the ingress of the perchlorate anion or co-ion ejection for the maintenance of electroneutrality. However, in Chapter 2 it was noted that in $LiClO_4$ concentrations below 0.5M, the resident layer mass of $OsPVP_{100}$ coatings does not vary with $LiClO_4$ concentration. This behaviour is considered to reflect the permselectivity of these layers. Under these conditions, the only available neutral species within the polymer are the initially imbibed solvent molecules. It is therefore suggested that the initial decrease in the Φ_{ClO4^-} -charge plot represents the egress of solvent molecules rather than co-ion ejection. The egress of solvent may result from volume constraints imposed by the polymer structure, requiring solvent egress for the incorporation of the anion. Furthermore, it is suggested that this solvent egress mechanism is responsible for the observed increase in layer rigidity during redox switching (see Fig. 5.9).

Upon further oxidation of the layer (35 to 60 μC), the Φ_{ClO4^-} -charge plot is constant. This behaviour may reflect either the sole influx of the anion or exactly balancing solvent motion in opposite directions. As oxidation proceeds beyond 60 μC, the Φ_{ClO4^-} plot increases and becomes positive at ca. 100 μC. Within this region

Table 5.5. The oxidation/ reduction potentials of the $Os^{II/III}$ couple and their associated half-mass and half-charge potentials for $OsPVP_{100}$ coated crystals in $LiClO_4$.

$LiClO_4$ Conc.(M)	Oxidation[a]			Reduction[a]		
	$E_{1/2}$ (Ox.)	$E_{1/2}$ (q)	$E_{1/2}$ (m)	$E_{1/2}$ (Red.)	$E_{1/2}$ (q)	$E_{1/2}$ (m)
0.01	318	318	330	209	206	197
0.05	285	284	296	189	188	182
0.10	266	266	288	170	170	158
0.50	227	226	244	145	150	129
1.00	215	217	226	125	128	119
2.00	194	190	218	118	119	87
4.00	198	194	245	92	104	63

(a) All potentials (mV vs SCE) measured at 1 mVs^{-1} at ambient temperatures (20 ± 2° C).

Fig. 5.11. Mass- and Φ_{ClO4}^- -charge plots for data in Fig. 5.10.

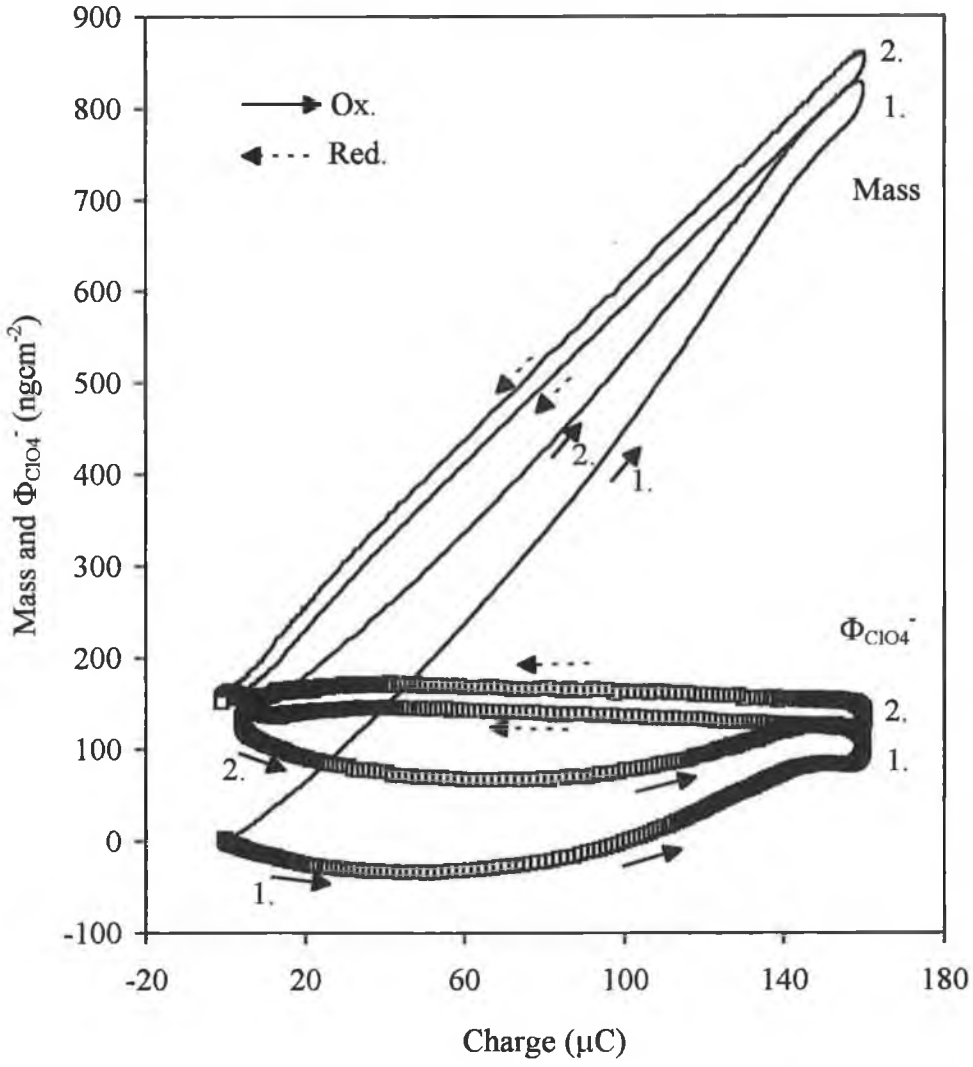

solvent ingress clearly dominates solvent egress. Upon cessation of the anodic charge, the mass of the layer continues to increase. This behaviour likely reflects the slow influx of solvent and highlights that solvent motion is hindered under these conditions [26-29]. Upon reduction, the Φ_{ClO4}^- -charge plot remains essentially constant and may reflect either the sole motion of the anion or counterbalancing solvent motion. The overall behaviour during the second voltammetric scan is similar

to that observed during the first.

Within the confines of these experiments, exact quantitation of these effects is not possible. Within the concentration range of 0.01M to 4.0M $LiClO_4$, the normalised mass change for the first voltammetric scan is independent of the $LiClO_4$ concentration and suggests that the layer is permselective. The average overall normalised mass change is 114 (±4) $gmol^{-1}$ and reflects the **net** influx of a single anion and ca. 1 solvent molecule per Os^{III} site. Because of the existence of bi-directional (counterbalancing) mass transfer processes, the level of solvent ingress is in fact greater than this. Our in-ability to separate the exact contributions of solvent ingress and egress prevents further quantitation.

In all $LiClO_4$ concentrations, the overall normalised mass change for the second voltammetric scan is less than that observed for the first. Within the concentration range of 0.01M to 0.1M $LiClO_4$, an average overall normalised mass change of 93 (±3) $gmol^{-1}$ is observed, which is less than that predicted for the motion of the anion. Similar behaviour has been previously reported for this polymer in $NaClO_4$ electrolytes [4,13]. Under these conditions solvent egress dominates solvent ingress. Within the concentration range of 0.5M to 4.0M $LiClO_4$, an average overall normalised mass change of 102 (±3) $gmol^{-1}$ is observed which suggests that only anions are transferred. Fig. 5.12 illustrates the mass and Φ_{ClO4^-} -charge plots for an $OsPVP_{100}$ coated crystal in 1.0M $LiClO_4$. The scan rate was 5 mVs^{-1} and the gravimetric surface was 1.28×10^{-8} $molcm^{-2}$. The Φ_{ClO4^-} -charge plot clearly highlights that, although the normalised mass change for the second scan is close to that predicted for anion motion, bi-directional solvent transfer is still observed. As was observed in 0.1M $LiClO_4$ (see Fig. 5.11), solvent egress dominates the initial oxidation process, whilst solvent ingress dominates the later processes. Within the timescale of this experiment, the overall effects of these solvent transfer phenomena are exactly balancing.

Fig. 5.12. Mass- and Φ_{ClO4}^- -charge plots for an $OsPVP_{100}$ coated crystal in 1.0M $LiClO_4$. Scan rate is 5 mVs^{-1}. Gravimetric surface coverage is 1.28 x 10^{-8} $molcm^{-2}$.

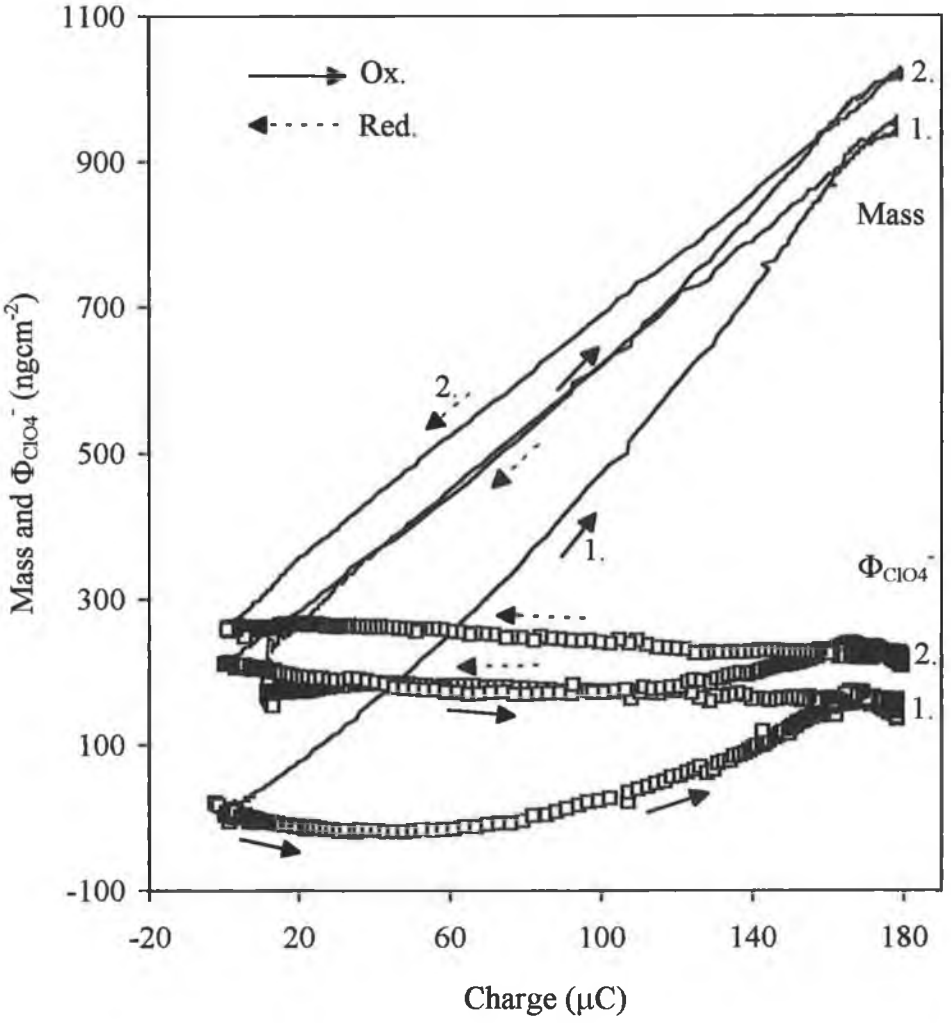

The difference in the overall normalised mass changes for the first and second scans is likely a consequence of additional solvent transfer during the first scan. Similar behaviour was observed for $OsPVP_{33}$ coatings in these electrolytes (see Section 5.3.1.2). Failure of the mass-charge plot to close illustrates that a component of the transferred mass is trapped within the layer during the first voltammetric scan. This trapped component is not ionic, as there is no evidence for charge trapping

during the experiment. In Chapter 2, it was noted that in this $LiClO_4$ electrolyte concentration, $OsPVP_{100}$ layers are apparently permselective. Therefore, under these conditions, the trapped species are likely to be solvent molecules. As was observed for $OsPVP_{33}$ coatings (see Section 5.3.1.2), the additional solvent component of the first voltammetric scan becomes trapped during this scan.

5.3.2.2. Gravimetric surface coverages of 1.87 to 4.92 x 10^{-8} molcm^{-2}.

In 2.0M and 4.0M $LiClO_4$, the normalised mass changes accompanying redox switching of $OsPVP_{100}$ coatings are dependent on the polymer surface coverage. Table 5.6. summarises the overall normalised mass changes for $OsPVP_{100}$ coatings, gravimetric surface coverage 1.87 to 4.92 x 10^{-8} molcm^{-2}, in these $LiClO_4$ concentrations. These normalised mass changes are greater than those quoted in Table 5.4. This behaviour is likely a consequence of the breakdown in layer permselectivity and the subsequent influx of $Li^+ClO_4^-$ during redox switching [1,14]. The non-permselective nature of $OsPVP_{100}$ layers in high $LiClO_4$ electrolyte concentrations was illustrated in Chapter 2. Assuming that solvent transfer due to activity considerations is the same as for lower $LiClO_4$ concentrations, the net increase in the normalised mass may be calculated [14,29]. In 2.0M $LiClO_4$, the overall normalised mass changes associated with the first and second scans are 163 ($\pm$10) gmol^{-1} and 139 ($\pm$8) gmol^{-1} respectively. These correspond to net mass increases of 53 gmol^{-1} and 39 gmol^{-1} respectively, compared with the normalised mass changes observed for thinner $OsPVP_{100}$ coatings, and represent the influx of 0.5 (0.2) and 0.4 (0.1) unhydrated (hydrated) salt molecules per redox site. Whilst the exact hydration number of this species in polymers is unknown, these values may be viewed as the upper and lower limits for salt influx within these polymers. Similarly, in 4.0M $LiClO_4$, the larger overall normalised mass changes represent the influx of 0.7 (0.3) and 0.6 (0.2) unhydrated (hydrated) salt molecules per redox site.

Table 5.6. The effect of $LiClO_4$ electrolyte concentration on the normalised mass change accompanying redox switching of $OsPVP_{100}$ coated crystals. Gravimetric surface coverages are 1.87 to 4.92 $x10^{-8}$ $molcm^{-2}$.

$LiClO_4$ Conc. (M)	Normalised Mass Change ($gmol^{-1}$)			
	1 mVs^{-1} (a)		5 mVs^{-1} (a)	
	Scan 1	Scan 2	Scan 1	Scan 2
2.00	163 (9)	139 (5)	162 (10)	139 (8)
4.00	189 (11)	179 (10)	195 (15)	168 (12)

(a) Errors quoted in brackets represent the variations between different films.

* signifies measurements made on one film only.

This breakdown in layer permselectivity was not observed in $NaClO_4$ electrolytes [4]. However, for $OsPVP_{100}$ coatings of the same thickness used in the $NaClO_4$ studies [4], permselective layer behaviour is observed in these $LiClO_4$ studies (see Section 5.3.2.1).

Fig. 5.13 illustrates the mass- and Φ_{ClO4^-} -charge plots for a 5 mVs^{-1} voltammetric scan of an $OsPVP_{100}$ coated crystal in 2.0 M $LiClO_4$. The gravimetric surface coverage was 2.27 x 10^{-8} $molcm^{-2}$. There is no apparent mass loss from the layer at any stage of polymer oxidation. However, this may reflect either the absence of solvent egress or the fact that salt influx during the initial 35 μC of osmium oxidation is sufficient to mask the egress of solvent.

Fig. 5.13. Mass- and Φ_{ClO4}^- -charge plots for an $OsPVP_{100}$ coated crystal in 2.0M $LiClO_4$. Scan rate is 5 mVs^{-1}. Gravimetric surface coverage is 2.27 x 10^{-8} $molcm^{-2}$.

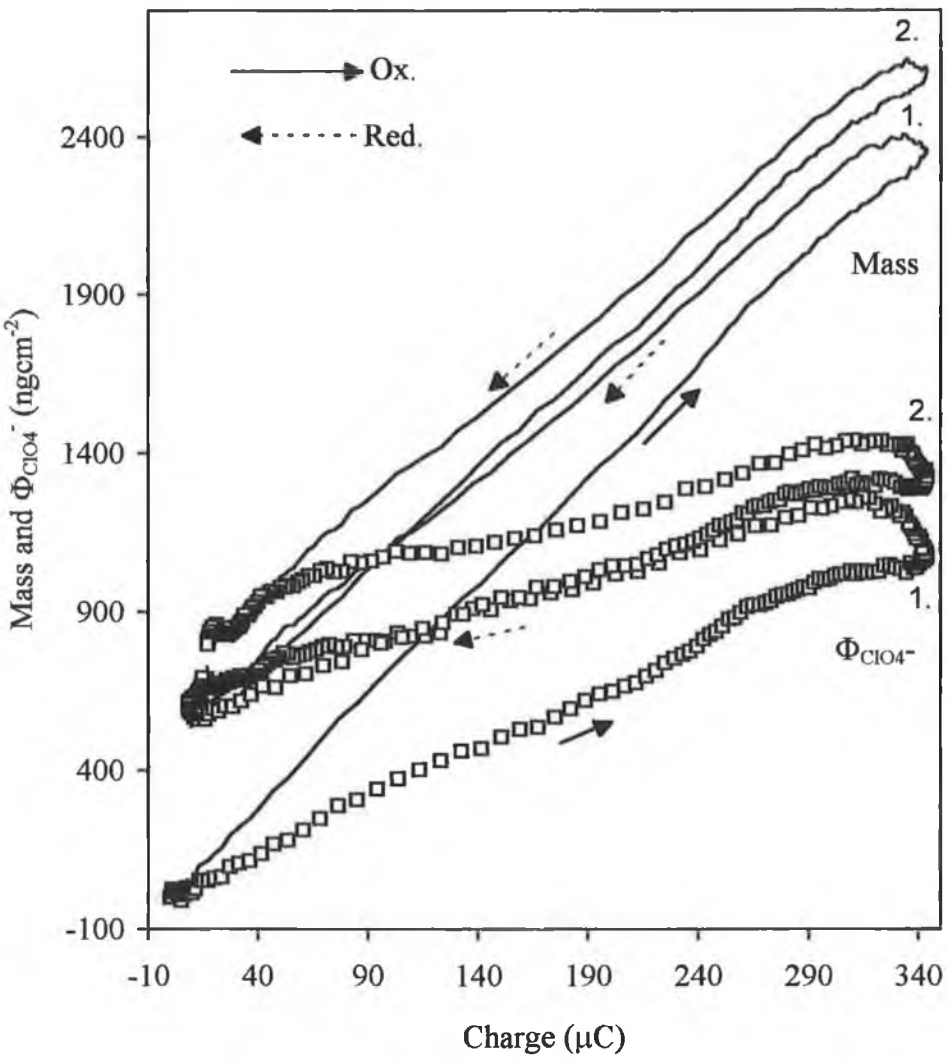

In summary, for $OsPVP_{100}$ coatings of gravimetric surface coverages of 0.52 to 1.57 x 10^{-8} $molcm^{-2}$, the second scan steady-state normalised mass changes are similar to those observed in $NaClO_4$ and illustrate that anion transfer dominates mass ingress during polymer oxidation. The Φ_{ClO4}^- -charge plots for these steady-state mass changes illustrate that there is solvent motion in both directions and that solvent

egress dominates solvent ingress during the initial oxidation (ca. 20%) of the polymer. As a consequence of this behaviour the normalised mass change for the second voltammetric scan is less than the mass of the perchlorate anion.

These steady-state mass changes are observed only following a break-in of the layer during the first voltammetric scan. The overall normalised mass changes accompanying the first voltammetric scan are greater than those observed during the second voltammetric scan as a consequence of the additional influx of solvent. This solvent component becomes trapped within the layer during the first voltammetric scan. The Φ_{ClO4^-}-charge plots for this data illustrate that, although the overall normalised mass change is ca. 114 (±5) $gmol^{-1}$, solvent egress is in evidence during the initial oxidation process. Therefore, for both voltammetric scans, the overall normalised mass changes quoted reflect the net normalised mass change during the $Os^{II/III}$ oxidation process.

5.3.3. Effect of Experimental Timescale on Mass Transfer Through $OsPVP_{33}$ Films.

In Chapter 3, the rate of charge transport through $OsPVP_{33}$ electrode coatings, as determined by cyclic voltammetry, $D_{CT}(CV)$, was observed to increase slightly on increasing the concentration of the contacting electrolyte from 0.1M to 1.0M $LiClO_4$. Activation parameters, estimated for the charge transport process, suggest that ion motion is limiting. In this section, mass transfer processes are studied using cyclic voltammetry under semi-infinite diffusion conditions (scan rates of 50-500 mVs^{-1}) to probe for interfacial mass transfer limitations. Table 5.7. summarises the normalised mass changes associated with redox switching of $OsPVP_{33}$ coatings, at scan rates of 50-500 mVs^{-1}, as a function of the contacting $LiClO_4$ electrolyte concentration. The normalised mass changes are sub-divided into ΔM_{ETE} and ΔM_{TOT}, where ΔM_{ETE} signifies the "end-to-end" mass change associated with the positive scan, and ΔM_{TOT} signifies the "total" mass change observed, including the additional mass increase on reversal of the scan direction. Where only one value is quoted, ΔM_{ETE} is equal to ΔM_{TOT}. These values are reproducible to within 10% for determinations on different films and 6% for repeated determinations on a single film. Table 5.7. also includes the charge transport rates evaluated for these $OsPVP_{33}$ coatings using the Randles-Sevcik equation, $D_{CT}(CV)$. $D_{CT}(CV)$ is reproducible to within 10% for determinations on different layers and 4% for repeated determinations on a single film. The mass and charge transport properties of these layers are dependent on the polymer surface coverage. The data in Table 5.7. are therefore presented for two approximate gravimetric surface coverage ranges.

5.3.3.1. Gravimetric surface coverages of 0.5 to 0.99 x 10^{-8} $molcm^{-2}$.

In Section 5.3.1.1, a study of the slow scan voltammetric changes in polymer populations during redox switching revealed that, for $OsPVP_{33}$ films of this surface coverage, electroneutrality is maintained by the influx of a single perchlorate anion

Table 5.7. The effect of $LiClO_4$ electrolyte concentration on the normalised mass change accompanying redox switching of $OsPVP_{33}$ coated crystals at fast cyclic voltammetric scan rates.

$LiClO_4$ Conc. (M)	D_{CT} (CV) x 10^{-11} cm^2s^{-1} (A)	(B)	Scan Rate (mVs^{-1})	Normalised Mass Change ($gmol^{-1}$) (A) ΔM_{ETE}	(A) ΔM_{TOT}	(B) ΔM_{ETE}	(B) ΔM_{TOT}
0.01	1.06	0.62	50	104 (3)		129*	144*
			100	104 (1)		127*	145*
			200	109 (3)		145*	169*
			500	111 (5)		136*	169*
0.05	1.21	1.01	50	110*		108 (5)	116 (8)
			100	108*		104 (3)	118 (8)
			200	107*		115 (7)	130 (6)
			500	103*		110 (6)	126 (7)
0.10	2.14	1.30	50	102 (1)		116*	
			100	112 (3)		124*	
			200	107 (3)		111*	
			500	108 (7)		117*	
0.50	2.60	2.03	50	101 (1)		115 (4)	
			100	101 (4)		111 (2)	
			200	107 (3)		105 (6)	
			500	101 (5)		109 (8)	
1.0	2.72	2.40	50	102 (4)		115 (1)	
			100	98 (1)		112 (2)	
			200	101*		117 (6)	
			500	110 (8)		113 (3)	
2.0	2.69	2.32	50	104 (5)		107 (4)	
			100	106*		108 (2)	
			200	100 (4)		107 (3)	
			500	106 (6)		114 (1)	
4.0	2.69	2.29	50	100 (2)		116 (5)	
			100	108*		126 (6)	
			200	102 (7)		117 (4)	
			500	102*		122 (8)	

A) Gravimetric surface coverages are 0.5 to 0.99 x 10^{-8} $molcm^{-2}$ $OsPVP_{33}$.

B) Gravimetric surface coverages are 1.1 to 5.8 x 10^{-8} $molcm^{-2}$ $OsPVP_{33}$.

and ca. 0.2 molecules of water per redox site (averaged over the complete oxidation). This solvent component of the mass transfer is delineated from the anion flux and is only observed after ca. 20-30% of osmium oxidation. Column A of Table 5.7. summarises the charge transport rates and the normalised mass changes associated with the redox switching of these $OsPVP_{33}$ coated crystals. For these layers, $\Delta M_{ETE} = \Delta M_{TOT}$. Furthermore, these normalised mass changes are independent of the $LiClO_4$ concentration of the contacting electrolyte and the experimental timescale. The average normalised mass change of 105 (±4) $gmol^{-1}$ is similar in magnitude to the slow scan data presented in Section 5.3.1.1.

Within the concentration range of 0.5M to 4.0M $LiClO_4$, the estimated charge transport rates and normalised mass changes are similar to those observed in $HClO_4$ electrolytes (see Chapter 4) and illustrate that the mass and charge transport properties of these layers are comparable in both electrolytes. Furthermore, within this concentration range, $D_{CT}(CV)$ is essentially independent of the electrolyte concentration. Within the concentration range of 0.01M to 0.1M $LiClO_4$, although the normalised mass changes observed for these $OsPVP_{33}$ are identical to those observed at higher $LiClO_4$ concentrations, the charge transport rates observed are reduced. For this polymer, a similar decrease in $D_{CT}(CV)$ on decreasing the electrolyte concentration from 1.0M to 0.1M $LiClO_4$ was observed in Chapter 3. This decrease in $D_{CT}(CV)$ is not a consequence of a decrease in the osmium site concentration as the admittance characteristics of these layers are almost identical in all $LiClO_4$ concentrations studied (see Chapter 2).

Fig. 5.14 illustrates the mass-potential plots for a 8.95 x 10^{-9} $molcm^{-2}$ $OsPVP_{33}$ coated crystal during a 50 mVs^{-1} cyclic voltammetric experiment in 0.01M $LiClO_4$. The characteristics of these plots are similar to those observed in more concentrated $LiClO_4$ solutions and in $HClO_4$ electrolytes. Mass and charge trapping during this experiment are again associated with the kinetic isolation of Os^{III} states. The mass and charge (not shown) data require 4 voltammetric scans before

Fig. 5.14. Mass-potential plots for an $OsPVP_{33}$ coated crystal in 0.01M $LiClO_4$. Scan rate is 50 mVs^{-1}.Gravimetric surface coverage is 8.95 x 10^{-9} $molcm^{-2}$.

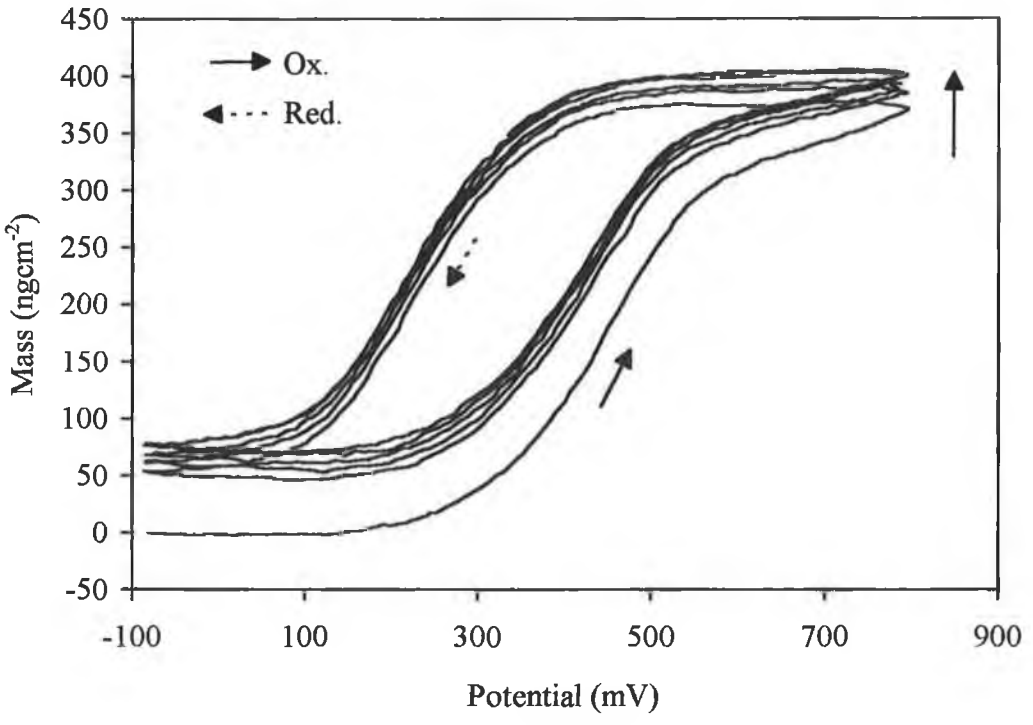

Fig. 5.15. Mass- and Φ_{ClO4}^- -charge plots for data in Fig. 5.14.

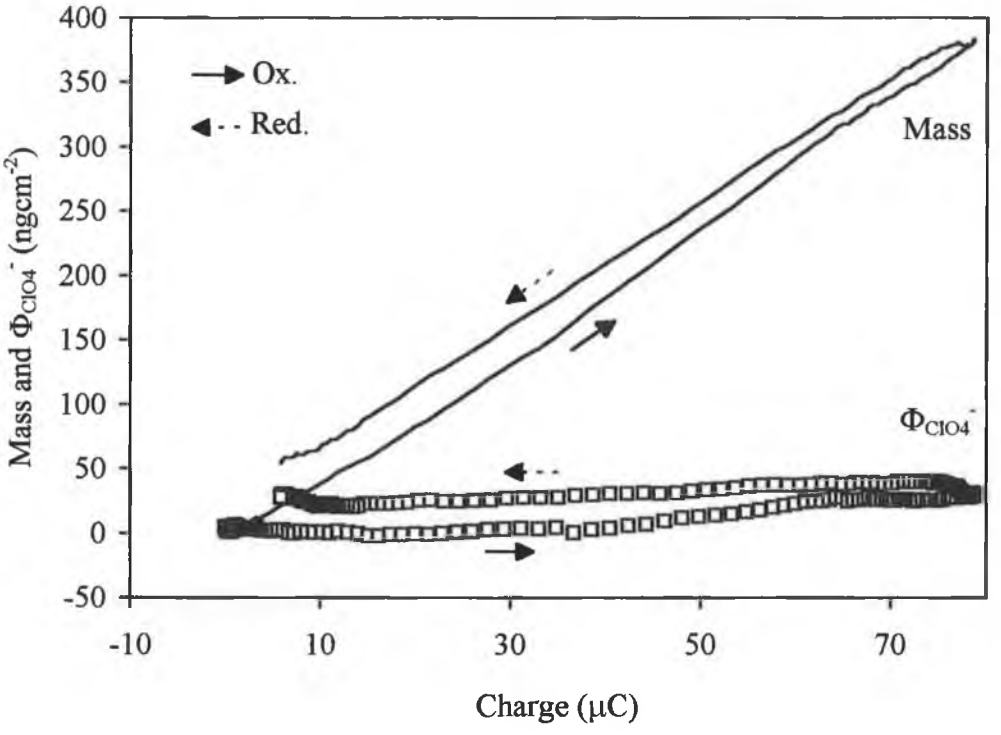

reproducible steady state changes are observed. Fig. 5.15 illustrates the corresponding mass- and Φ_{ClO4^-} -charge plots for the data in Fig. 5.14. The presence of hysteresis in these plots illustrates that the transfer of neutral species, namely solvent, is hindered and is in keeping with the observations made in acidic solutions (see Chapter 4). However, compared with the data obtained in more concentrated $LiClO_4$ solutions and in $HClO_4$ electrolytes (e.g. see Fig. 4.13 in Chapter 4) these plots exhibit greater hysteresis. It is suggested, therefore, that greater solvent limitations exist in 0.01M $LiClO_4$ and, whilst the origins of this effect are unknown, it is considered that it may result in the observed decrease in D_{CT}(CV) in low $LiClO_4$ electrolyte concentrations. This dependence of the rate of charge transport on the facility for interfacial solvent transfer has been previously demonstrated for $OsPVP_{100}$ crystal coatings in $HClO_4$ electrolytes [18].

5.3.3.2. Gravimetric surface coverages of 1.1 to 5.8 x 10^{-8} molcm^{-2}.

In Section 5.3.1.2, it was demonstrated that for slow scan voltammetric experiments, the normalised mass changes observed during redox switching of $OsPVP_{33}$ coatings of this surface coverage are different from those observed for thinner $OsPVP_{33}$ coatings. The normalised mass change for the first voltammetric scan is larger than for subsequent scans and is considered to reflect greater solvent influx. Mass transfer reaches its steady-state only during the second voltammetric scan. Under these steady-state conditions, within the concentration range of 0.05M to 4.0M $LiClO_4$, the mass transfer properties of these layers are identical to those of the thinner $OsPVP_{33}$ layers.

Column B of Table 5.7. summarises the charge transport rates and the normalised mass changes associated with redox switching of these $OsPVP_{33}$ crystal coatings (gravimetric surface coverages of 1.1 to 5.8 x 10^{-8} molcm^{-2}). Only the first voltammetric scan is considered. In 0.01M and 0.05M $LiClO_4$, ΔM_{TOT} is greater than ΔM_{ETE}. ΔM_{TOT} is similar to the slow scan voltammetric data discussed in Section

5.3.1.2. That ΔM_{ETE} is smaller, illustrates that solvent motion is lagging and that anion and solvent transfer are delineated processes. The existence of solvent motion limitations during the first voltammetric scan of these $OsPVP_{33}$ films was previously highlighted in Section 5.3.1.2. Fig. 5.16 illustrates the mass-potential plots for a 2.05 x 10^{-8} molcm^{-2} $OsPVP_{33}$ coating in 0.01M $LiClO_4$. Fig. 5.17 illustrates the corresponding mass- and Φ_{ClO4^-} -charge plots for this data. In Fig. 5.17, the Φ_{ClO4^-} data continues to increase on cessation of the anodic charge, illustrating the slow influx of solvent and the discrepancy between ΔM_{ETE} and ΔM_{TOT}.

Within the concentration range of 0.1M to 4.0M $LiClO_4$, ΔM_{ETE} and ΔM_{TOT} are identical and this illustrates that, in these $LiClO_4$ concentrations, solvent motion is relatively less hindered than in lower $LiClO_4$ concentrations. Fig. 5.18 illustrates the mass-potential plot for a 1.82 x 10^{-8} $OsPVP_{33}$ coated crystal in 1.0M $LiClO_4$. Fig. 5.19 illustrates the corresponding mass- and Φ_{ClO4^-} -charge plots for the data in Fig. 5.18. Compared with Fig. 5.17 (0.01M $LiClO_4$), the Φ_{ClO4^-} -charge plot clearly illustrates that solvent motion, although lagging the anion, is completed during the oxidative cycle. The normalised mass changes observed within this $LiClO_4$ concentration range are independent of the experimental timescale and the concentration of the contacting electrolyte. An average normalised mass change of 114 (±6) gmol^{-1} is observed and is similar to the slow scan data discussed in Section 5.3.1.2.

The effect of the bathing $LiClO_4$ electrolyte concentration on the charge transport properties of these layers is summarised in Table 5.7. and illustrated in Fig. 5.20. The $LiClO_4$ concentration is illustrated in log format for presentation purposes. In 0.01M and 0.1M $LiClO_4$, the rate of charge transport is faster within thinner $OsPVP_{33}$ coatings. This behaviour may reflect either a larger concentration of osmium sites in the relatively more compact thinner coatings (see Chapter 2) or more hindered mass transfer within the thicker $OsPVP_{33}$ coatings.

Fig. 5.16. Mass-potential plots for an $OsPVP_{33}$ coated crystal in 0.01M $LiClO_4$. Scan rate is 50 mVs^{-1}.Gravimetric surface coverage is 2.05 x 10^{-8} $molcm^{-2}$.

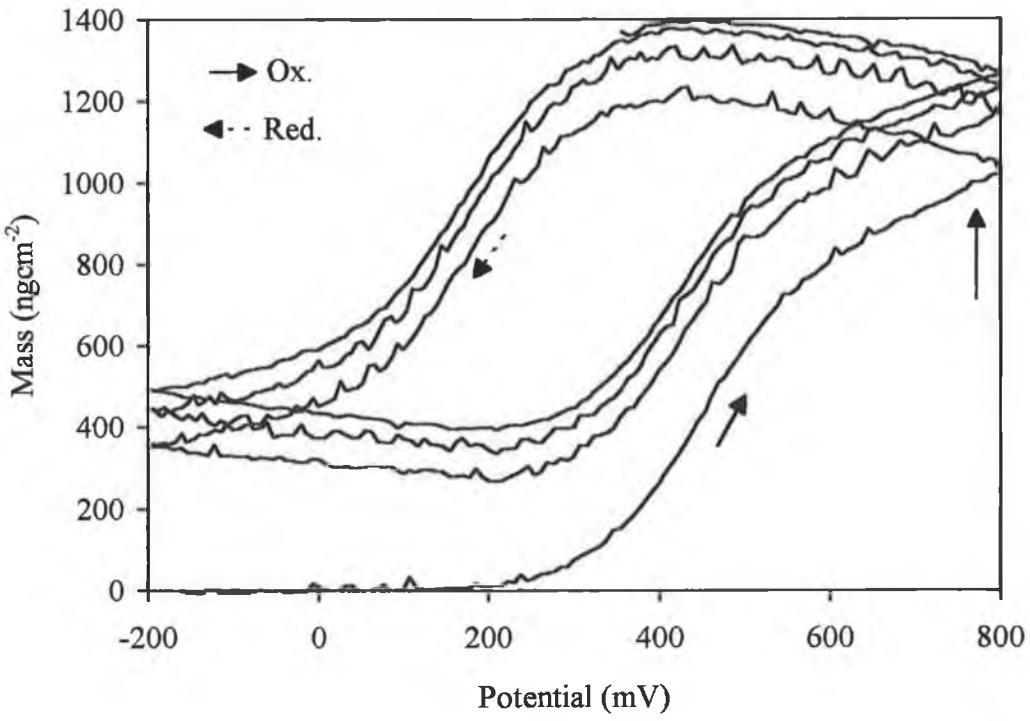

Fig. 5.17. Mass- and Φ_{ClO4}^- -charge plots for data in Fig. 5.16.

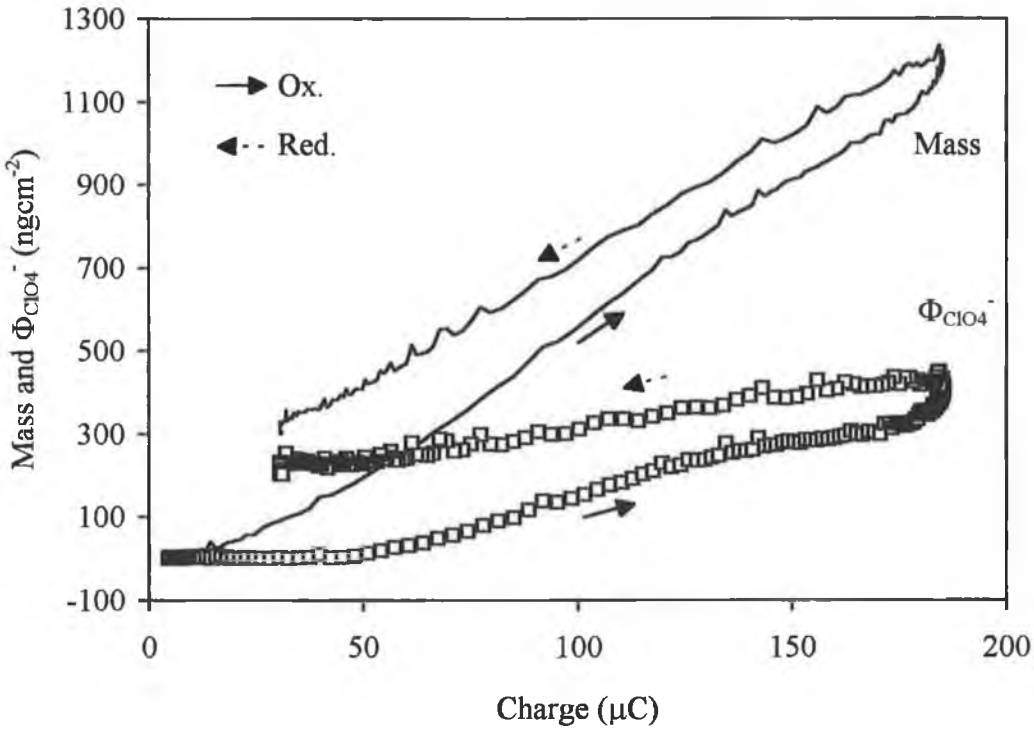

Fig. 5.18. Mass-potential plots for an $OsPVP_{33}$ coated crystal in 1.0M $LiClO_4$. Scan rate is 50 mVs^{-1}. Gravimetric surface coverage is 1.82×10^{-8} $molcm^{-2}$.

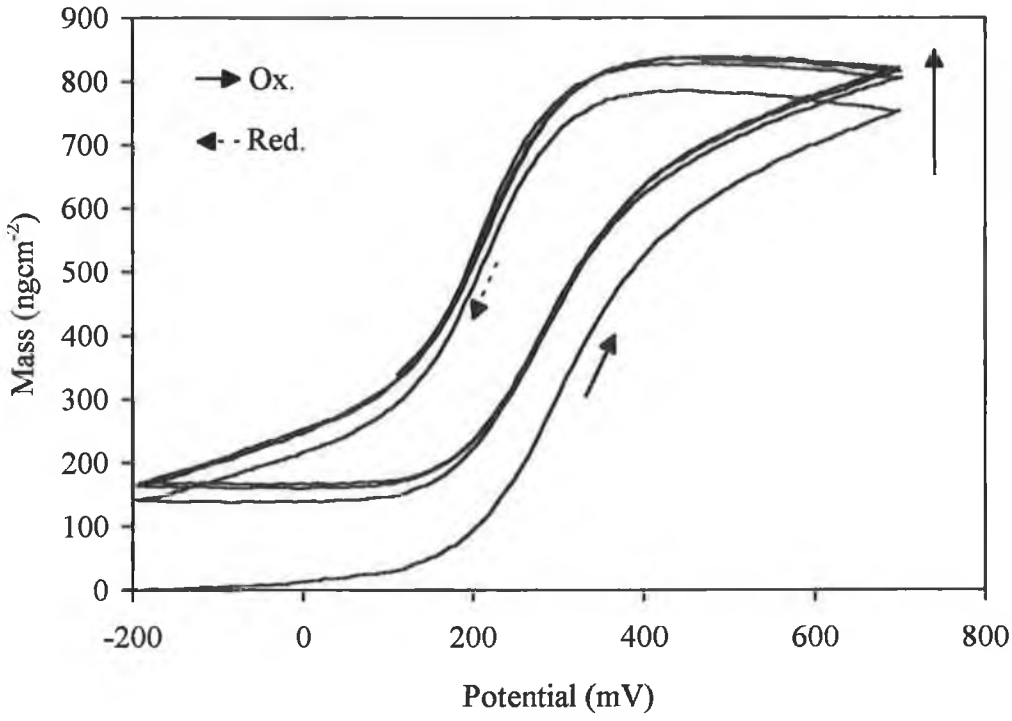

Fig. 5.19. Mass- and Φ_{ClO4}^- -charge plots for data in Fig. 5.18.

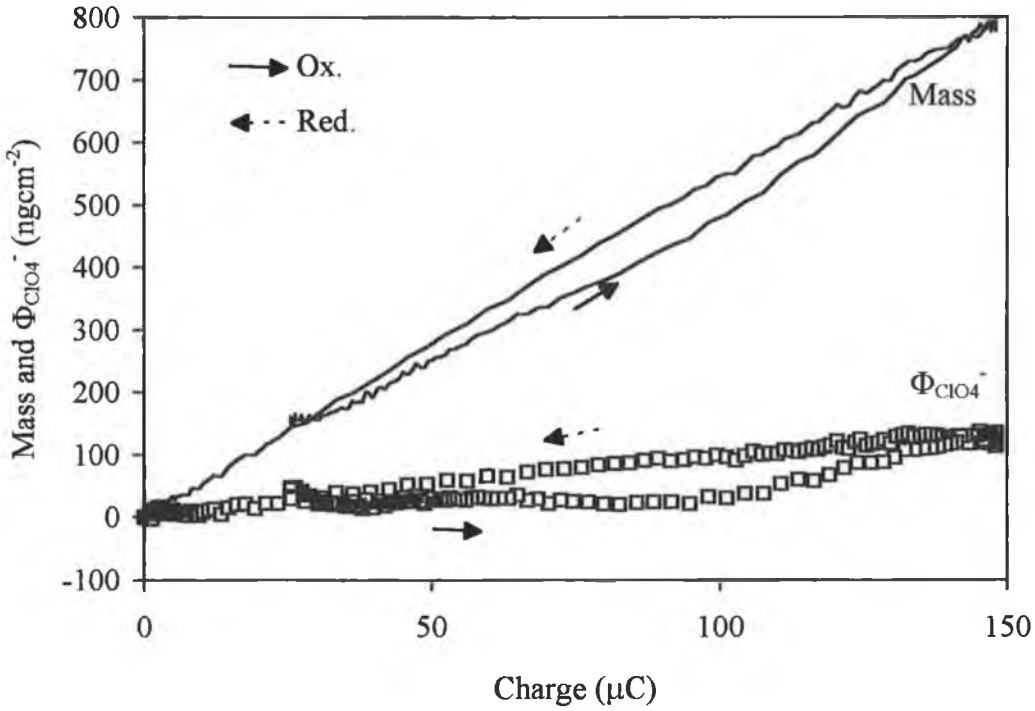

Fig. 5.20. The effect of $LiClO_4$ electrolyte concentration on the rate of charge transport, $D_{CT}(CV)$, through $OsPVP_{33}$; A (Δ) gravimetric surface coverages are 0.5 to 0.99 x 10^{-8} molcm^{-2} , B (□) gravimetric surface coverages are 1.1 to 5.8 x 10^{-8} molcm^{-2}; and (o) $OsPVP_{100}$ coated crystals.

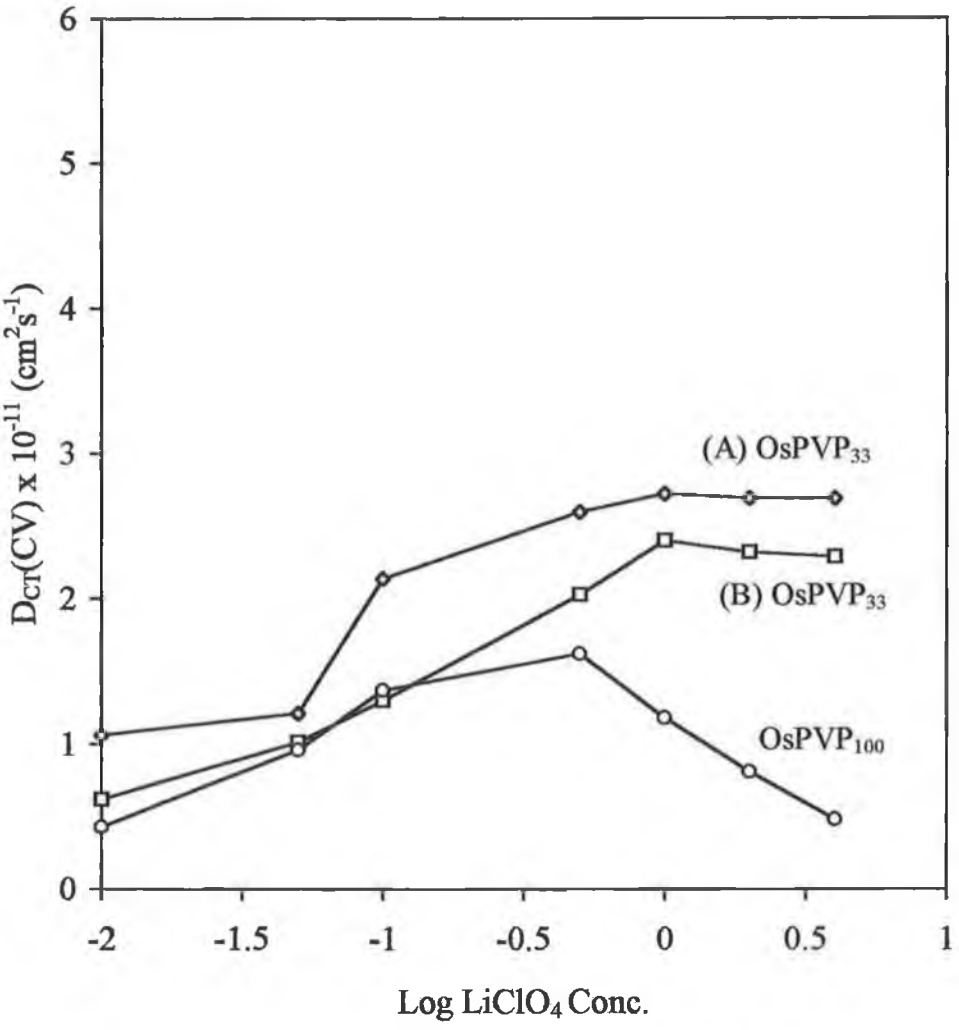

In Fig. 5.20, the rate of charge transport follows the same concentration dependence for both $OsPVP_{33}$ surface coverage ranges. Within the concentration range on 0.5M to 4.0M $LiClO_4$, $D_{CT}(CV)$ is essentially independent of the $LiClO_4$ electrolyte concentration. On decreasing the electrolyte concentration, $D_{CT}(CV)$ decreases. In 0.01M $LiClO_4$ the rate of charge transport is 3 times smaller than that observed in 1.0M $LiClO_4$. Comparison of Fig. 5.16 (0.01M $LiClO_4$) and Fig. 5.18 (1.0M $LiClO_4$) illustrates that in 0.01M $LiClO_4$ a greater number of voltammetric scans are required before steady-state mass changes are observed. This behaviour suggests that mass transfer in these $OsPVP_{33}$ coatings is relatively more impeded in lower $LiClO_4$ concentrations. Comparison of Fig. 5.17 (0.01M $LiClO_4$) and Fig. 5.19 (1.0M $LiClO_4$) illustrates that in 0.01M $LiClO_4$ the mass- and Φ_{ClO4^-} -charge plots exhibit greater hysteresis than those observed in 1.0M $LiClO_4$. Furthermore, the Φ_{ClO4^-} data continues to increase on cessation of the anodic charge in 0.01M $LiClO_4$. These observations clearly illustrate that interfacial solvent transfer is more hindered in 0.01M $LiClO_4$, which may explain the observed decrease in $D_{CT}(CV)$.

Within the concentration range of 0.5M to 4.0M $LiClO_4$ $D_{CT}(CV)$ is essentially independent of the $LiClO_4$ concentration of the contacting electrolyte. This point is reflect in the similarity of the normalised mass changes observed under these conditions and suggests that mass transfer is similarly limiting in these $LiClO_4$ concentrations.

5.3.4. Effect of Experimental Timescale on Mass Transfer Through $OsPVP_{100}$ Films.

Table 5.8. summarises the normalised mass changes associated with redox switching of $OsPVP_{100}$ coatings, at scan rates of 50-500 mVs^{-1}, as a function of the contacting $LiClO_4$ electrolyte concentration. These data are reproducible to within 10% for determinations on different films and 7% for repeated determinations on a single film. Table 5.8. also includes the charge transport rates evaluated for these $OsPVP_{100}$ layers using the Randles-Sevcik equation, $D_{CT}(CV)$. $D_{CT}(CV)$ is reproducible to within 10% for determinations on different layers and 6% for repeated determinations on single layers. Whilst the mass transfer properties of $OsPVP_{100}$ coatings are dependent on the polymer surface coverage (see Section 5.3.2), the charge transport properties of these $OsPVP_{100}$ coatings are independent of the surface coverage. The following discussion is, therefore, applicable to all $OsPVP_{100}$ coatings over the complete gravimetric surface coverage range studied i.e. 0.52 to 4.92 x 10^{-8} $molcm^{-2}$.

In Table 5.8., ΔM_{ETE} is less than ΔM_{TOT} for all $OsPVP_{100}$ coatings in each $LiClO_4$ concentration and illustrates that solvent transfer is lagging the anion. The existence of solvent motion limitations was previously highlighted in Section 5.3.2.1. Within experimental error, ΔM_{TOT} is independent of the experimental timescale and the $LiClO_4$ electrolyte concentration and is similar to the slow scan data discussed for both $OsPVP_{100}$ surface coverage ranges in Section 5.3.2.1 and Section 5.3.2.2. Fig. 5.21 illustrates the mass-potential plots for a 1.87 x 10^{-8} $molcm^{-2}$ $OsPVP_{100}$ coated crystal during a 50 mVs^{-1} cyclic voltammetric experiment in 0.1M $LiClO_4$. This plot exhibits considerable mass trapping, associated with the kinetic isolation of Os^{III} sites. Typically 3-4 voltammetric scans are required for the establishment of reproducible, steady-state mass changes. Fig. 5.22 illustrates the corresponding mass- and Φ_{ClO4^-} - charge plots for the data in Fig. 5.21. As was observed in Section 5.3.2.1, there is a decrease in Φ_{ClO4^-} for the initial 25 μC of osmium oxidation. This decrease is

Table 5.8. The effect of $LiClO_4$ electrolyte concentration on the normalised mass change accompanying redox switching of $OsPVP_{100}$ coated crystals at fast cyclic voltammetric scan rates.

$LiClO_4$ Conc. (M)	D_{CT} (CV) x 10^{-11} cm^2s^{-1}	Scan Rate (mVs^{-1})	Normalised Mass Change ($gmol^{-1}$)			
	A. and B.		A.		B.	
			ΔM_{ETE}	ΔM_{TOT}	ΔM_{ETE}	ΔM_{TOT}
0.01	0.43	50	104*	112*	119 (7)	130 (6)
		100	100*	111*	123 (5)	139 (8)
		200	101*	114*	116 (3)	138 (10)
		500	105*	115*	107 (4)	121
0.05	0.96	50	111 (4)	119 (5)	111 (4)	119 (5)
		100	105 (7)	115 (6)	105 (7)	115 (6)
		200	110	116 (5)	110	116 (5)
		500	125 (6)	-	125 (6)	-
0.10	1.37	50	109 (1)	117 (2)	109 (1)	117 (2)
		100	110 (4)	116 (5)	110 (4)	116 (5)
		200	106 (2)	111 (6)	106	111 (3)
		500	110 (10)	116 (4)	110 (10)	116 (4)
0.50	1.62	50	109 (6)	119 (4)	109 (6)	119 (4)
		100	115 (6)	120 (7)	115 (6)	120 (7)
		200	113 (1)	126 (10)	113 (1)	126 (10)
		500	114 (5)	122 (9)	114 (5)	122 (9)
1.0	1.18	50	117 (4)	121 (3)	117 (4)	121 (3)
		100	128 (2)	133 (3)	128 (2)	133 (3)
		200	129 (4)	132 (5)	129 (4)	132 (5)
		500	135 (5)	--	135 (5)	--
2.0	0.81	50	113 (6)	120 (7)	148 (5)	166 (10)
		100	119 (5)	129 (1)	143 (2)	165 (3)
		200	107 (8)	119 (10)	138 (3)	160 (6)
		500	105 (3)	127 (5)	132 (2)	161
4.0	0.48	50	107 (2)	119 (3)	191*	199*
		100	105 (2)	115 (6)	180*	192*
		200	108 (4)	119 (7)	170*	180*
		500	108 (5)	119 (1)	175*	189*

A) Gravimetric surface coverages are 0.52 to 1.57 x 10^{-8} $molcm^{-2}$ $OsPVP_{100}$.

B) Gravimetric surface coverages are 1.87 to 4.92 x 10^{-8} $molcm^{-2}$ $OsPVP_{100}$.

Fig. 5.21. Mass-potential plots for an $OsPVP_{100}$ coated crystal in 0.1M $LiClO_4$. Scan rate is 50 mVs^{-1}. Gravimetric surface coverage is 1.87×10^{-8} $molcm^{-2}$.

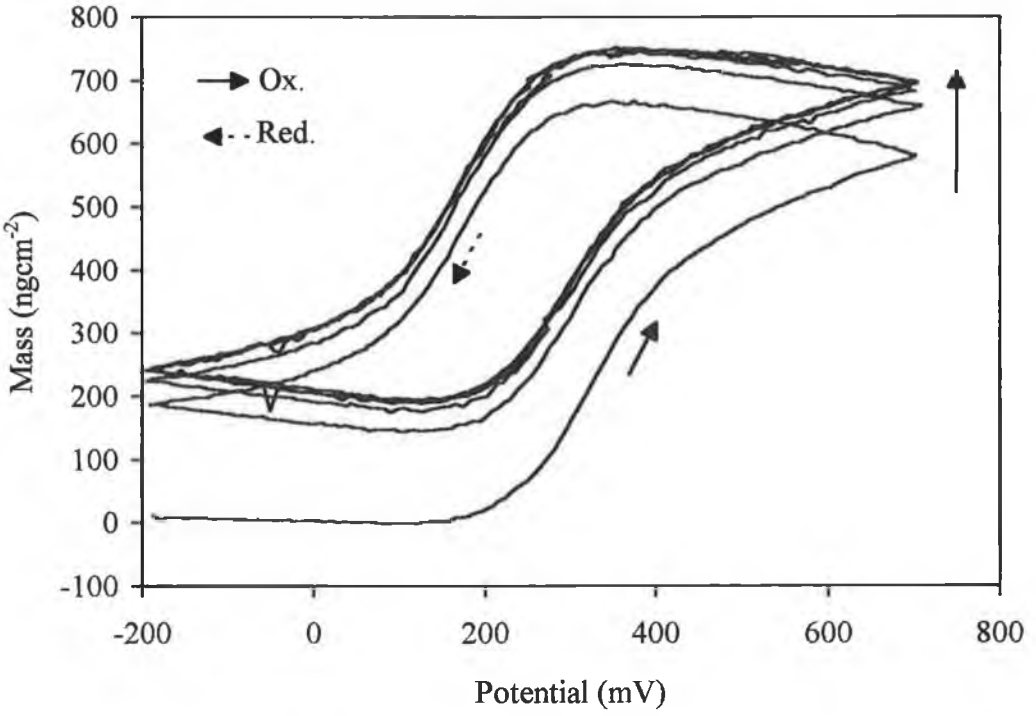

Fig. 5.22. Mass- and Φ_{ClO4^-} -charge plots for data in Fig. 5.21.

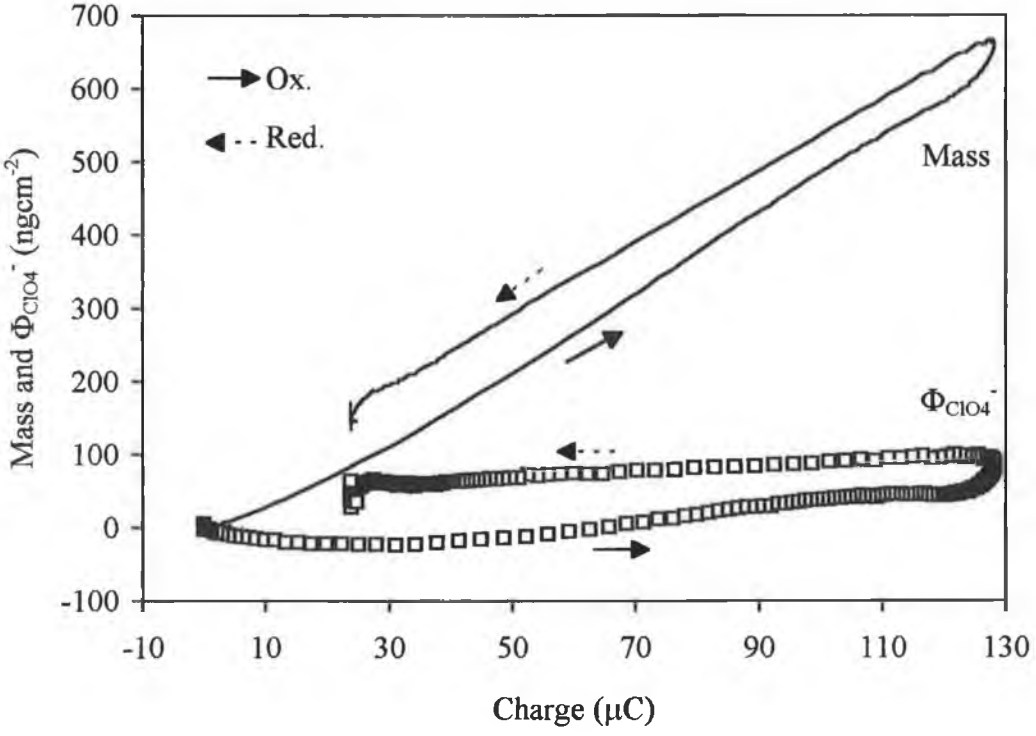

considered to reflect solvent egress accompanying the influx of the charge compensating counterion. As oxidation proceeds, Φ_{ClO4^-} becomes positive, which illustrates the influx of solvent in response to activity constraints. Φ_{ClO4^-} continues to increase on cessation of the anodic charge, thus highlighting the slow influx of solvent and the discrepancy between ΔM_{TOT} and ΔM_{ETE}. On reversal of the scan direction there is no apparent change in the Φ_{ClO4^-} data, suggesting that either there is counterbalancing species motion or that anion egress solely occurs.

The variation in the rate of charge transport through $OsPVP_{100}$ coatings, as a function of the contacting $LiClO_4$ electrolyte concentration, is summarised in Table 5.8. and illustrated in Fig. 5.20. Within the concentration range of 1.0M to 4.0M $LiClO_4$, $D_{CT}(CV)$ is slower for the $OsPVP_{100}$ polymer compared with the corresponding charge transport rates observed for thick $OsPVP_{33}$ coatings. These differences in $D_{CT}(CV)$ may reflect the more hindered mass transfer processes within $OsPVP_{100}$ coatings (see below).

Within the concentration range of 0.01M to 0.5 M $LiClO_4$, $D_{CT}(CV)$ increases with increasing $LiClO_4$ concentration. Similar behaviour was observed for $OsPVP_{33}$ coatings in Section 5.3.3. Fig. 5.23 illustrates the mass-potential plots for a 1.87 x 10^{-8} molcm^{-2} $OsPVP_{100}$ coated crystal in 0.01M $LiClO_4$. Fig. 5.24 illustrates the corresponding mass- and Φ_{ClO4^-} -charge plots for this data. Comparison of Fig. 5.21 (0.1M $LiClO_4$) and Fig. 5.23 (0.01M $LiClO_4$) illustrates that, in 0.01M $LiClO_4$, a greater number of voltammetric scans are required before steady-state mass changes are observed. This behaviour suggests that mass transfer is relatively more hindered in low $LiClO_4$ concentrations. Furthermore, comparison of Fig. 5.22 (0.1M $LiClO_4$) and Fig. 5.24 (0.01M $LiClO_4$) illustrates that, in 0.01M $LiClO_4$, the mass- and Φ_{ClO4^-} -charge plots exhibit greater hysteresis than those observed in 0.1M $LiClO_4$. These observations suggest that solvent transfer is relatively more impeded in 0.01M

Fig. 5.23. Mass-potential plots for an $OsPVP_{100}$ coated crystal in 0.01M $LiClO_4$. Scan rate is 50 mVs^{-1}.Gravimetric surface coverage is 1.87 x 10^{-8} $molcm^{-2}$.

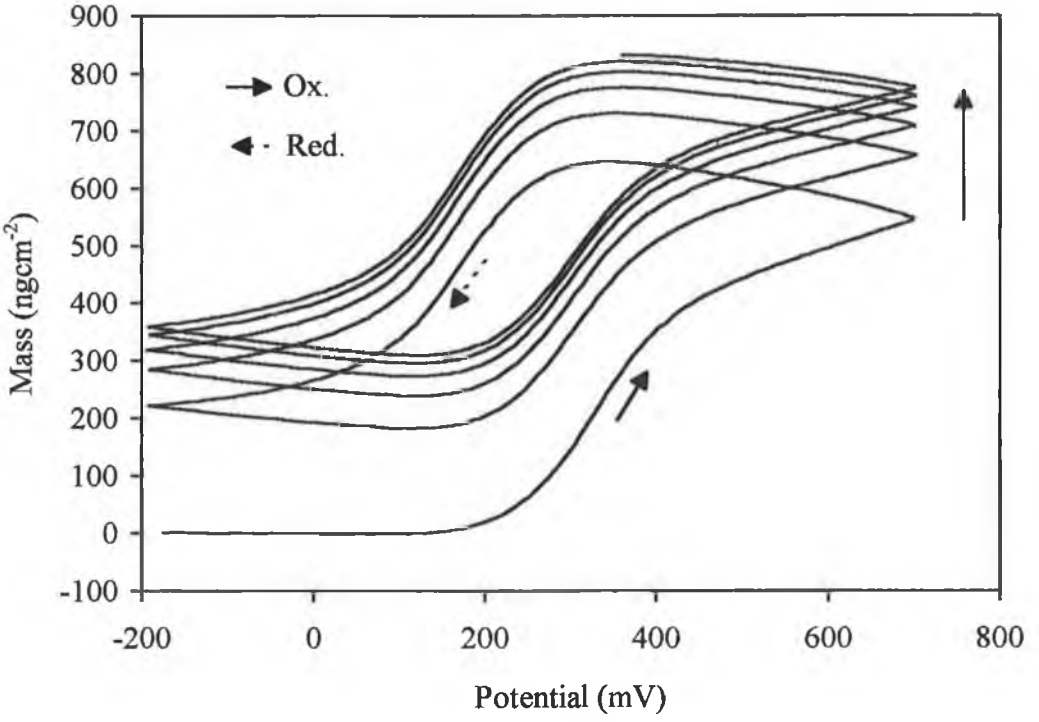

Fig. 5.24. Mass- and Φ_{ClO4^-} -charge plots for data in Fig. 5.23.

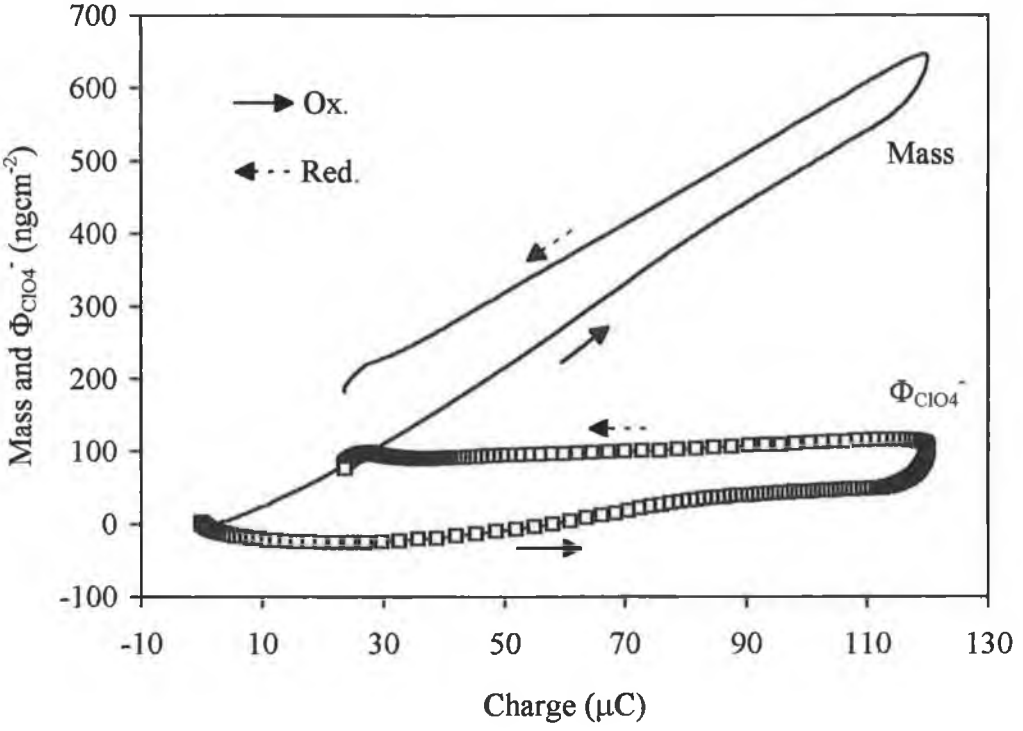

$LiClO_4$. This behaviour may result in the observed decrease in D_{CT}(CV) in 0.01M $LiClO_4$.

Within the concentration range of 0.5M to 4.0M $LiClO_4$, the rate of charge transport through $OsPVP_{100}$ coatings decreases by almost a factor of 4. In Section 5.3.2.2 it was noted that within this $LiClO_4$ concentration range, these layers are no longer permselective and salt influx occurs during redox switching. Fig. 5.25 illustrates the mass potential plots for a 1.87 x 10^{-8} PVP_{100} coated crystal in 4.0 M $LiClO_4$. It is apparent from this plot that even after 6 voltammetric scans the layer mass changes have not attained their steady-state. In Fig. 5.21 it was noted that for the same layer in 0.1M $LiClO_4$, steady-state mass changes were observed after only 4 scans. This behaviour suggests that mass transfer is more hindered in high $LiClO_4$ concentrations. Fig. 5.26 illustrates the corresponding mass- and Φ_{ClO4^-} -charge plots for the data in Fig. 5.25. The continued increase in Φ_{ClO4^-} on cessation of the positive scan reflects the slow influx of both solvent and salt species. The greater hysteresis in this plot, compared with the corresponding data in 0.1M $LiClO_4$ (see Fig. 5.22) illustrates that neutral species motion is relatively more hindered under these conditions. It is therefore considered that the observed decrease in D_{CT}(CV) with increasing $LiClO_4$ concentration reflects the more hindered transfer of net neutral species. This decrease in D_{CT}(CV) in high $LiClO_4$ concentrations, was not observed for $OsPVP_{33}$ coatings (see Section 5.3.3). For $OsPVP_{33}$ coatings in 4.0M $LiClO_4$, $\Delta M_{TOT} = \Delta M_{ETE}$. Consequently, in this electrolyte, interfacial solvent transfer is less hindered within the $OsPVP_{33}$ polymer.

These experiments illustrate that for both redox polymers, solvent transfer limitations exist under these dynamic conditions, independent of the $LiClO_4$ electrolyte concentration and the polymer surface coverage. An apparent trend between the rate of charge transport and the ease of solvent motion through these polymers has been illustrated. A similar correlation was observed previously for the $OsPVP_{100}$ polymer in $HClO_4$ electrolytes [18].

Fig. 5.25. Mass-potential plots for an $OsPVP_{100}$ coated crystal in 4.0M $LiClO_4$. Scan rate is 50 mVs^{-1}. Gravimetric surface coverage is 1.87×10^{-8} $molcm^{-2}$.

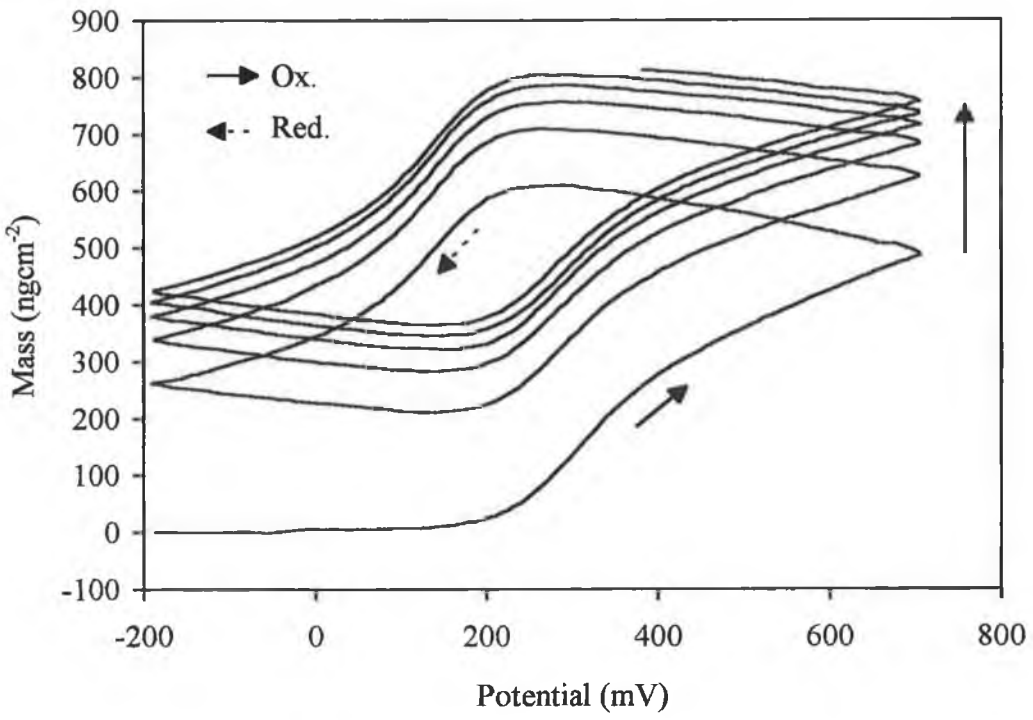

Fig. 5.26. Mass- and Φ_{ClO4}^- -charge plots for data in Fig. 5.25.

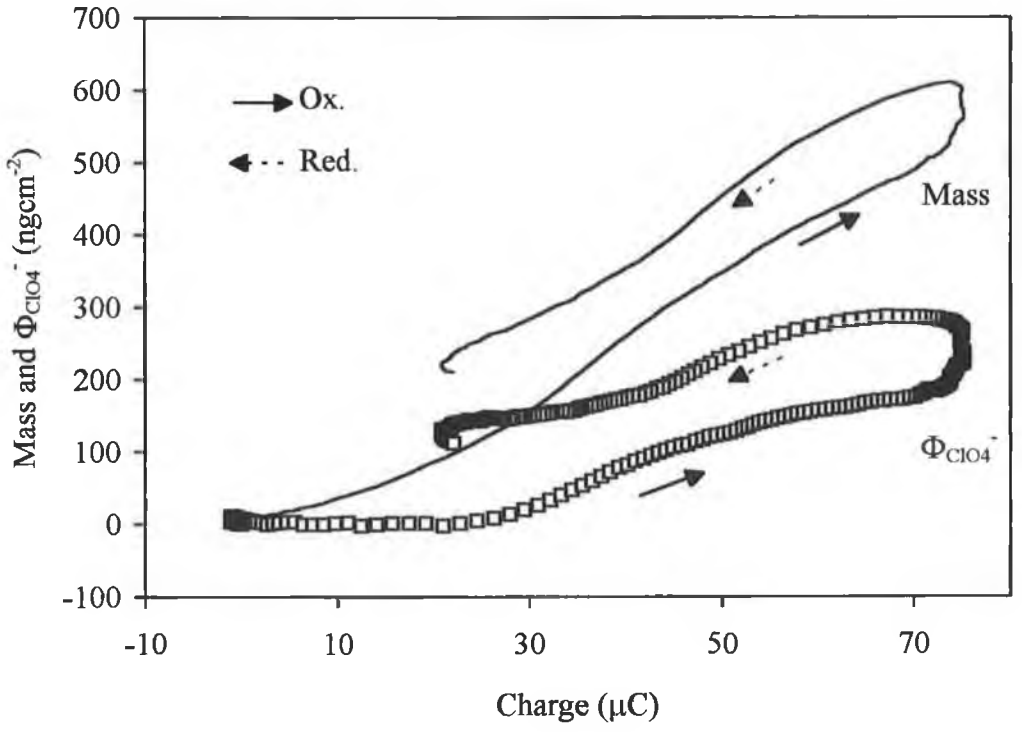

5.3.5. Comparison of $OsPVP_{33}$ and $OsPVP_{100}$ Films.

The redox-switching-induced mass transfer properties of these polymers in $LiClO_4$ electrolytes are different. For the $OsPVP_{33}$ polymer, redox switching is accompanied by the initial ingress of the anion and the subsequent influx of the anion and ca. 0.5 molecules of solvent per Os^{III} site. For the $OsPVP_{100}$ polymer, the perchlorate anion is again the dominant ion, however, solvent transfer occurs in both directions during polymer oxidation. Consequently, although the net normalised mass changes for both polymers are similar, the existence of this compensatory solvent transfer phenomena for the $OsPVP_{100}$ polymer, suggests that the level of solvent ingress for the $OsPVP_{100}$ polymer is in fact greater than that observed for the $OsPVP_{33}$ polymer. Similarly, in $HClO_4$, the level of solvent ingress during redox switching is greater for the $OsPVP_{100}$ (see Chapter 4). This reduced level of interfacial solvent transfer for the $OsPVP_{33}$ polymer clearly reflects the more hydrophobic nature of the $OsPVP_{33}$ copolymer backbone.

Furthermore, during redox switching, the permselective behaviour of these polymers are very different. In Chapter 2, it was illustrated that these polymers behave permselectively (non-permselectively) in electrolyte concentrations less than (greater than) 0.5M $LiClO_4$. During redox switching, the $OsPVP_{33}$ polymer behaves permselectively in all $LiClO_4$ concentrations. However, for thicker $OsPVP_{100}$ coatings, permselectivity breakdown is observed in electrolyte concentrations in excess of 1.0M $LiClO_4$. That permselective layer behaviour is observed for $OsPVP_{33}$ coatings over a greater $LiClO_4$ concentration range than for $OsPVP_{100}$ coatings is considered to reflect the more compact and hydrophobic nature of the $OsPVP_{33}$ copolymer. Similar observations were reported for this polymer in $HClO_4$ electrolytes (see Chapter 4). These observations clearly highlight the different chemical properties of the $OsPVP_{33}$ and $OsPVP_{100}$ polymers and their influence on the redox-switching-induced mass response.

5.4. Conclusions.

The mass transfer properties of $OsPVP_{33}$ polymer coatings, gravimetric surface coverages of 0.5 to 0.99 x 10^{-8} molcm^{-2}, are identical in $LiClO_4$ and $HClO_4$ electrolytes. This behaviour illustrates that anion motion, rather than cation motion is responsible for the maintenance of electroneutrality within these layers during redox switching. Similarly, anion motion is responsible for the maintenance of electroneutrality within $OsPVP_{100}$ coatings in these electrolytes.

Break-in effects are observed for both polymers during the first voltammetric scan. As a consequence of this behaviour, solvent becomes trapped within these layers during redox cycling. The normalised mass changes for the first and successive scans are different with steady-state mass changes being achieved following the first voltammetric scan.

The quantity of solvent transferred during redox switching is quite small for both polymers. For the $OsPVP_{33}$ polymer, solvent transfer is delineated from the anion transfer and is observed only after ca. 25-35% of the total charge change. This solvent is equivalent to 0.5-1.0 molecules of solvent per Os^{III} site, depending on the polymer surface coverage. For the $OsPVP_{100}$ polymer, solvent transfer occurs in both directions during polymer oxidation, with solvent egress dominating the initial 25% of the total charge change. The existence of these bi-directional solvent transfer processes prevents an accurate quantitation of the overall solvent changes . However, the net normalised mass change of 114 gmol^{-1} suggests that at least 1 solvent molecule per Os^{III} site enters the layer during polymer oxidation.

Under dynamic experimental conditions, interfacial solvent transfer is impeded in both polymers. The electrolyte dependence of the charge transport rate highlights the relationship between the ease of solvent transfer and the rate of charge transport, with D_{CT}(CV) being reduced in electrolytes in which solvent transfer becomes relatively more impeded.

5.5. References.

1. A.R. Hillman, D.C. Loveday and S. Bruckenstein, J. Electroanal. Chem., 274 (1989) 157.
2. A.R. Hillman, M.J. Swann and S. Bruckenstein, J. Electroanal. Chem., 291 (1990) 147.
3. S. Bruckenstein, C.P. Wilde, M. Shay and A.R. Hillman, J. Phys. Chem., 94 (1990) 787.
4. A.J. Kelly and N. Oyama, J. Phys. Chem., 95 (1991) 9579.
5. B.J. Feldman and O.R. Melroy, J. Electroanal. Chem., 234 (1987) 213.
6. C.S.C. Bose, S. Basak and K. Rajeshwar, J. Phys. Chem., 96 (1992) 9899.
7. M.C. Miras, C. Barbero, R. Kotz, O. Haas and V.M. Schmidt, J. Electroanal. Chem., 338 (1992) 279.
8. G. Inzelt, J. Electroanal. Chem., 287 (1990) 171.
9. C. Baker, Y-J Qiu and J.R. Reynolds, J. Phys. Chem., 95 (1991) 4446.
10. J.R. Reynolds, M. Pyo and Y-J Qiu, J. Electrochem. Soc., 141 (1994) 35.
11. D. Orata and D.A. Buttry, J. Am. Chem. Soc., 109 (1987) 3574.
12. P.T. Varineau and D.A. Buttry, J. Phys. Chem., 91 (1987) 1292.
13. A.J. Kelly, T. Ohsaka, N. Oyama, R.J. Forster and J.G. Vos, J. Electroanal. Chem., 287 (1990) 185.
14. A.P. Clarke, J.G. Vos, A. Glidle and A.R. Hillman, J. Chem. Soc. Faraday Trans., 89 (1993) 1695.
15. R. Borjas and D.A. Buttry, J. Electroanal. Chem., 280 (1990) 73.
16. A. Glidle, A.R. Hillman and S. Bruckenstein, J. Electroanal. Chem., 318 (1991) 411.
17. A.P. Clarke, J.G. Vos, A.R. Hillman and A. Glidle, J. Electroanal. Chem., 389 (1995) 129.
18. A.P. Clarke, Ph.D. Thesis, Dublin City University, (1992).

19. S. Bruckenstein, C.P. Wilde, M. Shay, A.R. Hillman and D.C. Loveday, J. Electroanal. Chem., 258 (1989) 457.

20. S. Bruckenstein and A.R. Hillman, J. Phys. Chem., 92 (1988) 4837.

21. A.R. Hillman, N.A. Hughes and S. Bruckenstein, J. Electrochem. Soc., 139 (1992) 74.

22. A.R. Hillman and S. Bruckenstein, J. Chem. Soc. Faraday Trans., 89 (1993) 339.

23. M.D. Ward, J. Electrocham. Soc., 135 (1988) 2747.

24. G. Inzelt and J. Bacskai, J. Electroanal. Chem., 308 (1991) 255.

25. A.R. Hillman, N.A. Hughes and S. Bruckenstein, Analyst, 119 (1994) 167.

26. A.R. Hillman, D.C. Loveday and S. Bruckenstein, J. Electroanal. Chem., 300 (1991) 67.

27. A.R. Hillman, M.J. Swann and S. Bruckenstein, J. Phys. Chem., 95 (1991) 3271.

28. A.R. Hillman, D.C. Loveday, M.J. Swann, S. Bruckenstein and C.P. Wilde, J. Chem. Soc. Faraday Trans., 87 (1991) 2047.

29. A.R. Hillman, D.C. Loveday, M.J. Swann, S. Bruckenstein and C.P. Wilde, Analyst, 117 (1992) 1251.

30. E.F. Bowden, M.F. Dautartas and J.F. Evans, J. Electroanal. Chem., 219 (1987) 91.

Chapter 6.

The Effect of Acetonitrile On the Mass and Charge Transport Properties of $[Os(bipy)_2(PVP_{100})_{10}Cl]^+$ Metallopolymer Films.

6.1. Introduction.

The structure of electroactive polymers has a profound influence on their electrochemical properties and is dependent on the identity of the counterion[1-5], the temperature [6-9] and the nature of the contacting solvent [10-12]. The influence of the counterion identity (and by implication film structure) on the redox-switching-induced solvent transfer properties of electroactive films has been demonstrated. For PVF films, oxidation in PF_6^- [5] and ClO_4^- [5,13] electrolytes is accompanied by the influx of small quantities of solvent, reflecting the compact nature of the film in these electrolytes. By comparison, in Cl^- [5] electrolytes, PVF layers are so extensively solvent swollen that the Sauerbrey equation is no longer accurate. For $OsPVP_{100}$ films, the redox-switching-induced mass changes are dependent on the electrolyte anion [3,4,14,15]. In ClO_4^- [3,14,15] electrolytes, in which these layers are compact, the level of solvent ingress is typically only 0-2.6 molecules of solvent per osmium site. In pTS^- [4,14,15] electrolytes, in which these layers are swollen, the level of solvent ingress is 4-20 molecules of solvent per osmium site, depending on the polymer surface coverage. For TCNQ films, the level of solvent influx is determined by the hydration number of the electrolyte cation [8,9].

The electrochemistry of PVF [16,17], Ru^{III}(edta) incorporated in PVP [11] and TCNQ [10] films are dependent on the solvent of the contacting electrolyte. Changes in the voltammetric behaviour of these polymer systems in various bathing solvents were discussed in terms of different solvent swelling effects. Additionally, the electrochemical properties of TCNQ coatings are greatly altered by temperature induced swelling variations [6,7]

The inter-relationship between polymer swelling and the rate of charge transport through electroactive films has been clearly illustrated [1,2,7,10,12,18-20]. Enhanced charge transport rates are frequently observed for swollen polymer films. This behaviour is typically discussed in terms of more facile ion transport and greater flexibility of the polymer chains on swelling of the polymer backbone

[1,2,7,10,12,18-20]. The charge transport properties of the $OsPVP_{100}$ metallopolymer are dependent on the identity of the counterion [21-24]. For example, in swelling electrolytes (H_2SO_4), charge transport rates, as estimated by cyclic voltammetry, are 10-100 times greater than those observed in compacting electrolytes ($LiClO_4$). Kinetic mass transfer studies of this particular polymer suggest that the structural (counterion) dependence of the charge transport rate may reflect the ease of solvent transfer [15], with solvent transfer being comparatively more hindered in compact films.

The aim of this chapter is to probe the relationship between the structure of $OsPVP_{100}$ films and their mass and charge transfer properties by systematically swelling the polymer layer. The influence of adding acetonitrile, which can solubilise this polymer, to aqueous electrolyte systems on the mass and charge transfer properties of this material is investigated. In aqueous perchlorate electrolytes, $OsPVP_{100}$ electrode coatings are compact and contain only small quantities of solvent [3,15]. Charge transport rates in $LiClO_4$ are amongst the lowest reported for this metallopolymer and reflect the difficulties for ion influx and transfer within these compact structures [23,24]. This electrolyte, therefore, provides a useful environment in which to probe the effects of solvent swelling on the electrochemical response of the $OsPVP_{100}$ metallopolymer.

6.2. Experimental.

6.2.1. Apparatus.

The EQCM and electrochemical apparatus have been described in Chapter 4 and Chapter 3 respectively.

6.2.2. Materials.

The synthesis of $[Os(bipy)_2(PVP_{100})_{10}Cl]Cl$ was described in Chapter 2. HPLC grade MeCN (0.02% H_2O) was used as supplied. All mixed solvents were prepared with Milli-Q H_2O and a constant 0.1M $LiClO_4$ electrolyte concentration was used in each case. Electrolytes are identified in terms of the percentage of non-aqueous solvent i.e. 30% MeCN signifies 0.1M $LiClO_4$ prepared in 30:70 (v:v) MeCN : H_2O.

6.2.3. Procedures.

Glassy carbon electrodes (3 and 7mm diameter) were drop coated from a 0.25% w/v ethanolic solution of $OsPVP_{100}$ polymer, as described in Chapter 3. The rate of charge transport and the associated activation parameters were evaluated for these electrode coatings, as a function of the MeCN content of the bathing electrolyte, using cyclic voltammetry (see Chapter 3 for experimental details). The influence of adding methanol to the contacting electrolyte, another organic electrolyte in which the polymer is soluble, on the charge transport properties of these layers was also probed. These results are not discussed in this chapter but are included in the Appendix.

Quartz crystal coatings were prepared, as described in Chapter 2, from the same $OsPVP_{100}$ polymer solution. To probe the influence of MeCN on the rigidity of these coatings, the admittance characteristics of the coated crystals were recorded in

each mixed solvent electrolyte, in order of increasing acetonitrile concentration. The layers were equilibrated for three hours in each solvent mixture by voltammetric cycling over the $Os^{II/III}$ couple, prior to the recording of the open circuit admittance spectra associated with the Os^{II} oxidation state. The existence of swelling effects is clearly illustrated and the importance of differentiating between "true" mass changes and deleterious contributions from polymer viscoelasticity is emphasised.

The change in layer mass accompanying redox switching of these $OsPVP_{100}$ crystal coatings was studied as a function of the MeCN content of the contacting electrolyte and the experimental timescale (1 to 500 mVs^{-1}).

Gravimetric surface coverages for these studies were in the range of 0.28 x 10^{-8} to 5.22 x 10^{-8} $molcm^{-2}$. The admittance and mass transfer characteristics of these coatings are dependent on the polymer surface coverage, reflecting different degrees of film swelling.

6.3. Results and Discussion.

6.3.1. Effect of MeCN on the Layer Rigidity and Resident Layer Mass of $OsPVP_{100}$ Films.

Fig. 6.1 illustrates the change in crystal resonance of an $OsPVP_{100}$ coated crystal in 0.1M $LiClO_4$ as the MeCN content of the contacting electrolyte is increased from 0% (100% H_2O) to 30%. The electrolyte concentration is 0.1M $LiClO_4$ for each mixed solvent system. The gravimetric surface coverage was 1.32×10^{-8} molcm^{-2}. This layer was voltammetrically cycled for three hours in each mixed solvent electrolyte, alternating between 1 and 50 mVs^{-1} scan rates, prior to the recording of these open circuit spectra. Table 6.1 summaries the characteristic features of these admittance spectra i.e. the admittance maximum, peak width at half max. admittance (PWHM) and the shift in frequency of maximum admittance. Table 6.1 also includes the change in layer mass calculated from the shift in resonant frequency, assuming the validity of the Sauerbrey equation (see below).

Fig. 6.2 illustrates the corresponding change in crystal resonance of an uncoated crystal in the same solutions. Comparison of Fig. 6.2 with Fig. 6.1 reveals that, as the MeCN content of the bathing electrolyte is increased form 0% to 30%, the shape of the crystal resonance broadens slightly. This behaviour is not associated with the viscous properties of the contacting electrolyte (see Fig. 6.2) and therefore reflects a loss in rigidity of the $OsPVP_{100}$ coating [3,4,15,19,25]. However, the PWHM of the admittance spectrum upon addition of 30% MeCN is only 3% greater than that observed for the uncoated crystal, which is unlikely to invalidate the Sauerbrey equation. With increasing MeCN content of the contacting electrolyte, there is a decrease in the frequency of maximum admittance. This corresponds to a decrease in the resonant frequency of the coated crystal. These data are summarised in Table 6.1 and reflect an increase in the resident layer mass. This increase in layer

Fig. 6.1. Admittance spectra for an $OsPVP_{100}$ coated crystal as a function of the MeCN content of the bathing electrolyte. Gravimetric surface coverage is 1.32×10^{-8} molcm^{-2}. Spectra were recorded at open circuit following voltammetry.

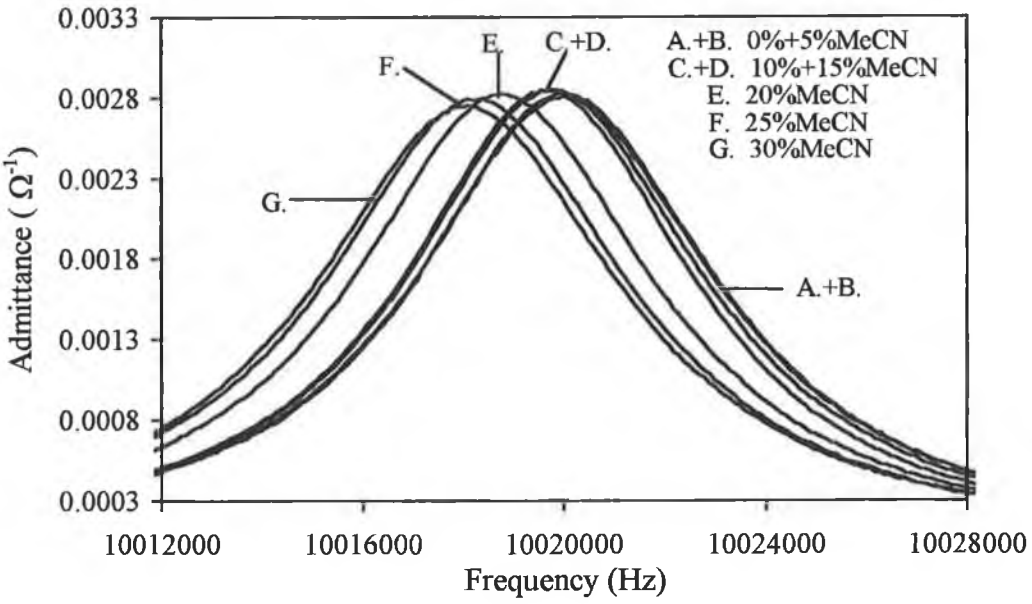

Fig. 6.2. Admittance spectra for an uncoated crystal as a function of the MeCN content of the bathing electrolyte.

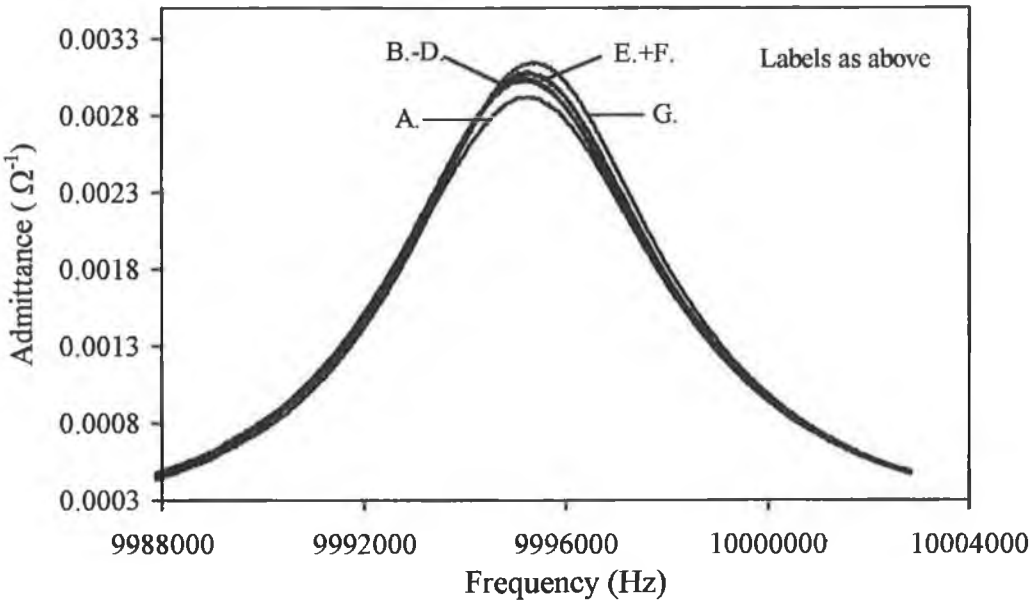

Table 6.1. Admittance data obtained at open circuit for an $OsPVP_{100}$ coated crystal in 0.1M $LiClO_4$, as a function of the MeCN content of the electrolyte. Gravimetric surface coverage is 1.32×10^{-8} molcm^{-2}.

% MeCN	Admittance[(a)] ($\Omega^{-1} \times 10^{-2}$)	PWHM[(a)] (Hz)	Δf[(a,b)] (Hz)	Mass per polymer unit[(b)] (g pol equiv^{-1})
H_2O	0.281	7300	--	--
5%	0.283	7250	-100	33
10%	0.285	7200	-200	65
15%	0.285	7200	-400	131
20%	0.283	7200	-1250	408
25%	0.280	7250	-1750	571
30%	0.276	7400	-2000	653

a) Data resolution is 20 Hz.

b) Estimated from shift in resonant frequency and corrected for the viscous load of the contacting electrolyte.

mass, coupled with the observed slight decrease in layer rigidity, clearly reflect swelling phenomena and are a consequence of the solubility of the polymer coating in this organic solvent.

Fig. 6.3 illustrates the change in layer mass of this $OsPVP_{100}$ coating as a function of the MeCN content of the electrolyte. The data is taken from Table 6.1 and has been corrected for the viscous load of the electrolyte. The addition of MeCN to the contacting electrolyte induces polymer swelling and an accompanying increase in layer mass. In 15-20% MeCN, the layer mass increases quite dramatically and is accompanied by slight broadening of the crystal resonance (see Table 6.1). However, as was discussed above, the resultant change in layer rigidity is not sufficient to invalidate the Sauerbrey equation. Unfortunately, identification of this additional mass component of the resident layer mass is not straight-forward and may be associated with the ingress of either solvent (water or acetonitrile), salt (as a consequence of the breakdown on permselectivity) or combinations of all three.

Fig. 6.4 illustrates the change in crystal resonance of a thicker $OsPVP_{100}$ coated crystal under the same experimental conditions used in Fig. 6.1. The gravimetric surface coverage was 3.05×10^{-8} molcm^{-2}. All spectra were recorded at open circuit following voltammetric cycling for 3 hours. Table 6.2 summarises the characteristic features associated with these spectra. Table 6.2 also includes the change in layer mass calculated from the shift in resonant frequency, correcting for the viscous load of the electrolyte.

The admittance characteristics of this thicker $OsPVP_{100}$ layer are qualitatively similar to those observed for the thinner $OsPVP_{100}$ coating (see Table 6.1). Upon addition of MeCN to the contacting electrolyte, the shape of the crystal resonance broadens, which again illustrates swelling of the polymer coating in this solvent. This swelling effect is accompanied by a decrease in the resonant frequency (increase in the resident layer mass).

Fig. 6.3. The influence of MeCN on the resident layer mass of $OsPVP_{100}$ crystal coatings. Gravimetric surface coverage is □) 1.32 x 10^{-8} molcm^{-2} and Δ) 3.05 x 10^{-8} molcm^{-2}.

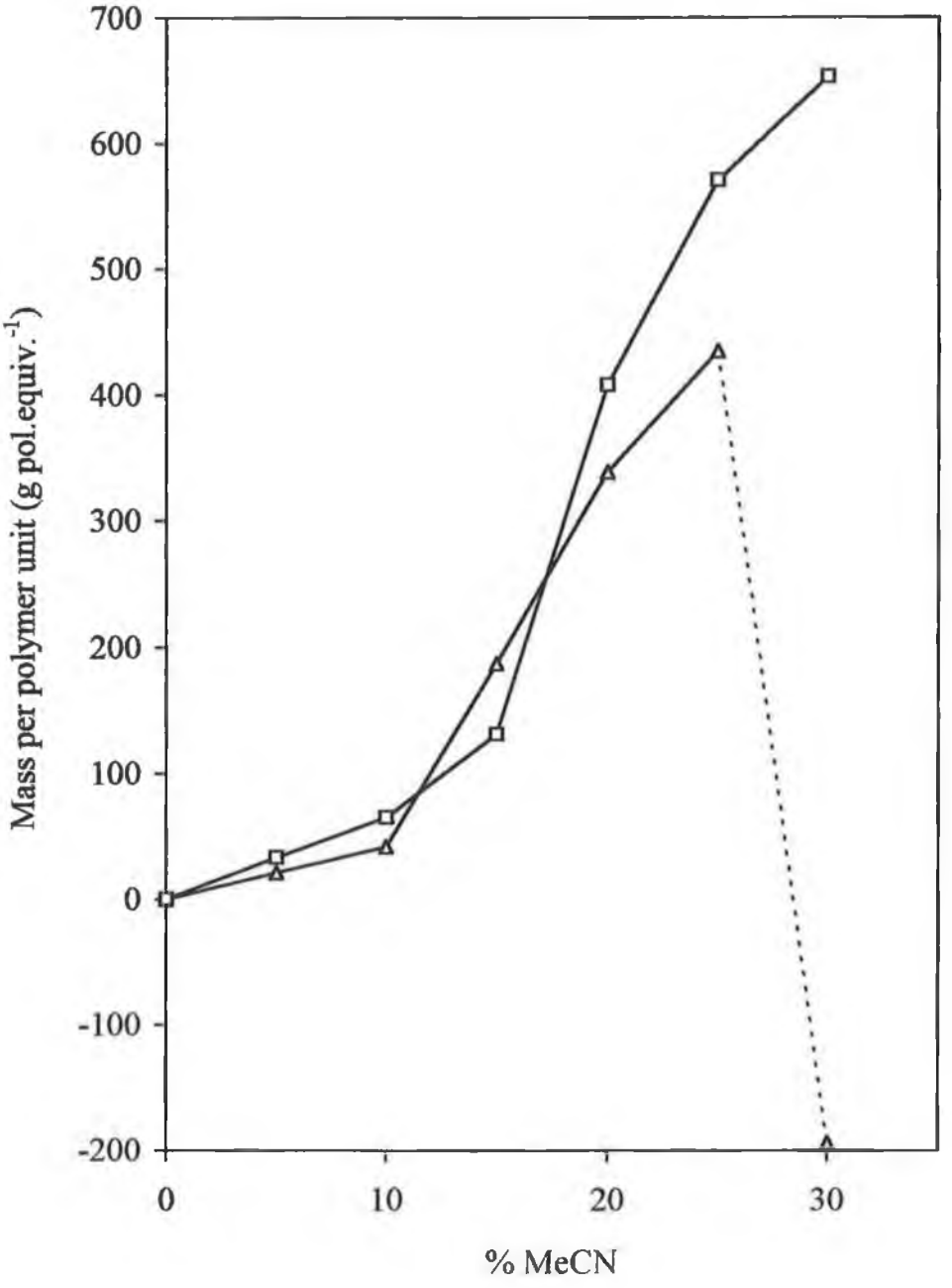

Fig. 6.4. Admittance spectra for an $OsPVP_{100}$ coated crystal as a function of the MeCN content of the bathing electrolyte. Gravimetric surface coverage is 3.05×10^{-8} molcm^{-2}. Spectra were recorded at open circuit following voltammetry. Labels as in Fig. 6.1.

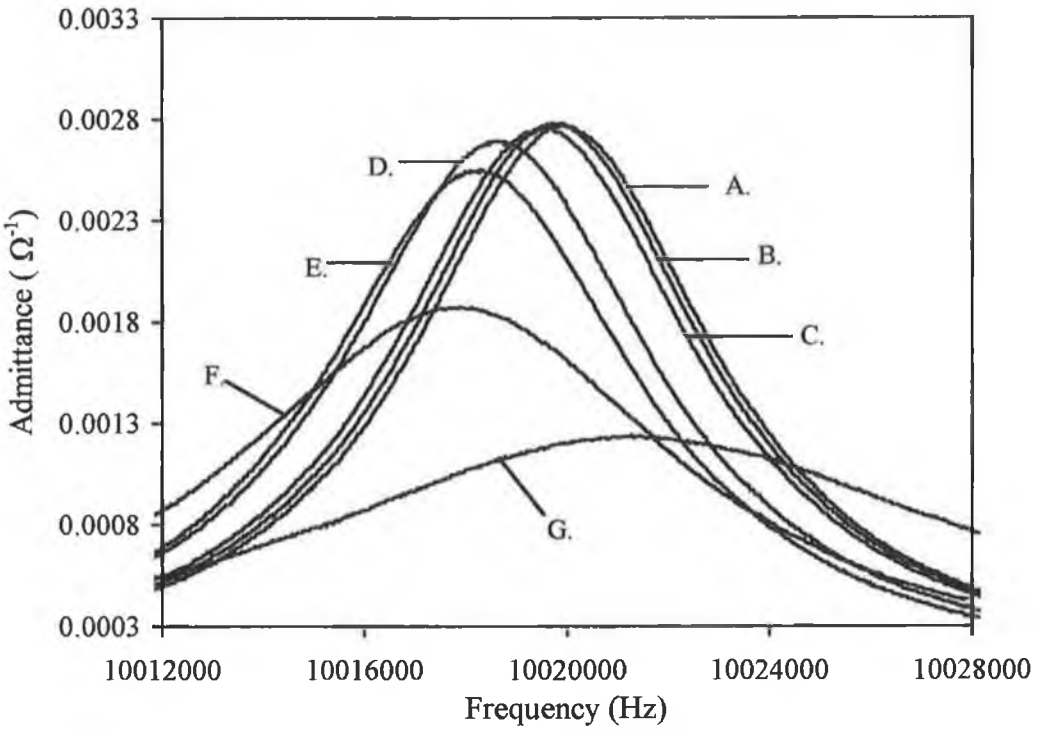

The change in layer mass, as a function of the MeCN content of the electrolyte, is illustrated in Fig. 6.3. Within the concentration range of 0% to 10% MeCN, the change in layer mass per polymer equivalent, is quantitatively similar for both layers. In MeCN concentrations in excess of 10%, there is a sharp increase in the resident layer mass. Similar behaviour was observed for the thinner $OsPVP_{100}$ coating (see Fig. 6.3) and reflects the substantial mobile species uptake that occurs in these higher MeCN concentrations. However, these swelling effects are dramatically accentuated for the thicker $OsPVP_{100}$ coating in the higher MeCN concentrations.

Table 6.2. Admittance data obtained at open circuit for an $OsPVP_{100}$ coated crystal in 0.1M $LiClO_4$, as a function of the MeCN content of the electrolyte. Gravimetric surface coverage is 3.05×10^{-8} molcm^{-2}.

% MeCN	Admittance[(a)] ($\Omega^{-1} \times 10^{-2}$)	PWHM[(a)] (Hz)	Δf[(a,b)] (Hz)	Mass per polymer unit[(b)] (g pol equiv^{-1})
H_2O	0.277	7350	---	--
5%	0.278	7325	-150	21
10%	0.276	7350	-300	42
15%	0.269	7550	-1325	187
20%	0.255	7650	-2400	339
25%	0.187	10750	-3075	435
30%	0.124	16775	+1375	---

a) Data resolution is 20Hz.

b) Estimated from shift in resonant frequency and corrected for the viscous load of the contacting electrolyte; where the Sauerbrey equation is still valid (see text).

It is suggested that the greater swelling effects observed for the thicker $OsPVP_{100}$ layer are a consequence of the greater requirement for solvent/ salt influx for the establishment of equilibrium neutral species levels.

Within the concentration range of 0-25% MeCN, it is considered that, for this thicker layer, the Sauerbrey equation is applicable (see below). However, in 30% MeCN the resonant frequency of the crystal increases and suggests that the resident layer mass has decreased. In this electrolyte, the PWHM has increased by ca. 130% relative to the PWHM for this layer in 100% H_2O and thus illustrates extensive swelling of the polymer coating. Under these conditions the Sauerbrey equation is unlikely to be valid. Consequently, the observed increase in resonant frequency at this MeCN concentration does not represent a decrease in layer mass but reflects contributions from the viscoelastic properties of the solvent swollen layer. This behaviour is discussed in greater detail in Section 6.3.3.2.

In summary, the addition of MeCN to the contacting electrolyte induces swelling of these layers, resulting in (or from) an increase in the resident layer mass. The degree of polymer swelling depends on the polymer surface coverage. These swelling phenomena have a profound influence on the electrochemical induced mass transfer properties of these coatings.

6.3.2. Effect of MeCN on the Slow Scan Voltammetric Behaviour of $OsPVP_{100}$ Films.

The voltammetric characteristics of $OsPVP_{100}$ coatings on glassy carbon electrodes were studied as a function of the MeCN content of the bathing electrolyte. In this section the influence of acetonitrile on the slow scan rate voltammetric characteristics (scan rates less than 10 mVs^{-1}) are discussed. The influence of

acetonitrile on the diffusional response of these coatings is discussed in Section 6.3.4.

Fig. 6.5A illustrates the 1 mVs^{-1} cyclic voltammetric behaviour of an $OsPVP_{100}$ coated electrode in aqueous 0.1M $LiClO_4$. The characteristic features of this voltammogram i.e. the peak-to-peak separation (ΔE_p), the full width at half maximum current (FWHM) and the half wave potential ($E_{1/2}$), are summarised in Table 6.3. The half wave potential ($E_{1/2}$) is taken as the average of the anodic and cathodic peak potentials. The ratio of the anodic to cathodic peak currents (i_{pa}/i_{pc}) is close to unity for all solvent combinations. In Fig. 6.5A, the presence of diffusional tailing is indicative of a diffusional controlled electrochemical response. A plot of i_p vs $v^{1/2}$ is linear for 5 to 500 mVs^{-1} scan rates and again indicates a diffusional rather than a surface response. In aqueous 0.1M $LiClO_4$, surface coverages estimated from the area under the anodic peak, correcting for background, are ca. 25-35% smaller than those estimated by exhaustive coulometry. Therefore, within this experimental timescale only 65-75% of the redox sites within the layer are electroactive. This behaviour, coupled with the observed diffusional limited response, is characteristic of perchlorate electrolytes and is considered to reflect hindered charge transport through the compact $OsPVP_{100}$ layers.

Table 6.3 highlights the influence of acetonitrile on the voltammetric characteristics of 1 mVs^{-1} cyclic voltammograms for this same $OsPVP_{100}$ layer. These characteristics are indistinguishable from those observed during experiments on individual polymer coatings. The addition of MeCN to the electrolyte greatly alters the voltammetric characteristics of the polymer layer. On increasing the MeCN content of the electrolyte, a gradual transition from diffusion controlled voltammetric behaviour to surface behaviour is observed. Fig. 6.5B illustrates the cyclic voltammetric behaviour of this layer in 20% MeCN. The voltammetric characteristics are significantly different from those observed in 100% H_2O (see Fig. 6.5A). The peak-to-peak separation is essentially zero and the FWHM is 90 mV.

Fig. 6.5. 1 mVs^{-1} cyclic voltammetric behaviour of an $OsPVP_{100}$ coated glassy carbon electrode. Coulometric surface coverage is 4.3×10^{-8} $molcm^{-2}$.

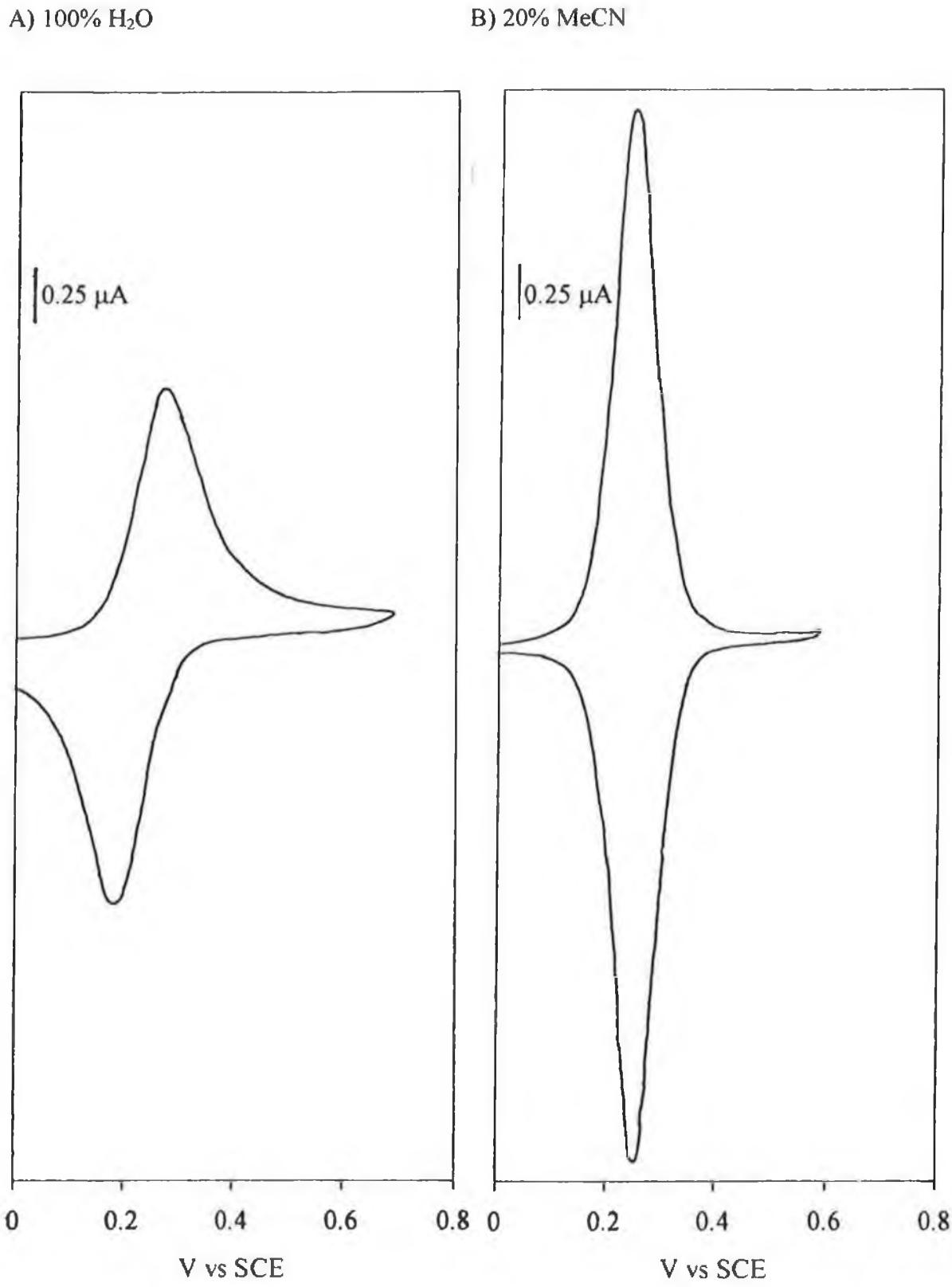

Table 6.3. The effect of MeCN on the characteristic parameters of 1 mVs^{-1} cyclic voltammograms of $OsPVP_{100}$ coated electrodes in 0.1M $LiClO_4$.

% MeCN	FWHM[a,b] (mV)	ΔE_p[a,b] (mV)	$E_{1/2}$[a,b,c] (mV)
0%	140	95	230
5%	115	50	230
10%	100	30	250
15%	90	15	248
20%	90	5	248
25%	90	5	250
30%	90	5	248

a) Estimated from 1 mVs^{-1} cyclic voltammogram.

b) Error on measurement is ±5 mV.

c) Estimated from the average of the anodic and cathodic peak potentials.

These features are characteristic of a one electron oxidation/ reduction of surface confined species and represent ideal surface behaviour [26]. In this mixed solvent electrolyte, the surface coverage of osmium sites estimated from the area under the anodic peak is identical to the coverage estimated by exhaustive coulometry. This illustrates that the complete layer is now electroactive within these experimental timescales.

The observed transition in the voltammetric behaviour from solution to surface behaviour, coupled with the oxidation of larger portions of these modifying layers upon addition of MeCN to the contacting electrolyte, clearly reflect more rapid charge transport processes compared with those observed in aqueous $LiClO_4$. Considering the solubility of the polymer in this solvent (see Section 6.3.1), it seems likely that these voltammetric observations are a direct consequence of solvent induced swelling effects. Therefore, it is considered that the occurrence of surface behaviour on addition of 20% MeCN to the contacting electrolyte reflects swelling of the polymer layer and the more favourable mass and change transport processes within these swollen structures. These effects are examined in greater detail in the following sections.

6.3.3. Effect of MeCN on the Layer Mass Changes Accompanying Redox Switching of $OsPVP_{100}$ Films.

The influence of these swelling phenomena on mobile species transfer during redox switching of these electroactive layers was probed. In the course of these experiments it was observed that the surface coverage had a significant effect on the redox-switching-induced mass change. This behaviour reflects the dependence of the degree of polymer swelling on the polymer surface coverage, as was discussed in Section 6.3.1. From the $OsPVP_{100}$ crystal coatings examined, two surface coverage ranges of different mass transfer behaviour were identified a) 0.28 to 1.93 x 10^{-8}

molcm^{-2} and b) 2.15 to 5.22 x 10^{-8} molcm^{-2}. The data for both surface coverages are discussed individually.

6.3.3.1. Gravimetric surface coverages of 0.28 to 1.93 x 10^{-8} molcm^{-2}.

In Section 6.3.1, the influence of MeCN on the rigidity and layer mass of a 1.32 x 10^{-8} molcm^{-2} $OsPVP_{100}$ coating was examined. Upon addition of MeCN to the contacting electrolyte, the layer swells and the resident layer mass increases. However, despite this solvent induced swelling of the layer, it is considered that the Sauerbrey equation is still valid.

For the work reported here, the crystal resonance shape of $OsPVP_{100}$ coated crystals was studied as a function of the $Os^{II/III}$ oxidation states, to probe for possible deleterious swelling variations during redox switching. Fig. 6.6 illustrates the change in crystal resonance of an $OsPVP_{100}$ coated crystal during an oxidative 5 mVs^{-1} cyclic voltammetric scan in 20% MeCN. The gravimetric surface coverage was 1.15 x 10^{-8} molcm^{-2}. In Fig. 6.6, the resonant frequency decreases during polymer oxidation. This behaviour represents an increase in layer mass and suggests that anion influx is responsible for the maintenance of electroneutrality. The shape of the crystal resonance is similar in both Os^{II} and Os^{III} redox states, which indicates that the layer rigidity is not compromised during redox switching [11,17,19,20,25]. This observation clearly illustrates that the Sauerbrey equation is valid under these conditions and corroborates the findings in Section 6.3.1.

Furthermore, Fig. 6.7 illustrates the change in layer mass for $OsPVP_{100}$ coatings of different surface coverage in 20% MeCN. It is anticipated that, for layers behaving viscoelastically, the mass change for thicker films will be reduced and these plots will exhibit concave curvature [27,28]. The linearity of this plot, therefore illustrates that the viscoelastic properties of the layer do not contribute to the mass response in this MeCN concentration.

Fig. 6.6. Admittance spectra for an $OsPVP_{100}$ coated crystal during redox switching in 0.1M $LiClO_4$ (20% MeCN) at 5 mVs^{-1}. Gravimetric surface coverage is 1.15×10^{-8} $molcm^{-2}$.

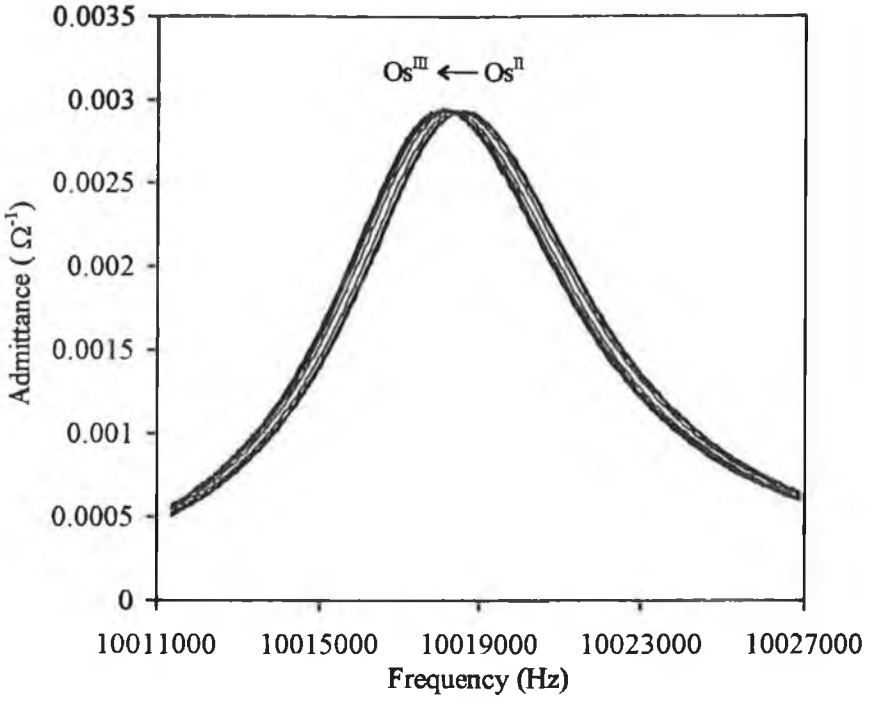

Table 6.4 summarises the overall normalised change in layer mass, during redox switching of $OsPVP_{100}$ coated crystals, as a function of the MeCN content of the bathing electrolyte. The voltammetric scan rates were 1 and 5 mVs^{-1}. These mass changes are associated with the maintenance of electroneutrality within the $OsPVP_{100}$ coatings during the $Os^{II/III}$ oxidation process. The normalised mass changes are reproducible to within 10% for determinations on different films and 3% for repeated determinations on a single film.

The change in layer mass during redox switching of $OsPVP_{100}$ coatings in 0.1M $LiClO_4$ has been discussed in Chapter 5. For the data presented here only the first voltammetric scan is considered.

Fig. 6.7. Change in layer mass accompanying $Os^{II/III}$ oxidation of $OsPVP_{100}$ coated crystals in 0.1M $LiClO_4$ (20% MeCN). Coulometric surface coverages are 0.48 to 3.00 x 10^{-8} molcm^{-2}.

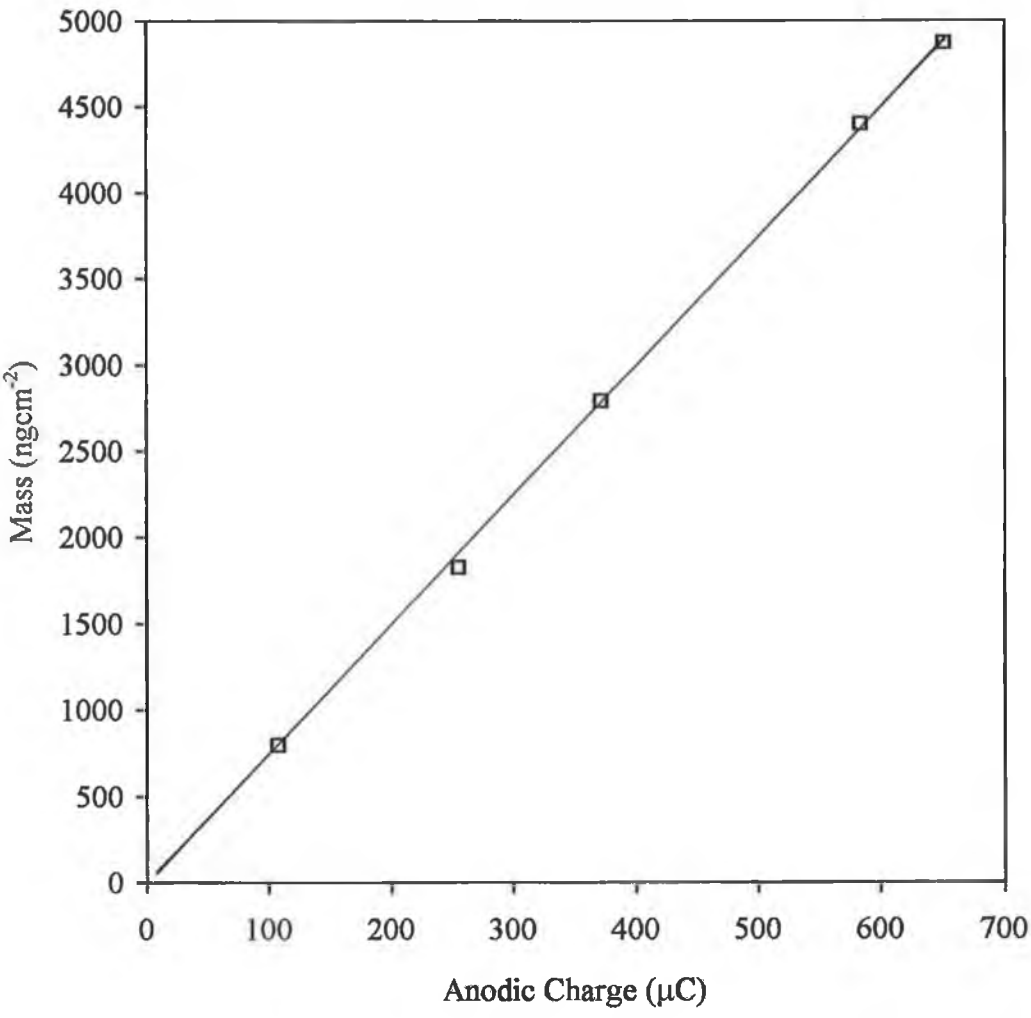

Table 6.4. The effect of MeCN on the normalised mass change accompanying redox switching of $OsPVP_{100}$ crystal coatings in 0.1M $LiClO_4$. Gravimetric surface coverages are 0.28 to 1.93 x 10^{-8} molcm^{-2}.

% MeCN	Normalised Mass Change ($gmol^{-1}$)	
	A. 1 mVs^{-1} [a]	B. 5 mVs^{-1} [a]
0	114 (2)	112 (3)
5	141 (6)	134 (1)
10	167 (5)	160 (4)
15	159 (1)	155 (4)
17.5	151*	159 (2)
20	160 (7)	162 (3)
22.5	161 (2)	156 (4)
25	167*	165 (7)
30	314 (17)	345 (19)

(a) errors quoted in brackets represent the variations between 2 different films.

* signifies measurements made on one film only.

On addition of 5% MeCN to the contacting electrolyte, the overall redox-switching-induced mass change increases from 112 (±3) $gmol^{-1}$ to 134 (±1) $gmol^{-1}$. This increase in normalised mass change, upon addition of MeCN to the contacting electrolyte, is likely a consequence of the more swollen polymer structure that exists in this electrolyte (see Section 6.3.1). Fig. 6.8 illustrates the change in layer mass for an $OsPVP_{100}$ coated crystal in 5% MeCN. The scan rate was 5 mVs^{-1} and the gravimetric surface coverage was 1.29 x 10^{-8} $molcm^{-2}$. Fig. 6.9 illustrates the corresponding mass and Φ_{ClO4^-}-charge plots for the data in Fig. 6.8. The behaviour in Fig. 6.8 and Fig. 6.9 is qualitatively similar to that observed in 100% H_2O and has been discussed in Chapter 5. In 100% H_2O, there is an initial decrease in the Φ_{ClO4^-}-charge data which is considered to reflect the egress of solvent from the layer (see Chapter 5). Although this behaviour is not apparent in Fig. 6.9, it cannot be discounted, as the additional mass influx may be sufficient to mask the egress mechanism. The substantial hysteresis in both the mass- and Φ_{ClO4^-}-charge plots indicates that interfacial neutral species transfer is retarded [29-32].

Table 6.5 summarises the potentials of half-total-charge change and half-total-mass change, for both oxidative and reductive processes, obtained during 5 mVs^{-1} cyclic voltammetric experiments. Also included are the corresponding anodic and cathodic peak potentials. Within the concentration range of 0-10% MeCN the potentials of half-total-mass change and half-total-charge change are delineated. This behaviour illustrates that mass transfer is relatively more hindered than charge transfer and is consistent with the observation of hysteresis in the mass-charge plot of Fig. 6.9.

Within the concentration range of 10% to 25% MeCN, the normalised mass change accompanying redox switching increases to 160 (±4) $gmol^{-1}$. This greater mass change, compared with 0% and 5% MeCN is not a consequence of viscoelastic contributions from the swollen polymer (see Fig. 6.6 and Fig. 6.7), but reflects an increase in the normalised mass change as a consequence of greater species

Fig. 6.8. Cyclic voltammogram and mass-potential plot for an $OsPVP_{100}$ coated crystal in 0.1M $LiClO_4$ (5% MeCN). Scan rate is 5 mVs^{-1}. Gravimetric surface coverage is 1.29×10^{-8} $molcm^{-2}$.

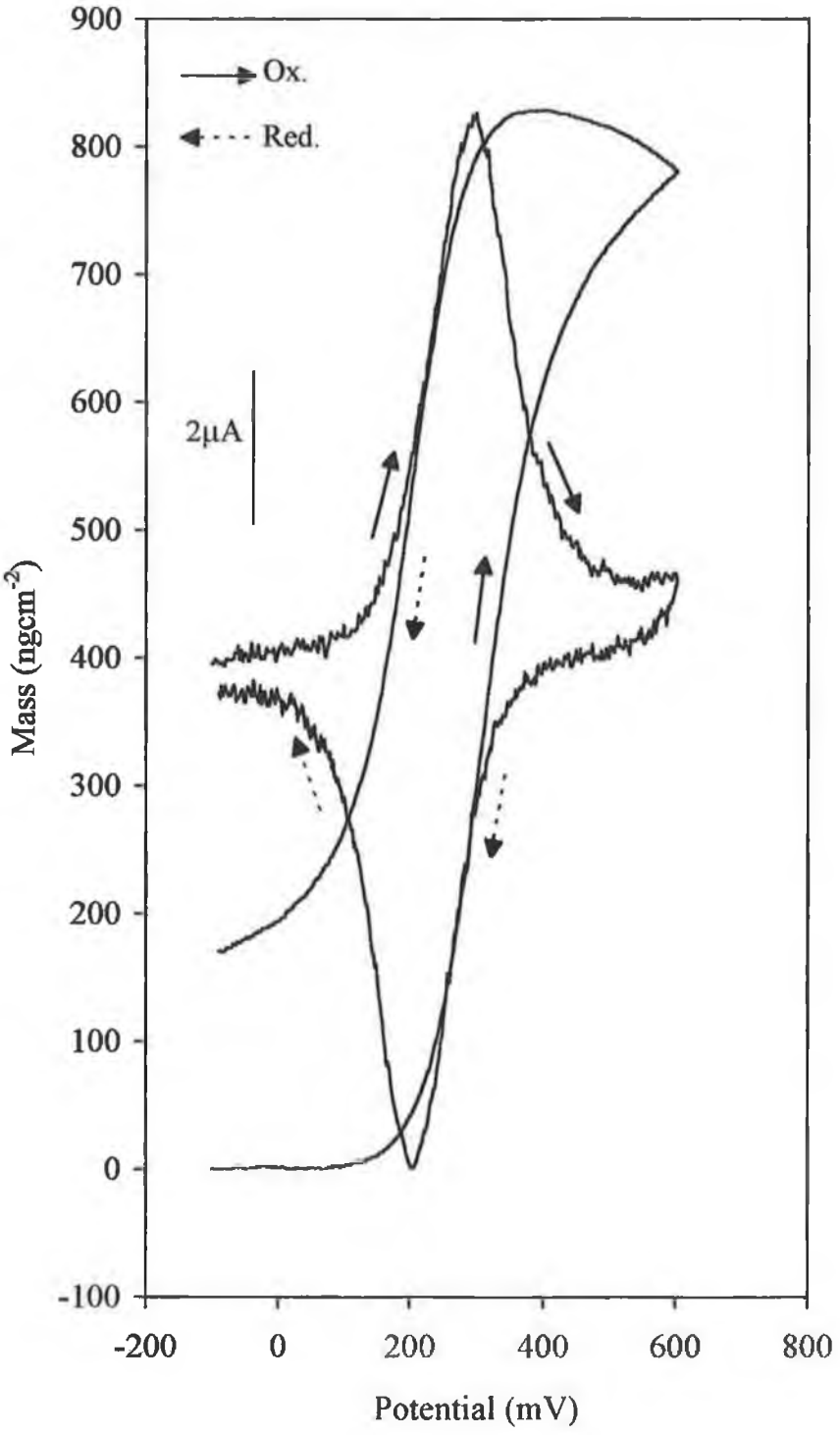

Fig. 6.9. Mass- and Φ_{ClO4}^- -charge plots for data in Fig. 6.8.

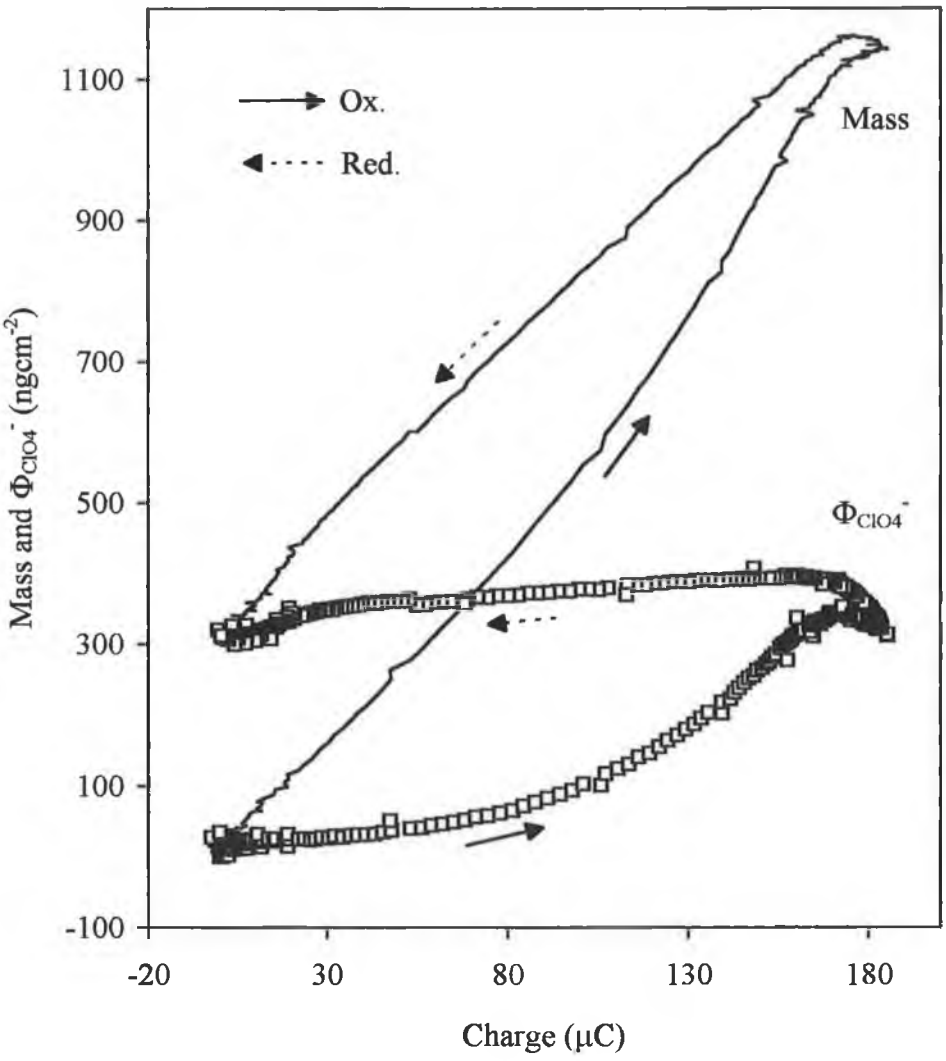

influx during polymer oxidation.

Fig. 6.10 illustrates the cyclic voltammogram and change in layer mass of an $OsPVP_{100}$ coated crystal (same layer as in Fig. 6.8) during a 5 mVs^{-1} voltammetric scan in 20% MeCN. The cyclic voltammogram is characteristic of ideal surface behaviour. This transition between solution and surface behaviour was discussed in Section 6.3.2. Under these conditions the complete layer is electroactive and the coulometric and gravimetric surface coverages are essentially identical

Table 6.5. The oxidation/ reduction potentials of the $Os^{II/III}$ couple and their associated half-mass and half-charge potentials for $OsPVP_{100}$ coated crystals as a function of MeCN electrolyte content.

% MeCN	Oxidation[a]			Reduction[a]		
	$E_{1/2}$ (Ox.)	$E_{1/2}$ (q)	$E_{1/2}$ (m)	$E_{1/2}$ (Red.)	$E_{1/2}$ (q)	$E_{1/2}$ (m)
0	260	258	284	158	156	148
5	265	268	282	191	191	172
10	251	251	264	227	225	218
15	247	247	244	222	222	224
17.5	244	245	239	234	236	232
20	239	240	239	235	235	235
22.5	237	237	238	232	231	228
25	239	244	238	233	228	229
30	250	254	247	250	241	241

(a) All potentials (mV vs SCE) measured at 1 mVs^{-1} at ambient temperatures (20 ± 2^{o} C).

Fig. 6.10. Cyclic voltammogram and mass-potential plot for an $OsPVP_{100}$ coated crystal in 0.1M $LiClO_4$ (20% MeCN). Scan rate is 5 mVs^{-1}. Gravimetric surface coverage is 1.29×10^{-8} $molcm^{-2}$.

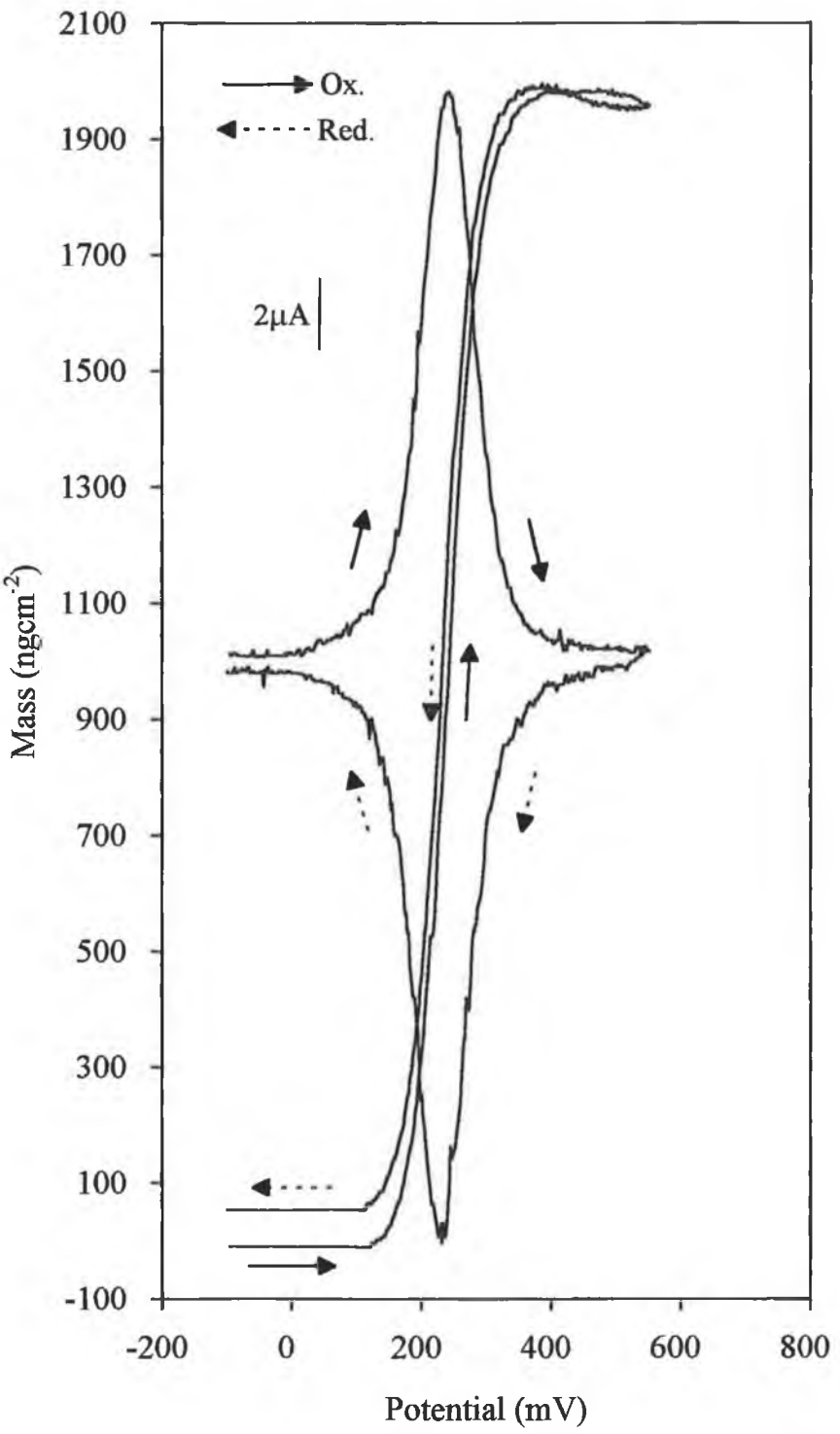

(< 10% difference). The mass-potential and charge-potential (not shown) plots exhibit minimal hysteresis. This, coupled with the absence of a scan rate dependence of the normalised mass change (see Table 6.4), attests to the achievement of at least pseudo-equilibrium on the timescale of these experiments [29,30].

Fig. 6.11 illustrates the corresponding mass and Φ_{ClO4^-} -charge plots for the data in Fig. 6.10. The absence of hysteresis in the mass-charge plot illustrates that, compared with the data in 5% MeCN (see Fig. 6.9), mass transfer across the electrolyte polymer interface is less hindered for this relatively more swollen layer. Furthermore, within the concentration range of 15-30% MeCN, the potentials of half-mass and half-charge change coincide, reflecting concomitant mass and charge transfer (see Table 6.5). Assuming that anion motion is responsible for the maintenance of electroneutrality (see below) then the Φ_{ClO4^-} -charge plot represents the motion of net neutral species. The monotonic increase in the Φ_{ClO4^-} -charge data suggests that the motion of solvent is associated with the anion.

To aid in the identification of the individual contributions of the different neutral species to the overall mass change, the experiment was repeated using deuterated solvents i.e. D_2O and CD_3CN. This approach has been successfully employed previously and can provide unambiguous identification of solvent contributions to the overall mass change [4,14,33]. Table 6.6 summarises the normalised mass changes associated with the oxidation of the 1.29×10^{-8} molcm^{-2} $OsPVP_{100}$ coating in 20% acetonitrile using a) 80% H_2O, 20% MeCN, b) 80% D_2O, 20% MeCN and c) 80% H_2O, 20% CD_3CN. The use of D_2O and CD_3CN should, in theory, result in increased mass changes of 11% and 7% respectively if either water or acetonitrile are solely responsible for the neutral species component of the normalised mass change (assuming of course that solvent transfer occurs in one direction only). The solvent component of the total mass change during polymer oxidation, calculated by subtraction of the mass change associated with anion motion, is 2% (D_2O) and 10% (CD_3CN) greater than that observed in the protonic solvents.

Fig. 6.11. Mass- and Φ_{ClO4}^- -charge plots for data in Fig. 6.10.

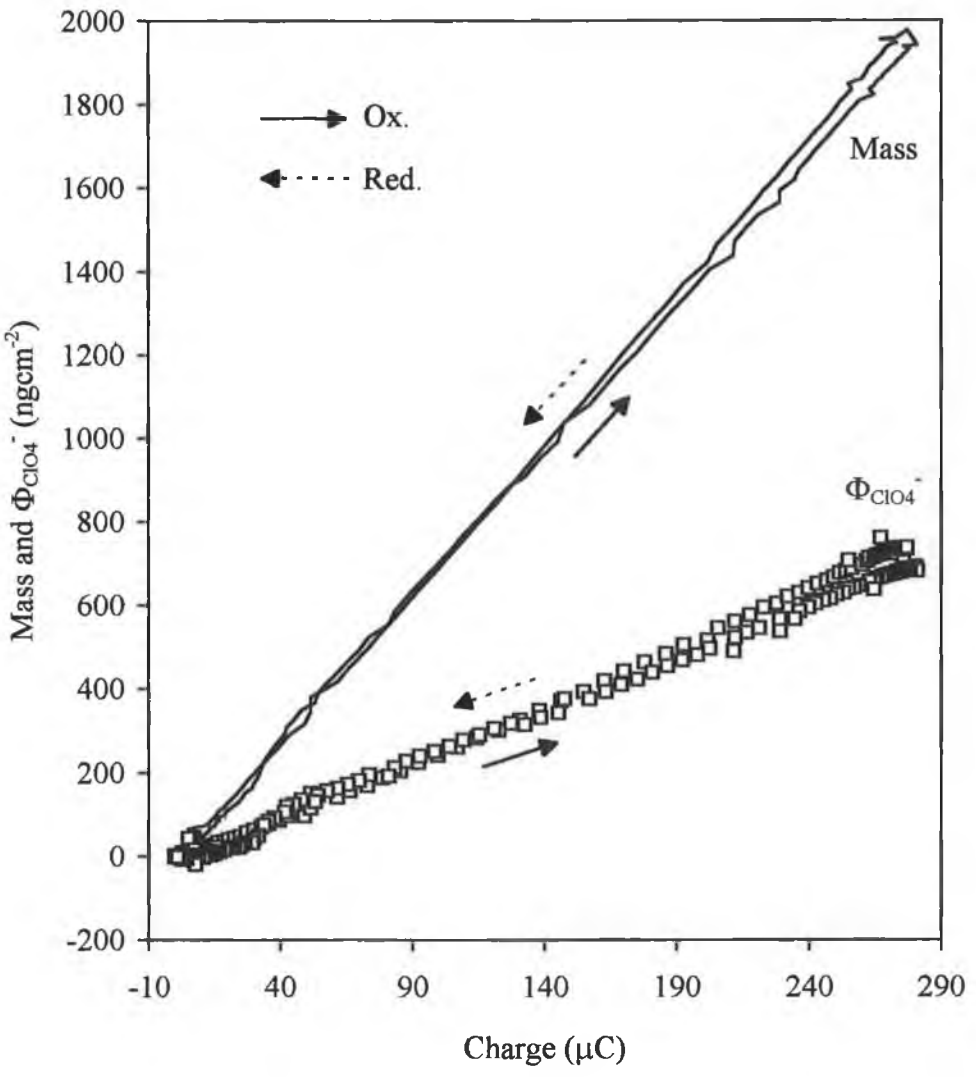

For this analysis the data were reproducible to within ± 2% and suggest that the layer is permselective during redox switching and that the dominant neutral species component of the normalised mass change is acetonitrile. Furthermore, it would appear that, compared with the data in 0% MeCN (see Chapter 5), solvent transfer now occurs in one direction only. Therefore, the overall normalised mass change of 160 (±4) $gmol^{-1}$ may be equated with the influx of 1 perchlorate anion and ca. 1.4 molecules of acetonitrile per Os^{III} site. The data presented in the following

Table 6.6. The effect of using deuterated solvents on the normalised mass change accompanying redox switching of an $OsPVP_{100}$ coated crystal in 0.1M $LiClO_4$ (20% MeCN). Scan rate is 5 mVs^{-1}. Gravimetric surface coverage is 1.29 x 10^{-8} $molcm^{-2}$

	H_2O : MeCN (80:20)	D_2O : MeCN (80:20)	H_2O : CD_3CN (80:20)
Γ_c [a] (x 10^{-8} $molcm^{-2}$)	1.26	1.25	1.25
ΔM [b] ($ngcm^{-2}$)	1982	1975	2038
ΔM_{TOT} [c] ($gmol^{-1}$)	157	158	163
ΔM_{Sol} [c] ($gmol^{-1}$)	58	59	64

(a) Estimated from the area under the anodic peak.

(b) Change in layer mass during polymer oxidation.

(c) Normalised mass change assuming validity of the Sauerbrey equation.

section corroborate these observations.

In 30% MeCN, the overall normalised mass change increases to 345 (±19) $gmol^{-1}$. Fig. 6.12 illustrates the change in crystal resonance of a 1.15 x 10^{-8} $OsPVP_{100}$ coated crystal during an oxidative 5 mVs^{-1} scan in 30% MeCN. The constant shape of the crystal resonance during redox switching illustrates that viscoelastic contributions to the normalised mass change are negligible. Therefore, the increase in the normalised mass change in 30% MeCN is "real" and represents an increase in the quantity of species transferred during redox switching. This increase in the normalised mass change is likely a consequence of the more swollen polymer structure that exists in this MeCN concentration (see Section 6.3.1).

Fig. 6.13 illustrates the cyclic voltammogram and change in layer mass of a 2.80 x 10^{-9} $molcm^{-2}$ $OsPVP_{100}$ coated crystal during a 5 mVs^{-1} voltammetric scan in 30% MeCN. The qualitative behaviour of these plots is identical to that observed in 20% MeCN (see Fig. 6.10). To identify the additional component of the normalised mass change in 30% MeCN, the experiment was repeated with deuterated solvents. Table 6.7 summarises the normalised mass changes associated with the $Os^{II/III}$ oxidation process for these experiments. The solvent component of the total mass change during polymer oxidation is 2% (D_2O) and 9% (CD_3CN) greater than that observed with protonic solvents. For this analysis, the data were reproducible to within ± 2%. The increase in the normalised mass change observed in 30% MeCN may therefore be equated with the additional influx of MeCN. Clearly, under these swelling conditions, this layer is still permselective during redox switching. Therefore, the normalised mass change of 345 (±19) $gmol^{-1}$ may be equated with the influx of 1 anion and ca. 6 molecules of MeCN per redox site.

Fig. 6.12. Admittance spectra for an $OsPVP_{100}$ coated crystal during redox switching in 0.1M $LiClO_4$ (30% MeCN) at 5 mVs^{-1}. Gravimetric surface coverage is 1.15 x 10^{-8} $molcm^{-2}$.

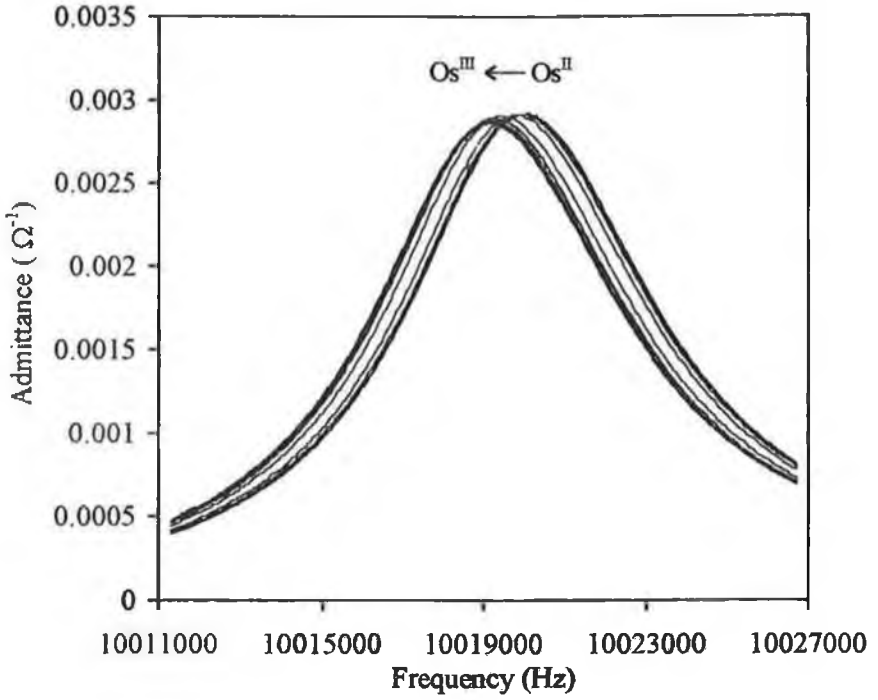

Fig. 6.13. Cyclic voltammogram and mass-potential plot for an $OsPVP_{100}$ coated crystal in 0.1M $LiClO_4$ (30% MeCN). Scan rate is 5 mVs^{-1}. Gravimetric surface coverage is 2.80 x 10^{-9} $molcm^{-2}$.

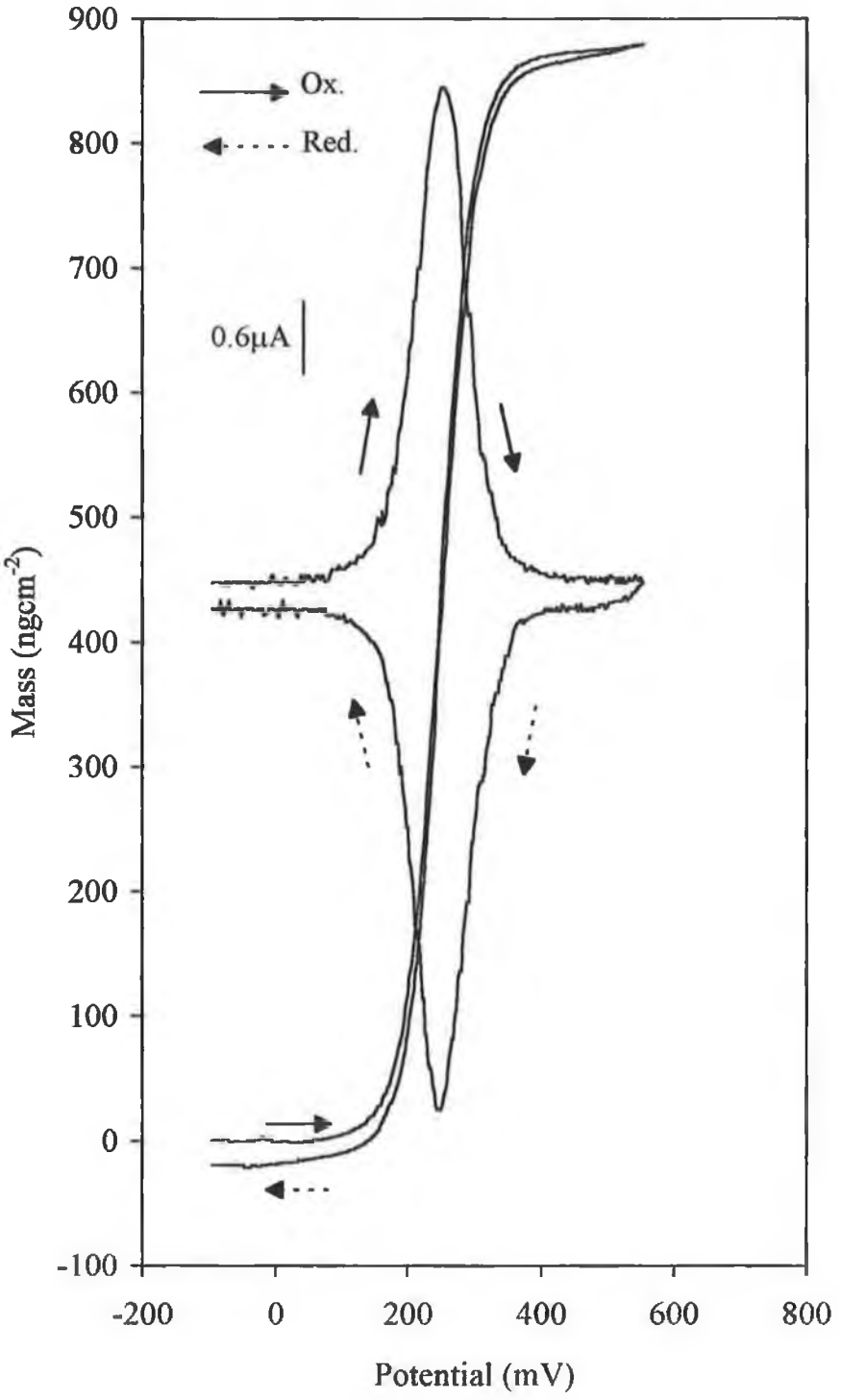

Table 6.7. The effect of using deuterated solvents on the normalised mass change accompanying redox switching of an $OsPVP_{100}$ coated crystal in 0.1M $LiClO_4$ (30% MeCN). Scan rate is 5 mVs^{-1}. Gravimetric surface coverage is 2.80 x 10^{-9} $molcm^{-2}$

	H_2O : MeCN (70:30)	D_2O : MeCN (70:30)	H_2O : CD_3CN (70:30)
$\Gamma_c^{(a)}$ (x 10^{-9} $molcm^{-2}$)	2.72	2.77	2.76
$\Delta M^{(b)}$ ($ngcm^{-2}$)	887	888	959
$\Delta M_{TOT}^{(c)}$ ($gmol^{-1}$)	326	321	347
$\Delta M_{Sol}^{(c)}$ ($gmol^{-1}$)	227	222	248

(a) Estimated from the area under the anodic peak.

(b) Total shift in resonant frequency during polymer oxidation.

(c) Normalised mass change assuming validity of the Sauerbrey equation.

6.3.3.2. Gravimetric surface coverages of 2.15 to 5.22 x 10^{-8} molcm^{-2}.

Within the concentration range of 0% to 20% MeCN, the redox-switching-induced mass changes are independent of the $OsPVP_{100}$ surface coverage (see Fig. 6.7). For $OsPVP_{100}$ coatings of 2.15 to 5.22 x 10^{-8} molcm^{-2}, the normalised mass change increases to 357 (±18) gmol^{-1} in 25% MeCN. Similar behaviour was observed for thinner $OsPVP_{100}$ layers, under rigid layer conditions, in 30% MeCN (see Table 6.4). and suggests that the thicker $OsPVP_{100}$ layers may be rigid in 25% MeCN. If layer rigidity is maintained under these conditions, then the normalised mass change of 357 (±18) gmol^{-1} can be equated with the influx of a single anion and ca. 6 molecules of MeCN per Os^{III} site. On increasing the MeCN content of the electrolyte to 30%, the sign of the redox-switching-induced shift in resonant frequency changes for these thicker layers. Fig. 6.14 illustrates the cyclic voltammogram and frequency-potential plot for a 3.05 x 10^{-8} $OsPVP_{100}$ coated crystal during a 5 mVs^{-1} voltammetric scan in 30% MeCN. This diagram illustrates that redox switching of this layer is accompanied by an increase in the resonant frequency. However, the following points are noted which clearly indicate that the layer is non-rigid and that the observed increase in resonant frequency does not reflect a change in the layer mass, but contributions from the viscoelastic properties of this solvent swollen layer. Firstly, the shape of the crystal resonance of a 3.05 x 10^{-8} $OsPVP_{100}$ coated crystal broadened dramatically in 30% MeCN (see Fig. 6.4). This behaviour clearly indicates that the layer is extensively swollen. Secondly, during redox processes in 30% MeCN, the admittance peak decreases monotonically. This behaviour is illustrated in Fig. 6.15 for a 2.41 x 10^{-8} molcm^{-2} $OsPVP_{100}$ coated crystal during a 5 mVs^{-1} oxidative scan. Therefore, under these "non-rigid layer" conditions, the change in layer mass during redox switching can not be accurately evaluated.

Fig. 6.14. Cyclic voltammogram and frequency-potential plot for an $OsPVP_{100}$ coated crystal in 0.1M $LiClO_4$ (30% MeCN). Scan rate is 5 mVs^{-1}. Gravimetric surface coverage is 3.05 x 10^{-8} $molcm^{-2}$.

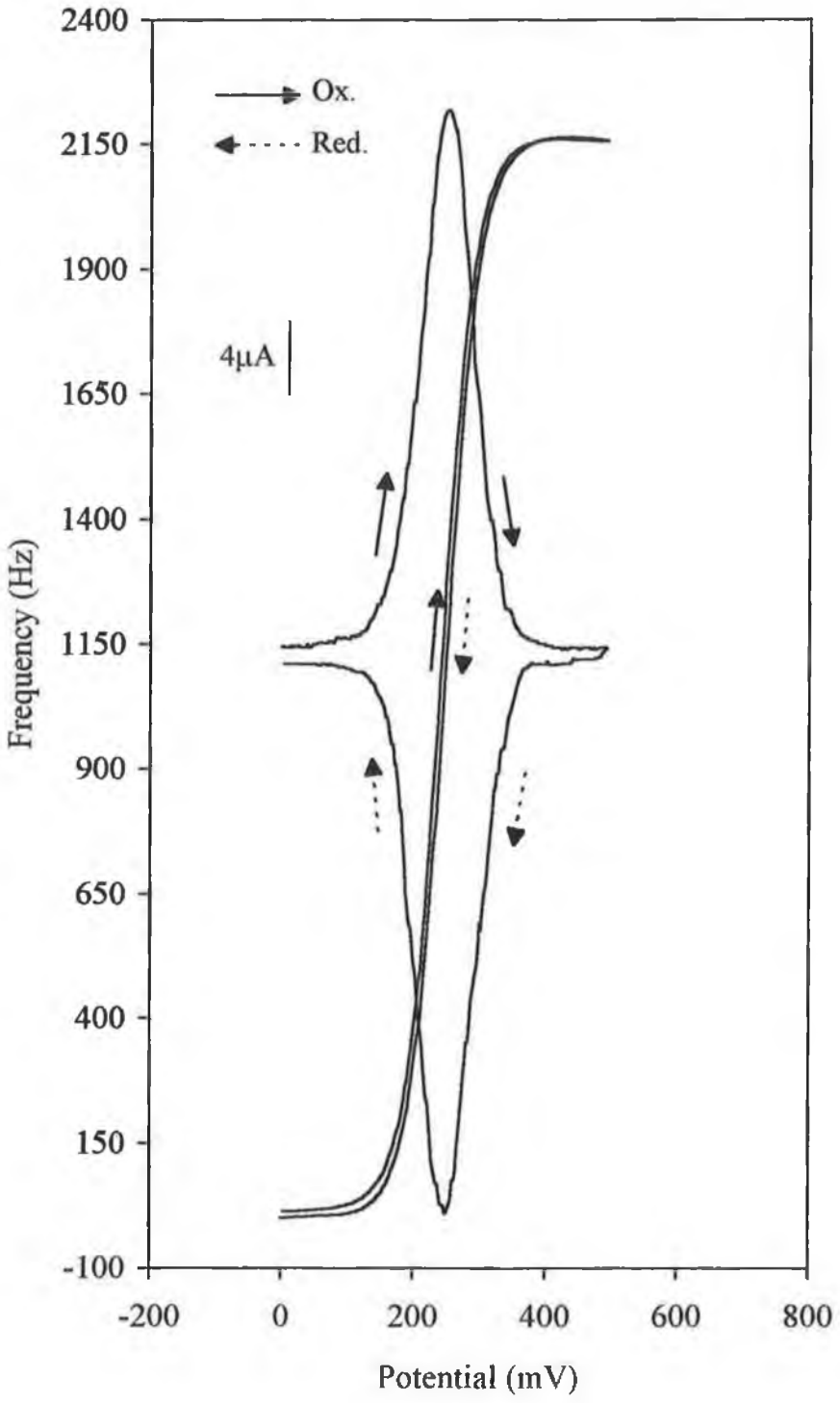

Fig. 6.15. Admittance spectra for an $OsPVP_{100}$ coated crystal during redox switching in 0.1M $LiClO_4$ (30% MeCN) at 5 mVs^{-1}. Gravimetric surface coverage is 2.41 x 10^{-8} $molcm^{-2}$.

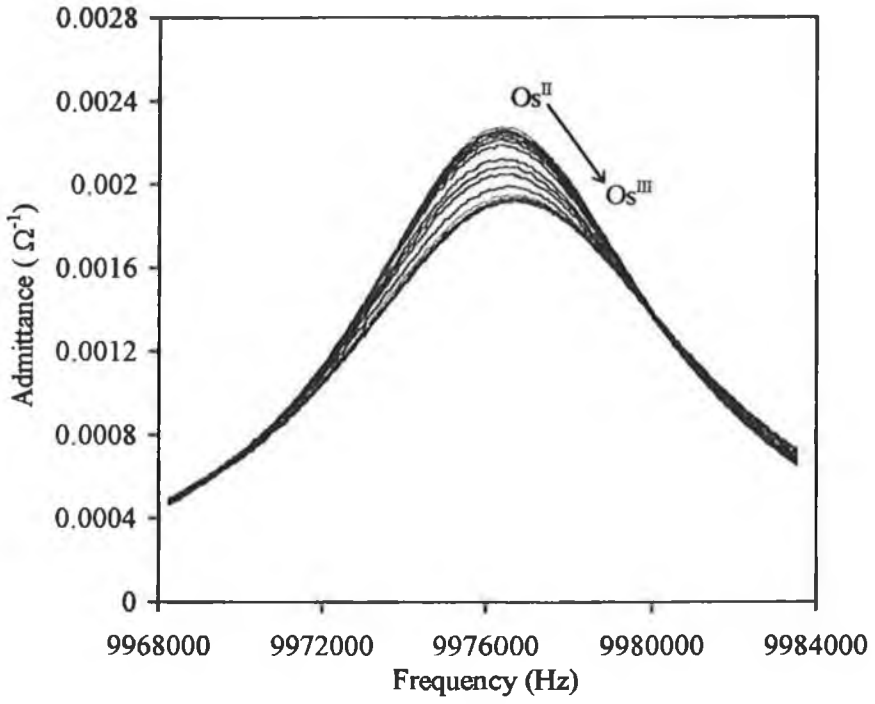

In summary, the addition of MeCN to the contacting electrolyte induces swelling of $OsPVP_{100}$ layers. The degree of polymer swelling depends on the polymer surface coverage. These swelling phenomena have a profound influence on the electrochemically induced mass transfer properties of these coatings. With increasing concentration of MeCN and, by implication, increased layer swelling, the magnitude of the redox-switching-induced mass change increases substantially. This increase is a result of greater quantities of solvent (MeCN) transfer during redox switching of these solvent swollen films.

6.3.4. Effect of MeCN on the Charge Transport and Transient Mass Transfer Properties of $OsPVP_{100}$ Films.

The influence of acetonitrile on the charge transport properties of $OsPVP_{100}$ coated electrodes (3 mm glassy carbon) was studied using cyclic voltammetric ($D_{CT}(CV)$) and chronoamperometric ($D_{CT}(PS)$) techniques, as illustrated in Chapter 3. Activation parameters associated with the charge transport process were estimated from the temperature dependence of the charge transport diffusion coefficients. The interfacial mass transfer properties of $OsPVP_{100}$ coated crystals were studied using cyclic voltammetry, under semi-infinite diffusion conditions (50-500 mVs^{-1}), to probe for mass transfer limitations. The combined data from these experiments are presented in the following section.

Fig. 6.16 illustrates the dependence of the anodic peak current on the square root of scan rate, as a function of the MeCN content of the electrolyte, for scan rates of 50-500 mVs^{-1}. The linearity of these plots indicates a semi-infinite diffusion response. Fig. 6.17 illustrates Cottrell plots, for times up to 20 ms, as a function of the MeCN content of the electrolyte. These plots are linear and intercept at the origin, which is again consistent with a diffusional response.

Table 6.8 summarises the charge transport rates for the $Os^{II/III}$ oxidation, $D_{CT}(CV)$ and $D_{CT}(PS)$, as a function of the MeCN concentration of the bathing electrolyte. The estimated charge transport rates are reproducible to within 10% for determinations on different coatings and 5% for repeated determinations on a single coating. The influence of MeCN on $D_{CT}(CV)$ is illustrated in Fig. 6.18. This data highlight the profound influence of MeCN on the rate of charge transport through these $OsPVP_{100}$ films. In this organic solvent, $OsPVP_{100}$ layers swell (see Section 6.3.1). It is therefore considered that the trend of increased $D_{CT}(CV)$ is real and does not reflect an increase in the concentration of electroactive sites. Under these swelling conditions, the concentration of electroactive sites will in fact be less

Fig. 6.16. The effect of MeCN on the anodic peak currents of 50 to 500 mVs^{-1} cyclic voltammograms for an $OsPVP_{100}$ coated electrode in 0.1M $LiClO_4$. Coulometric surface coverage is 4.30×10^{-8} $molcm^{-2}$.

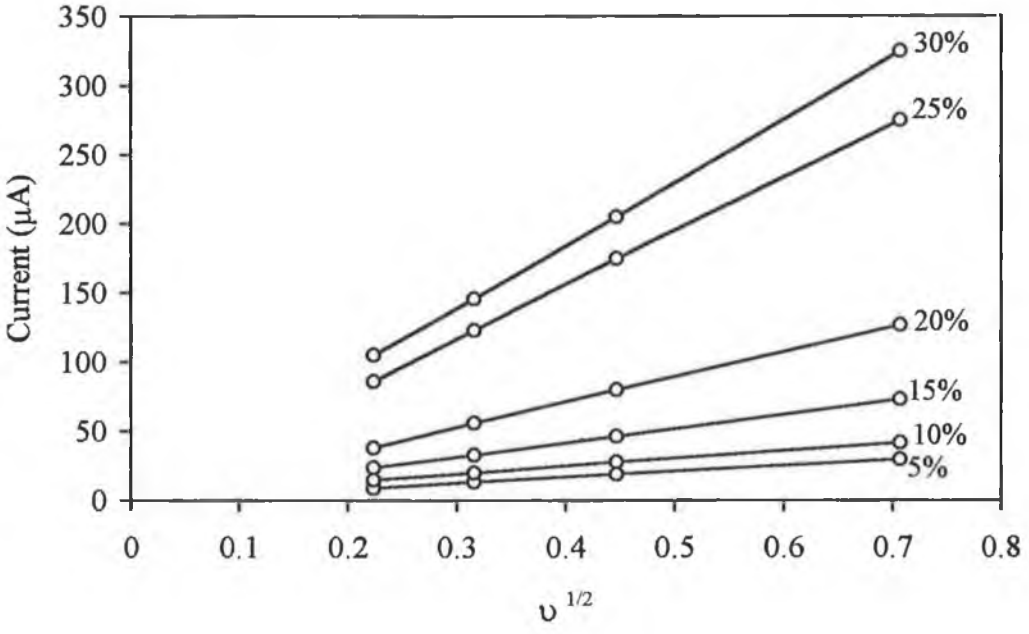

Fig. 6.17. The effect of MeCN on the chronoamperometric response of an $OsPVP_{100}$ coated electrode in 0.1M $LiClO_4$. Coulometric surface coverage is 4.30×10^{-8} $molcm^{-2}$.

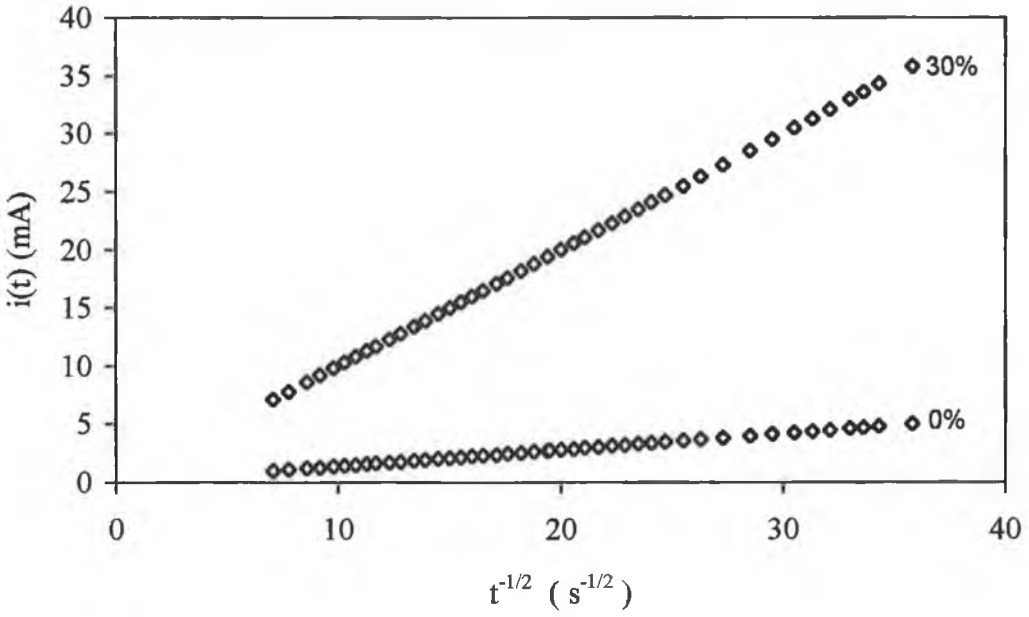

Table 6.8. The effect of MeCN on the rate of charge transport through $OsPVP_{100}$ films as determined by cyclic voltammetry, $D_{CT}(CV)$, and chronoamperometry, $D_{CT}(PS)$, in 0.1M $LiClO_4$. The coulometric surface coverages are 2.0 to 6.0 x 10^{-8} molcm^{-2}.

% MeCN	D_{CT} (CV) x 10^{-11} [a] ($cm^2 s^{-1}$)	D_{CT} (PS) x 10^{-10} [a] ($cm^2 s^{-1}$)
0%	1.2	1.1
5%	1.9	1.4
10%	3.5	1.5
15%	12	3.1
20%	76	13
25%	132	28
30%	171	49

(a) The variations between individual coatings are ±10%.

Fig. 6.18. The effect of MeCN on the rate of charge transport through $OsPVP_{100}$ films as determined by cyclic voltammetry, $D_{CT}(CV)$.

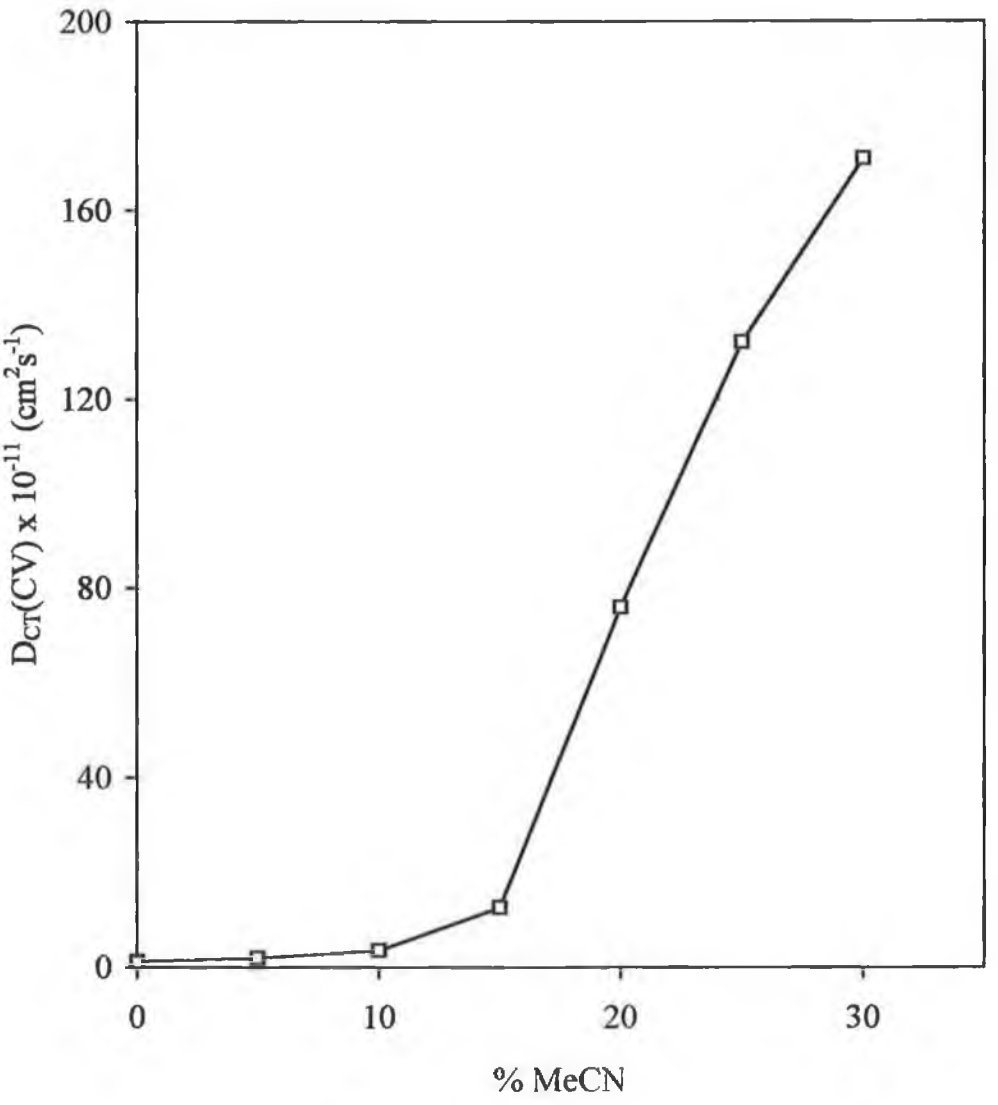

than 0.7M. The quoted charge transport rates may therefore be viewed as the lower limit for charge transport under these conditions. On addition of MeCN to the contacting electrolyte, $D_{CT}(CV)$ increases and then continues to increase with further increases in the MeCN concentration. Above an electrolyte content of 15% MeCN, $D_{CT}(CV)$ increases quite dramatically (see Fig. 6.18). $D_{CT}(CV)$ continues to increase as the MeCN electrolyte content is increased above 30% MeCN. However, in these concentrations the layer is insufficiently stable to allow for accurate measurements to be made.

The effect of the MeCN bathing electrolyte concentration on the activation parameters for charge transport, as estimated by both cyclic voltammetry and potential step techniques, is illustrated in Table 6.9. These data are reproducible to within 10-15% for determinations on different films and 5% for repeated determinations on the same film. $E_a(CV)$ increases with increasing MeCN content of the electrolyte and reaches a maximum of 79 ± 5 kJmol^{-1} in 15% MeCN. This increase in activation energy is accompanied by a transition from a negative to a positive entropy term. In MeCN concentrations in excess of 15%, there is a gradual decrease in $E_a(CV)$ which is accompanied by a decrease in the activation entropy. In 30% MeCN, $E_a(CV) = 57 \pm 4$ kJmol^{-1} and is coupled to a negative entropy term.

Table 6.10 summarises the normalised mass changes associated with redox switching of $OsPVP_{100}$ coatings at scan rates of 50-500 mVs^{-1} as a function of the bathing MeCN concentration. The gravimetric surface coverages are 0.28 to 1.93 x 10^{-8} molcm^{-2}. These values are reproducible to within 9% for determinations on different films and 6% for repeated determinations on a single film. Table 6.10 also includes the charge transport rates estimated for these $OsPVP_{100}$ coatings using the Randles-Sevcik equation, $D_{CT}(CV)$. $D_{CT}(CV)$ is reproducible to within 10% for determinations on different layers and 5% for repeated determinations on single layers. There is a discrepancy between the charge transport rates quoted in Table 6.10 and Table 6.8. Within the concentration range of 15 to 30% MeCN, the charge

Table 6.9. The effect of MeCN on the activation parameters for charge transport through $OsPVP_{100}$ films as determined by cyclic voltammetry and chronoamperometry in 0.1M $LiClO_4$. Coulometric surface coverages are 2.0 to 6.0 x 10^{-8} molcm^{-2}.

% MeCN	E_a(CV) (kJmol^{-1})	$\Delta S(CV)^{\neq}$ (Jmol^{-1}K^{-1})	$\Delta G(CV)^{\neq}$ (kJmol^{-1})	E_a(PS) (kJmol^{-1})	$\Delta S(PS)^{\neq}$ (Jmol^{-1}K^{-1})	$\Delta G(PS)^{\neq}$ (kJmol^{-1})
0%	44	-72	63	20	-137	58
10%	72	28	61	36	-79	57
15%	79	66	57	55	-6	54
20%	72	53	54	67	42	52
25%	67	42	52	57	15	50
30%	57	-24	62	47	-54	61

The variations between individual coatings are ±10%.

Table 6.10. The effect of MeCN on the normalised mass change accompanying redox switching of $OsPVP_{100}$ coated crystals at fast voltammetric scan rates. Gravimetric surface coverages are 0.28 to 1.93 x 10^{-8} molcm^{-2}.

% MeCN	D_{CT} (CV) x 10^{-11} cm^{2}s^{-1}	Scan Rate (mVs^{-1})	Normalised Mass Change (gmol^{-1})	
			ΔM_{ETE}	ΔM_{TOT}
0%	1.61	50	109 (4)	117 (3)
		100	114 (1)	116 (2)
		200	107 (2)	119 (2)
		500	108 (2)	119 (3)
5%	2.04	50	138 (2)	142 (3)
		100	144 (2)	151 (1)
		200	149 (2)	152 (1)
		500	149 (4)	155 (5)
10%	3.21	50	165 (3)	
		100	159 (4)	
		200	155 (2)	164 (4)
		500	145 (5)	169 (5)
15%	7.93	50	167 (1)	
		100	159 (4)	
		200	170 (3)	
		500	171 (7)	
20%	11.0	50	171 (6)	
		100	175 (6)	
		200	169 (7)	
		500	182 (3)	
25%	15.9	50	172 (5)	
		100	182 (4)	
		200	169 (5)	
		500	169 (6)	
30%	29.8	50	332 (16)	
		100	325 (11)	
		200	341 (14)	
		500	345 (21)	

Where only one value quoted $\Delta M_{ETE}=\Delta M_{TOT}$.

Errors quoted in brackets represent the variations between 2 different films.

transport rates estimated for the EQCM experiments (Table 6.10) are considerably smaller than those observed for the charge transport studies on glassy carbon electrodes (Table 6.8). This discrepancy is probably a consequence of surface coverage differences. The data in Table 6.10 were obtained for surface coverages of 0.28 to 1.93 x 10^{-8} molcm^{-2}, while the data in Table 6.8 were obtained for surface coverages within the range of 2.0 to 6.0 x 10^{-8} molcm^{-2}. EQCM studies with $OsPVP_{100}$ coatings of this surface coverage (2.0 to 6.0 x 10^{-8} molcm^{-2}) yielded charge transport rates of the same magnitude as those quoted in Table 6.8.

In aqueous 0.1M $LiClO_4$, the occurrence of a diffusional limited response at slow cyclic voltammetric scan rates and the charge transport rate of 1 x 10^{-11} cm^{2}s^{-1}, as estimated by cyclic voltammetry, reflect slow charge transport within these compact layers. The activation energy associated with the charge transport process, $E_a(CV)$, is 44 $\pm$ 6 kJmol^{-1}. This activation energy is coupled with a negative entropy term which suggests that ion motion is rate limiting [34]. In this electrolyte (100% H_2O), ΔM_{ETE} is less than ΔM_{TOT}, which suggests that solvent motion is hindered. Fig. 6.19 illustrates the mass-potential plots for a 1.87 x 10^{-8} molcm^{-2} $OsPVP_{100}$ coated crystal during a 50 mVs^{-1} cyclic voltammetric experiment in 0.1M $LiClO_4$ (100% H_2O). In Fig. 6.19, steady-state mass changes are only achieved after 4 voltammetric scans. This behaviour illustrates that, as was discussed in Chapter 5, interfacial mass transfer processes are hindered. Fig. 6.20 illustrates the corresponding mass- and Φ_{ClO4^-}-charge plots for this data. As was discussed in Chapter 5, the hysteresis in Fig. 6.20 indicates that solvent motion is lagging anion motion. Consequently, interfacial solvent motion is the slowest of the mass transfer processes accompanying redox switching [29-32].

Addition of MeCN to the bathing electrolyte results in a transition from diffusion limited responses to ideal surface behaviour in slow scan rate cyclic voltammetric experiments. However, diffusional responses are still observed at faster

Fig. 6.19. Mass-potential plots for an $OsPVP_{100}$ coated crystal in 0.1M $LiClO_4$ (0% MeCN). Scan rate is 50 mVs^{-1}.Gravimetric surface coverage is 1.87 $x10^{-8}$ $molcm^{-2}$.

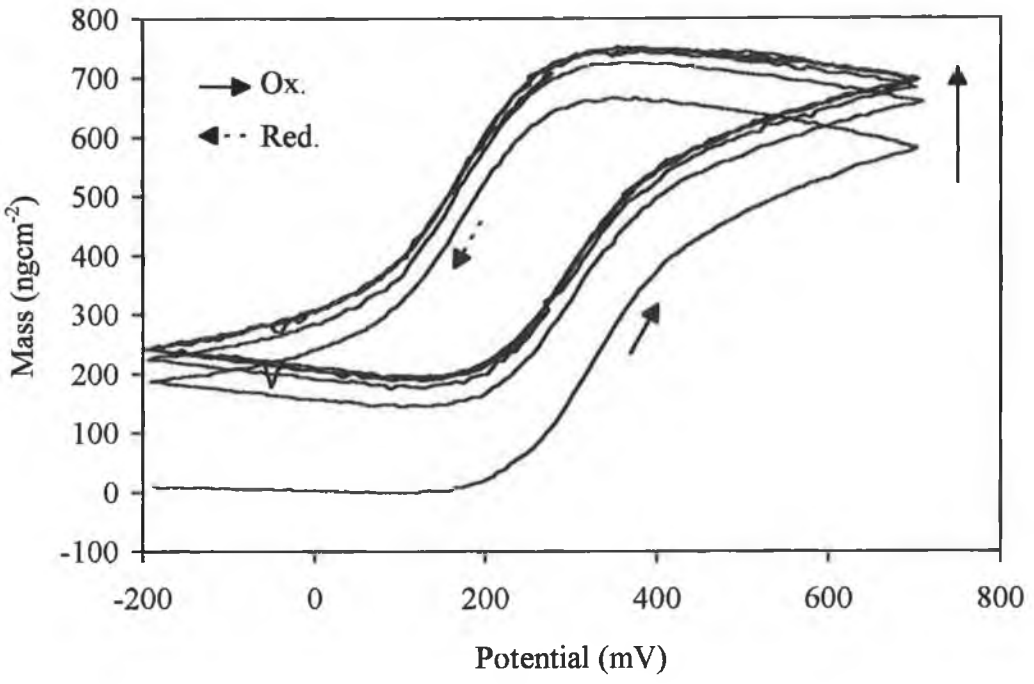

Fig. 6.20. Mass- and Φ_{ClO4}^- -charge plots for data in Fig. 6.19.

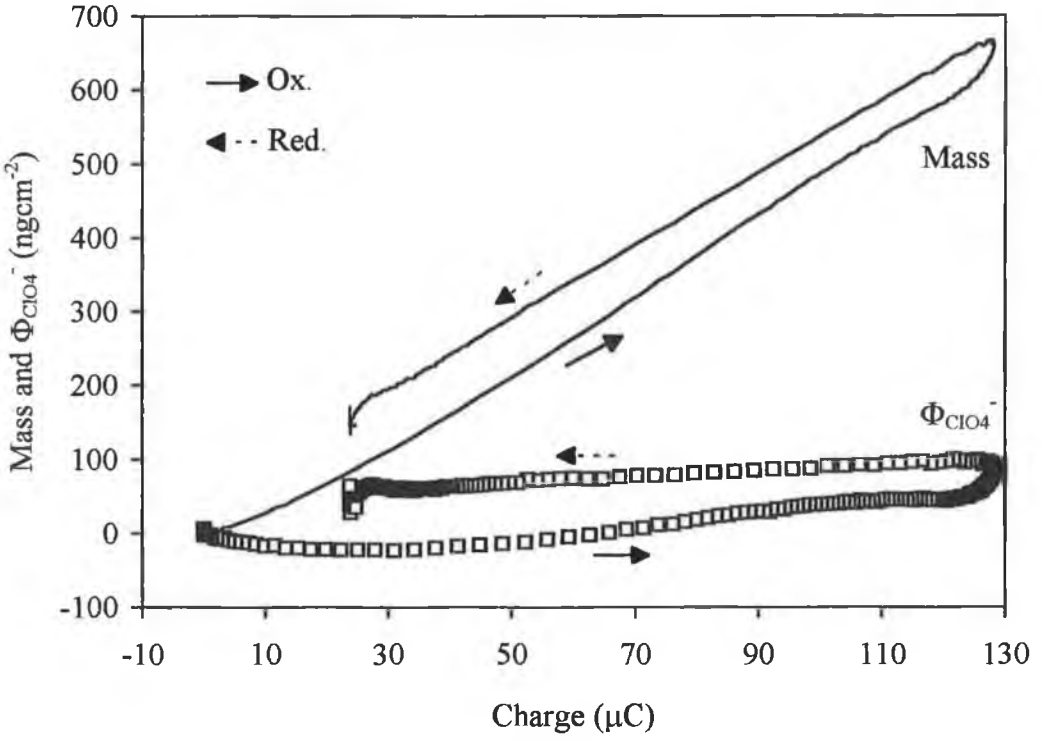

scan rates (see Fig. 6.16). $D_{CT}(CV)$ increases dramatically as the concentration of MeCN in the bathing electrolyte is increased. In 15% MeCN, $D_{CT}(CV)$ is 12.6 x 10^{-11} cm^2s^{-1} and represents a 10 fold increase in charge transport rate compared to aqueous 0.1M $LiClO_4$ (100% H_2O).

The increase in $D_{CT}(CV)$ is accompanied by an increase in the activation energy for electron transfer. The entropy term in 15% MeCN is positive and suggests that a transition in rate controlling process has occurred. It has been suggested previously that this positive entropy may be associated with polymer chain motion limitations [21-24]. Swelling of these layers will increase the osmium site-to-site separation. This transition to polymer motion limitation may, therefore, reflect the requirement for motion of the polymer chains to reduce the intersite separation to allow for electron hopping.

Fig. 6.21 illustrates the mass-potential plots for a 1.65 x 10^{-8} $molcm^{-2}$ $OsPVP_{100}$ coating during a 50 mVs^{-1} cyclic voltammetric experiment in 15% MeCN. Fig. 6.22 illustrates the corresponding mass- and Φ_{ClO4^-} -charge plots for this data. Comparison of Fig. 6.19 (0% MeCN) and Fig. 6.21 (15% MeCN) illustrates that steady-state mass changes are achieved after four voltammetric scans in 0% MeCN and 2 voltammetric scans in 15% MeCN. This, coupled with the fact that ΔM_{ETE} and ΔM_{TOT} are equal in 15% MeCN (see Table 6.10) indicates that interfacial mass transfer is comparatively more facile in the solvent swollen layers that exist in this electrolyte. The Φ_{ClO4^-} -charge plots support these observations. Comparison of Fig. 6.20 (0% MeCN) and Fig. 6.22 (15% MeCN) illustrates that in 0% MeCN solvent motion is limiting whilst in 15% MeCN the absence of hysteresis indicates that the system is under electroneutrality control [29-32]. This may indicate either ion or electron motion limitations [29-32]. It is considered, however, that ion motion is likely the limiting process as the observed charge transport rate is more than an order of magnitude less than the charge transport rates reported for analogous PVI polymers under electron transfer control [35]. It can be clearly seen from these mass

Fig. 6.21. Mass-potential plots for an $OsPVP_{100}$ coated crystal in 0.01M $LiClO_4$ (15% MeCN). Scan rate is 50 mVs^{-1}. Gravimetric surface coverage is 1.65×10^{-8} $molcm^{-2}$.

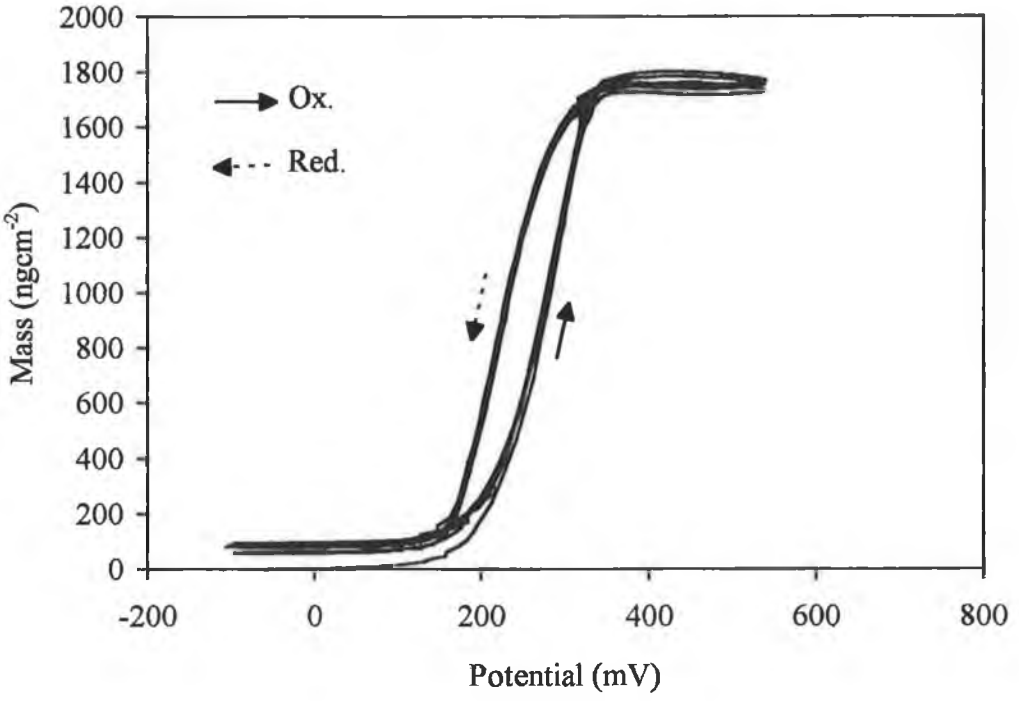

Fig. 6.22. Mass- and Φ_{ClO4}^- -charge plots for data in Fig. 6.21.

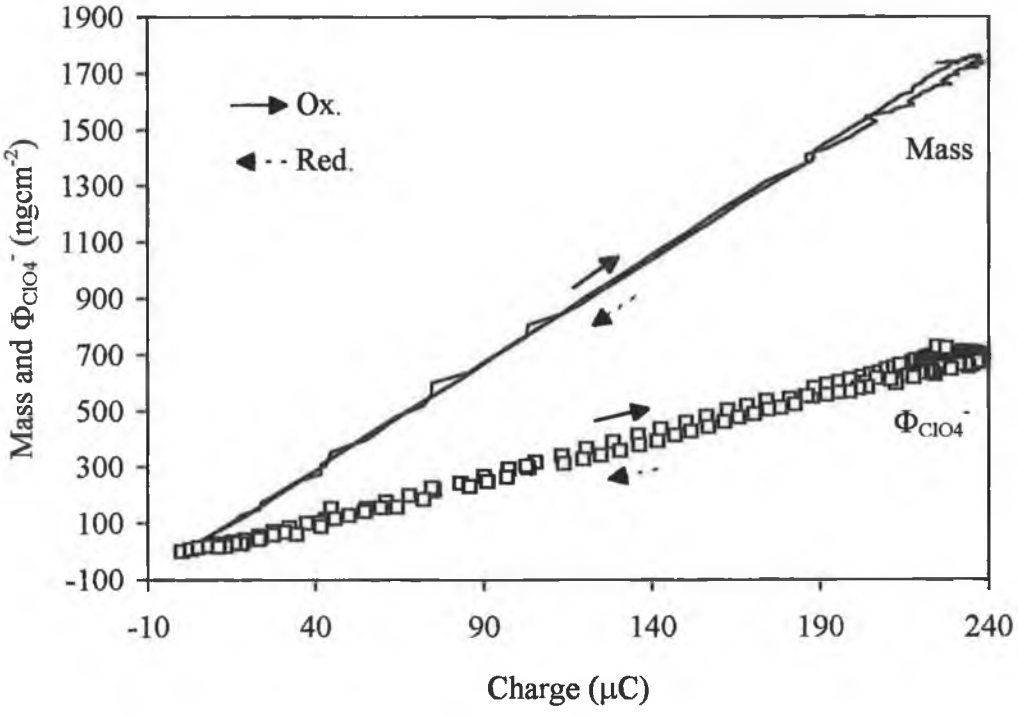

transfer studies that the increase in $D_{CT}(CV)$ in these mixed solvent electrolytes is a consequence of more facile interfacial mass transfer processes within these solvent swollen layers. This inter-relationship between the polymer structure, the facility for solvent transfer and the rate of charge transport through this redox polymer has been illustrated previously [14,36].

Above 15% MeCN, $D_{CT}(CV)$ continues to increase. In 30% MeCN $D_{CT}(CV)$ is 1.71×10^{-9} cm^2s^{-1} (see Table 6.8) and represents a 100 fold increase in the charge transport rate compared with corresponding values obtained in aqueous 0.1M $LiClO_4$. This is one of the fastest charge transport rates reported for this particular polymer. For the analogous 1 in 10 loaded poly(N-vinyl imidazole) polymer, similar charge transport rates were only observed under conditions where electron hopping appeared to be rate limiting [35]. In MeCN concentrations in excess of 15%, $E_a(CV)$ decreases. The magnitude of the entropy decreases and in 30% MeCN the sign of this entropy term changes from positive to negative. This apparent change in the activation parameters, on increasing the MeCN content of the contacting electrolyte from 15% to 30% MeCN, is surprising but is considered accurate. The numerical errors on both the activation and entropy data, within this MeCN concentration range, are not sufficient to account for these changes. Furthermore, changes in the osmium intersite separation due to swelling are not sufficient to account for the change in the sign of the entropy term. Therefore, the decrease in the activation energy, coupled with the change in the sign of the entropy term, suggest that the processes limiting charge transport have changed. This suggestion is supported by the observed 10 fold increase in $D_{CT}(CV)$ within this concentration range. This negative entropy term is associated with either ion motion or electron hopping as being rate limiting [34]. Within the swollen structures that exist in this concentration of MeCN it is considered unlikely that ion motion will be rate determining. The entropy term may therefore reflect electron hopping as being rate determining.

Mass transport studies under these conditions provide little additional

information. Charge transport rates of this magnitude were only observed for $OsPVP_{100}$ crystal coatings of 2.15 to 5.22 x 10^{-8} molcm^{-2} in 30% MeCN, as was discussed above. However, for coatings of this surface coverage in 30% MeCN, the Sauerbrey equation is no longer applicable (see Section 6.3.3.2). That this ten fold increase in D_{CT}(CV) is only observed for surface coverages in excess of 1.93 x 10^{-8} molcm^{-2}, suggests that it is a direct consequence of the greater swelling of these thicker $OsPVP_{100}$ layers (see Section 6.3.1). This behaviour again highlights the more favourable charge transport properties of these coatings when swollen.

The effect of the MeCN on the rate of charge transport, as estimated by potential step chronoamperometry, D_{CT}(PS), was also studied. No mass transfer measurements were made for these short timescale experiments. Table 6.8 and Table 6.9 highlight the influence of acetonitrile on D_{CT}(PS) and the associated activation parameters respectively. This data is reproducible to within 10% for determinations on different films and 7% for repeated determinations on the same film. Fig. 6.23 illustrates the change of D_{CT}(PS) as a function of the MeCN content of the contacting electrolyte.

D_{CT}(PS) is less sensitive to the MeCN content of the electrolyte than D_{CT}(CV) and remains essentially constant as the MeCN content of the bathing electrolyte is raised from 0% to 10%. As the MeCN content of the bathing electrolyte is increased above 10% MeCN, D_{CT}(PS) increases and this increase in charge transport rate becomes quite dramatic above 15% MeCN (see Fig. 6.23). The overall increase in D_{CT}(PS) from 0 to 30% MeCN represents an approximate 50 fold increase in charge transport rate. E_a(PS) increases with increasing MeCN concentration and is associated with a change in the sign of the entropy term (negative to positive). In electrolyte concentrations in excess of 20% MeCN, E_a(PS) decreases. In 30% MeCN there is a return to a negative entropy term. This overall behaviour is qualitatively similar to that observed by cyclic voltammetry, which

Fig. 6.23. The effect of MeCN on the rate of charge transport through $OsPVP_{100}$ films as determined by potential step, $D_{CT}(PS)$.

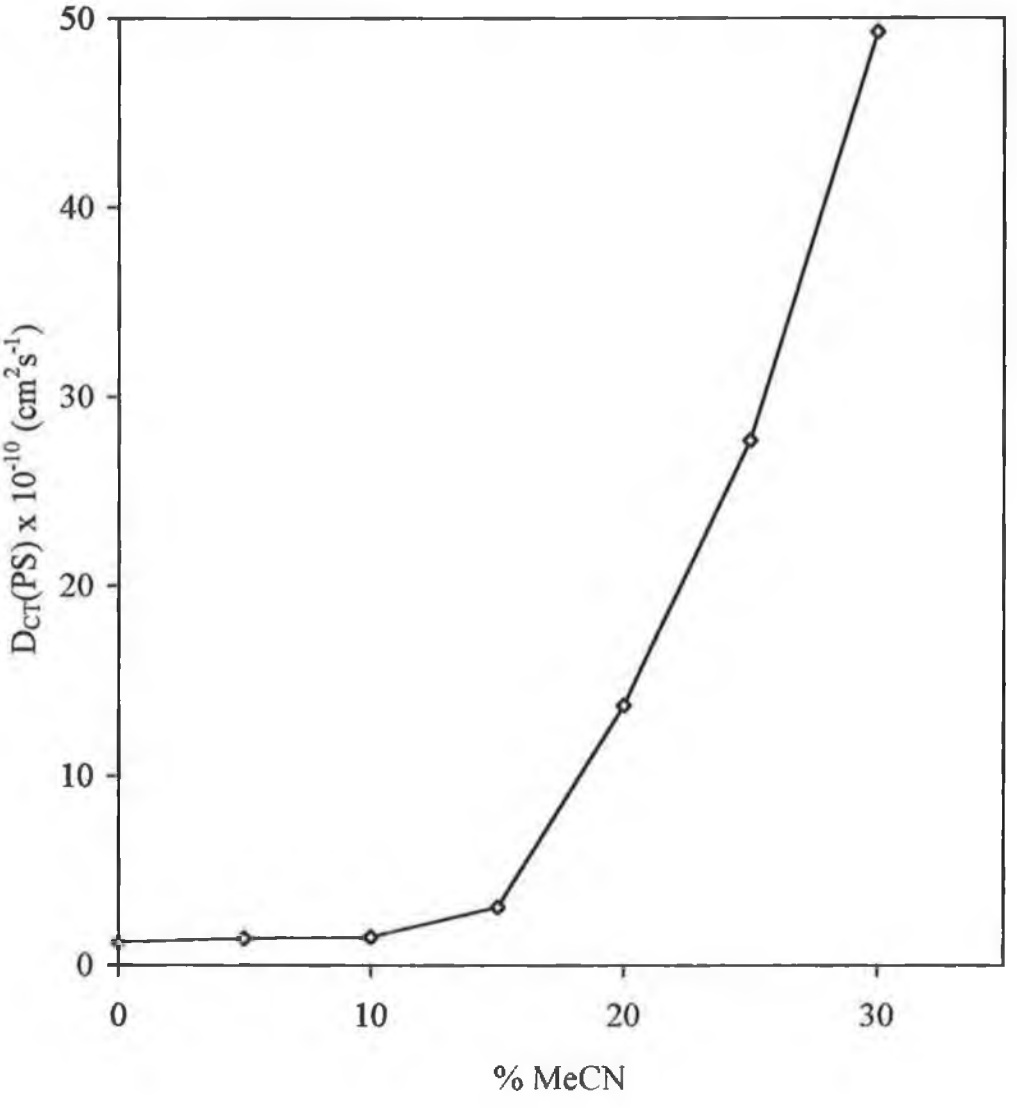

suggests that the nature of the rate determining step is not dependent on the experimental timescale.

In aqueous 0.1M $LiClO_4$, D_{CT}(PS) differs from D_{CT}(CV) by an order of magnitude (see Table 6.8). As was discussed in Chapter 3, the dependence of the rate of charge transport on the experimental technique used in its measurement is commonly observed for osmium and ruthenium metallopolymers [21-24,37,38]. It has been proposed that these differences may represent a dependence on the experimental time scale or the region of the film in which it is evaluated [21,22,24,38]. The activation data in this electrolyte are consistent with ion motion limitations controlling both D_{CT}(CV) and D_{CT}(PS). This observation suggests that, under these conditions, the nature of the rate determining step is not dependent on the experimental timescale and that the large activation energy for cyclic voltammetry reflects a greater ion motion limitation. This is not surprising considering the nature of ion motion is decidedly different for the two techniques. In CV, the more extensive oxidation of the layers requires counterion diffusion to occur over larger regions of the layer than in short timescale PS experiments. Furthermore, the quantity of diffusing counterions is considerably larger in cyclic voltammetry experiments.

Alternatively, it is also possible that the larger D_{CT}(PS) may reflect a greater concentration of redox centres in the relatively more compact base layer. However, the difference between D_{CT}(CV) and D_{CT}(PS) would require differential swelling of over 300% [21,22,24,38].

In mixed solvent systems, where the layers are extensively swollen, D_{CT}(PS) and D_{CT}(CV) are similar. Under these conditions, the nature of the equilibrium established within the layer is identical for both techniques and is independent of the experimental timescale.

6.4. Conclusions.

The nature of the interaction between solvent and polymer has a profound influence on the charge and mass transfer properties of $OsPVP_{100}$ polymer coatings. This behaviour highlights the importance of the structural properties of the polymer backbone. On addition of MeCN to the contacting electrolyte, $OsPVP_{100}$ coatings swell. The degree of polymer swelling is dependent on the MeCN content of the bathing electrolyte and the polymer surface coverage. Despite these swelling phenomena, and with the exception of polymer surface coverages of 2.15 to 5.22 x 10^{-8} molcm^{-2} in 30% MeCN, the Sauerbrey equation is applicable for all conditions under investigation. These swelling phenomena have a profound influence on the magnitude of the redox-switching-induced mass response. With increased swelling of the polymer layer, the overall normalised mass change increases. This behaviour is a consequence of more facile mass transfer within the swollen polymer structures that exist in these mixed solvent electrolytes. The additional mass component of the normalised change has been identifies as MeCN by using isotopic substitution.

Furthermore, these swelling phenomena dramatically improve the charge transport properties of these layers. 10-100 fold increases in the rate of charge transport are observed on swelling of the $OsPVP_{100}$ polymer. These enhanced charge transport rates are likely a consequence of more facile mass transfer processes within these solvent swollen layers. It is noted that the situation which favours rapid electron exchange i.e. a high concentration of closely packed redox sites, will result ion diffusion limitations.

6.5. References.

1. S.M. Oh and L.R. Faulkner, J. Electroanal. Chem., 269 (1989) 77.
2. S.M. Oh and L.R. Faulkner, J. Am. Chem. Soc., 111 (1989) 5613.
3. A.P. Clarke, J.G. Vos, A. Glidle and A.R. Hillman, J. Chem. Soc. Faraday Trans., 89 (1993) 1695.
4. A.P. Clarke, J.G. Vos, A.R. Hillman and A. Glidle, J. Electroanal. Chem., 389 (1995) 129.
5. P.T. Varineau and D.A. Buttry, J. Phys. Chem., 91 (1987) 1292.
6. G. Inzelt, Electrochim. Acta, 34 (1989) 83.
7. G. Inzelt, L. Szabo, J.Q. Chambers and R.W. Day, J. Electroanal. Chem., 242 (1988) 265.
8. G. Inzelt, J. Electroanal. Chem., 287 (1990) 171.
9. G. Inzelt and J. Bacskai, J. Electroanal. Chem., 308 (1991) 255.
10. P. Joo and J.Q. Chambers, J. Electrochem. Soc., 132 (1985) 1345.
11. N. Oyama and F.C. Anson, J. Electrochem. Soc., 127 (1980) 641.
12. A.H. Schroeder and F.B. Kaufman, J. Electroanal. Chem., 113 (1980) 209.
13. A.R. Hillman, D.C. Loveday and S. Bruckenstein, J. Electroanal. Chem., 274 (1989) 157.
14. A.J. Kelly, T. Ohsaka, N. Oyama, R.J. Forster and J.G. Vos, J. Electroanal. Chem., 287 (1990) 185.
15. A.J. Kelly and N. Oyama, J. Phys. Chem., 95 (1991) 9579.
16. P. Daum and R.W. Murray, J. Electroanal. Chem., 103 (1979) 289.
17. P. Daum and R.W. Murray, J. Phys. Chem., 85 (1981) 389.
18. T. Kawai, T. Kuwabara, S. Wang and K. Yoshino, J. Electrochem. Soc., 137 (1990) 3739.
19. R. Borjas and D.A. Buttry, J. Electroanal. Chem., 280 (1990) 73.
20. N. Oyama, T. Tatsuma and K. Takahashi, J. Phys. Chem., 97 (1993) 10504.

21. R.J. Forster, J.G. Vos and M.E.G. Lyons, J. Chem. Soc. Faraday Trans., 87 (1991) 3761.

22. R.J. Forster and J.G. Vos, J. Electroanal. Chem., 314 (1991) 135.

23. R.J. Forster, A.J. Kelly, J.G. Vos and M.E.G. Lyons, J. Electroanal. Chem., 270 (1989) 365.

24. R.J. Forster and J.G. Vos, Electrochim. Acta, 37 (1992) 159.

25. A. Glidle, A.R. Hillman and S. Bruckenstein, J. Electroanal. Chem., 318 (1991) 411.

26. A.J. Bard and L.R. Faulkner, Electrochemical Methods: Fundamentals and Applications, Wiley, New York, (1980).

27. D. Orata and D.A. Buttry, J. Am. Chem. Soc., 109 (1987) 3574.

28. D.A. Buttry, Applications of the Quartz Crystal Microbalance to Electrochemistry, in A.J. Bard (Ed.) Electroanalytical Chemistry, Marcel Dekker, New York, (1991), Vol.17, 1.

29. A.R. Hillman, M.J. Swann and S. Bruckenstein, J. Phys. Chem., 95 (1991) 3271.

30. A.R. Hillman, D.C. Loveday, M.J. Swann, S. Bruckenstein and C.P. Wilde, Analyst, 117 (1992) 1251.

31. A.R. Hillman, D.C. Loveday, M.J. Swann, B. Bruckenstein and C.P. Wilde, J. Chem. Soc. Faraday Trans., 87 (1991) 2047.

32. A.R. Hillman, D.C. Loveday and S. Bruckenstein, J. Electroanal. Chem., 300 (1991) 67.

33. S.J. Lasky and D.A. Buttry, J. Am. Chem. Soc., 110 (1988) 6258.

34. P. Daum, J.R. Lenhard, D.R. Rolison and R.W. Murray, J. Am. Chem. Soc., 102 (1980) 4649.

35. R.J. Forster and J.G. Vos, Langmuir, 10 (1994) 4330.

36. A.P. Clarke, Ph.D. Thesis, Dublin City University, (1992).

37. R.J. Forster and J.G. Vos, J. Inorganic and Organometallic Polymers, 1 (1991) 67.

38. D. Leech, R.J. Forster, M.R. Smyth and J.G. Vos, J. Mater. Chem., 1 (1991) 629.

Chapter 7.

Concluding Comments.

7.1. Concluding Comments.

In this work, the influence of the nature of the polymer backbone on the open circuit and electrochemical properties of $[Os(bipy)_2(PVP_x)_{10}Cl]^{+}$ electrode coatings has been investigated. The predominant part of this work has centred around the effects of introducing styrene moieties into the poly (4-vinylpyridine) polymer backbone. The techniques used in the characterisation of these metallopolymers were electrochemical (CV, PS and the EQCM) and non-electrochemical based (admittance analysis). What has clearly emerged from these studies is the strong dependence of the electrochemical properties of these $[Os(bipy)_2(PVP_x)_{10}Cl]^{+}$ films on the nature and properties of the polymer backbone.

The open circuit admittance characteristics of $[Os(bipy)_2(PVP_x)_{10}Cl]^{+}$ coated crystals were investigated as a function of the styrene content of the polymer backbone. This technique enables the rigidity and resident layer mass of these polymer coatings to be studied and provides a means of probing the different chemical properties of the individual polymers. For these metallopolymers, there is a notable decrease in layer mass and, by implication, an increase in layer rigidity, on increasing the styrene content of the polymer backbone. The origins of these effects are twofold. Firstly, incorporation of styrene moieties into the polymer backbone increases the hydrophobicity of the polymer layer. As a consequence, the level of solvent imbibition decreases with increasing styrene content of the polymer backbone. Secondly, incorporation of styrene moieties into the polymer backbone reduces the PVP content of the polymer. As a consequence, in $HClO_4$ electrolytes, the requirement for anion influx for the maintenance of electroneutrality within the protonated backbone is proportionally reduced. For all polymers examined, the open circuit mass increase accompanying protonation in $HClO_4$ electrolytes accounts for the counter-anion requirement for the maintenance of electroneutrality plus the demands for ion solvation. Furthermore, for all polymers in 0.5M $HClO_4$, there is good correlation between the mass change observed and the mass change anticipated,

assuming complete protonation of the polymer backbone.

The electrochemical mass transfer and charge transport properties of these redox polymers are also influenced by the nature of the polymer backbone. In $HClO_4$ electrolytes, the rate of charge transport through these materials is dependent on the styrene content of the polymer backbone. In 0.1M $HClO_4$, $D_{CT}(CV)$ is faster for the $OsPVP_{100}$ polymer compared with the copolymers. However, in 1.0M $HClO_4$, $D_{CT}(CV)$ is slower for the $OsPVP_{100}$. This behaviour is a consequence of the different properties of these polymers and reflects the more open $OsPVP_{100}$ polymer structure in 0.1M $HClO_4$ and the more crosslinked $OsPVP_{100}$ polymer structure in 1.0M $HClO_4$; compared with the styrene based copolymers.

The mass transfer studies of the $OsPVP_{100}$ and $OsPVP_{33}$ polymers also highlight subtle differences in the electrochemical properties of these materials. During redox switching of these polymers in perchlorate electrolytes, the quantity of solvent transferred is quite small. This behaviour reflects the compact nature of these coatings. For the $OsPVP_{33}$ polymer, the level of interfacial solvent transfer is reduced, reflecting the more hydrophobic nature of this particular polymer. The permselectivity of these polymers is clearly dependent on the composition of the polymer backbone. For the $OsPVP_{100}$ polymer, there is a breakdown in layer permselectivity in perchlorate concentrations in excess of 1.0M. However, for the $OsPVP_{33}$ polymer, layer permselectivity is maintained over the complete perchlorate electrolyte concentration range studied. This behaviour is quite surprising and is likely a consequence of the more hydrophobic and compact nature of the $OsPVP_{33}$ polymer backbone. For both polymers, under dynamic experimental conditions, interfacial solvent transfer is impeded. This behaviour is clearly a consequence of the compact nature of these polymer in perchlorate electrolyte. For these polymers, the $HClO_4$ and $LiClO_4$ electrolyte concentration dependence of the charge transport rate correlates quite well with the facility for solvent transfer.

The influence of the polymer morphology on the electrochemical properties of

the $OsPVP_{100}$ polymer is profound. Swelling of this polymer in mixed solvent electrolytes greatly facilitates the interfacial transfer of mobile species during redox switching. Consequently, swelling of these layers is accompanied by an increase in the resident layer mass at open circuit. Furthermore, during redox switching the quantity of solvent transferred increases. For these electrochemical experiments, the additional solvent component of the normalised redox-switching-induced mass change has been identified as acetonitrile from isotopic substitution experiments. Finally, as a consequence of these swelling phenomena and the improvements in the facility for solvent transfer, the rate of charge transport is greatly enhanced.

The developments presented here have important implications for the design and development of electrochemical sensors based on these redox materials. Firstly, improvements in the rigidity and, by implication, the stability of metallopolymer coatings can be achieved by altering the composition of the polymer backbone. Secondly, the applicability of these materials to areas such as electrocatalysis is intrinsically dependent on their charge transport properties, as these will limit both the sensitivity and response times of these systems. Consequently, the addition of organic solvents to aqueous solutions represents a useful approach to controlling the rate of charge transport through these materials. 100 fold increases in the charge transport rate may be simply achieved by adding acetonitrile to the contacting electrolyte. Furthermore, the degree of polymer swelling may be varied by altering the organic solvent content of the contacting electrolyte which will allow for greater control of the selectivity of these materials towards solution species. By controlling the swelling and charge transport properties of the electrode modifying materials, their mediating properties can be tailor-made to suit the particular system under investigation.

Appendix.

#21.5US568801/ELSEVI/EA—1013/ELE02T0

Pergamon

Electrochimica Acta, Vol. 41, No. 0, pp. 00–00, 1996

0013-4686(95)00501-3 $9.50 + 0.00

0013–4686(95)00501–3

THE INFLUENCE OF ACETONITRILE AND METHANOL ON THE CHARGE TRANSPORT PROPERTIES OF $[Os(bipy)_2(PVP)_{10}Cl]Cl$ FILMS

DAVID M. KELLY and JOHANNES G. VOS
School of Chemical Sciences, Dublin City University, Dublin 9, Ireland

(*Received* ?????? 1996)

Abstract—The influence of solvent composition on the electrochemical properties of electrodes modified with $[Os(bipy)_2(PVP)_{10}Cl]Cl$ films, where bipy is 2,2′-bipyridyl and PVP is poly(4-vinylpyridine), is investigated. The addition of acetonitrile or methanol to aqueous $LiClO_4$ electrolyte solutions, greatly alters their electrochemical behaviour. The apparent diffusion coefficient for homogeneous charge transport (D_{CT}) has been evaluated using cyclic voltammetry and chronoamperometry. The charge transport rate is enhanced upon the addition of 5–60% of these solvents. Thermodynamic parameters evaluated for the charge transport process suggest that, upon polymer swelling, the rate limiting process changes from ion movement to polymer chain motion. This behaviour is interpreted in terms of the more facile transport of charge compensating counterions because of increased swelling of the layer in the presence of organic solvent

Key words: polymer modified electrode, charge transport, osmium, solvent dependence.

INTRODUCTION

The influence of metal loading, electrolyte type and concentration and temperature on the kinetics of homogeneous and heterogeneous electron transport have been reported for thin films of $[Os(bipy)_2(POL)_xCl]Cl$, where bipy is 2,2′-bipyridyl, POL is poly(4-vinylpyridine) or poly(N-vinylimidazole) and x signifies the metal to polymer loading[1–7]. It is generally accepted that charge transport in such redox polymers proceeds by an electron-hopping process[8]. This process is in-turn accompanied by the motion of charge compensating counterions, solvent and polymer chain segments. The interplay between these processes will ultimately determine the rate at which charge may be transported through these materials[9]. What has clearly emerged from these studies is the profound influence of the physico-chemical properties of these materials and the role of counterion-polymer interactions on the rate of charge percolation through these redox polymers[1, 3, 5, 6]. EQCM studies of the mass transport properties of $[Os(bipy)_2(PVP)_{10}Cl]Cl$ have confirmed these observations and have highlighted the influence of solvent transport on the charge transport process[10, 11].

The electrochemistry of plasma polymerised vinylferrocene[12, 13], Ru^{III}(edta) incorporated in PVP[14] and TCNQ[15] is dependent on the solvent of the contacting electrolyte. Changes in the voltammetric behaviour of these polymer systems for different bathing solvents are typically discussed in terms of different solvent swelling effects.

To probe the relationship between the structural properties of redox polymers and the charge transport process, the influence of the nature of the bathing electrolyte solvent on the electrochemical properties of $[Os(bipy)_2(PVP)_{10}Cl]Cl$ films was investigated. Previously, electrochemical studies of this polymer were predominantly undertaken in aqueous electrolyte. In this contribution the influence of adding acetonitrile and methanol, which can solubilise this polymer, to aqueous electrolyte systems on the charge transport properties of this material is reported. In aqueous perchlorate electrolytes $[Os(bipy)_2(PVP)_{10}Cl]Cl$ electrode coatings are compact and contain only small quantities of solvent[11, 16]. Charge transport rates in $LiClO_4$ are amongst the lowest reported for this metallopolymer and reflect the difficulties for ion influx and transport within these compact structures[5]. This electrolyte, therefore, provides a useful environment in which to probe the effects of solvent swelling on the electrochemical properties of this metallopolymer. Charge transport rates for the $Os^{II/III}$ oxidation, characterised by the diffusion coefficient D_{CT}, were measured by cyclic voltammetry and chronoamperometry. Activation energies associated with the charge transport process were estimated from the temperature dependence of the diffusion coefficient.

MATERIALS

The redox polymer, $[Os(bipy)_2(PVP)_{10}Cl]Cl$, was prepared as previously described[17]. $LiClO_4$ was analytical grade. HPLC grade MeCN (0.02% H_2O) and MeOH (0.02% H_2O) were used as supplied. All mixed solvents were prepared with Milli-Q H_2O and

* Author to whom correspondence should be addressed.

a constant 0.1 M $LiClO_4$ electrolyte concentration was used in each case. Electrolytes are identified in terms of the percentage of non-aqueous solvent *ie* 30% MeCN signifies 0.1 M $LiClO_4$ prepared in 30 : 70 MeCN : H_2O.

APPARATUS AND PROCEDURES

Glassy carbon electrodes (3 mm dia.) shrouded in PTFE (Metrohm) were used for the analysis. Electrode coatings were prepared by droplet evaporation using a 0.25% w/v enthanolic solution of the metallopolymer. Coatings were allowed to dry in a solvent saturation chamber for 24 h prior to use. The electrochemical cell was thermostated and all charge transport rates are quoted at 25°C ± 1°C. A saturated potassium calomel electrode (*sce*) and a 1 cm^2 platinum mesh counter electrode were used. All potentials are quoted with respect to the *sce* without regard to liquid junction potentials. Electrochemical measurements were made using an EG&G PAR 175 universal programmer and a 363 potentiostat. Where necessary, *ir* compensation was achieved *via* positive feedback circuitry. Coulometric measurements were made using a 379 digital coulometer. Transient current measurements were made over the time range 0 to 20 ms by means of a Philips 3311 digital storage oscilloscope interfaced to a BBC microcomputer for data integration and allowing signal averaged results to be obtained. For both the redox active potential step and for background correction, five current decays were averaged. Potential steps for background correction were made between −0.3 and 0.0 V, where no redox reaction occurred, and were linearly extrapolated.

Diffusion coefficients and activation parameters were estimated on fresh coatings to minimise memory effects[18]. Diffusion coefficients were typically reproducible to within 10% for determinations on three different coatings and 4% for repeated determinations on single coatings. Activation parameters were reproducible to within 10–20% for determinations on two different coatings and 5% for repeated determinations on single coatings. The concentration of osmium centres within the films was estimated as 0.7 M from density measurements of the dry polymer (1.2 g cm^{-3}) in non-swelling solvent. Surface coverages were 79d by integrating the area under the anodic peak of a background corrected slow sweep rate cyclic voltammogram (1 mV s^{-1}). Alternatively, the charge passed during exhaustive oxidation of the layers was monitored using coulometry. Surface coverages were typically in the range of 2–6 × 10^{-8} mol cm^{-2}.

Estimation of D_{CT}: Fig. 1 illustrates the dependence of the anodic peak current on the square root of the scan rate, as a function of the MeCN content of the electrolyte, for scan rates of 50–500 mV s^{-1}. The linearity of these plots suggests a semi-infinite diffusion response. Charge transport rates, $D_{CT}(cv)$, from cyclic voltammograms obtained under these conditions, were estimated using the Randles-Sevcik equation[19];

$$i_p = 0.4463(nF)^{3/2} A D_{CT}^{1/2} C v^{1/2}/(RT)^{1/2} \qquad (1)$$

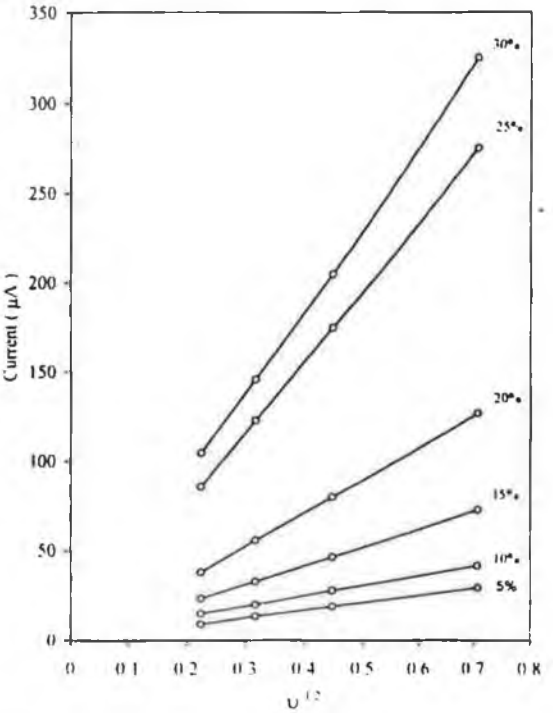

Fig. 1. The effect of MeCN on the anodic peak currents of 50 to 500 mV s^{-1} cyclic voltammograms for an $[Os(bipy)_2(PVP)_{10}Cl]Cl$ coated electrode in 0.1 M $LiClO_4$. Surface coverage 4.3 × 10^{-8} mol cm^{-2}.

where n is the number of electrons passed, F is the Faraday constant, A is the electrode area, D_{CT} is the apparent charge transport diffusion coefficient, C is the concentration of electroactive sites, v the sweep rate, R the gas constant and T the absolute temperature.

Figure 2 illustrates Cottrell plots, for times up to 20 ms, as a function of the MeCN content of the electrolyte. These plots are linear and exhibit zero current intercepts, which is consistent with a semi-infinite diffusional response. Charge transport rates were estimated from these plots using the Cottrell equation[20] and are identified as D_{CT}(PS), where PS signifies potential step;

$$i(t) = \frac{nFAD_{CT}^{1/2} C}{(\pi t)^{1/2}} \qquad (2)$$

Migrational enhancement of the diffusional response may be diagnosed by a non-zero intercept in the Cottrell plot[21] or by the presence of a peak in the $It^{1/2}$ vs. $t^{1/2}$ plot[22]. Neither of these features were observed in this investigation. The experimentally determined parameter is $D_{CT}^{1/2} C$, where C is the concentration of electroactive sites within the polymer and has been estimated as 0.7 M. Within these experiments the polymer layers become extensively solvent swollen. The concentration of electroactive sites is, therefore, likely to be less than 0.7 M. All trends of increased D_{CT} therefore reflect enhanced charge transport rates and may be viewed as the lower limit for charge transport under these conditons[7].

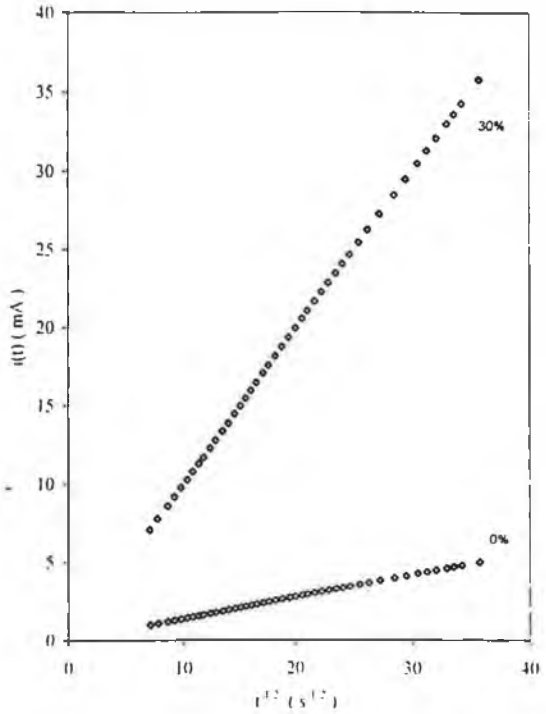

Fig. 2. The effect of MeCN on the chronoamperometric response of an $[Os(bipy)_2(PVP)_{10}Cl]Cl$ coated electrode in 0.1 M $LiClO_4$. Surface coverage 4.3×10^{-8} mol cm^{-2}.

Activation parameters: The evaluation of the activation parameters associated with homogeneous charge transport can provide additional information about the rate limiting process for charge transport. In the work reported here, linear plots of $\ln D_{CT}$ vs. T^{-1} were obtained in each mixed solvent system investigated. Activation energies were determined from the temperature dependence of both D_{CT}(cv) and D_{CT}(PS) over the temperature range of 275–308 K using the Arrhenius equation[23]:

$$D_{CT} = D_{CT}^{O} \exp(-E_a/RT) \quad (3)$$

where D_{CT}^{O} is the pre-exponential factor for physical diffusion.

The activation entropy, ΔS^{*}, was estimated from the Eyring equation[24]:

$$D_{CT}^{O} = e\delta^2(k_B T/h) \exp(\Delta S^{*}/R) \quad (4)$$

where e is the base of the natural log, k_B is the Boltzmann constant, h is Planck's constant, and δ is the equilibrium separation of vicinal redox sites. Assuming a rigid rod structure in the metallopolymer backbone, the osmium intersite separation may be approximated as 25 Å from crystal structure data for the separation of adjacent monomer units in the poly(4-vinylpyridine) backbone[25]. It is accepted that activation parameters are of limited accuracy since the extent of film swelling at a given electrolyte concentration and temperature is unknown. However, the ability to distinguish between rate determining cases such as ion diffusion or polymer chain motion is unlikely to be affected and observed trends should remain valid[2, 3, 5, 7].

RESULTS AND DISCUSSION

General layer behaviour

Figure 3 illustrates the cyclic voltammetric behaviour of an $[Os(bipy)_2(PVP)_{10}Cl]Cl$ coated electrode in aqueous 0.1 M $LiClO_4$ at a scan rate of 1 mV s^{-1}. The characteristic features of this voltammogram *ie* the peak-to-peak separation (ΔE_p), the full width at half maximum current (FWHM) and the half wave potential ($E_{1/2}$), are summarised in Table 1. $E_{1/2}$ is taken as the average of the anodic and cathodic peak potentials. The ratio of anodic to cathodic peak currents (i_{pa}/i_{pc}) was unity for all solvent combinations. In Fig. 3 the presence of diffusion tailing and the ΔE_p of 95 mV are indicative of a diffusional controlled electrochemical response. A plot of i_p vs. $v^{1/2}$ is linear for scan rates up to 500 mV s^{-1} and again reflects a diffusional response. In aqueous 0.1 M $LiClO_4$ surface coverages estimated from the area under the anodic peak, correcting for background, are *ca.* 25% smaller than those estimated by exhaustive coulometry. Therefore, within these experimental timescales only 75% of the redox sites within the layer is electroactive, thus illustrating the slow transport of charge through these compact layers in aqueous $LiClO_4$.

Table 1 summaries the influence of acetonitrile and methanol on the voltammetric characteristics of

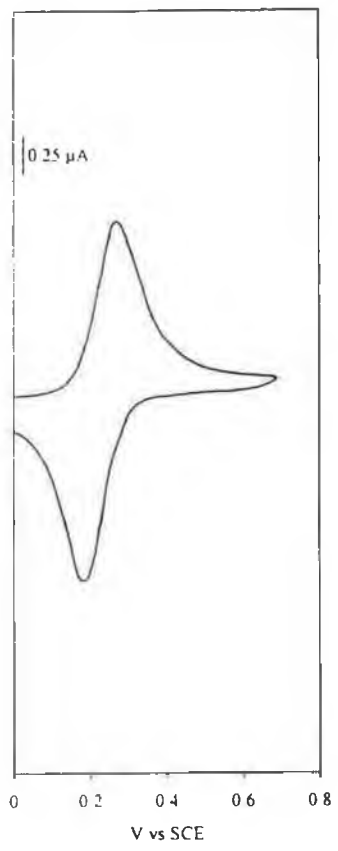

Fig. 3. Cyclic voltammogram of an $[Os(bipy)_2(PVP)_{10}Cl]Cl$ coated electrode in aqueous 0.1 M $LiClO_4$. Scan rate 1 mV s^{-1}. Surface coverage 5.6×10^{-8} mol cm^{-2}.

Table 1. The effect of MeCN and MeOH on the characteristic parameters of 1 mV s^{-1} cyclic voltammograms of $[Os(bipy)_2(PVP)_{10}Cl]Cl$ coated electrodes in 0.1 M $LiClO_4$. The surface coverages are 2–6 × 10^{-8} mol cm^{-2}.

	MeCN			MeOH		
% Solvent	FWHM[a,b] (mV)	ΔE_p[a,b] (mV)	$E_{1/2}$[a,b,c] (mV)	FWHM[a,b] (mV)	ΔE_p[a,b] (mV)	$E_{1/2}$[a,b,c] (mV)
0	140	95	230	135	95	233
5	115	50	230			
10	100	30	250	125	65	233
15	90	15	248			
20	90	5	248	105	35	238
25	90	5	250			
30	90	5	248	100	20	240
40				95	15	243
50				90	5	248
60				90	0	250

[a] Estimated from 1 mV s^{-1} cyclic voltammogram.
[b] Error on measurement is ±5 mV.
[c] Estimated from the average of the anodic and cathodic peak potentials.

1 mV s^{-1} cyclic voltammograms for this same polymer layer. These characteristics are indistinguishable from those observed during experiments on individual polymer coatings. The addition of MeCN to the electrolyte greatly alters the voltammetric characteristics of the polymer layer. On increasing the MeCN content of the electrolyte, a gradual transition from diffusion controlled voltammetric behaviour to surface behaviour is observed at this scan rate. However, at higher scan rates (> 20 mV s^{-1}) diffusion behaviour is still obtained. Figure 4 illustrates the 1 mV s^{-1} cyclic voltammetric behaviour of this layer in 20% MeCN. The voltammetric characteristics are significantly different from those observed in 100% H_2O (see Fig. 3). The peak-to-peak separation is essentially zero and the peak width at half height is 90 mV. These features are characteristic of a one electron oxidation reduction of surface confined species[26, 27]. Also, the surface coverage of osmium sites estimated from the area under the anodic peak is identical to the coverage estimated by exhaustive coulometry. This illustrates that the complete layer is now electroactive within these experimental timescales.

The behaviour in MeOH is similar to that observed in MeCN (see Table 1). Addition of MeOH to the electrolyte again results in a transition from solution to surface behaviour, however, surface behaviour is only observed in MeOH concentrations above 45%.

For both solvents, the observed transition in the voltammetric behaviour from solution to surface behaviour, coupled with the oxidation of larger portions of these modifying layers upon addition of these solvents to the contacting electrolyte, clearly reflect more rapid charge transport processes compared with those observed in aqueous $LiClO_4$. Considering the solubility of this polymer in these solvents it is suggested that these voltammetric observations are a direct consequence of solvent induced swelling effects. The observed dissolution of these layers in 40% (70%) MeCN (MeOH) clearly illustrates this point. The transition between solution and surface behaviour reflects swelling of the polymer layer and the more favourable transport properties within these swollen structures. In both solvents, $E_{1/2}$ shifts from 233 mV in H_2O to 250 mV in 20 (50%) MeCN (MeOH). This shift in $E_{1/2}$ may reflect the more solution like nature of the swollen polymer layer.

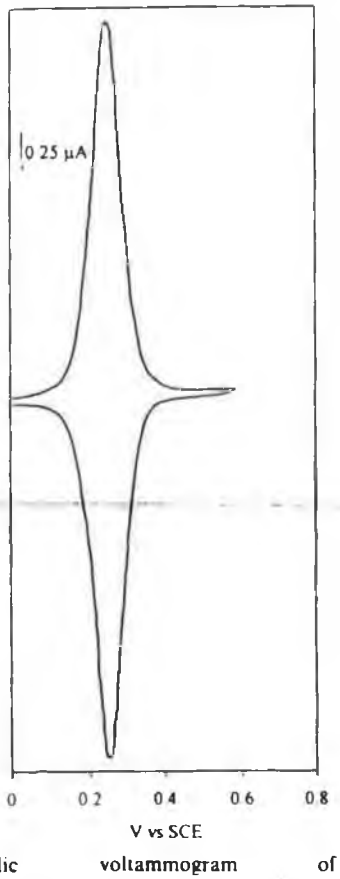

Fig. 4. Cyclic voltammogram of an $[Os(bipy)_2(PVP)_{10}Cl]Cl$ coated electrode in 0.1 M $LiClO_4$, 20% MeCN. 80% H_2O. Scan rate 1 mV s^{-1}. Surface coverage 5.6 × 10^{-8} mol cm^{-2}.

Charge transport properties

Charge transport rates for the $Os^{II/III}$ oxidation, $D_{CT}(cv)$ and $D_{CT}(PS)$, as a function of MeCN and MeOH concentration are summarised in Table 2. The data highlight the profound influence of these solvents on the rate of charge transport through $[Os(bipy)_2(PVP)_{10}Cl]Cl$ films. Above an electrolyte content of 15% MeCN $D_{CT}(cv)$ increases quite dramatically (see Fig. 5). $D_{CT}(cv)$ continues to increase as the MeCN electrolyte content is increased above 30% MeCN. However, at these concentrations the layer is insignificantly stable to allow for accurate measurements to be made. The effect of the MeCN bathing electrolyte concentration on the activation parameters for charge transport, as estimated by both cyclic voltammetry and potential step techniques, is illustrated in Table 3. The value of $E_a(cv)$ increases with increasing MeCN content of the electrolyte and reaches a maximum of 79 ± 5 kJ mol^{-1} in 15% MeCN. This increase in activation energy is accompanied by a transition from a negative to a positive entropy term. In MeCN concentrations greater than 15%, there is a gradual decrease in $E_a(cv)$ which is accompanied by a decrease in the activation entropy. In 30% MeCN, $E_a(cv) = 57 \pm 4$ kJ mol^{-1} and is coupled to a negative entropy term.

Table 2. The effect of MeCN and MeOH on the rate of charge transport through $[Os(bipy)_2(PVP)_{10}Cl]Cl$ films as determined by cyclic voltammetry ($D_{CT}(cv)$) and chronoamperometry ($D_{CT}(PS)$) in 0.1 M $LiClO_4$. The surface coverages are $2–6 \times 10^{-8}$ mol cm^{-2}

% Solvent	$D_{CT}(cv) \times 10^{11}$ [a] (cm^2 s^{-1})		$D_{CT}(PS) \times 10^{10}$ [a] (cm^2 s^{-1})	
	MeCN	MeOH	MeCN	MeOH
0	1.2	1.2	1.1	1.2
5	1.9		1.4	
10	3.5	1.2	1.5	1.2
15	12		3.1	
20	76	1.1	13	1.1
25	132		28	
30	171	3.5	49	1.3
40		11		2.7
50		25		6.1
60		100		10

[a] The reproducibility between layers is $\pm 10\%$.

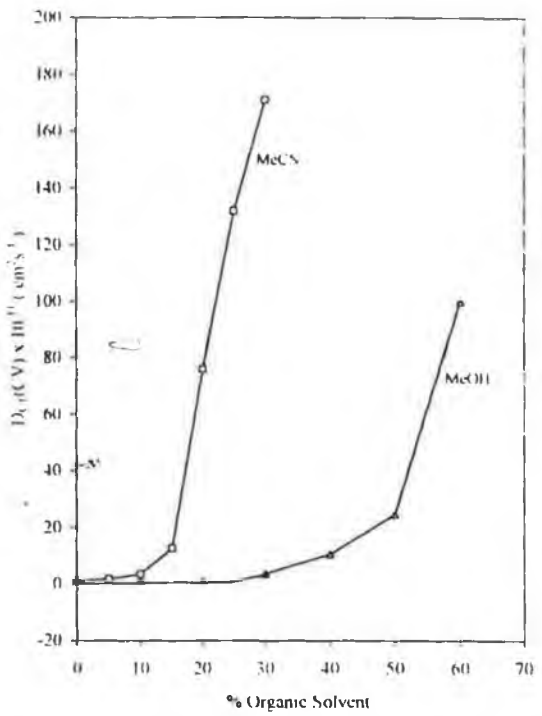

Fig. 5. The effect of MeCN (□) and MeOH (△) on the rate of charge transport through $[Os(bipy)_2(PVP)_{10}Cl]Cl$ films as determined by cyclic voltammetry, $D_{CT}(cv)$.

In aqueous 0.1 M $LiClO_4$, the occurrence of a diffusional limited response at slow cyclic voltammetric scan rates and the charge transport rate of 1×10^{-11} cm^2 s^{-1}, as estimated by cyclic voltammetry, reflect slow charge transport within these compact layers. The energy of activation, $E_a(cv)$, associated with the charge transport process is 44 ± 6 kJ mol^{-1}. This activation energy is associated with a negative entropy term. It is suggested that this negative entropy term is associated with either ion motion or electron hopping as being rate determining[28]. It is considered that, in this case, ion motion rather than electron hopping limitations dominate the charge transport properties as charge transport rates for cases where electron hopping is the rate determining step are typically two order of magnitudes higher[7]. Addition of MeCN results in a transition from diffusion limited responses to ideal surface voltammetric behaviour in slow scan rate cyclic voltammetric experiments. Furthermore, $D_{CT}(cv)$, increases dramatically as the concentration of this solvent in the bathing electrolyte is increased. In 15% MeCN $D_{CT}(cv)$ is 12.6×10^{-11} cm^2 s^{-1} and represents a 10 fold increase in charge transport rate compared pure aqueous $LiClO_4$. This behaviour most likely reflects the more facile transport properties of these solvent swollen layers and suggest that ion motion is no longer limiting. These observations are supported by the thermodynamic data. The increase in $D_{CT}(cv)$ is accompanied by an increase in the activation barrier for electron transfer. This behaviour suggest that higher pre-exponential factors rather than lower activation barriers are responsible for the increase in $D_{CT}(cv)$. It has been suggested that an increase in the matrix fluidity *eg* by solvent swelling, may increase the pre-exponential factor of equation (4) by increasing the collisional frequency[7].

The entropy term in 15% MeCN is positive and suggests that a transition in rate controlling process has occurred. This positive entropy may be associated with polymer chain motion[28]. Swelling of these layers increases the osmium site-to-site separation. This transition to polymer motion limitation may, therefore, reflect the requirement for motion of the polymer chains to reduce this inter-site separation to allow for electron hopping. Above 15% MeCN, $D_{CT}(cv)$ continues to increase. In 30% MeCN $D_{CT}(cv)$ is 1.71×10^{-9} cm^2 s^{-1} and represents a 100 fold increase in charge transport rate compared with that observed in aqueous $LiClO_4$. This is one of the

fastest charge transport rates reported for this particular polymer. For the analogous 1 in 10 loaded poly(N-vinyl imidazole) polymer, similar charge transport rates were only observed under conditions where electron hopping appeared to be rate limiting[7]. In MeCN concentrations greater than 15%, $E_a(cv)$ decreases. The magnitude of the entropy decreases and in 30% MeCN the sign of this entropy term changes from positive to negative. This apparent change in the activation parameters, on increasing the MeCN content of the contacting electrolyte from 15% to 30% MeCN, is surprising but is considered accurate. The numerical errors on both the activation and entropy data, within this MeCN concentration range, are not sufficient to account for these changes. Furthermore, changes in the osmium intersite separation due to swelling are not sufficient to account for the change in sign of the entropy term. Therefore, the decrease in the activation energy coupled with the change in the sign of the entropy term suggest that the processes limiting charge transport have changed. This suggestion is supported by the observed 10 fold increase in $D_{CT}(cv)$ within this concentration range. This negative entropy term is associated with either ion motion or electron hopping as being rate limiting[28]. Within the swollen structures that exist in this concentration of MeCN it is considered unlikely that ion motion will be rate determining. The entropy term may therefore reflect electron hopping as being rate determining. However, more detailed studies are needed to substiantiate this.

The effect of the MeCN content of the bathing electrolyte on $D_{CT}(PS)$ and the associated activation parameters is summarised in Tables 2 and 3 respectively. $D_{CT}(PS)$ is less sensitive to the MeCN content of the electrolyte than $D_{CT}(cv)$ and remains essentially constant as the MeCN content of the bathing electrolyte is raised from 0% to 10%. As the MeCN content of the bathing electrolyte is increased above 10% MeCN, $D_{CT}(PS)$ increases and this increase in charge transport rate becomes quite dramatic above 15% MeCN (see Fig. 6). The overall increase in $D_{CT}(PS)$ from 0% to 30% MeCN represents an approximate 50 fold increase in charge transport rate. $E_a(PS)$ increases with increasing MeCN concentration and is associated with a change in the sign of the entropy term (negative to positive). Above 20% MeCN $E_a(PS)$ decreases and at 30% MeCN there is a return to a negative entropy term. This overall behaviour is qualitatively similar to that observed by cyclic voltammetry and may again reflect a transition between rate determining process with, firstly polymer motions and then electron hopping limiting the rate of charge transport through these swollen layers.

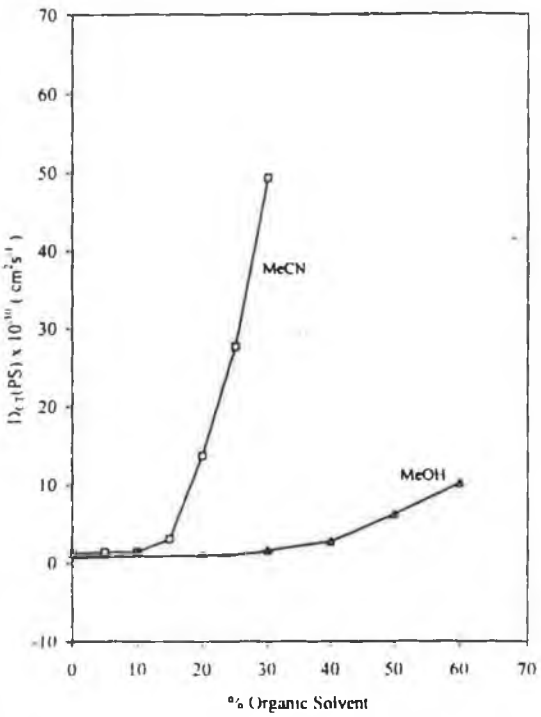

Fig. 6. The effect of MeCN (□) and MeOH (△) on the rate of charge transport through $[Os(bipy)_2(PVP)_{10}Cl]Cl$ films as determined by chronoamperometry, $D_{CT}(PS)$.

The effect of MeCN content on $D_{CT}(cv)$ and $D_{CT}(PS)$ is summarised in Table 2. The influence of MeOH on the rate of charge transport is less profound than that observed in MeCN. $D_{CT}(cv)$ and $D_{CT}(PS)$ remain essentially constant for MeOH electrolyte concentrations up to 20% and 30% respectively. Increasing the MeOH content of the electrolyte above these concentrations results in an increase in both $D_{CT}(cv)$ and $D_{CT}(PS)$. In MeOH, the fastest charge transport rates are observed in 60% MeOH, as these layers dissolve in higher MeOH concentrations. In this concentration of MeOH, $D_{CT}(cv)$ and $D_{CT}(PS)$ are identical and reflect 100 and 10 fold increases in charge transport rates respectively, compared with pure aqueous $LiClO_4$. The

Table 3. The effect of MeCN on the activation parameters for charge transport through $[Os(bipy)_2(PVP)_{10}Cl]Cl$ films as determined by cyclic voltammetry and chronoamperometry in 0.1 M $LiClO_4$. Surface coverages are $2–6 \times 10^{-8}$ mol cm^{-2}

% MeCN	$E_a(cv)$ (kJ mol^{-1})	$\Delta S(cv)'$ (J mol^{-1} K^{-1})	$\Delta G(cv)'$ (kJ mol^{-1})	$E_a(PS)$ (kJ mol^{-1})	$\Delta S(PS)'$ (J mol^{-1} K^{-1})	$\Delta G(PS)'$ (kJ mol^{-1})
0	44(6)	−72(12)	63(1)	20(5)	−137(16)	59(2)
10	72(5)	28(4)	62(2)	36(2)	−79(7)	57(1)
15	79(5)	66(7)	57(2)	55(3)	−6(4)	54(2)
20	72(2)	53(5)	54(1)	67(2)	42(5)	52(1)
25	67(6)	42(8)	52(1)	57(4)	15(4)	50(1)
30	57(4)	−24(4)	62(3)	47(3)	−54(5)	60(4)

Errors quoted in brackets.

effect of MeOH on the temperature dependence of $D_{CT}(cv)$ and $D_{CT}(PS)$ is summarised in Table 4. $E_a(cv)$ increases with increasing MeOH electrolyte concentration reaching a maximum value of $111 \pm 5\,kJ\,mol^{-1}$ in 40% MeOH. This increase in activation energy is associated with a change in the sign of the entropy term. Activation energies were not obtained in 60% MeOH as the layers were insufficiently stable over the duration of the experiment. $E_a(PS)$ remains essentially constant as the MeOH concentration of the electrolyte is increased from 0% to 30%. $E_a(PS)$ increases in MeOH concentrations greater than 30% and is again associated with a change in the sign of the entropy term.

The influence of MeOH on the electrochemical properties of $[Os(bipy)_2(PVP)_{10}Cl]Cl$ is qualitatively similar but not as dramatic as that observed in MeCN. A larger MeOH content is required to induce surface behaviour and to produce the same increase in charge transport rate as MeCN. This most likely reflects the poorer solubility of the films in MeOH and, therefore, the lower degree of polymer swelling in this solvent. The data in MeOH follow similar trends to those observed in MeCN. The increase in $D_{CT}(cv)$ and $D_{CT}(PS)$ with increasing MeOH concentration is accompanied by a transition from negative to positive entropy. This behaviour may again reflect a transition in the rate determining process from ion movement to polymer segmental motion. The similarity in this behaviour suggests that the controlling processes in both solvents are similar and that the degree of solvent swelling of these layer ultimately dominates the electrochemical response in these solvents.

Comparison of $D_{CT}(cv)$ and $D_{CT}(PS)$

In aqueous 0.1 M $LiClO_4$, $D_{CT}(PS)$ differs from $D_{CT}(cv)$ by an order of magnitude (see Table 2). The dependence of the rate of charge transport on the experimental technique used in its measurement is commonly observed for osmium and ruthenium metallopolymers[1–3, 5, 6, 29]. It has been proposed that these differences may represent a dependence on the experimental timescale or the region of the film in which it is evaluated[2, 3, 5, 29]. The thermodynamic data in this electrolyte are consistent with ion motion limitations controlling both $D_{CT}(cv)$ and $D_{CT}(PS)$. This observation suggests that, under these conditions, the nature of the rate determining step is not dependent on the experimental timescale and that the large activation energy for cyclic voltammetry reflects a greater ion motion limitation. This is not surprising considering the nature of ion motion is decidedly different for the two techniques. In *cv*, the more extensive oxidation of the layers requires counterion diffusion to occur over larger regions of the layer than in short timescale PS experiments. Furthermore, the quantity of diffusing counterions is considerably larger in cyclic voltammetry experiments.

Alternatively, it is also possible that the larger $D_{CT}(PS)$ may reflect a greater concentration of redox centres in the relatively more compact base layer. However, the difference between $D_{CT}(cv)$ and $D_{CT}(PS)$ would require differential swelling of over 300%[2, 3, 5, 29].

In both mixed solvent systems, $D_{CT}(cv)$ is found to be more sensitive to swelling of the films in low solvent concentrations. The increase in $D_{CT}(cv)$ is accompanied by an increase in $E_a(cv)$ and is considered to reflect more facile ion motion as a result of layer swelling. The insensitivity of $D_{CT}(PS)$ to swelling of the layer in the low organic solvent concentrations suggests that the outer portion of the layer is more swollen. Further swelling of the layer in higher organic solvent concentrations causes an increase in $D_{CT}(PS)$ which is accompanied by an increase in $E_a(PS)$. This likely reflects the progressive swelling of the base layer with increasing organic solvent concentration of the contacting electrolyte and the enhancement of charge transport rates as a consequence of more facile ion motion. In both solvents, when the layers are extensively swollen, $D_{CT}(PS)$ and $D_{CT}(cv)$ are similar and appear to be controlled by the same processes. This behaviour suggests that the nature of the equilibrium established within the layer is identical for both techniques and is independent of the experimental timescales.

CONCLUSION

The nature of the interaction between solvent and polymer has a profound influence on the electrochemical properties of $[Os(bipy)_2(PVP)_{10}Cl]Cl$ polymer coatings and highlights the importance of the structural properties of the polymer backbone. Swelling of these layers in both methanol and acetonitrile not only improves their charge transport properties but also changes the rate determining process. These improved responses may likely reflect more facile ion motion within the solvent swollen

Table 4 The effect of MeOH on the activation parameters for charge transport through $[Os(bipy)_2(PVP)_{10}Cl]Cl$ films as determined by cyclic voltammetry and chronoamperometry in 0.1 M $LiClO_4$. Surface coverages are $2–6 \times 10^{-8}$ mol cm^{-2}

% MeOH	$E_a(cv)$ (kJ mol^{-1})	$\Delta S(cv)^{\ddagger}$ (J mol^{-1} K^{-1})	$\Delta G(cv)^{\ddagger}$ (kJ mol^{-1})	$E_a(PS)$ (kJ mol^{-1})	$\Delta S(PS)^{\ddagger}$ (J mol^{-1} K^{-1})	$\Delta G(PS)^{\ddagger}$ (kJ mol^{-1})
0	44(6)	−72(12)	63(1)	20(5)	−137(16)	59(2)
10	51(3)	−52(5)	62(3)	24(3)	−124(13)	58(4)
20	63(4)	15(7)	62(1)	30(2)	−104(10)	58(4)
30	75(3)	39(4)	61(5)	31(4)	−99(15)	58(1)
40	111(5)	169(13)	58(4)	57(4)	−2(5)	55(1)
50	101(7)	143(12)	56(1)	87(6)	104(11)	54(2)

Errors quoted in brackets.

polymer network. It is noted that the situation which favours rapid electron exchange *ie* a high concentration of closely packed redox sites, will result in limited ion diffusion. Swelling of these layer allows for more facile ion diffusion but results in polymer chain motions being required to bring the osmium sites together to allow electron transfer to occur.

The addition of organic solvents to aqueous solutions represents a useful approach to controlling the rate of charge transport through these materials. One hundred-fold increases in the charge transport rate may be simply achieved by adding either acetonitrile or methanol to the contacting electrolyte. The applicability of these materials to areas such as electrocatalysis is intrinsically dependent on their charge transport properties, as these will limit both the sensitivity and response times of these systems. Furthermore, the degree of polymer swelling may be varied by altering the organic solvent content of the contacting electrolyte which will allow for greater control of the selectivity of these materials towards solution species. The developments presented here, therefore, have important implications for the design and development of electrochemical sensors based on these redox materials. By controlling the swelling and charge transport properties of the electrode modifying materials, their mediating properties can be tailor-made to suit the particular system under investigation.

Acknowledgements—The authors thank Dr R. J. Forster for helpful discussions and Forbairt, the Irish Science and Technology Agency, for financial support.

REFERENCES

1. R. J. Forster, A. J. Kelly, J. G. Vos and M. E. G. Lyons, *J. Electroanal. Chem.* **270**, 365 (1989).
2. R. J. Forster and J. G. Vos, *J. Electroanal. Chem.* **314**, 135 (1991).
3. R. J. Forster, J. G. Vos and M. E. G. Lyons, *J. Chem. Soc. Faraday Trans.* **87**, 3761 (1991).
4. R. J. Forster, J. G. Vos and M. E. G. Lyons, *J. Chem. Soc. Faraday Trans.* **87**, 3769 (1991).
5. R. J. Forster and J. G. Vos, *Electrochim. Acta* **37**, 159 (1992).
6. R. J. Forster and J. G. Vos, *J. Inorganic and Organometallic Polymers*, **1**, 67 (1991).
7. R. J. Forster and J. G. Vos, *Langmuir* **10**, 4330 (1994).
8. F. B. Kaufman and E. M. Engler, *J. Am. Chem. Soc.* **101**, 547 (1979).
9. F. B. Kaufman, A. H. Schroeder, E. M. Engler, S. R. Kramer and J. Q. Chambers, *J. Am. Chem. Soc.* **102**, 483 (1980).
10. A. J. Kelly, T. Ohsaka, N. Oyama, R. J. Forster and J. G. Vos, *J. Electroanal. Chem.* **287**, 185 (1990).
11. A. J. Kelly and N. Oyama, *J. Phys. Chem.* **95**, 9579 (1991).
12. P. Daum and R. W. Murray, *J. Electroanal. Chem.* **103**, 289 (1979).
13. P. Daum and R. W. Murray, *J. Phys. Chem.* **85**, 389 (1981).
14. N. Oyama and F. C. Anson, *J. Electrochem. Soc.* **127**, 640 (1980).
15. P. Joo and J. Q. Chambers, *J. Electrochem. Soc.* **132**, 1345 (1985).
16. A. P. Clarke, J. G. Vos, A. Glidle and A. R. Hillman, *J. Chem. Soc. Faraday Trans.* **89**, 1695 (1993).
17. R. J. Forster and J. G. Vos, *Macromolecules* **23**, 4372 (1990).
18. A. P. Clarke, J. G. Vos and A. R. Hillman, *J. Electroanal. Chem.* **356**, 287 (1993).
19. A. Sevcik, *Collect. Czech. Chem. Commun.* **44**, 327 (1948).
20. F. G. Cottrell, *Z. Phys. Chem.* **42**, 385 (1902).
21. W. T. Yap, R. A. Durst, E. A. Blubaugh and D. D. Blubaugh, *J. Electroanal. Chem.* **144**, 69 (1983).
22. W. T. Yap and R. A. Durst, *J. Electroanal. Chem.* **216**, 11 (1987).
23. S. M. Oh and L. R. Faulkner, *J. Electroanal. Chem.* **269**, 77 (1989).
24. R. C. Bowers and R. W. Murray, *Anal. Chem.* **38**, 461 (1966).
25. D. Ghesquiere, B. Ban and C. Chachaty, *Macromolecules* **10**, 743 (1977).
26. E. Laviron, *J. Electroanal. Chem.* **52**, 395 (1974).
27. A. P. Brown and F. C. Anson, *Anal. Chem.* **49**, 1589 (1977).
28. P. Daum, J. R. Lenhard, D. R. Rolison and R. W. Murray, *J. Am. Chem. Soc.* **102**, 4649 (1980).
29. D. Leech, R. J. Forster, M. R. Smyth and J. G. Vos, *J. Mater. Chem.* **1**, 629 (1991).